DIGITAL IMAGE PROCESSING

FOR NOISE REDUCTION IN MEDICAL ULTRASONICS

Thanasis Loupas

Thesis submitted for the Degree of Doctor of Philosophy
in the Medical Faculty, University of Edinburgh, July 1988.

TABLE OF CONTENTS

Abstract

The purpose of this project was to investigate the application of digital image processing techniques as a means of reducing noise in medical ultrasonic imaging.

Ultrasonic images suffer primarily from a type of acoustic noise, known as speckle, which is generally regarded as a major source of image quality degradation. The origin of speckle, its statistical properties as well as methods suggested to eliminate this artifact were reviewed. A simple model which can characterize the statistics of speckle on displays was also developed.

A large number of digital noise reduction techniques was investigated. These include frame averaging techniques performed by commercially available devices and spatial filters implemented in software. Among the latter, some filters have been proposed in the scientific literature for ultrasonic, laser and microwave speckle or general noise suppression and the rest are original, developed specifically to suppress ultrasonic speckle. Particular emphasis was placed on adaptive techniques which adjust the processing performed at each point according to the local image content. In this way, they manage to suppress speckle with negligible loss of genuine image detail.

Apart from preserving the diagnostically significant features of a scan another requirement a technique must satisfy before it is accepted in routine clinical practice is real-time operation. A spatial filter capable of satisfying both these requirements was designed and built in hardware using low-cost and readily available components. The possibility of incorporating all the necessary filter circuitry into a single VLSI chip was also investigated.

In order to establish the effectiveness and usefulness of speckle suppression, a representative sample from the techniques examined here was applied to a large number of abdominal scans and their effect on image quality was evaluated.

Finally, further improvements and possible uses of speckle suppression techniques in other fields were also considered.

CHAPTER 1

INTRODUCTION

1.1. Background

1.1.1. Medical imaging

The last decade has witnessed an unprecedented expansion of new modalities in medical imaging (Margulis & Shea, 1986). This development had started as early as the 1950's (Higson, 1987) but it was the emergence of the microelectronics technology which enabled the new modalities to be perfected and introduced in routine clinical use. Until not very long ago, the only practical method of obtaining useful images of the internal structure of the human body was by means of X-rays. Since then, the horizons of radiology have expanded beyond traditional X-ray imaging to embrace radioisotope and ultrasonic imaging, thermography, computed tomography, magnetic resonance imaging and digital radiography.

The concept of uniquely specified diseases is central to the Western model of medicine and their identification is an essential prerequisite for choosing the appropriate treatment. Modern radiological methods utilize the interaction of several types of energy with the human body to form images which provide anatomical and functional information about the structure being imaged. This information is vital not only for detecting but, most importantly, for assessing the spread of a disease. The wealth of diagnostic information offered by the new imaging modalities has without any doubt improved the health care and management of individual patients considerably. However it is essential to keep in mind that, despite its advantages, high-technology medicine is a very complex issue and the debate about its appropriate use is far from over. High-technology medicine is inappropriately used if the same objective could be achieved by simpler means, if the risks involved outweigh

the probable benefits, if the patient's condition is too serious to respond to treatment or if it diverts resources from activities that would bring greater benefits (Jennet, 1984). The last criticism is the one repeated most often, especially because of the escalating economic pressures in the Health Service. Nevertheless, the continuing advances in new technology combined with society's sensitivity to health care indicate that the field of medical imaging will continue its growth in the foreseeable future.

1.1.2. Ultrasonic imaging

One of the most important modalities in medical imaging is diagnostic ultrasound. The possibility of using ultrasonic pulses to obtain images of internal organs has been demonstrated as early as the late 1950's (Baum & Greenwood, 1958; Donald et al, 1958) but it is only recently that ultrasonic imaging has gained widespread acceptability in clinical practice. Since then, the field has expanded constantly and its applications grow year by year. The abdomen is a particularly fruitful area of application, as are the heart and the eye, but almost every medical discipline with an interest in imaging soft tissues has benefited from the growth of the field. Ultrasonic scanning has become an established tool in internal medicine, cardiology, ophthalmology, urology, neurology, paediatrics, gynaecology and especially obstetrics. It is estimated that over 50 million examinations are performed every year worldwide and their number continues to increase (Hill, 1986). Compared to other modalities, ultrasound possesses some unique characteristics which explain its current popularity.

- *Safety.* Although research in the biological effects of ultrasound started a long time ago, and it will certainly continue for even longer, no evidence has been found yet to suggest that present ultrasonic diagnostic practice represents a health risk for patients or operators (Wells, 1987).

- *Cost effectiveness.* Ultrasound is one of the less expensive

modalities as far as both equipment and running costs are concerned. For example, it is estimated that the cost of an ultrasonic examination is between 10 and 20 times lower than the equivalent figure for CT or NMR (Wells, 1986). Because of its cost effectiveness ultrasound is readily available and, consequently, it can reach wider groups of the population.

- *Speed of examination and patient comfort.* The real-time nature of ultrasonic scanning allows an examination to be completed in a few minutes. Also, the procedure for obtaining ultrasonic images introduces minimum patient inconvenience. These two factors reduce the amount of distress caused by the examination.

- *Information content.* In many cases, the information provided by ultrasonic scans cannot be obtained by other means. Also, the ability to display several images per second enhances the usefulness of the technique because it enables the examination of moving structures and monitoring of dynamic events.

Because of these characteristics, ultrasound is rapidly becoming an adjunct to physical examination and it is the favourite diagnostic approach even in centres where CT and NMR are available (Margulis & Shea, 1986). The previous statement does not imply, of course, that ultrasound is a kind of modern panacea. However, when its use is governed by prudence (Wells, 1986) it can improve the health care both from the point of view of the individual and the society as a whole.

1.1.3. Image quality

Image quality is of central importance for the success of an ultrasonic examination. The quality and consequently the clinical usefulness of ultrasonic images has improved dramatically since the early days of static B-scanners. Real-time operation has allowed the movement of internal structures to be studied and large volumes of tissue can be scanned in a short time (McDicken, 1981). Bistable displays have been replaced by grey scale displays which allow the visualization not only of strong echoes from organ boundaries but also the

low-level signals from soft tissue parenchyma which are more important from the diagnostic point of view (Hussey, 1985). The move from analog to 4, 6 or even 8-bit digital scan converters has improved the stability, accuracy, reliability and processing of the displayed information (Ophir & Maklad, 1979; Robinson & Knight, 1981). Electronic beam forming and dynamic focusing has improved spatial resolution considerably (Halliwell, 1987). Finally, image quality has improved as result of using sophisticated computer-controlled time gain compensation systems which adjust the gain function across as well as along the scan lines (Pye et al, 1988).

Despite all these advances, little has been done to reduce noise in ultrasonic images. A good definition of the term "noise", which tends to be a rather vague concept in general, is given by Cornsweet (p. 80, 1970) in his book "Visual perception".

> " In common usage, the term 'noise' refers to sounds that interfere with the sounds the listener wants to hear. These are generally sounds which are random in respect to the signal of interest. The term has now been generalized to include any signals, manifested in any form of energy, that occur irregularly with respect to the signal of interest and tend to obscure the signal."

Electronic noise limits the useful penetration depth of an ultrasonic scan but otherwise does not degrade image quality (Wells & Halliwell, 1981). However, ultrasonic images suffer from a type of acoustic noise called speckle which represents a major source of image quality degradation (Kremkau & Taylor, 1986). Speckle is an interference effect caused by the scattering of the ultrasonic pulse by microscopic tissue inhomogeneities (Morrison et al, 1980). The interference can be constructive or destructive depending on the relative phase differences of the scattered wavelets emanating from within the resolution cell (Wells & Halliwell, 1981). The resulting granular pattern, which is

commonly referred to as texture, can be wrongly interpreted as real whereas in fact it bears little resemblance to the actual tissue microstructure (Flax et al, 1981). The texture of soft tissues depends heavily on the imaging system as well as the tissue being imaged. Factors such as grey scale mapping, transducer focusing pattern and position relative to the body, or even the intervening tissue have a significant effect on texture (Jaffe & Harris, 1980a, 1980b; Kimme-Smith & Jones, 1984). For this reason, it is extremely difficult for a human observer to isolate the true tissue information contained in texture simply by visual inspection of the image. The practical consequences of speckle are:

- *Resolution.* The presence of speckle reduces the ability of a human observer to detect low-contrast lesions (Smith & Lopez, 1982). This is particularly important because in many diseases, such as tumours, the abnormal regions have only slightly different echogenicity from that of the surrounding normal tissue. The resolution of small structures, such as ducts and tracts, is also affected due to the noise masking effect.

- *Image interpretation.* The lack of direct analogy between the speckle pattern and the actual tissue microstructure makes ultrasonic scans difficult to interpret. The question of what is real and what artifactual introduces an element of uncertainty in the examination, reduces confidence in judgements about the clinical significance of a finding and demands a high degree of experience in order to make a correct diagnosis.

- *Image variability.* The strong dependence of texture on the scanner being used has been confirmed by several psychovisual experiments (Kimme-Smith Jones, 1984; Chivers et al, 1986). The disturbing implication of this finding is that the set of criteria employed by a radiologist in order to determine if a scan is abnormal has to be modified when a different machine is used.

- *Viewer efficiency.* Although no experimental data exist for medical ultrasound, it has been observed in other areas where this phenomenon is also encountered that speckle reduces the efficiency of a human observer by causing viewer fatigue (Rawson et al, 1976).

It is reasonable to expect that if speckle suppression can be achieved without loss of true tissue information, image quality will improve due to increased contrast and spatial resolution, enhanced viewer performance, reduced image variability and easier image interpretation. During this project, several established and original methods for speckle suppression were investigated. The common characteristic of all the techniques is that they perform speckle suppression by means of digital image processing.

1.1.4. Digital image processing

A digital image is an image f(x,y) that has discrete values both in spatial coordinates and in brightness. We may consider a digital image as an array of N X N picture elements (pixels) whose row and column indices identify a point in the image and the corresponding element value gives the grey scale level at that point. Typically, a digital image has 512 X 512 pixels with 256 grey levels.

Interest in digital image processing stems from two principal application areas; improvement of pictorial information for human interpretation and processing image data for autonomous machine perception. Initially, work was stimulated mainly by the space research program in the 1960's (Frieden, 1979). Since then, this area has experienced vigorous growth and has become an interdisciplinary subject with research performed in such fields as engineering, robotics, computer and information science, statistics, physics, biology and medicine. The burst of activity can be attributed mainly to three reasons:

- *Development of sophisticated algorithms.* In the early days, the majority of the techniques applied in image processing, such as linear filtering, were transplanted from the field of one dimensional signal processing. As researchers have become aware of the fact that pictorial information demands a different type of processing, more complex but also more effective techniques have emerged which take into account, to a lesser or greater extent, the characteristics of the

human visual system (Mastin, 1985).

- *Dedicated hardware for image processing.* The advances in semiconductor technology have enabled the design of special VLSI integrated circuits which can implement complex algorithms at a fraction of the time needed by a general purpose computer (Young & Liu, 1986; Proceedings of the IEEE, 1987). At the same time, the cost of dedicated hardware is decreasing constantly.

- *Growth in applications.* The initial progress in algorithm and hardware design has resulted in increased awareness of possible users about the potential of image processing which, in turn, has created greater demand for new applications and has stimulated research in new areas.

At the moment even the most sophisticated image processing system looks crude compared to the way a human observer analyses visual information. However, the continuing advances in microelectronics and the use of massively parallel processing devices (Uhr, 1986) should eventually result in systems which approach the efficiency, flexibility and capabilities of the human visual system.

Digital image processing is an essential part of many medical imaging techniques. Computers or dedicated hardware are used to generate, enhance and quantitate visual information in computed tomography, digital radiography, radioisotope and magnetic resonance imaging (Todd-Pokropek, 1980; Sklansky et al, 1986; Sharp, 1987). Although digital techniques have been used to some extent in ultrasonic imaging, mainly for data storage, their impact has been felt much less than in other modalities. However, digital image processing is becoming more and more suitable for the improvement of ultrasonic scans. The general trend towards an all-digital scanner means that echoes are available in digital form from as early as the radiofrequency stage. The decreasing cost and increasing speed of digital signal processing devices makes them compatible with the inexpensive and real-time nature of

ultrasound. Finally, the flexibility, accuracy, reliability and performance offered by digital techniques cannot be obtained by other methods. It is expected that during the next few years, image processing will play an important role in the improvement of ultrasonic image quality.

1.2. Aims and of overview of this project

The aim of this project was to investigate the application of digital image processing techniques as a means of reducing ultrasonic speckle.

Chapter 2 deals with ultrasonic speckle in some detail. The subjects covered are speckle generation, its statistical properties and their modification by the signal processing stages inside the scanner, the possible information carried by speckle about the tissue being imaged and a brief review of techniques proposed to eliminate this artifact.

It was considered essential to begin the experimental part of this project by examining the effectiveness and suitability of commercially available techniques for noise reduction. The only technique specifically aimed at noise reduction which has been incorporated into ultrasonic scanners so far is a form of temporal filtering called recursive averaging. This technique is examined in Chapter 3. Frame integration, which is another form of temporal filtering, is also included in this chapter.

Apart from commercially available techniques another, perhaps more important, objective was to review, apply and evaluate digital image processing algorithms which have appeared in the scientific literature with particular emphasis on adaptive, i.e. space-varying, techniques. Because ultrasonic imaging is a relatively new field, there are still only a few algorithms for acoustic speckle suppression. However similar artifacts are encountered in every field that uses a coherent source of radiation such as laser and microwave radar imaging. The increased awareness of researchers in these

fields about the image degradation caused by speckle has led to the development of a variety of methods to suppress it. Also, from the vast number of noise reduction algorithms available in the general image processing literature some could prove to be useful, even if they were not specifically developed for speckle suppression. A large number of noise reduction algorithms was examined during this phase of the project. The algorithms were modified, where appropriate, in order to take into account the special characteristics of ultrasonic speckle and were applied to digitized scans.

Experimentation with already existing noise reduction techniques was undertaken for two reasons. The first and obvious reason was to determine their suitability. The other reason was to identify their weaknesses and specify the desirable characteristics of an ideal speckle suppression algorithm, so that it would be possible to achieve better performance either by combining the positive features of well-known techniques or by following directions previously unexplored. During this phase of the project several new algorithms were developed with, admittedly, varying degrees of success. At the same period some time was devoted in deriving and studying theoretical properties of new algorithms in order to gain a better understanding of the way they operate. Chapter 4 describes some representative algorithms, both established and new, and presents results from their application to ultrasonic scans. The algorithms are classified as linear, nonlinear and adaptive according to their operation on the input data. Their common characteristics are that they perform spatial filtering, i.e. they use the noisy information contained in a single frame to produce a smooth image, and they are implemented in software.

The final objective of the project was to develop techniques which could be used in clinical practice. The most important requirement for the

clinical application of speckle suppression is real-time operation, in the sense that a scan should be processed in 1/10 - 1/20 of a second. This is by no means a trivial task because it involves several million numerical calculations per second. Computers cannot provide this kind of speed so they are effectively suitable only for off-line applications. However research in software techniques was considered, and was actually proved, essential for establishing the necessary features and determining the feasibility of algorithms suitable for real-time operation. Chapter 5 discusses the problems associated with the real-time implementation of digital image processing algorithms and describes the design of a hard-wired two dimensional filter which can perform real-time speckle suppression while preserving the important features of a scan.

From the image processing literature, it is evident that far more effort has been devoted in developing new algorithms than in evaluating their performance. In our opinion, this is indicative of the difficulties involved in performing a comprehensive and rigorous evaluation. In medicine, however, it is very important to assess the clinical usefulness of image processing techniques, despite the difficulties involved. The approach followed here was to apply frame averaging, software spatial filtering and hardware spatial filtering to a large number of scans obtained by using different scanners. Afterwards, the quality of the original and processed images was evaluated in terms of noise content, boundary definition, contrast, diagnostic information and overall preference both from the physician's and the physicist's point of view. The methodology and results of the clinical evaluation are presented in Chapter 6.

Finally, Chapter 7 discusses further developments and possible improvements. Other applications of noise suppression in ultrasonic imaging, apart from the ones investigated in this project, are also considered.

CHAPTER 2

ULTRASONIC SPECKLE

2.1. Introduction

Ultrasonic imaging utilizes the interaction of the human body with a high frequency pulse to form images which provide information about the acoustical properties of the tissue being scanned. Because of the complex and poorly understood nature of this interaction, the information provided by the scan is qualitative rather than quantitative, in the sense that image intensities correspond to a combination of several factors instead of a single acoustic tissue property. In general, B-scan images are based on the changes of the acoustic impedance inside a medium (Fatemi & Kak, 1980). The acoustic impedance Z can be defined as $Z=\rho c$ or $Z=(\rho\mu)^{1/2}$, where c is the speed of sound, ρ the density and μ the compressibility of the medium.

The returning echoes that form the ultrasonic image are generated mainly through the mechanisms of reflection and scattering (McDicken, 1981). Reflection occurs when the ultrasonic pulse encounters a large-scale interface separating two media of acoustic impedances Z_1 and Z_2. Assuming normal incidence, the reflected intensity I_r is given in terms of the incident intensity I_i by the plane wave reflection formula

$$I_r/I_i=(Z_1-Z_2)^2/(Z_1+Z_2)^2 \qquad (2.1)$$

This is of course an idealized situation which can nevertheless give us a rough estimate of the reflective properties of tissue interfaces. Reflection is responsible for the strong echoes received from organ boundaries such as the interface between liver and diaphragm.

Scattering, on the other hand, occurs when a wave is fragmented in several directions after interacting with tissue discontinuities of dimensions

similar to or smaller than the acoustic wavelength. This is a far more important echo generation mechanism because the backscattered wave provides information about the mean scattering strength of the internal structure of an organ, as opposed to just the location of interfaces, which can be correlated to the pathology of the tissue. It is also a far more complex phenomenon to analyse because of the mathematical difficulties involved and our incomplete knowledge of the tissue acoustic microstructure. However, because of its diagnostic significance scattering has attracted considerable attention both from the theoretical and experimental point of view. The current status of scattering theory is reviewed by Chivers (1977) and more recently by Dickinson (1986). All the theories that have been developed so far model tissue either as a continuous medium where the density and compressibility fluctuate from point to point about their mean values (inhomogeneous continuum model) or as a large collection of point scatterers embedded at random positions in an otherwise homogeneous medium (discrete scatterer model).

Figure 2.1 shows a typical ultrasonic scan of the liver, kidney and the diaphragm. The scan exhibits a characteristic granular pattern, commonly referred to as speckle, due to scattering of the ultrasonic pulse by microscopic tissue inhomogeneities. In the early days of grey scale ultrasonography, the origin and implications of speckle had been the cause of much confusion and misunderstandings. The first attempts to explain its nature (Burckhardt, 1978; Abbot & Thurstone, 1979; Morrison 1979; Morrison et al, 1980) used analogies from other fields where this phenomenon is also encountered, and in particular from laser imaging. Laser speckle has been studied extensively (see for example Journal of the Optical Society of America, special edition on speckle, November 1976) and some of the results are directly applicable to ultrasound. However, the analogies are somehow limited because laser speckle is

produced by a continuous wave reflected by a two-dimensional surface whereas ultrasonic speckle is produced by a finite length pulse propagating through a three-dimensional volume (Flax et al, 1981).

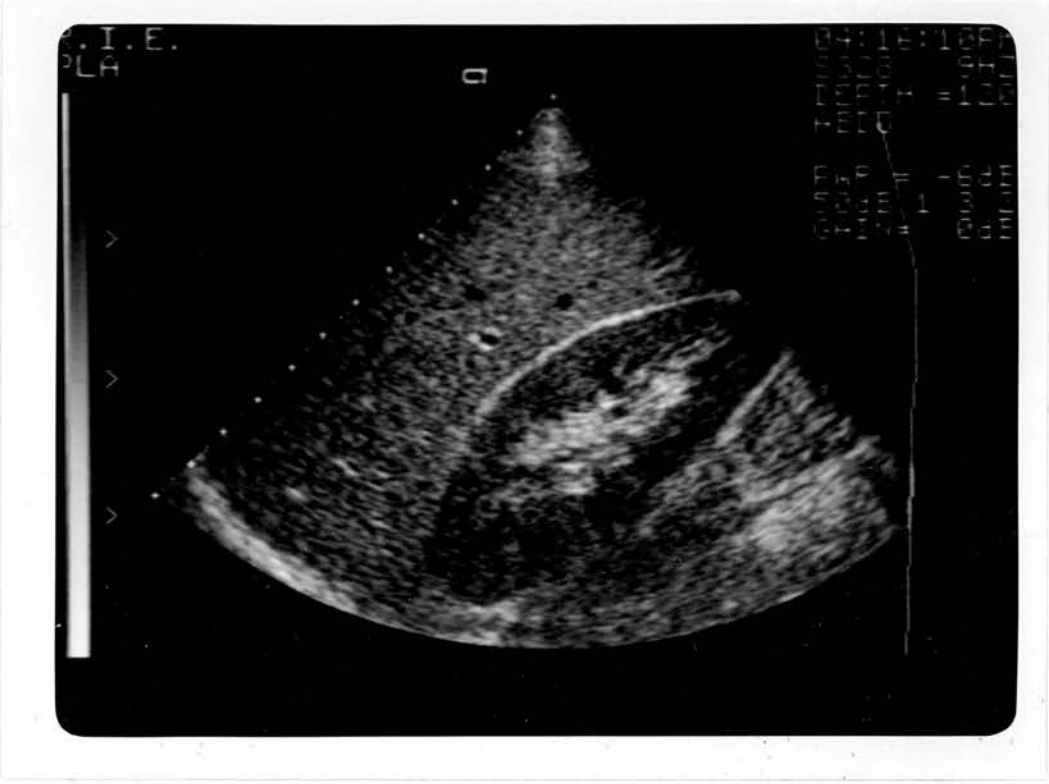

Figure 2.1 : Ultrasonic scan of the liver, right kidney and the diaphragm.

A qualitative explanation of how speckle is generated can be given by using the discrete scatterer tissue model. Let us considered Figure 2.2a which has been adapted from Wells & Halliwell (1981). Because of the finite width of the beam, at any time instant the pulse interacts with a three-dimensional volume element, the so called resolution cell, which includes a large number of scatterers of size and spacing comparable or smaller than the wavelength. Speckle is an interference effect due to the phase-sensitive addition by the transducer of the scattered wavelets emanating from within the resolution cell. Depending on the relative phase differences of the wavelets, predominantly constructive or destructive interference may occur. The extreme cases of interference caused by the addition of two pulses of the form shown in Figure 2.2b and having phase difference of zero, half and one wavelength, are

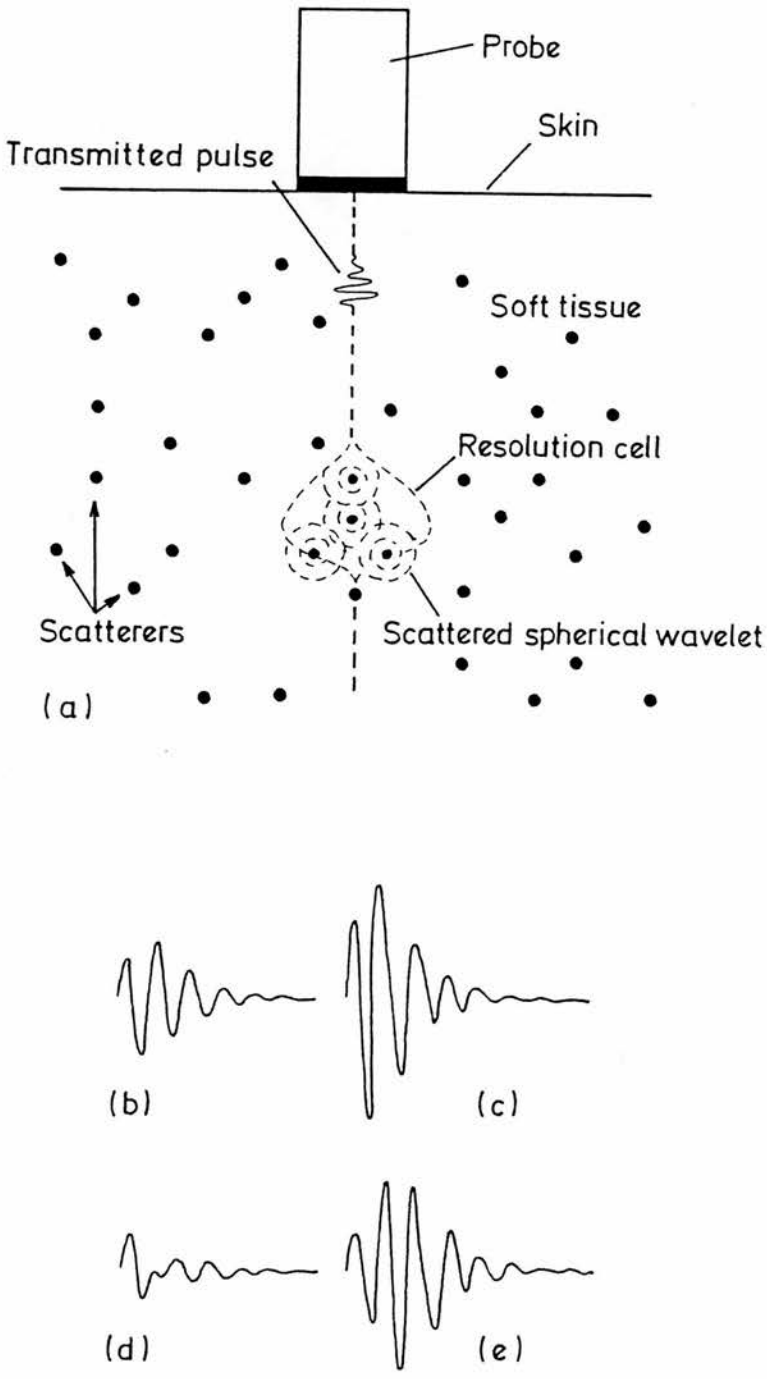

Figure 2.2 : **(a)** - Speckle generation. **(b), (e)** - Examples of constructive and destructive interference. Addition of two pulses of the form shown in **(b)** and having phase difference of zero **(c)**, half **(d)** and one wavelength **(e)**.

displayed in Figures 2.2c, d and e respectively (adapted from Morrison et al, 1980). The previous description of speckle generation ignores the effect of the intervening tissue on the scattered echoes. For a more realistic description, multiple scattering and phase distortion due to different acoustic velocities, frequency dependent attenuation and multiple interfaces should also be considered.

2.2. First-order statistics

The statistical properties of speckle have been studied by Burckhardt (1978) and Wagner et al (1983). Their analysis was based on the random walk problem which had been previously used to study laser speckle (Goodman, 1975). At a given time instant, the transducer receives N echoes scattered by the tissue inhomogeneities within the resolution cell. The k_{th} elementary contribution can be represented in phasor notation as $a_k=|a_k|\exp[j\phi_k]$, where $|a_k|$ is the magnitude and ϕ_k is the phase of the scattered wavelet.

The following assumptions are made:

- The number of scatterers N is very large.

- The phasors a_k are statistically independent. In other words, the joint probability density function , in short notation pdf, $f(a_1,a_2,...,a_N)$ is the product of the individual pdf's $f(a_k)$.

- The phases ϕ_k are uniformly distributed in the interval $[0,2\pi]$ and independent of the magnitudes $|a_k|$.

Then, the phase-sensitive addition by the transducer of the elementary phasors a_k corresponds to a two-dimensional random walk problem in the complex plane. From the central limit theorem (Middleton, Chapter 7, 1960), the transducer output A

$$A=\sum_{k=1}^{N}|a_k|\exp[j\phi_k]=A_R+jA_I \qquad (2.2)$$

has a joint pdf

$$f(A_R,A_I)=(1/2\pi\psi)\exp[-(A_R^2+A_I^2)/2\psi] \tag{2.3}$$

This is a circular Gaussian distribution with mean equal to 0 and variance equal to ψ. The parameter ψ is defined as

$$\psi=\sum_{k=1}^{N}|a_k^2|/2 \tag{2.4}$$

and provides information about the tissue scattering strength.

From probability theory (Papoulis, Chapter 7, 1981), the transform

$$z=g(x,y) \qquad\qquad w=h(x,y) \tag{2.5}$$

has a joint pdf $f_{zw}(z,w)$ which can be expressed in terms of the pdf $f_{xy}(x,y)$ as

$$f_{zw}(z,w)=f_{xy}(x_1,y_1)/|J(x_1,y_1)|+ \ldots+f_{xy}(x_n,y_n)/|J(x_n,y_n)| \tag{2.6}$$

where (x_1,y_1), $\ldots,(x_n,y_n)$ are real solutions of the simultaneous equations of (2.5) and the determinant of the Jacobian J(x,y) is defined as

$$|J(x,y)|=(\partial g(x,y)/\partial x)(\partial h(x,y)/\partial y)-(\partial g(x,y)/\partial y)(\partial h(x,y)/\partial x) \tag{2.7}$$

Using (2.6), it can be easily proven that the transform to polar coordinates $|A|=[A_R^2+A_I^2]^{1/2}$ and $\theta=\tan^{-1}(A_I/A_R)$ has a joint pdf

$$f(|A|,\theta)=(|A|/2\pi\psi)\exp[-|A|^2/2\psi] \tag{2.8}$$

Finally the pdf $f(|A|)$ of the envelope-detected signal $|A|$ is given by

$$f(|A|)=\int_0^{2\pi} f(|A|,\theta)d\theta = (|A|/\psi)\exp[-|A|^2/2\psi] \tag{2.9}$$

This is a Rayleigh distribution with mean m, variance σ^2 and signal-to-noise ratio SNR

$$m=[\pi\psi/2]^{1/2} \qquad \sigma^2=(4-\pi)\psi/2 \qquad SNR=[\pi/(4-\pi)]^{1/2}\simeq 1.91 \tag{2.10}$$

Despite the simplifications and assumptions made, (2.9) describes the first-order statistics of acoustic speckle accurately. Several workers have reported agreement between the Rayleigh distribution and experimental histograms of the envelope-detected signal, obtained by scanning tissue mimicking phantoms (Foster et al, 1983; Wagner et al, 1983; Zagzebski et al, 1985).

From (2.10), it can be seen that the mean of the envelope-detected signal is proportional to the standard deviation. This is a characteristic of multiplicative noise. Consequently, speckle can be modelled as

$$z=xn \qquad \text{or} \qquad z=x+xu \tag{2.11}$$

where
- z is the observed signal
- x is the true signal
- n=1+u is a noise term, statistically independent of x

The noise distribution can be found in the following manner. Assuming that an area of the same scattering strength ψ is scanned, from (2.10) the true signal x is equal to $[\pi\psi/2]^{1/2}$. Since x is constant, its pdf $f_x(x)$ is given by $f_x(x)=\delta[x-(\pi\psi/2)^{1/2}]$, where $\delta(x)$ is the delta function (Bracewell, Chapter 5, 1986). In order that z obeys the Rayleigh distribution of (2.9) the pdf $f_n(n)$ of the noise term n should be $f_n(n)=(\pi n/2)\exp[-n^2\pi/4]$ with mean $m_n=1$ and variance $\sigma_n^2=(4-\pi)/\pi$. By substituting $f_x(x)$, $f_n(x)$ into the following equation

$$f_z(z)=\int_{-\infty}^{+\infty}(1/|w|)f_x(w)f_n(z/w)dw \tag{2.12}$$

which gives the pdf of the product of two independent random variables (Papoulis, Chapter 7, 1981), it is straightforward to verify that the pdf $f_z(z)$ of the observed signal z is given by (2.9).

Envelope detection is the first of many signal processing stages inside the scanner which modify the statistics of speckle. When the echoes are finally displayed as a grey scale image, the Rayleigh distribution and the multiplicative noise model are no longer valid. For example, the histograms of Figure 2.3 correspond to the same 64 X 64 region of a tissue mimicking phantom[1] imaged under normal conditions (Figure 2.3a) and with the logarithmic compression circuit disconnected (Figure 2.3b). The images were obtained using a Marti real-time sector scanner manufactured by Fischer Ultrasound Ltd. Both histograms are quite different from the Rayleigh distribution with the histogram of Figure 2.3a having an almost Gaussian shape. Bamber & Cook-Martin (1987) have also commented upon the similarity between the Gaussian distribution and histograms of speckle calculated from grey scale images.

In order to obtain an idea about the statistics of speckle on displays, the simple signal transmission model of Figure 2.4 has been used. The form of the logarithmic compression is similar to the one used by Schomberg et al (1983) for the deconvolution of ultrasonic scans. The low-pass filter simulates the effect of the finite bandwidth of the amplifying stages and the interpolation/smoothing performed by the scan converter. Although it would be preferable to develop analytical expressions for the statistical distribution of speckle on displays, this is not possible because of the following reasons. The

[1]The tissue mimicking phantoms used in this work were the Cardiff resolution, grey scale and routine quality test objects (McCarty & Stewart, 1984).

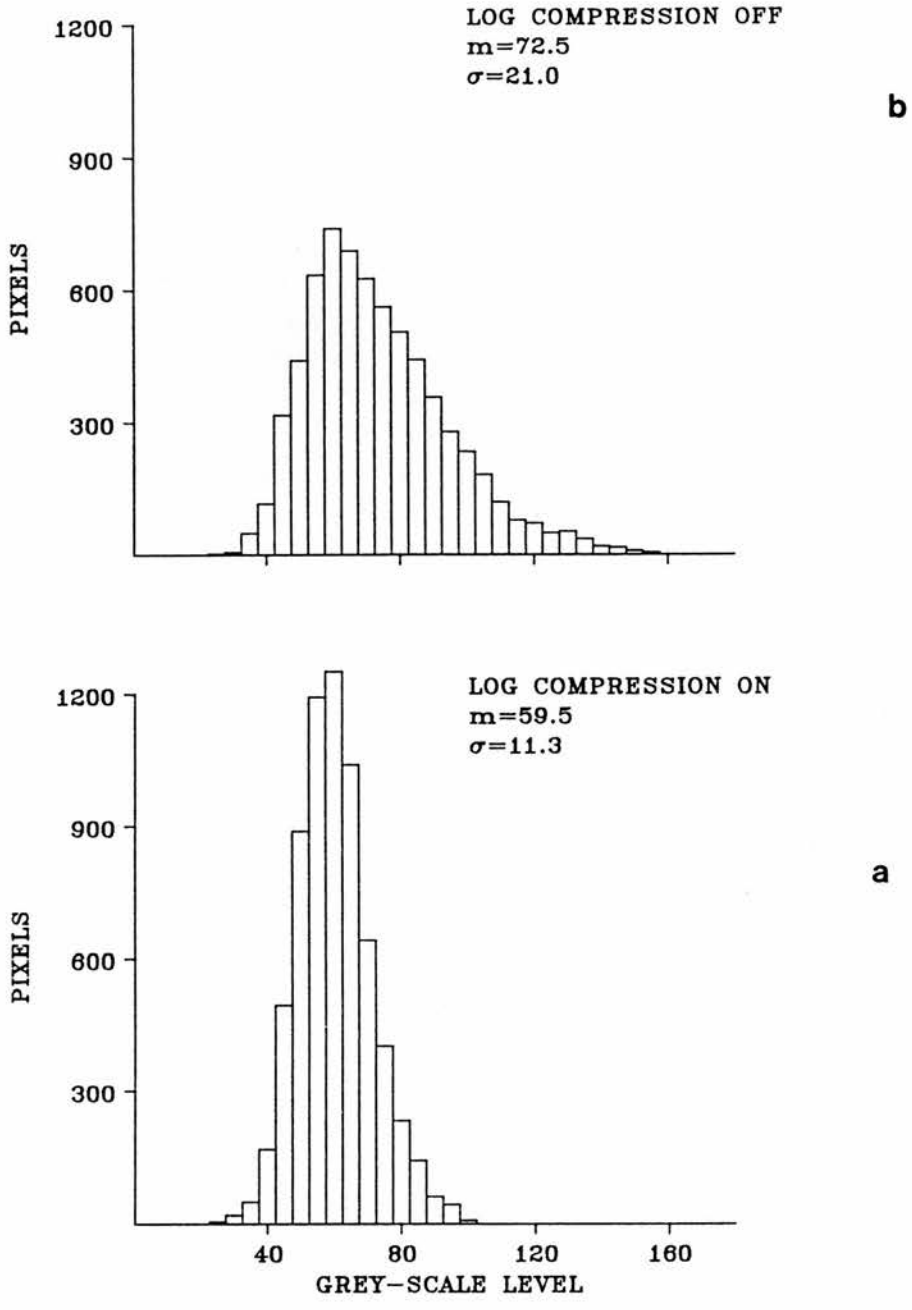

Figure 2.3 : Influence of signal processing on the statistics of acoustic speckle. Histograms calculated from the same 64 X 64 scan of a phantom under normal conditions **(a)** and with the log compression circuit disconnected **(b)**.

logarithmic transform of a Rayleigh variable x has been studied for the simple case $y=\ln x$ (Deutsch, Chapter 3, 1962) but the moments (e.g. mean, variance etc) of y cannot be obtained in closed form for the more general case $y=A\ln(Bx+1)$. In addition, the pdf of the output z of a linear system, like the low-pass filter of Figure 2.4, is in general intractable unless the input y is a Gaussian process (Davenport & Root, Chapter 9, 1958).

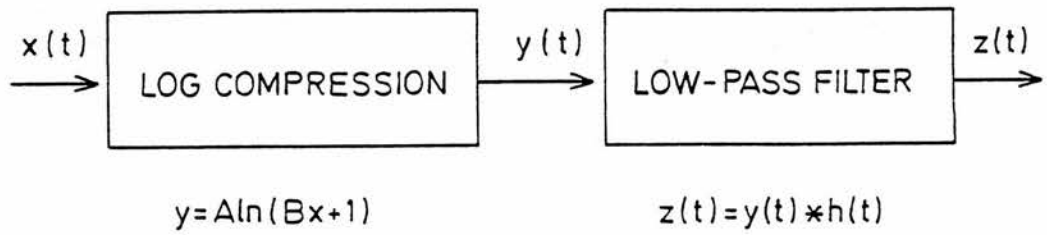

Figure 2.4 : Simple signal transmission model to simulate the processing stages inside the scanner. x(t), z(t) are the envelope-detected and displayed signals respectively.

Computer simulations are useful when analytical expressions cannot be obtained. In order to estimate the statistics of speckle on displays, a simulation program based on the model of Figure 2.4 was written. The starting point is the generation of a 10000-point random sequence. This is an uncorrelated Gaussian process, with mean and variance equal to 0 and ψ respectively, and corresponds to the radiofrequency signal of (2.2). Envelope detection is performed by means of the Hilbert transform (Bracewell, Chapter 12, 1986). The parameters A, B of the logarithmic compression and the low-pass filter coefficients are adjusted to obtain agreement with experimental data. As an example, Figure 2.5 displays the histograms of each stage for an input sequence with $\psi=2292$, $A=37$, $B=0.05$ and a simple 3-point running average filter. The envelope-detected signal exhibits the characteristic shape of the Rayleigh distribution (Figure 2.5a). The logarithmic transform distorts the Rayleigh distribution by compressing the right-hand tail of the histogram (Figure 2.5b) and low-pass filtering results in an almost Gaussian distribution

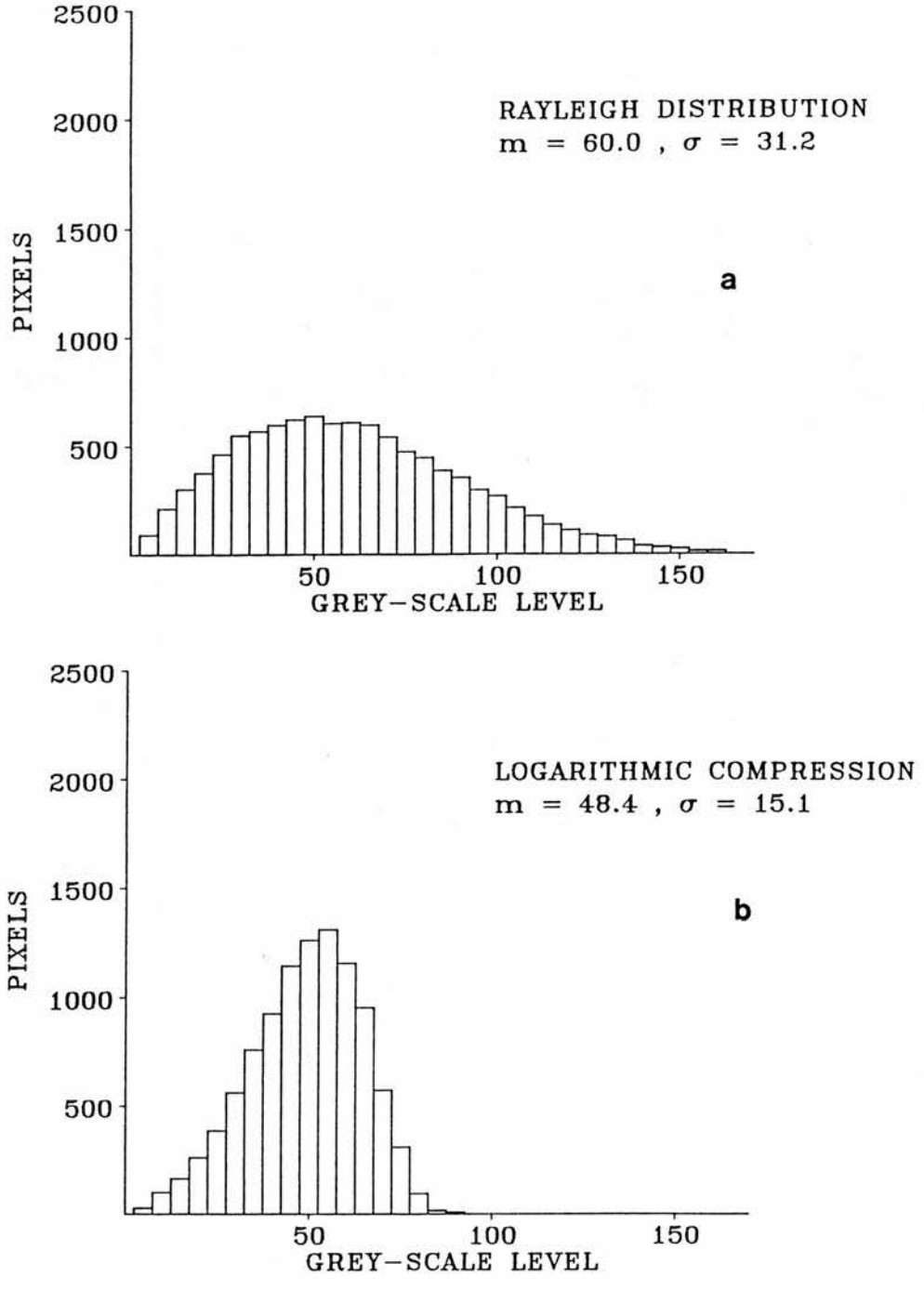

Figure 2.5 : Computer simulation of first-order statistics of speckle. Histograms of envelope-detected signal **(a)** and log compressed signal **(b)**.

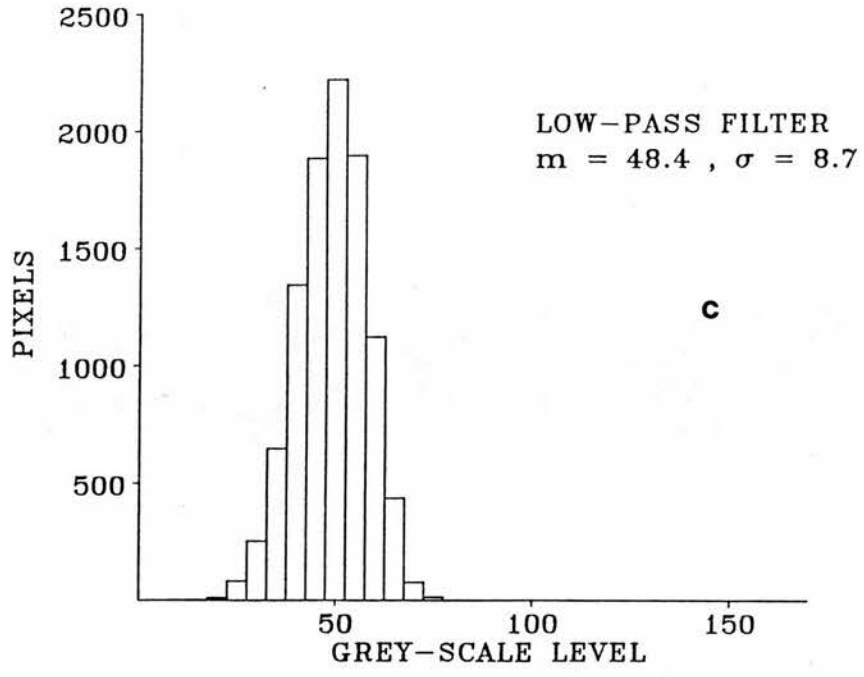

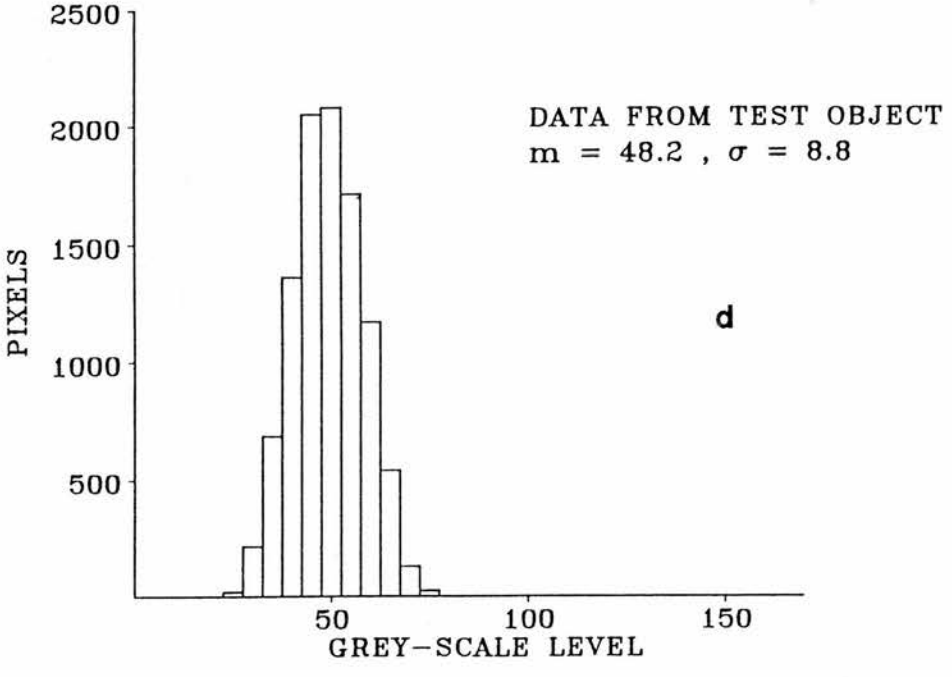

Figure 2.5 : Computer simulation of first-order statistics of speckle. **(c)** - Histogram of low-pass filtered signal. **(d)** - Experimental histogram calculated from scan of ultrasonic phantom.

(Figure 2.5c). Both the shape and moments of the final histogram agree quite well with experimental data, like the histogram of a 64 X 64 region from a tissue mimicking phantom shown in Figure 2.5d. Note that the actual histogram values in Figure 2.5d have been multiplied by $10000/64^2$ so that all four histograms are displayed with the same scale.

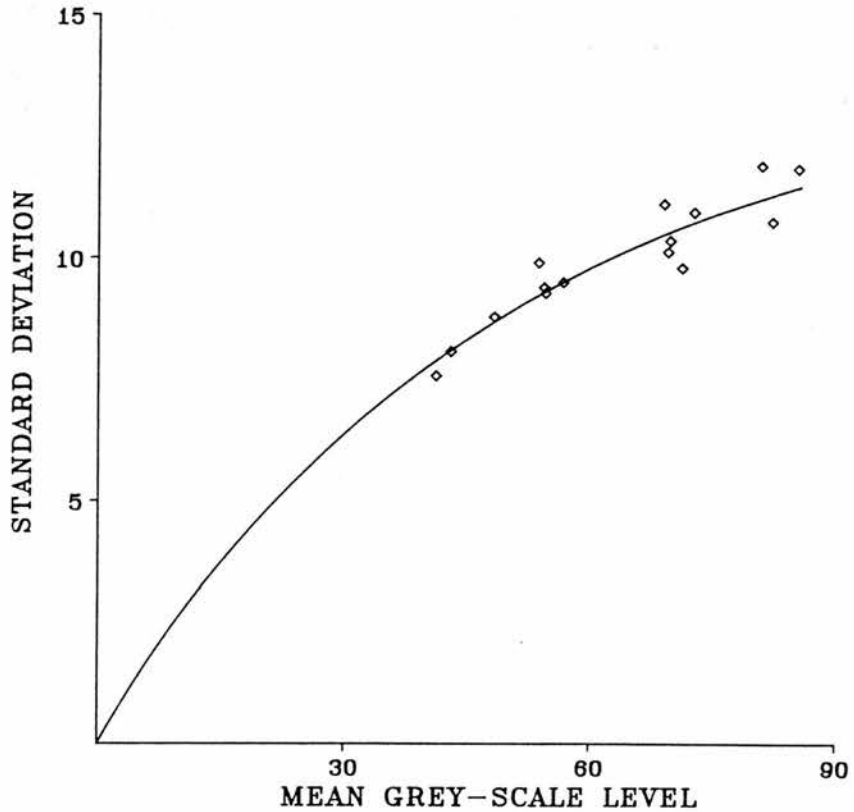

Figure 2.6 :Standard deviation vs the mean of ultrasonic speckle. Solid curve - computer simulation. Points - data obtained from ultrasonic phantoms using the Siemens Sonoline SX scanner.

The graph of the standard deviation vs the mean of speckle on displays is plotted in Figure 2.6. The solid curve was obtained by performing the computer simulation using different values for the variance ψ of the input sequence. The points represent experimental data obtained by calculating the mean and standard deviation of the pixels inside 64 X 64 regions from tissue mimicking phantoms. The regions chosen were judged to have uniform

intensities without reverberations or other artifacts and were imaged using the same time gain compensation settings. From Figure 2.6 it can be seen that speckle is no longer multiplicative in the sense that the mean m is proportional to the variance σ^2 rather than the standard deviation σ. This observation implies that the ratio σ^2/m is, at least approximately, constant and therefore it could be used to characterize speckle. An example is given by Figure 2.7a which is a scan of the liver and gallbladder. The local mean and variance of each pixel is calculated using a 9 X 9 pixel window and the quantity σ^2/m is displayed in Figure 2.7b as a grey scale image. Comparison between the two images shows that areas containing speckle in Figure 2.7a correspond to similar midgrey levels in Figure 2.7b, whereas resolvable structures have considerably higher intensities. The σ^2/m criterion is used extensively in the design of the adaptive filters of Chapter 4. Based on the assumption that σ^2/m is constant, speckle on displays can be now modelled as

$$z=x+x^{1/2}u \tag{2.13}$$

where
- z is the observed signal
- x is the true signal
- u is a noise term, statistically independent of x and having mean $m_u=0$

The first-order statistics of this noise model are studied in Section 4.4.1 (equations 4.27 - 4.30).

The following points could be made about the validity of the computer simulation and the choice of σ^2/m. First, the input of the computer program is an uncorrelated random sequence whereas speckle is correlated both in the axial and lateral direction (Wagner et al, 1983). Also, the simulation uses one-dimensional data to estimate the statistics of a two-dimensional signal. Finally, the assumption that σ^2/m has a constant value

a

b

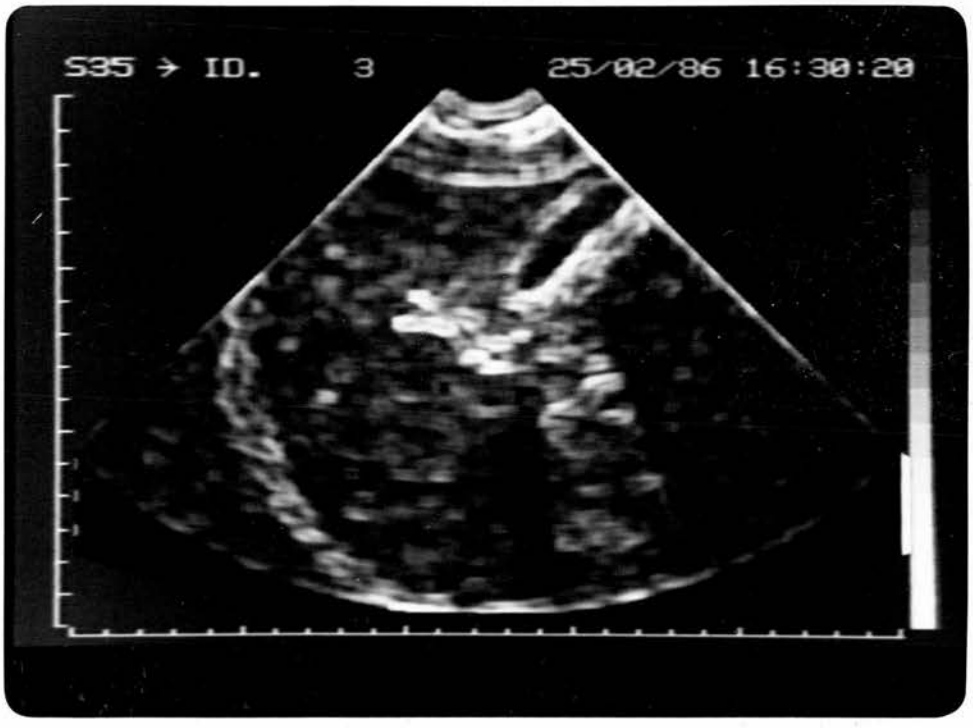

Figure 2.7 : **(a)** – Ultrasonic scan of the liver and gallbladder. **(b)** – Ratio of the local variance over the local mean, multiplied by a scaling factor and displayed as a grey scale image.

is only an approximation of the actual curve of Figure 2.6. Nevertheless, the purpose of this study was not to provide a comprehensive and rigorous treatment of the statistics of speckle on displays but simply to find a convenient and easily calculated quantity which could characterize speckle. The σ^2/m criterion has been found in practice to satisfy these requirements.

2.3. Information or noise ?

Should speckle and its spatial variation (texture) be regarded as true signal which provides information about the tissue pathology (Kossoff et al, 1976) or as undesirable noise which bears no relationship to the actual tissue microstructure (Burckhardt, 1978) ? This question has been the subject of several investigations. Their conclusions, although sometimes contradictory, have improved our understanding of the complicated mechanisms which govern the ultrasonic image formation.

The theoretical analysis presented in Section 2.2 assumes that the first-order statistics of speckle can be described in terms of general physical principles without references to the imaging system. The average intensity of speckle is related through (2.10) to the tissue scattering strength. This implies that a more accurate estimate of the tissue acoustical properties could be obtained by suppressing random signal fluctuations. Following similar methodology Wagner et al (1983) concluded that the second-order statistics of speckle and the quantities determined by them, such as the average speckle size, depend only on the transducer characteristics and reported very good agreement between their theoretical expressions and experimental data from phantoms and computer simulations (Smith & Wagner, 1984). However, they also warned that their results are applicable to clinical images only to the extent that tissue can be modelled as a gelatin matrix containing many small uniformly distributed scatterers.

The effect of the imaging system on texture has been the subject of qualitative studies by Jaffe & Harris (1980a; 1980b). They remarked that the transducer focusing pattern and the grey scale mapping modify the appearance of texture. According to them, the "true" tissue texture is not the one nearest the transducer but that which is displayed at regions of best focus, a comment also made by Kremkau & Taylor (1986).

Computer simulations which model the entire image formation process have been widely used to study the problem of ultrasonic texture because they allow the effect of individual parameters on the final image to be examined in a systematic manner. The validity of this approach has been demonstrated by Foster et al (1983) and Zagzebski et al (1985), who have developed three-dimensional models which take into account the transducer's as well as the scattering medium's properties and have achieved very good agreement between theory and experiment. Bamber and Dickinson (1980) have performed a two-dimensional simulation of speckle based on the inhomogeneous continuum tissue model. The results of the simulation suggest that there is a very complicated relationship between the ultrasonic scan of an object and the object itself. For objects of dimensions larger than the pulse wavelength (resolvable at least in theory) the scan exhibits a marked difference, demonstrated primarily by a finer texture, but is relatively insensitive to the pulse width and rise/fall times. On the other hand, for unresolvable structures the appearance of the scan depends heavily on the pulse characteristics. Flax et al (1981) have observed that fine texture is not indicative of high spatial resolution. They have also observed that the average speckle size is proportional to the distance from the transducer and inversely proportional to the number of scatterers used in the computer simulation program. Oosterveld et al (1985) and Thijssen et al (1987) have studied the effect of depth, attenuation and scatterer density on the first and

second-order statistics of texture. They concluded that the mean echo level is proportional to the square root of the scatterer density, as expected from (2.10), but it also depends on the depth increasing towards the focal point and decreasing beyond it. They also found that the lateral and axial dimensions of speckle decrease as the scatterer density increases. Attenuation has a major effect on the second-order statistics of speckle. For an attenuating medium the lateral width of speckle increases sharply with depth. They commented that the area around the focal point, which is preferred by the physicians because it has the best spatial resolution, has also the least constant lateral texture.

The effect of instrumentation parameters on texture has been confirmed by two psychovisual experiments. In the first experiment (Kimme-Smith & Jones, 1984), a specimen of bovine pancreas was scanned under different imaging conditions and a group of radiologists evaluated the visual similarity of the images. The analysis of the results demonstrated that the grey scale mapping, the transducer focusing pattern and the intervening tissue have a significant effect on texture whereas factors such as the distance from the transducer or the scan conversion algorithm used are relatively unimportant. In the second experiment (Chivers et al, 1986), scans of four tissue mimicking phantoms of different scattering properties were compared with a scan of normal liver to determine which phantom resembles liver texture more closely. The procedure was repeated for four scanners and the image similarity was judged by a group of twenty two observers. The results suggested that the model which resembles liver most closely varies from machine to machine. This result seem to support the hypothesis that the textures observed are characterized primarily by the scanner that produced them rather than the tissue mimicking phantom that was imaged.

From the above, it is clear that the average speckle intensity is a

useful quantity because it provides information about the tissue scattering strength. In fact, this is the most widely used criterion by radiologists when examining a scan. However, the spatial variation of speckle depends heavily on so many system parameters that it is almost impossible for a human observer to isolate the true tissue information. Consequently, judgements about the clinical significance of texture can be misleading. The lack of a direct correspondence between texture and the actual tissue microstructure plus the effects speckle has on image interpretation and variability, resolution and viewer efficiency (already mentioned in Section 1.1.3) support the argument that speckle is an undesirable signal which should be treated as noise.

On the other hand, since speckle results from the interaction of tissue with the ultrasonic pulse it is reasonable to assume that it should carry at least some information about the tissue being imaged. Considerable effort has been devoted in trying to extract this information. A group of techniques based on computer analysis of texture attempt to identify texture features which could be used as tissue signatures. These features include local histograms for studying Gaucher's disease (Shawker et al, 1981) or distinguishing between normal liver and carcinoma (Itoh et al, 1985), co-occurence matrices for classification of diffuse and malignant liver disease (Raeth et al, 1985) and grey level run-length histograms and grey level difference statistics for identification of acute myocardial ischemia (McPherson et al, 1986). A combination of textural features including first-order, second-order and Fourier domain features has been used by Nicholas et al (1986) to perform automatic discrimination between liver and spleen scans. Texture has also been used for automatic tissue segmentation (Mailloux et al, 1984; 1985).

The previous techniques are *ad hoc* in nature in the sense that the selection of texture features is made on a trial-and-error basis. Other groups

have attempted to associate the texture to the histological state of tissue. Sommer et al (1981) and Fellingham & Sommer (1984) have found that tissue exhibits periodic or semiperiodic structure which can be associated with pathology. For example, cirrhotic liver disease and Hodgkin's disease in the spleen result in coarser than normal histological appearance. They have been able to detect the periodic structure by analysing the autocorrelation of digitized echoes returning from the pathological site. Recently, a very interesting approach which relates the histology of tissue to the statistical properties of texture has been suggested. The statistical basis of this method is described in two publications by Wagner et al (1986; 1987a). According to this method, the tissue inhomogeneities are classified as diffuse or distributed specular scatterers. Diffuse scatterers have dimensions smaller than the pulse wavelength, obey Rayleigh statistics, are unresolvable and do not carry any tissue signature apart from the mean scattering strength. Distributed specular scatterers have dimensions comparable with the wavelength, obey Rician statistics, are partially resolvable and provide information about the semiperiodical structure of the tissue being imaged. The tissue signature can be obtained by calculating the power spectrum of the texture and stripping off the diffuse components. The technique has be proven to be useful for classification of liver disease (Insana et al, 1986), but attention is drawn to the need for removing the effects of the scanner in order to obtain accurate results (Wagner et al, 1987b).

The common characteristic of the texture analysis techniques discussed here, and indeed the vast majority of the tissue characterization techniques, is that the information is extracted by means of complicated numerical processing of the data performed by computers. The use of computers is necessary because the information, and especially the second-order statistical properties of texture, is not available from visual

inspection. The classic work of Julesz (Julesz at al, 1973; Julesz, 1975) in visual perception has proved that observers are sensitive to differences in the second-order properties of texture. However, by using simulated images of the type encountered in ultrasonic imaging Wagner et al (1985) have demonstrated that there is a wide range of texture discrimination tasks based on second-order statistics at which the human observer performs very poorly whereas a machine is very efficient.

In the light of the previous discussion, the original question of this section seems incomplete. In order to determine if speckle is information or noise the means by which the signal is analysed should also be specified. Machine analysis of texture seems to be a promising direction for tissue characterization. However, as far as visual interpretation of images is concerned, speckle not only does not convey any perceivable information but it also interferes with the perception of diagnostically significant features. It makes sense, therefore, to suppress the irrelevant data like speckle in order to enhance the features of the image which are relevant to the decision making process.

2.4. Review of ultrasonic speckle reduction techniques

It is generally hoped that speckle suppression could improve image quality and possibly increase the diagnostic potential of ultrasonic imaging. For this reason, speckle suppression has been, and still is, a very active area of research. Speckle suppression techniques must satisfy the following requirements in order to gain acceptability in clinical practice.

- *Adequate noise reduction and signal preservation.* Ultrasonic images are heavily corrupted by noise. However, unlike some other types of medical images they also possess sharp edges which in many cases, e.g. small blood vessels, have dimensions comparable to the speckle size. Consequently, the techniques should suppress speckle without degrading the resolution of the image by wiping out important features.

- *Real or near real-time operation.* It has been pointed out in Chapter 1 that one of the most important advantages of ultrasound is its real-time nature. Anything that disrupts the interactive procedure of scanning is inevitably of limited value.

- *Low complexity.* The more complex and expensive to implement a technique is, the more difficult it becomes to justify its use, especially in a low-cost modality like ultrasound.

Speckle suppression techniques have yet to gain acceptance in routine scanning. This can be attributed to the fact that they fail to satisfy one or more of the above requirements. The last part of this section presents a brief review of the techniques proposed so far and discusses some of their drawbacks. The vast majority of the techniques can be divided in two broad categories known as spatial filtering and compounding.

2.4.1. Spatial filtering

The task of spatial filtering in speckle suppression is to produce a smooth image by estimating the true signal intensity from the noisy information contained in a single frame. This is usually performed in the space instead of the frequency domain because it offers more flexibility and is easier to implement. Given a M X M digital image f(x,y), spatial filtering generates a smooth image g(x,y) whose grey level at each point (x,y) is the combination of the pixel intensities around a predefined neighbourhood of (x,y) in the original image f(x,y). Linear combinations of the pixel intensities have been proposed for noise reduction in echocardiography by Parker & Pryor (1982) and Hecker & Pöppl (1982). Alternatively, the combination can be nonlinear in the form of median filtering (Morikubo et al, 1985) or outlier removal (Schuster et al, 1986). The major drawback of both linear and nonlinear approaches is that they are space-invariant, in other words they perform the same type of operation in all parts of an image. Since the content of ultrasonic scans varies with location,

the filtering algorithms should ideally be able to distinguish between specular reflections, uniform areas of speckle and boundaries between regions of different scattering strength and perform the appropriate type of processing. However because of their space-invariance, linear and nonlinear filters tend to introduce blurring and loss of true image detail. In order to overcome these limitations, space-varying or adaptive techniques have been introduced recently which attempt to distinguish between different regions using some speckle characterization features. Dickinson (1982) has proposed a filter whose smoothing action is inversely proportional to the local mean. In this way strong echoes can be preserved, but at the expense of oversmoothing low level signals and blurring the boundaries of low-contrast focal lesions. The use of more sophisticated speckle characterization features based on the first-order statistics(Bamber & Daft, 1986; Loupas et al, 1987), or a combination of first and second-order statistics (Bamber & Cook-Martin, 1987) has resulted in better and more effective algorithms. A more detailed discussion on this subject is presented in Chapter 4.

2.4.2. Compounding

Compounding attempts to reduce speckle contrast by combining independent views of the same object obtained under different imaging conditions. This idea has been used before for speckle suppression in laser (Goodman, 1976) and microwave radar imaging (Porcello et al, 1976). Its origins, however, can be traced even further back to a fundamental theorem found in every textbook of probability theory. The theorem states that the addition of N independent, identically distributed random variables results in a new random variable having standard deviation reduced by $N^{1/2}$ and signal-to-noise ratio increased by the same factor. The key word in the concept of compounding is the term "independent views". Many authors have remarked that, unlike electronic noise or radioactive decay, speckle patterns

obtained at different times will always be identical provided that all the imaging parameters are kept constant (Morrison et al, 1980; Wells & Halliwell, 1981). Therefore the problem is how to generate independent ,i.e. uncorrelated, speckle patterns.

In spatial compounding, uncorrelated or partially uncorrelated views are obtained by examining the object from different angles. One way of achieving this is by changing the position of the transducer relative to the body. This idea has been extensively used in B-mode static imaging (Garret et al, 1975; Kossoff et al, 1976). In real-time scanning, a very simple form of spatial compounding superimposes several video frames on photographic film by keeping the camera lens open for a period of time and relies on slight patient movement to obtain partially uncorrelated speckle patterns (Bartrum & Crow, 1980; Sommer & Sue, 1983; Cunningham & Bacani, 1985). The digital equivalent of this technique (Sommer & Sue, 1983; Petrovic et al, 1986) is examined in Chapter 3 under the name frame integration. An alternative method for obtaining independent views of the object is to divide a multielement transducer into subapertures which share the same transmit/receive circuits in succession (Shattuck & von Ramm, 1982; Shattuck et al, 1984) or to use more than one transducer operating in parallel (Kossoff et al, 1985; Kerr et al, 1986).

In frequency compounding, partially uncorrelated views of the object are obtained by varying the centre frequency and/or the bandwidth of the transmitted pulse (Magnin et al, 1982; Melton & Magnin, 1984). A variation of this technique, known as split spectrum processing in the field of ultrasonic nondestructive testing (Newhouse et al, 1982; Karpur et al, 1987), separates the frequency spectrum of the received echoes in N components using adjacent band-pass filters and then combines the individual frequency components in a coherent or incoherent manner (Yoshida et al, 1985; 1986; Gehlbach & Sommer

1987a; 1987b; Galloway et al, 1988).

Under ideal conditions, compounding possesses certain advantages over filtering. In probability theory, compounding and spatial filtering are equivalent to estimating the properties of a random process by using information from independent repetitions (ensemble statistics) or a single observation of the process (time statistics) respectively. The true properties of the process are given by the ensemble statistics and time statistics are only an approximation, particularly when a non-stationary, non-ergodic, and correlated process like an ultrasonic image is examined. Another reason is that after filtering, but not after compounding, the output image exhibits increased autocorrelation which manifests itself as coarser texture. This is undesirable both from the point of view of a human observer who tends to tolerate uncorrelated noise more easily (Kozma & Christensen, 1976) and statistical decision theory which predicts that there is an inverse relationship between texture coarseness and contrast resolution (Smith et al, 1983). An additional advantage of spatial compounding is that it could improve the definition of specular reflections.

A successful example of spatial compounding is shown in Figure 2.8. The unprocessed image (Figure 2.8a) is a scan of a tissue mimicking phantom, obtained using a Siemens Sonoline SX real-time scanner with a 3.5 MHz transducer. By moving the transducer at 2mm increments, four scans parallel to the horizontal axis of the phantom and belonging to the same plane were obtained. The scans were then transferred to a computer and the amount of horizontal and vertical shift needed for perfect registration was calculated using a cross-correlation technique described by Pratt (Chapter 19.5, 1978). Finally the shifted scans were added on a pixel by pixel basis and the result is displayed in Figure 2.8b. From this figure it can be seen that, apart from reduced speckle contrast, the compound scan exhibits improved edge

a

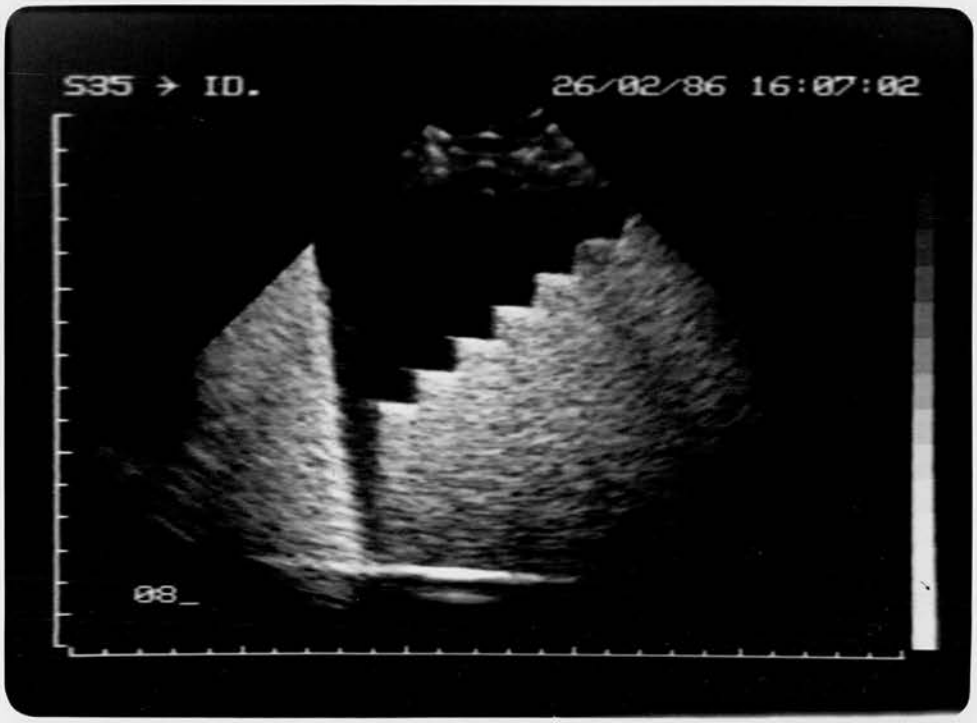

b

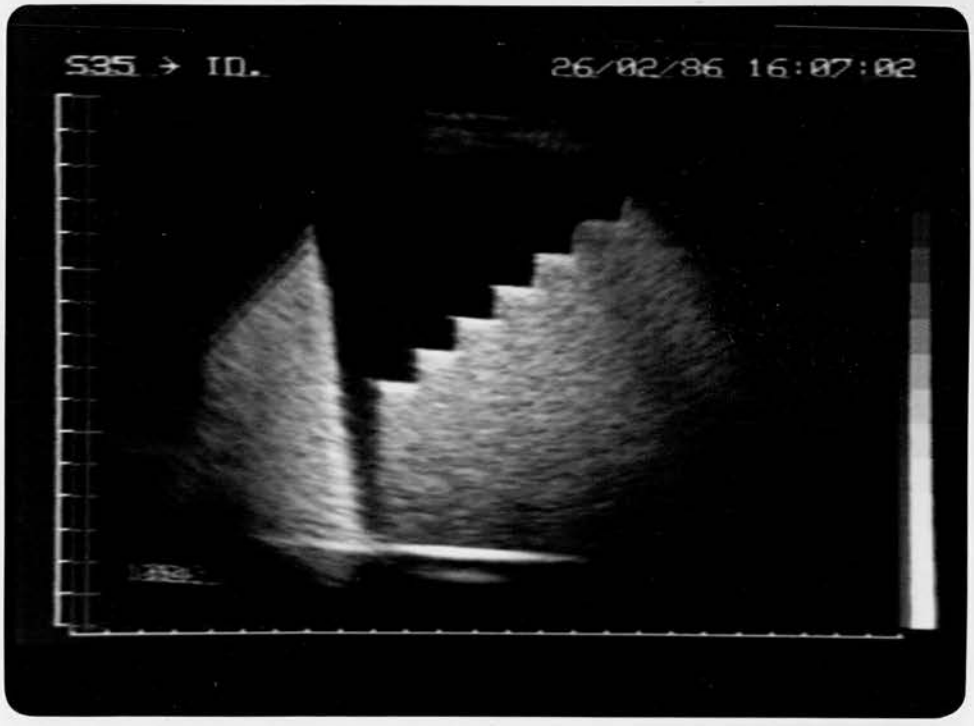

Figure 2.8 : **(a)** - Original scan of an ultrasonic phantom. **(b)** - Spatially compounded version of **(a)**.

definition, especially at the bottom part of the dark wedge.

Difficulties encountered in practice can make compounding inferior to filtering, despite its theoretical superiority. Ideally, the combined images must have uncorrelated speckle patterns but otherwise the image content of the scans should be identical. In spatial compounding, due to the dependence of factors such as the axial and lateral resolution, attenuation, refraction and acoustic velocity on the angle of insonification, the intensity or position of genuine structure can vary from image to image. This causes image blurring and loss of spatial resolution. Also, the means by which uncorrelated views of the same object are to be obtained poses more problems. The use of a moving transducer creates problems of registration and reduced frame rate. In addition, no system capable of operating in real-time has been reported up to now, probably because of the mechanical difficulties involved in the accurate and fast movement of the transducer between frames. The use of more than one transducer overcomes the previous problems but introduces increased hardware complexity and difficulties in accessing some organs. On the other hand, a multielement transducer involves a compromise between using all the elements as a single aperture for better lateral resolution and dividing them in subapertures for better noise reduction.

Frequency compounding has similar drawbacks. The intervening tissue does not create any problems, as in the case of spatial compounding, because the angle of insonification is fixed. However, the dependence of the axial and lateral resolution, attenuation and backscattering on the transmitted frequency can cause resolution loss and image blurring. Also, the division of the available bandwidth, in order to transmit different frequencies, results in an increase of the pulse length and, therefore, in poorer axial resolution.

The most important factor in the design of compound systems is the

rate of decorrelation of the speckle pattern achieved by altering the imaging parameters. Several attempts have been made in the past to measure experimentally and predict theoretically this rate. The most recent and comprehensive results have been presented by Trahey et al for lateral aperture translation (1986a) and centre frequency change (1986b). The same group has studied the reduction of speckle contrast in relation to the resolution loss and has found that spatial compounding offers a better tradeoff between these two quantities (Trahey et al, 1987). More importantly, they concluded that although target detectability improves with spatial compounding, always at the expense of point resolution, it actually deteriorates significantly with frequency compounding.

2.4.3. Speckle reduction via phase

A new method for speckle suppression has been proposed recently (Seggie & Leeman, 1987; Leeman & Seggie, 1987) which does not fall into either of the categories mentioned above. The technique is based on the instantaneous frequency, defined as the time derivative of the radiofrequency signal phase, which originates from frequency modulated imaging (Ferrari et al, 1982; Seggie et al, 1987). The local fluctuations in the amplitude of the instantaneous frequency are used to determine points of an A-scan line where destructive interference has occurred. These points serve as speckle markers. The echoes on either side of the marker are then combined to reduce speckle This approach has certain similarities with the adaptive filtering techniques in the sense that both attempt to identify areas where speckle is present, but on the whole is quite different because it uses a deterministic rather than a statistical quantity to characterize speckle. The authors have applied their technique on a simple cyst phantom and have obtained better noise reduction indices than in compounding. However, it is not possible to judge the potential of the technique, and especially how successful it is in preserving

important image features, because no clinical images have been presented so far.

2.4.4. Commercially available techniques

Although speckle has not been addressed directly by the designers of ultrasonic equipments, modern scanners utilize simple forms of both spatial filtering and compounding to produce a smooth image. Straight averaging of typically two pixels along and two pixels across an A-scan line is a common feature of most scan converters. However, this approach cannot be extended to fully suppress speckle by averaging more pixels because it will introduce severe blurring and loss of true image detail. Another technique which has recently been incorporated into scanners is a form of temporal processing. This technique, known as recursive or frame-to-frame averaging, generates a new output frame by performing a weighted sum of the current input and the previous output frames. This can be regarded as a form of spatial compounding because it is the transducer's displacement relative to the body that generates partially uncorrelated speckle patterns. Recursive averaging is discussed in the following chapter.

CHAPTER 3

FRAME AVERAGING TECHNIQUES

3.1. Introduction

As was mentioned in the previous chapter, a digital signal processing technique which can be found in an increasing number of real-time scanners performs averaging of successive video frames to reduce noise in the image. This operation makes use of a recursion formula between the current input and the previous output in order to produce a new output frame. Although a variety of names such as temporal filtering, temporal processing, digital averaging, running averaging etc have been used to describe this type of noise reduction, recursive averaging is the term preferred here so that it can be distinguished from straight averaging or frame integration which makes use only of the previous inputs in order to produce a new output frame.

Both recursive averaging and frame integration belong to the same general category of frame averaging techniques. The introduction of frame averaging in ultrasonic scanning can be interpreted as an acknowledgment by the manufacturers of the need to produce a less noisy image. Its cost-effective implementation has been made possible by the widespread use of digital scan converters and the decreasing costs of random access memories for storing digital images. The same idea has been applied before in many fields including electron microscopy and digital subtraction angiography and has been found particularly effective in suppressing intensity fluctuations (noise) which vary with time. However speckle, which is the main type of noise encountered in ultrasonic imaging, does not vary with time if all the imaging conditions are kept constant. As a consequence, frame averaging techniques have to rely on small changes in the transducer's position relative to the body in order to obtain partially uncorrelated speckle patterns and eventually reduce speckle contrast. From this point of view they can be

regarded as a simple form of spatial compounding.

Recursive averaging is the only feature offered by scanners specifically for noise reduction. Although no studies on its clinical benefits have been reported so far, experience has shown that this type of processing has been accepted by physicians who tend to use it frequently, particularly when scanning "noisy" patients. For the above reasons, it was considered essential to evaluate its performance as a first step towards determining the value of speckle suppression. In order not to be restricted only to scanners which offer this option, it was decided that the image processor which was about to be purchased for digitizing and transferring data to a computer should offer recursive averaging. The image processor finally chosen (Crystal manufactured by Microconsultants Ltd.) can also perform frame integration. The Crystal has over one Megabyte of dynamic memory and can store up to two images digitized at 576 rows by 530 columns by 8 bits resolution. Unlike other image processors which need a supervising computer, the Crystal has been designed to work autonomously. This inevitably restricts the ease with which it can be controlled by a computer but, at the same time, it is very useful because it makes the processor mobile and suitable for use in a clinical environment.

3.2. Recursive averaging

The operation of recursive averaging results in a live image. At a given time instant which corresponds to frame number i, the output frame O_i is the weighted sum of the present input frame I_i and the previous output frame O_{i-1}, where the frames are added on a point-by-point basis. Figure 3.1a shows this operation in a block diagram form with (x,y) representing the pixel which belongs to row x and column y of the digitized image and Z^{-1} denoting a delay of one frame. Recursive averaging can be defined in terms of a simple equation

$$O_i(x,y)=nI_i(x,y)+(1-n)O_{i-1}(x,y) \qquad (3.1)$$

The weighting factor n takes the discrete values n=1, 1/2, $1/2^2$, ..., $1/2^M$ with M=12 for the Crystal. Sometimes the inverse of the weighting factor F=1/n=1, 2, 2^2, ..., 2^M is given. F is usually referred to by the term "number of frames". However, it must be noted that the statement "recursive averaging for 4 frames" simply means that F=4 (n=1/4) and not that 4 frames were added.

The fact that n, F take only values which are powers of 2 is very convenient for hardware implementation. Maher et al (1988) have examined the Intellect 100 image processor manufactured by the same company as the Crystal and found that recursive averaging is performed according to the formula

$$O_i(x,y)=n[I_i(x,y)-O_{i-1}(x,y)]+O_{i-1}(x,y) \qquad (3.2)$$

which is simply a rearrangement of (3.1). The current output pixel $O_i(x,y)$ is calculated by subtracting the previous output from the current input value, shifting m positions to the left ($n=1/2^m$) and adding the result to the previous output value. Everything is performed in integer based arithmetic without the need for expensive, slow and complicated hardware multipliers.

The weighting factor n determines how fast the output can follow changes of the input and represents a tradeoff between noise reduction and blurring due to patient movement. If it is assumed that a jump of the input occurs at frame N, i.e. $I_i(x,y)=A$ for $1\leq i<N$ and $I_i(x,y)=B$ for $N\leq i<+\infty$, the output $O_N(x,y)$ will be equal to

$$O_N(x,y)=nB+(1-n)A \qquad (3.3)$$

In a similar manner, the output $O_{N+i-1}(x,y)$ after i frames will be

$$O_{N+i-1}(x,y)=Bn\sum_{k=0}^{i-1}(1-n)^k+A(1-n)^i \tag{3.4}$$

which can be simplified further if the sum of the geometric series in (3.4) is substituted by

$$\sum_{k=0}^{i-1}(1-n)^k=[1-(1-n)^i]/[1-(1-n)] \tag{3.5}$$

By defining the quantity c as the ratio of the difference between the input $I_{N+i-1}(x,y)$ and the output $O_{N+i-1}(x,y)$ over the original intensity jump B-A we obtain the expression

$$i=ln(c)/ln(1-n) \tag{3.6}$$

By taking into account the fact that a frame corresponds to 1/25 s, the values of Table 3.1 have been calculated from (3.6) for c=0.1 and 0.01.

Table 3.1

n	c=0.1	c=0.01
1/2	0.14	0.27
1/4	0.32	0.64
1/8	0.69	1.38
1/16	1.43	2.85
1/32	2.90	5.80

For example if n=1/16 and a change of the input occurs, the difference between the input and the output will be smaller than 10% and 1% of the original jump after 1.43 and 2.85 s respectively.

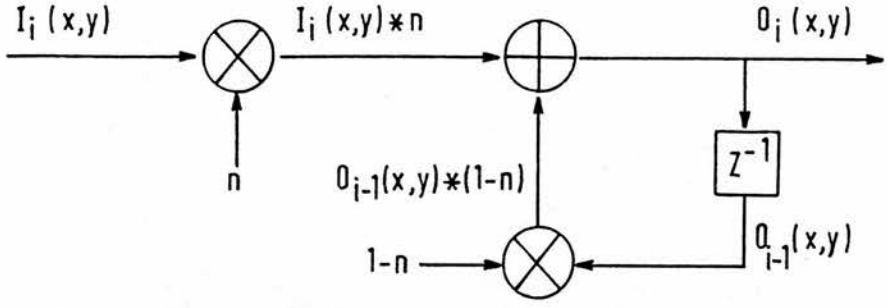

a Recursive averaging

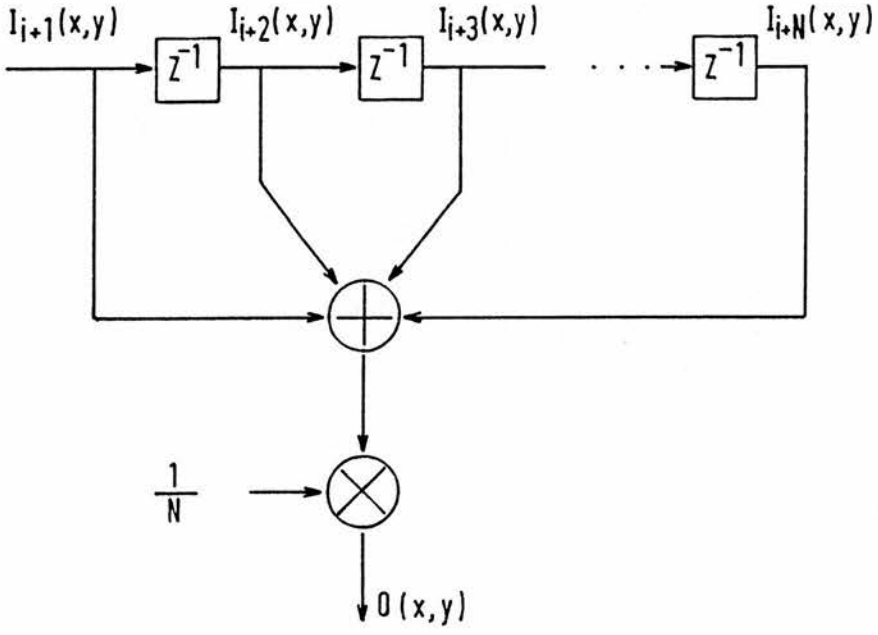

b Integration

Figure 3.1 : (a) - Block diagram of recursive averaging. **(b)** - Block diagram of integration.

3.3. Frame integration

The second noise reduction technique offered by the Crystal is called integration and results in a frozen image. This operation is performed simply by adding N consecutive video frames and dividing the sum by N to produce a normalized image, as it can be seen by the block diagram of Figure 3.1b and the following equation

$$O(x,y)=[\sum_{k=i+1}^{i+N} I_k(x,y)\ ]/N \tag{3.7}$$

The number of frames N has to be a power of 2, i.e. $N=1, 2, 2^2, ..., 2^M$, with M=11 for the Crystal. Integration is also implemented very easily in hardware by adding the N successive frames in a point-by-point basis and then shifting the sum m positions to the left, where $N=2^m$ (Maher et al, 1988). N determines the tradeoff between noise reduction and blurring due to patient movement. The duration of integration can be found by multiplying the number of frames N by 1/25 s.

3.4. Recursive averaging versus frame integration

It is interesting to compare the noise suppression capabilities of the two frame averaging techniques examined here. Let us assume that the input terms $I_i(x,y)$ belong to a sequence of independent, identically distributed random variables X_k, k=1, 2, ..., $+\infty$, with mean $E\{X_k\}$ equal to 0 and variance σ_{in}^2 equal to $E\{X_k^2\}-E^2\{X_k\}=E\{X_k^2\}$. Integration for N frames will be examined first. From (3.7)

$$E\{O_N(x,y)\}=E\{[\sum_{k=i+1}^{i+N} X_k\ ]/N\}=NE\{X_k\}/N=0 \tag{3.8}$$

and

$$E\{O_N^2(x,y)\}=E\{[\sum_{k=i+1}^{i+N} X_k\ ]^2/N^2\} \tag{3.9}$$

Since X_k are mutually independent, the expected value $E\{X_iX_j...X_k\}$ is equal to $E\{X_i\}E\{X_j\}...E\{X_k\}=0$ for any combination of the indices i, j, ..., k. Then

$$E\{O_N^2(x,y)\}=NE\{X_k^2\}/N^2 \tag{3.10}$$

or the variance of the integrated output σ_{INT}^2 is related to the variance of the input σ_{in}^2 by the formula

$$\sigma_{INT}^2=\sigma_{in}^2/N \tag{3.11}$$

For the case of recursive averaging we assume that processing starts at frame 1 and the first output is equal to the first input. Then from (3.1)

$$O_1(x,y)=I_1(x,y)=X_1$$

$$O_2(x,y)=nX_2+(1-n)X_1$$

Similarly, the output after N frames is given by

$$O_N(x,y)=n\sum_{k=0}^{N-2}(1-n)^{N-2-k}X_{k+2} + (1-n)^{N-1}X_1 \tag{3.12}$$

The mean of $O_N(x,y)$ is equal to

$$E\{O_N(x,y)\}=nE\{X_k\}\sum_{k=0}^{N-2}(1-n)^{N-2-k} + (1-n)^{N-1}E\{X_1\}=0 \tag{3.13}$$

Again, because of the independence of the random variables X_k the expected value $E\{O_N^2(x,y)\}$ is equal to

$$E\{O_N^2(x,y)\}=n^2E\{X_k^2\}\sum_{k=0}^{N-2}(1-n)^{2(N-2-k)} + (1-n)^{2(N-1)}E\{X_1^2\} \tag{3.14}$$

By using (3.5) to calculate the sum of the geometric series and performing a few algebraic simplifications we arrive at the following expression for the variance σ^2_{RAV} of the output after recursive averaging

$$\sigma^2_{RAV}=\sigma^2_{in}[n+2(1-n)^{2N-1}]/(2-n) \tag{3.15}$$

If the number of frames N during which recursive averaging is performed is large, the output variance reaches a constant value

$$\sigma^2_{RAV}=\sigma^2_{in}n/(2-n) \tag{3.16}$$

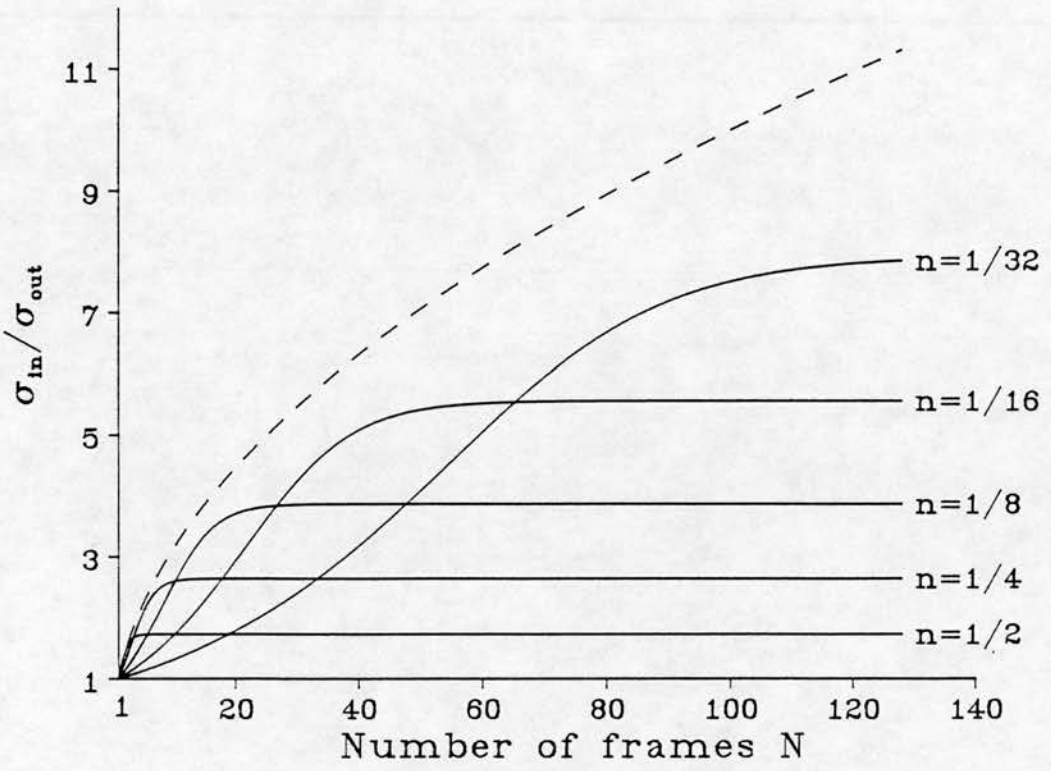

Figure 3.2 : Noise reduction offered by integration (broken curve) and recursive averaging (solid curves). N is the number of frames from the start of processing; n is the weighting factor for recursive averaging; σ_{in}, σ_{out} are the standard deviations of the unprocessed and processed signals respectively.

Figure 3.2 plots the ratio of the input standard deviation σ_{in} over the output standard deviation σ_{out}, which describes the noise reduction achieved, for the case of integration (broken curve) and recursive averaging (solid curve)

with the weighting factor n equal to 1/2, 1/4, 1/8, 1/16 and 1/32. From this figure it can be seen that integration is more effective in suppressing noise than recursive averaging. Another point, perhaps not very well appreciated from equation (3.15) but clearly demonstrated by Figure 3.2, is that the number of frames N from the start of recursive averaging until maximum noise reduction is reached increases dramatically as the weighting factor n becomes smaller.

It must be noted that the values of Figure 3.2 represent the maximum possible noise reduction when the input sequence consists of independent terms. For the case of ultrasonic scans, the noise reduction achieved is considerably smaller because the speckle patterns obtained during the application of frame averaging are strongly correlated.

3.5. Applications

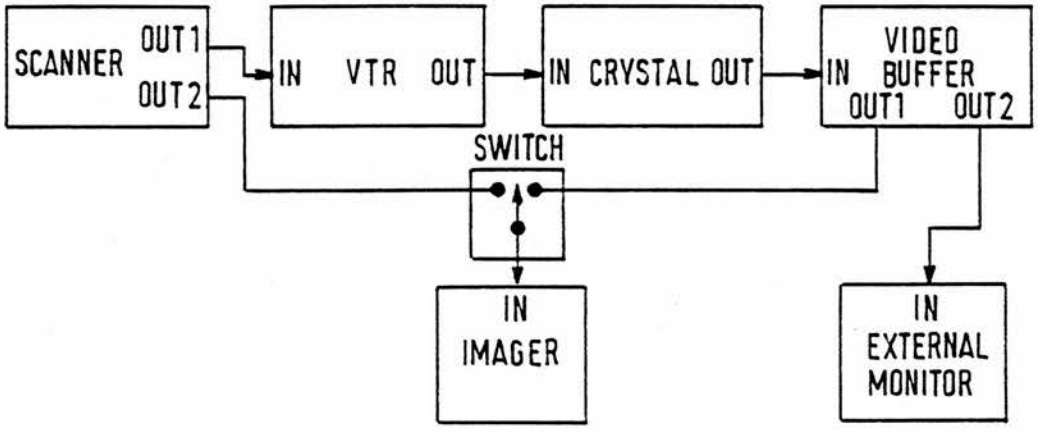

Figure 3.3 : Experimental set up for the clinical evaluation of frame averaging.

Recursive averaging and frame integration were clinically evaluated using the set up of Figure 3.3. The image processor was connected to one of the video outputs of the scanner and the processed images were displayed on an external monitor. The original and processed scans were routed through a switch, which selected either one or the other, to the input of a EMI

multiformat imager. Every care was taken, by adjusting the gain of Crystal's input amplifier and using a video buffer, that both types of images had the same contrast and brightness levels. For each anatomical view two unprocessed and two processed images were photographed on standard X-ray film following the procedure described below.

1. While the image processor performs recursive averaging find suitable view.
2. Freeze image on both the scanner and external monitor simultaneously. Take photographs 1 (unprocessed I) and 2 (recursive averaging).
3. Unfreeze image on scanner. Having frozen image on external monitor as a guide, scan patient to find the same view.
4. Start integration
5. At the end of integration freeze images on scanner and external monitor. Take photographs 3 (unprocessed II) and 4 (integration).

For recursive averaging a value of n=1/4 was chosen which offers reasonable noise reduction but also allows the output to follow the input relatively fast. For example, from Table 3.1 we see that if an intensity jump in the input occurs at a certain time, the difference between the output and the input will become smaller than 10% and 1% of the original jump after 0.32 and 0.64 s respectively. For the integration a value of N=32 frames was chosen which corresponds to a time interval of 1.28 s. The patients were instructed to hold their breath during processing.

The results of the clinical evaluation which included 145 views (580 images in total) from 73 patients are presented in Chapter 6. The main limitation of frame averaging is that the quality of the processed images depends heavily on factors such as patient movement, which cannot be controlled by the operator. Depending on the amount of movement, a

processed scan can be identical, smoother or severely blurred compared to the original. A successful application of frame averaging techniques is shown in Figure 3.4. Figures 3.4a and 3.4c are unprocessed scans of the pancreas. Speckle has been reduced considerably in the scans of Figure 3.4b (recursive averaging) and 3.4d (integration) but also boundaries between areas of different echogenicity are better defined. The processed images were judged to have superior quality by the radiologist who was responsible for the clinical evaluation. On the other hand, Figure 3.5 shows an example where frame averaging produces images of inferior quality. Recursive averaging (Figure 3.5b) has almost no effect on the original scan of Figure 3.5a, apart from a slight decrease in sharpness, whereas integration results in an image (Figure 3.5d) which suffers from severe blurring and loss of image detail.

In conclusion, frame averaging offers the advantage of simple and low-cost implementation in hardware but it also has the drawback of introducing blurring which results in image quality degradation. Two clinical applications of integration which have been reported recently use different approaches to overcome the problem of blurring. Cunningham & Bacani (1985) have implemented an analog form of integration which superimposes several video frames on photographic film by keeping the camera lens open for a period of time. In order to overcome the problem of blurring, they have found it necessary to repeat this procedure at least six times for the same view to make sure that an image of quality superior to that of the original has been obtained. Petrovic et al (1986) have applied digital integration to echocardiography. Their solution for avoiding blurring is to use a special triggering method based on the ECG so that only heart scans corresponding to the same point of the cardiac cycle are integrated. To our knowledge, there have been no reports so far on clinical applications of recursive averaging in ultrasonic imaging. A possible improvement of this technique could be

achieved by using a motion detector similar to the one described by Jaffe et al (1982) for use in digital subtraction angiography, so that speckle is suppressed but moving structures remain unaffected. In this way, a less noisy image could be generated without having to pay the price of blurring.

a

b

Figure 3.4 : Scan of the pancreas. **(a)** - Unprocessed I. **(b)** - Recursive averaging.

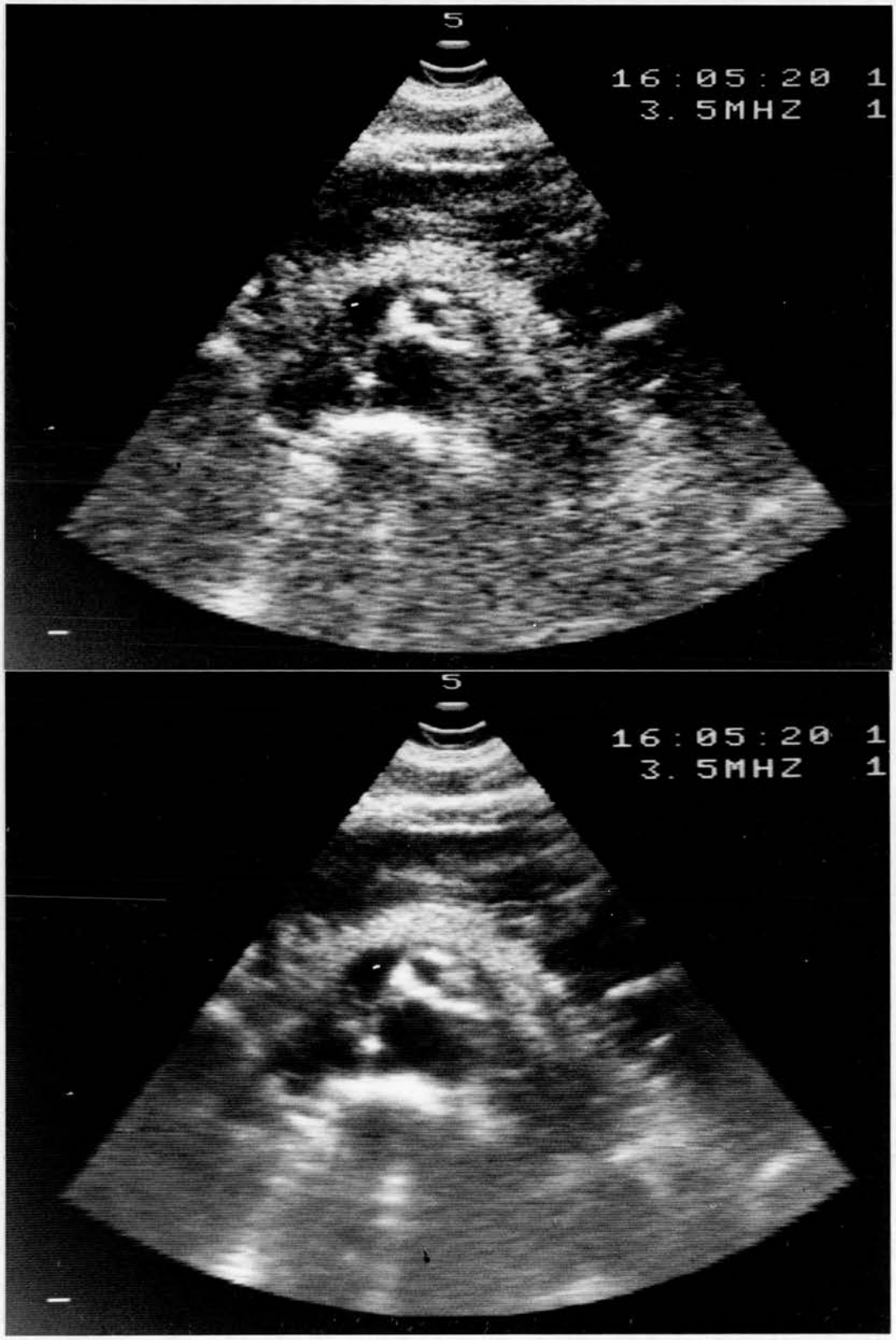

Figure 3.4 : Scan of the pancreas. **(c)** - Unprocessed II. **(d)** - Integration.

Figure 3.5 : Scan of the liver and kidney. **(a)** - Unprocessed I. **(b)** - Recursive averaging.

Figure 3.5 : Scan of the liver and kidney. **(c)** - Unprocessed II. **(d)** - Integration.

CHAPTER 4

SPATIAL FILTERING

4.1. Introduction

The common characteristic of the techniques described in Chapter 3 is that they perform temporal filtering. Each new pixel is calculated from data belonging to previous frames and, therefore, obtained at different times. On the contrary, spatial filtering utilizes the information contained in the two-dimensional space domain defined by the x, y coordinates, with x and y corresponding to the rows and columns of a digitized scan. In principle, techniques developed for temporal filtering can also be used for spatial filtering and vice versa. In fact when image processing by means of two-dimensional spatial filtering was still new, most of the applications were based on extensions of techniques developed for processing one-dimensional time signals. In a similar manner, it is not only possible from the mathematical point of view but also highly desirable to extend the algorithms of this chapter so that they operate on three-dimensional data defined by the two spatial coordinates x, y and the time coordinate t. The only reason for not having done this, is technical problems associated with the acquisition and storage of a large number of consecutive video frames.

The algorithms of this chapter estimate the true grey scale level of a pixel (x,y) from a combination of the pixel intensities in a predefined neighbourhood around (x,y). The neighbourhood is called the filter window or filter size and is usually a square area of M X M pixels, centred at point (x,y). The algorithms are classified as linear, nonlinear or adaptive according to the type of operation they perform on the data inside the window. All the algorithms have been implemented in software. The corresponding programs, written in Fortran 77, can be found in Appendix B. Filtering has been applied to abdominal images which were recorded on video tape during clinical

examination. The images were then digitized by the Crystal at 576 X 530 by 8 bits resolution and, through a parallel Direct Memory Access interface, were transferred to a DEC PDP11/23 PLUS minicomputer for storage and processing. The PDP11 has certain limitations with a very small random access memory and a slow processing speed being the most important from our point of view. These limitations inevitably created several problems in the development and application of complex and time consuming algorithms. The purchase of a DEC MicroVax II minicomputer, which offered a 20-fold increase in processing speed and unlimited (virtual) memory, greatly enhanced the possibility for experimentation although this happened only when the project was approaching its completion.

Evaluating the performance of different filters can be a very difficult task. Ideally, a quantitative measure should be used but no agreement exists among the image processing community on which measures are the most appropriate. A commonly used quantity is the Mean Square Error between the noise-free and the processed image (Chin & Yeh, 1983). This approach has been used for the evaluation of filters applied to images corrupted by computer generated noise but it is obviously not applicable in our case because the noise-free image is not available. Sometimes, quantitative measures can give contradictory and confusing results. For example, according to the information content and entropy indices an image corrupted by computer generated noise has better quality than both the processed and original image (Deekshatulu et al, 1985). An interesting remark on this subject has been made by Mastin (1985) who performed a quantitative and qualitative evaluation of several noise smoothing algorithms. He concluded that it is the human observer's perception of quality rather than a statistical measure that defines the "best" filter. A possible explanation for this is that a human observer makes his judgements by scanning an image in a highly selective

rather than a point-by-point manner. He chooses specific areas from which he extracts certain features and, in essence, weighs these areas more heavily than the rest of the image (Granrath, 1981). On the other hand, a quantitative measure which treats the image in a global manner with all the points having equal importance cannot simulate satisfactorily the human visual system.

Because of the problems associated with quantitative measures, it was decided to assess the various filters' performance using visual comparisons. An evaluation and clinical assessment of software techniques, based on a large number of scans, is presented in Chapter 6. However, due to space limitations, the comparisons in the present chapter are based only on the two original images of Figure 4.1 which were obtained using a 3.5 MHz Siemens Sonoline SX scanner.

The top image, which is a scan of normal liver, gallbladder and the hepatic vein, has been chosen for determining how well the filters preserve high-contrast edges and small details. Of particular interest here are the small portal tracts in the left part of the scan and the small branch of the hepatic vein. The bottom image of Figure 4.1, which is a scan of secondary metastasis in the liver, is used to assess the filters' ability to preserve and enhance subtle grey scale variations like the hypoechoic metastatic lesions in the liver parenchyma. In order to facilitate the process of visual comparisons the 64 X 64 areas enclosed by the squares in Figure 4.1 have been enlarged by a factor of two and are displayed as 128 X 128 images at the top right corner of the scans. Also, the 64-point vertical intensity profiles along the column indicated by the markers just above and below the squares are displayed on the top left corner of the scans. The same format has been followed throughout this chapter.

When comparing images processed by various filters it is very

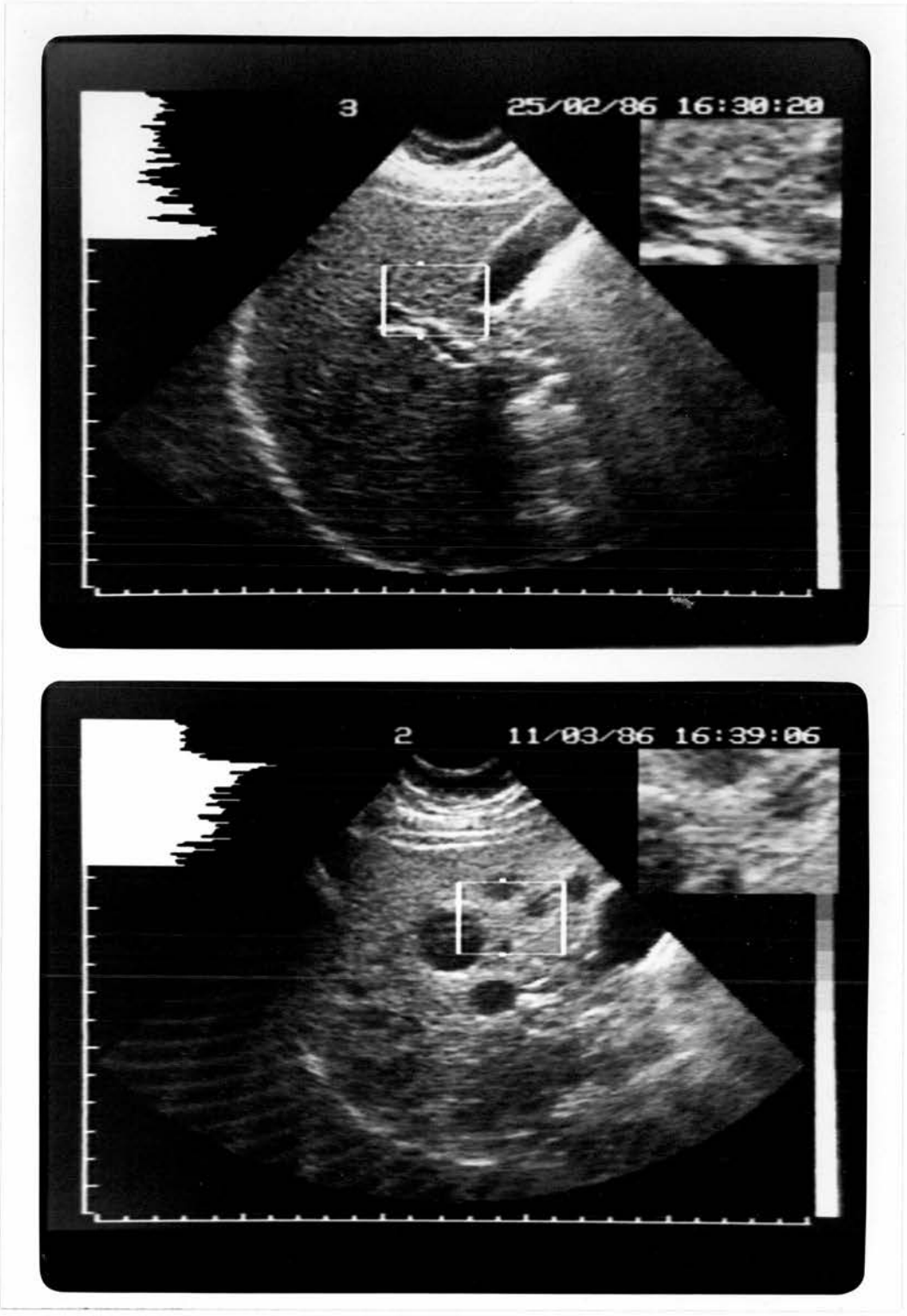

Figure 4.1 : Unprocessed abdominal scans. **(a)** - Liver, kidney and gallbladder. **(b)** - Liver metastasis. The magnified regions display the hepatic vein (top) and metastatic deposits (bottom).

important to appreciate the whole range of differences, no matter how subtle they are. In our opinion, the best way to achieve this is by taking advantage of some image processors' ability to store a number of images and display instantaneously one or another at the push of a button. This is equivalent to the comparison of one-dimensional signals where superposition of the signals is the best way to appreciate the existing differences (see for example Figures 4.5a and 4.5b in this chapter). The comments made about the performance of the various filters were formed following this method of visual comparison which is unfortunately not available to the reader. Because the reader has to rely on photographs of the scans in order to compare the filters, every care was taken to ensure that the quality of images presented in this chapter is the highest possible. For this reason, the photographs of this chapter were taken using a Scopix 300R imager manufactured by Agfa Gevaert which offers the best quality among all the imagers available to us and also minimizes loss of image detail because it produces a positive image directly from the computer display onto photographic paper.

4.2. Linear filters

A two-dimensional filter is defined as an operator $T[\bullet]$ that transforms an input sequence $\{I(x,y)\}$ to an output sequence $\{O(x,y)\}$

$$\{O(x,y)\}=T[\{I(x,y)\}] \tag{4.1}$$

If the operator $T[\bullet]$ satisfies the principle of superposition, that is, if

$$T[\{aI_1(x,y)+bI_2(x,y)\}]=aT[\{I_1(x,y)\}]+bT[\{I_2(x,y)\}] \tag{4.2}$$

the filter is said to be linear (Cappellini & Emiliani, 1986). Linear filters are based on the concept of the frequency spectrum. According to this concept, a digital signal is assumed to be composed of cosine and sine terms with varying frequencies. The minimum frequency is, of course, zero and from the

sampling theorem (Bracewell, Chapter 10, 1986) the maximum frequency is half the digitizing frequency. The relative contributions of each frequency can be determined by taking the discrete Fourier transform of the signal. An N X N digital image f(x,y) and its discrete Fourier transform F(u,v) are related through the following equations

$$F(u,v)=N^{-1}\sum_{x=0}^{N-1}\sum_{y=0}^{N-1} f(x,y)\exp[-j2\pi(ux+vy)/N] \tag{4.3}$$

and

$$f(x,y)=N^{-1}\sum_{u=0}^{N-1}\sum_{v=0}^{N-1} F(u,v)\exp[j2\pi(ux+vy)/N] \tag{4.4}$$

where the spatial and frequency coordinates x,y and u,v take values in the range [0,N-1]. Both the discrete Fourier transform F(u,v) and its inverse f(x,y) are assumed to be periodic with period N. For example

$$F(u,v)=F(u+N,v)=F(u,v+N)=F(u+N,v+N) \tag{4.5}$$

The power spectrum $|F(u,v)|^2$, defined as the product of F(u,v) with its complex conjugate $F^*(u,v)$, gives an indication of the signal's energy at each point (u,v) of the frequency plane. A point to remember is that since the origin of the space domain is at (x_0=0,y_0=0) the origin of the frequency domain is at (u_0=0,v_0=0) as well. This can be appreciated better by examining the 3D plot of Figure 4.2a which is a 64 X 64 image with all pixels equal to zero apart from those in the central 7 X 7 square which are equal to 1/49. Its power spectrum is shown in Figure 4.2b with the origin of the spatial frequency axes at point (u_0=0,v_0=0). In general it is more appropriate to shift F(u,v) so that the origin of axes is at the centre (N/2,N/2) of the frequency plane. The corresponding power spectrum is shown in Figure 4.2c. A shifted version

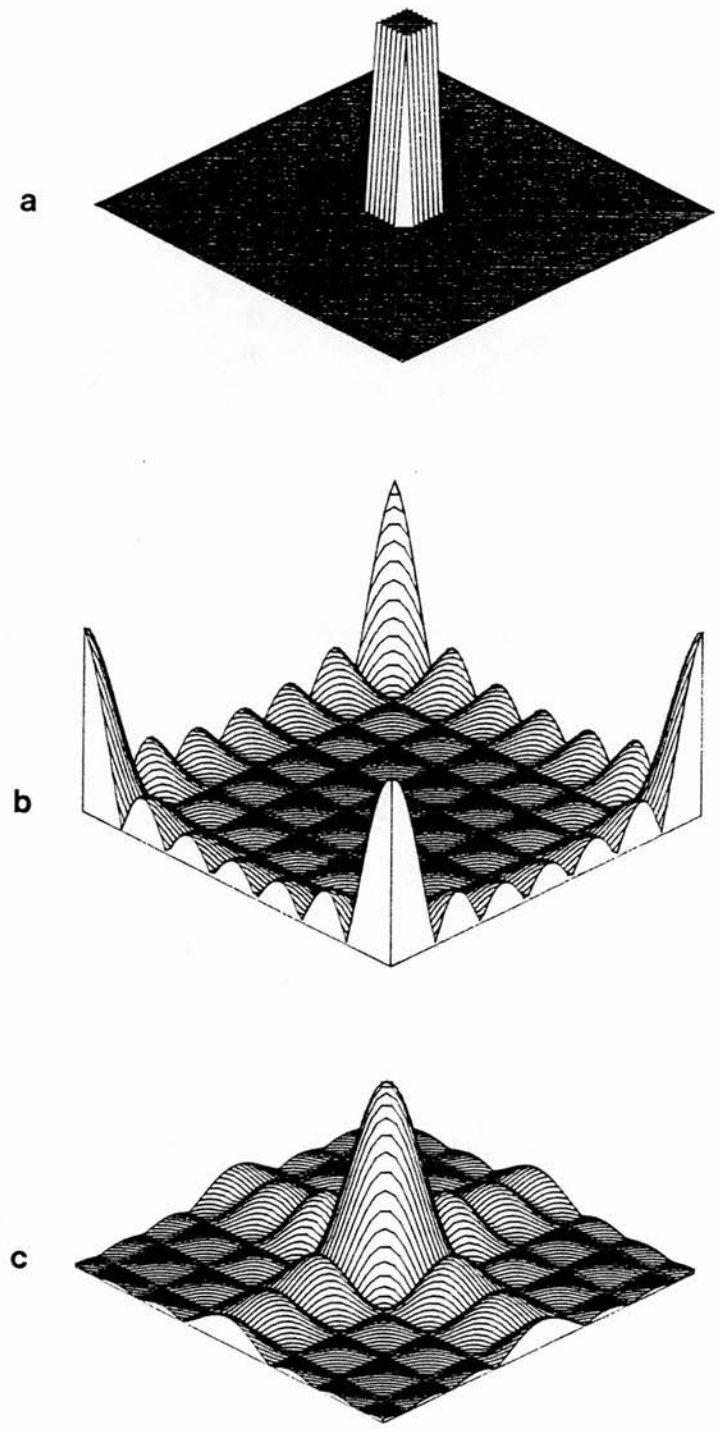

Figure 4.2 : **(a)** – Impulse response of a 7 X 7 running average filter. **(b), (c)** – Power spectrum before and after shifting the origin of the frequency plane.

F(u',v') of the Fourier transform F(u,v) (u'=u−N/2, v'=v−N/2) can be obtained using the following expression from Gonzalez & Wintz (Chapter 3, 1987).

$$F(u',v')=N^{-1}\sum_{x=0}^{N-1}\sum_{y=0}^{N-1} f(x,y)(-1)^{x+y}\exp[-j2\pi(u'x+v'y)/N] \tag{4.6}$$

Then the spatial angular frequencies $\omega_x=2\pi u'/N$, $\omega_y=2\pi v'/N$ take values between $-\pi$ and π whereas the normalized frequencies $\omega_x/2\pi$, $\omega_y/2\pi$ take values between −0.5 and 0.5. Linear filters assume that signal and noise occupy different non-overlapping parts of the frequency spectrum. Smoothing is performed by allowing frequencies corresponding to the signal to pass through the filter unaffected (passband zone) whereas parts of the spectrum occupied by noise, usually high frequencies, are suppressed (stopband zone).

Linear filtering can be performed either in the frequency or in the space domain. In the frequency domain, the Fourier transform $I_f(u,v)$ of the input image I(x,y) is connected to the Fourier transform $O_f(u,v)$ of the output image O(x,y) through the filter transfer function or frequency response H(u,v), which takes values between 1 in the passband and 0 in the stopband zone.

$$O_f(u,v)=H(u,v)I_f(u,v) \tag{4.7}$$

The equivalent operation in the space domain is based on the inverse Fourier transform of H(u,v) which is called the impulse response or convolution mask of the filter. For a 2K+1 X 2K+1 window and impulse response h(x,y) (x=−K, ..., K y=−K, ..., K), each point of the output image O(m,n) is calculated as the convolution of the pixel intensities inside the window with h(x,y).

$$O(m,n)=\sum_{x=-K}^{K}\sum_{y=-K}^{K} h(x,y)I(m-x,n-y) \tag{4.8}$$

Hence, the Fourier transform substitutes convolution in the space domain by

multiplication in the frequency domain. Although both methods are common, filtering by means of convolution was chosen here because it is easier to implement on the PDP11 and also in order to take advantage of the Crystal's ability to perform fast convolution.

The impulse response of the filter described by (4.8) has a finite extent. This type of filter is called finite impulse response (FIR) and is nonrecursive because the output depends only on a given number, equal to the window size, of input values. Another type of filter, known as infinite impulse response (IIR), utilizes feedback from previous output values, i.e. IIR filters are recursive. Although each type has its own advantages and disadvantages, FIR filters were chosen because: they offer excellent linear phase characteristics; they are always stable since no feedback paths are used; the design techniques for FIR filters are generally simpler than those for IIR filters.

Filter design involves the calculation of the convolution mask h(x,y) so that the resulting filter has a specified frequency response. The simplest FIR filter is the running average, with all the convolution coefficients equal to $1/(2K+1)^2$, where 2K+1 X 2K+1 is the window size. In this case (4.8) can be written as

$$O(m,n)=(2K+1)^{-2} \sum_{x=-K}^{K} \sum_{y=-K}^{K} I(m-x,n-y) \qquad (4.9)$$

The impulse response of a 7 X 7 running average filter is displayed as a 3D plot in Figure 4.2a and its power spectrum is plotted in Figure 4.2c. Running averages are very popular because they can be implemented without any multiplications and offer the maximum noise reduction for a given window size. However, as it can be seen from Figure 4.2c their power spectrum

exhibits ripple in the stopband zone and, consequently, a certain amount of high frequencies is allowed to pass through the filter.

If one wants a filter with well-behaved frequency response more sophisticated FIR filters must be used. In order to design filters with a specified frequency response, a number of computer programs which implement filter design algorithms were written in Fortran. The programs were executed on the University's mainframe computer which offers a comprehensive package of numerical algorithms (NAG Library) including discrete Fourier transforms. Because linear filtering has not proved very successful, only a brief description of the design algorithms will be given here. The first two algorithms are based on a prototype one-dimensional filter designed using the window method (Oppenheim & Schafer, Chapter 5, 1975; Rabiner et al, 1979). The algorithm of Kato & Matsumoto (1982) obtains the frequency response H(u,v) of a two-dimensional filter by rotating the one-dimensional response of the prototype filter and then performs the inverse Fourier transform of H(u,v) in order to obtain the impulse response h(x,y). The second algorithm, known as the McClellan transform (McClellan & Chan, 1977), extends the prototype one-dimensional filter in two dimensions using a transformation of the frequency response based on the family of Chebyshev polynomials. The above methods produce filters with approximately circular frequency response. Sometimes it is desirable to define different cutoff frequencies along the u, v axes in the frequency domain. This can be achieved by multiplying an ideal impulse response with appropriate two-dimensional window functions (Fiasconaro, 1979). Finally, the algorithm based on the polygonal approximation (Hecker & Pöppl, 1982) enables the design of filters having frequency response of arbitrary shape. In this case, instead of cutoff frequencies the stopband zone is specified by the coordinates of a series of points in the frequency plane.

A large number of filters was designed using the above algorithms with frequency responses chosen on a trial-and-error basis, although the power spectra of images containing uniform speckle were also calculated to obtain an idea of the frequency content of speckle. Figure 4.3a shows the impulse response of a low-pass filter designed using the McClellan transform with a window size of 9 X 9 and normalized cutoff frequency equal to 0.12. The corresponding power spectrum is displayed in Figure 4.3b. Application of this filter to the images of Figure 4.1 results in the processed images shown in Figure 4.4. Comparisons with the original scans show that although the low-pass filtered images are smoother, they still exhibit a considerable amount of speckle and also suffer from blurring and loss of image detail.

Similar results were obtained with other filters. The conclusion of this study is that linear filtering is not suitable for speckle suppression in ultrasonic images. In fact, this statement is not restricted only to ultrasonic images but it is generally accepted for a wide range of other types of images as well. The inadequacy of linear filters is directly related to their poor performance in edge/detail preservation. Many features of an image such as edges, which convey important information to a human observer, are displayed as sharp grey scale variations. The spectral content of these variations extends to infinity and therefore overlaps with the noise spectrum. Consequently, any attempt to suppress noise is accompanied by blurring of these information-bearing structures and loss of fine detail. Also, space-invariant linear filtering assumes that images are stationary, in the sense that their statistical properties and local content are position independent, something which is obviously not a valid assumption for ultrasonic scans. As a result a filter which is optimum for one part of an image could be completely inappropriate for another part.

The computational efficiency of linear filters depends heavily on the

CONVOLUTION MASK OF LOW – PASS FILTER

–1	–1	0	1	1	1	0	–1	–1
–1	0	3	7	8	7	3	0	–1
0	3	10	16	18	16	10	3	0
1	7	16	25	28	25	16	7	1
1	8	18	28	32	28	18	8	1
1	7	16	25	28	25	16	7	1
0	3	10	16	18	16	10	3	0
–1	0	3	7	8	7	3	0	–1
–1	–1	0	1	1	1	0	–1	–1

a

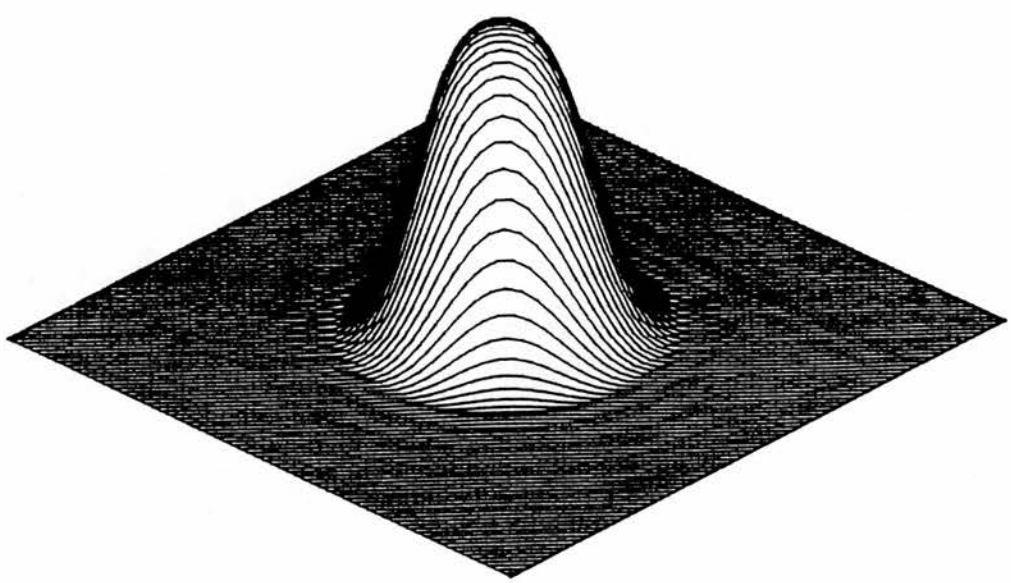

b

Figure 4.3 : Linear filtering. **(a)** - Impulse response. **(b)** - Power spectrum.

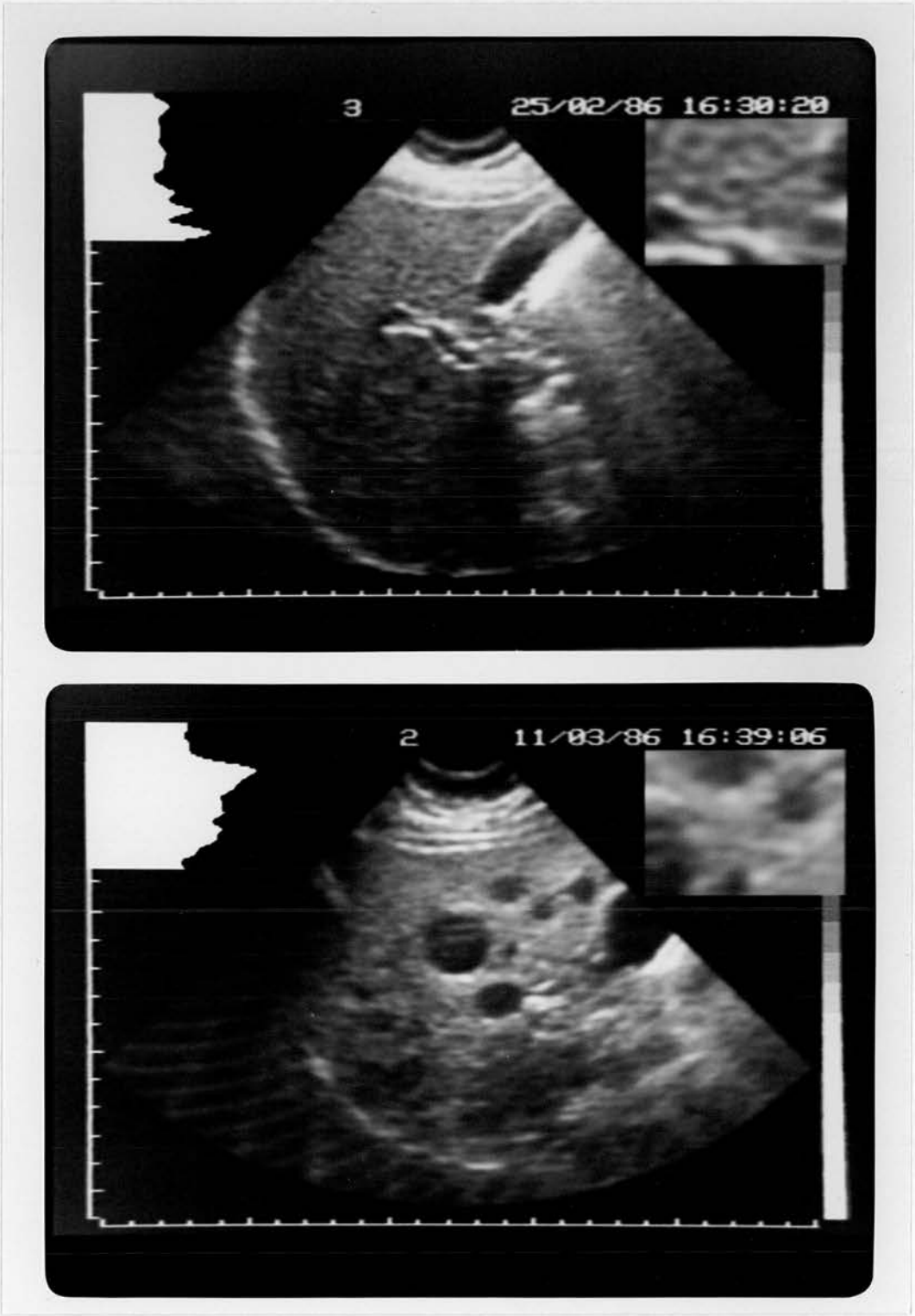

Figure 4.4 : Linear filtering applied to the original scans of Figure 4.1.

way they are implemented. For a straightforward implementation of a 9 X 9 filter with real coefficients on the MicroVax, 200 s of CPU are needed to process a scan. The very slow execution time is due to the fact that for each pixel 81 real multiplications, which tend to be time consuming, and 81 additions must be performed. On the other hand, the Crystal can perform the same operation with integer instead of real convolution coefficients in only 5 s. This speed is achieved using a fast hardware multiplier/accumulator. More recently special very large scale integration (VLSI) circuits have become available which can perform linear filtering even faster. For example, the IMS A100 84-pin device manufactured by Inmos can perform convolution of a 512 X 512 by 16 bits image with a 32-point 16-bit mask in 1/10 s (Inmos Ltd, 1986a). These new devices open up the possibility of space-varying filtering in real or near real-time. More specifically, a number of filters which offer varying degrees of smoothing, could be applied to an image in parallel. The output image could then be formed by assigning to each pixel a value from one of the filtered images according to the local image content.

4.3. Nonlinear filters

Despite the simplicity of the analysis, design and implementation of linear filters and the fact that they can suppress noise very effectively in many applications, their usefulness in image processing is limited. The main reason, discussed in the previous section, is that they cause image degradation due to blurring of important information-bearing features such as edges. In addition, the concept of frequency selective filtering on which they are based can only be applied when signal and noise are separated in the frequency domain, i.e. in the presence of signal-independent additive noise. Even then, linear filters are optimum, in the sense that they offer maximum noise reduction for a given window size, only if the noise has Gaussian distribution (Bovik et al, 1983). In recent years, considerable effort has been devoted to the development of

nonlinear smoothers which could overcome these limitations. By definition, nonlinear filters do not satisfy the superposition principle of (4.2). Since the vast majority of mathematical methods used in signal processing assume that this principle is satisfied, new tools have to be developed to analyse the properties and performance of nonlinear filters. This is not always possible but even when it is the analysis can be extremely complicated. As a result, nonlinear filter design methods based on a sound mathematical theory are not available yet. Instead, nonlinear filters are used in an *ad hoc* and heuristic manner. However, despite these drawbacks they have proved useful in numerous applications and, judging from the number of publications in the signal processing literature, their popularity is increasing rapidly.

Although a large number of nonlinear filters was investigated during the course of this project, due to space limitations, only a few representative examples will be described in detail here, with the rest mentioned briefly in the review which follows. Among the first nonlinear techniques used for suppression of signal-dependent noise was homomorphic filtering (Oppenheim et al, 1968). This approach uses a grey scale transformation which can, at least approximately, decouple the noise from the signal and has been found to yield better results than linear techniques for a variety of noise models (Arsenault & Denis, 1983). Another class of filters, probably the most important, was introduced to signal processing from the field of robust statistical estimation theory (David, 1970; Huber 1981). This class is known as order statistics or rank order filters (Heygster, 1982; Bovik et al, 1983). Other types of nonlinear filters include nonlinear or generalized means (Kundu et al, 1984; Pitas & Venetsanopoulos, 1986a) and techniques which compare the pixels inside the window with the central pixel and perform selective averaging based on the results of these comparisons (Davis & Rosenfeld, 1978; Lee, 1983a; Pomalaza-Raez & McGillem, 1984). At the present, the general trend is

to develop families which encompass many types of already known filters. One such family which includes homomorphic, order statistics, generalized means and linear filters is known as nonlinear order statistics filters (Pitas & Venetsanopoulos, 1986b). Another attempt to unify linear and nonlinear techniques has been made by Maragos & Schafer (1987a; 1987b) using the theory of mathematical morphology (Serra, 1982). Mathematical morphology originates from the field of pattern recognition but recently it has found applications in general noise smoothing (Stevenson & Arce, 1987), radar speckle suppression (Crimmins, 1985) and ultrasonic speckle suppression (Billon, 1988).

4.3.1. Median filtering

The median is the most popular member of the general nonlinear family of order statistics filters. Initially, the sample median had been used by statisticians as a more robust alternative to the sample mean for estimating the central value of a population. Its effectiveness as a noise suppression filter was first observed by Tukey (1971) who used it for smoothing time series data. Since then, the median has found numerous applications in signal and image processing, including medical imaging (Ioannidis et al, 1984; Ritenour et al, 1984). Median filtering is performed by replacing each point of the input by the median value of all the terms inside a window centred at this point, after the terms have been ordered in ascending or descending order. For example, if the window includes 2K+1 terms I_i (i=1, ..., 2K+1), the median O_{med} is equal to

$$O_{med}=\text{median}\{I_1, I_2, ..., I_{2K+1}\}=I_{(K+1)} \tag{4.10}$$

where $I_{(K+1)}$ denotes the $(K+1)_{th}$ largest term.

The smoothing action of the median is based on the concept of monotonicity. A point is regarded as noise if it represents an excursion from

the local monotonicity of the signal which is insufficiently supported by the values in its vicinity (Velleman, 1977). The deterministic properties of the median, i.e. its effect on non random signals, have been studied by Tyan (1981) and Gallagher & Wise (1981) and the following results have been obtained for the one-dimensional case. A median filter of arbitrary length preserves a monotonic sequence. If, however, the input contains segments of different monotonicity (e.g. increasing and decreasing segments), it is preserved by a median of 2K+1 points only if it consists of monotonic segments of any length connected by constant segments with a length of at least K+1 points. Therefore, a median of 2K+1 points will preserve edges and impulses (spikes) of at least K+1 points long whereas shorter impulses will be eliminated. These properties of the median are illustrated by the example of Figure 4.5. The solid curve of Figure 4.5a corresponds to an ideal step edge whereas the broken curve is obtained by adding Gaussian noise plus a positive impulse. Figure 4.5b shows the results of applying a 5-point median (solid curve) and a 5-point running average (broken curve) to the noisy signal. Comparison between the two curves demonstrates that the median offers better performance because it has preserved the sharp transition of the edge and has suppressed the impulse. On the contrary, the running average filter has changed the step edge to a ramp, something which is equivalent to edge blurring in a grey scale image, and has not managed to suppress the impulse. Another interesting property of the median is that repeated filtering results in a "root" signal which remains invariant to any subsequent filtering. For a signal of length L and a 2K+1-point median, a "root" signal will be obtained after [3(L-2)]/[2(K+1)] passes at the most (Wendt et al, 1986).

Analysing the statistical properties of median filters can be an extremely complicated task due to their nonlinear nature, as can be seen from the statistics of the weighted median presented in Appendix A. Nevertheless,

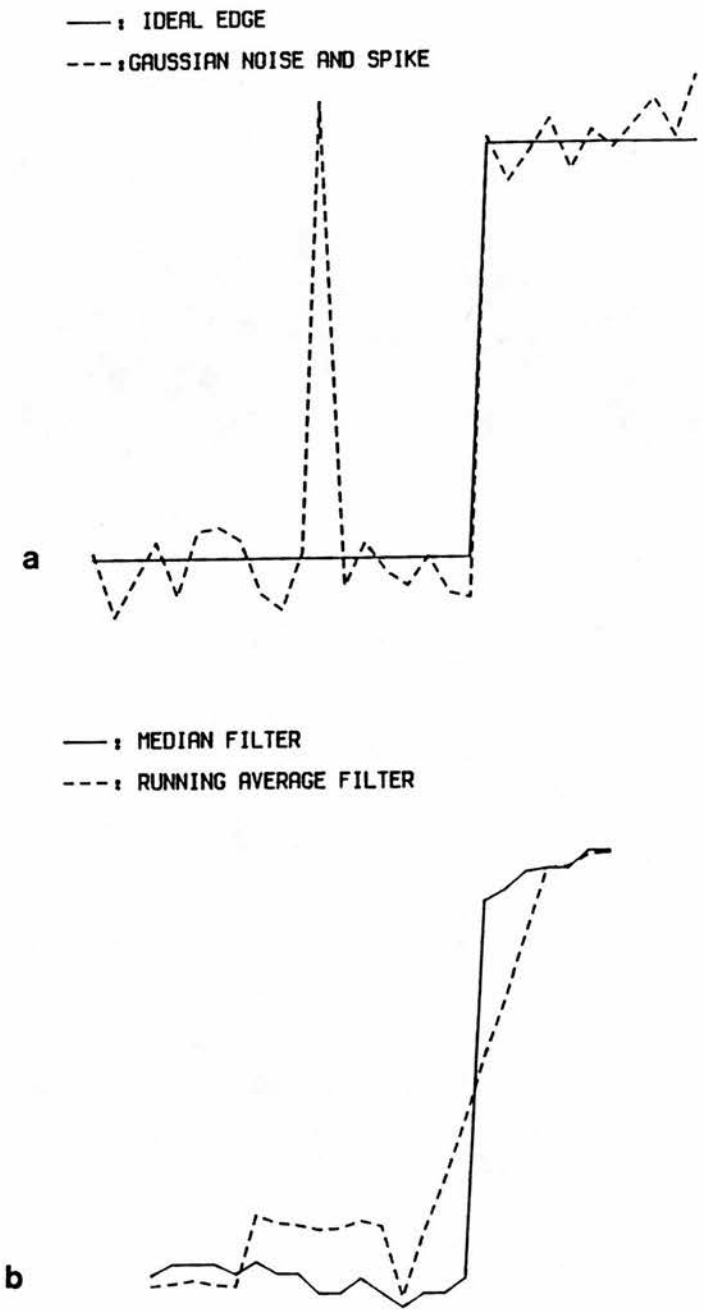

Figure 4.5 : Comparison between linear and nonlinear filtering. **(a)** - Ideal step edge corrupted by uncorrelated additive Gaussian noise plus a positive spike. **(b)** - 5-point median and running average filtering of the noisy signal.

over the last few years a considerable amount of work has been done in this area which has increased the understanding of the median operation and has helped in making its use more efficient and better suited to specific applications. Justusson (1981) has derived the probability density functions of the median for several signal plus noise cases. More general results for arbitrary input sequences have been obtained by Nodes & Gallagher (1984) and Liao et al (1985), for the one and two-dimensional case respectively. The statistics of the median have been used to predict its performance in noise suppression and signal preservation. The median is very efficient in suppressing impulsive and Laplacian noise as well as any other type of noise having a long-tailed distribution, but offers less noise suppression than the running average for short-tailed noise distributions, like the Gaussian (Justusson, 1981; Bovik et al, 1983). Also, the median introduces less distortion to edges corrupted by noise than linear filters, irrespective of the noise distribution (Justusson, 1981; Pomalaza-Raez & McGillem, 1984).

Instead of the multiplications and addition used in linear filtering, the calculation of the median is based on comparisons. For a N-point window, the straightforward calculation involves ordering the terms inside the window until the $[(N+1)/2]_{th}$ largest (or smallest) term has been found, an operation which needs $3(N^2-1)/8$ comparisons. This corresponds to 2460 comparisons per pixel for a 9 X 9 window. Alternative methods for calculating the median, which offer considerable increase in speed over the straightforward ordering method, have been proposed in the literature (Ataman et al, 1980; Rao & Rao, 1986). Huang's histogram update algorithm (Huang et al, 1979) which is the most suitable for software implementation has been used here. An even faster algorithm has been reported recently (Ahmad & Sundararajan, 1987), which has the additional advantage of being independent of the image content and the number of grey scale levels, but it offers only marginal speed improvement for

the type of images considered in this project.

The results of applying a 7 X 7 median filter to the scans of Figure 4.1 are shown in Figure 4.6. From the processed scans it can be seen that speckle has been suppressed substantially, more than by the linear filter in Figure 4.4, and some areas like the metastatic deposits shown in detail in the magnified region of the bottom scan have better defined boundaries. However, the processed scans suffer from loss of genuine image detail, like the small branch of the hepatic vein shown in the magnified region of the top scan. Also, some edges have been blurred and in general the quality of the processed image is not regarded as satisfactory.

As far as computational efficiency is concerned, the median is the best among the filters considered in this chapter with only 30 s of CPU time needed to process a scan on the MicroVax. Furthermore, due to the interest in median filtering applications, integrated circuits which can perform median filtering in real-time are becoming increasingly common. The first report on this subject was published in 1983 (Oflazer, 1983) and described a VLSI chip capable of performing one-dimensional 5-point median filtering at data rates of up to 10 MHz. More recently, a VLSI device manufactured by LSI Logic became commercially available which can perform 8 X 8 median filtering on input data digitized at 20 MHz (Bursky, 1987). However, despite the fact that it is now possible to perform median filtering in real-time this is not judged to be the solution to the problem of ultrasonic speckle. The median's property of eliminating spikes is not of particular relevance to ultrasonic images which are corrupted by Gaussian-like rather than impulsive noise. In addition signal preservation deteriorates rapidly as the window size increases in order to provide adequate noise reduction, resulting in loss of image detail. Experimentation with a large number of scans has suggested that the most useful property of the median for our application is the ability to preserve

Figure 4.6 : Median filtering applied to the original scans of Figure 4.1.

boundaries between areas of slightly different echogenicity. It would be, therefore, desirable to have a filter which incorporates this feature but overcomes some of the limitations of the median. This is the subject of the following subsection.

4.3.2. Double Window Modified Trimmed Mean Filtering

In recent years, there have been several efforts to develop general classes of filters which possess some desirable features of the median but also improve some aspects of its performance.

In an attempt to combine the properties of linear and nonlinear filters, Nieminen et al (1987) have suggested a class of FIR-median hybrid filters which use linear FIR substructures in conjunction with median operations.

Bovik et al (1983) have introduced a generalization of the median, called order statistics (OS) filters, which uses a linear combination of the ordered values inside the window. For the one-dimensional case, the output O_{OS} of the filter is given by

$$O_{OS}=\sum_{i=1}^{2K+1} w_i I_{(i)} \qquad (4.11)$$

where, $I_{(i)}$ is the i_{th} largest value among the 2K+1 terms I_1, ..., I_{2K+1} and w_i is the corresponding weight coefficient. By selecting the appropriate weights w_i, filters which are optimum for specific noise distributions can be obtained. For example, the optimum filters for Gaussian, impulsive and uniform noise are the running average ($w_i=1/(2K+1)$, i=1, ..., 2K+1), the median ($w_i=0$ for $i\neq K+1$ and $w_{K+1}=1$) and the min/max filter ($w_1=w_{2K+1}=0.5$ with the rest of the weights equal to zero), respectively.

A slightly different class known as a-trimmed means (a-TM) (Bednar & Watt, 1984) is obtained if a number T of samples is deleted from each end

of the ordered data set and the remaining 2(K−T)+1 terms are averaged with weights equal to 1/[2(K−T)+1] so that

$$O_{a-TM}=\sum_{i=T+1}^{2K+1-T} I_{(i)}/[2(K-T)+1] \qquad (4.12)$$

T is defined in terms of a parameter a ($0\leq a\leq 0.5$) by $T=\lfloor a(2K+1)\rfloor$ where $\lfloor x\rfloor$ denotes the largest integer which does not exceed x . Although the a−TM filters possess the characteristics of both the running average (a=0) and the median (a=0.5), the idea of averaging a fixed number of terms (the median value and K−T terms on each side of the median in the ordered set) is not ideal because it does not take into account the local image content.

Better performance can be achieved by using the modified trimmed mean (MTM) filter (Lee & Kassam, 1985) which calculates the median O_{med} and then averages only samples which fall within the range $[O_{med}-q, O_{med}+q]$, where q is a threshold determined by the standard deviation of the noise and the minimum edge height to be preserved. A contradiction associated with the MTM filter is that the window size should be small, so that the median preserves small details, but at the same time large, in order to provide adequate noise reduction. One way to overcome this contradiction is to use a small window of 2K+1 points to calculate the median O_{med} and a larger window of 2L+1 points for the averaging operation. The resulting filter is known as the double window modified trimmed mean (DW−MTM) filter (Lee & Kassam, 1985). Its output O_{DW} is equal to

$$O_{DW}=\sum_{i=1}^{2K+1} w_i I_i / \sum_{i=1}^{2L+1} w_i \qquad (4.13)$$

where

$$w_i=1 \quad \text{for } |I_i-O_{med}| \leq q$$
$$w_i=0 \quad \text{for } |I_i-O_{med}| > q \tag{4.14}$$

The DW-MTM filter utilizes a two-step procedure to calculate the output. The median of the terms inside the small window provides a first estimate of the true signal value. Then a better, less noisy, estimate is obtained by averaging only the terms inside the larger window whose absolute difference from the median is smaller or equal to q.

The threshold q is determined by the standard deviation of the noise. From Section 2.2, the standard deviation of speckle is proportional to the square root of the local mean. This property can be incorporated into the DW-MTM filter if we approximate the local mean m by the local median O_{med} and choose q as

$$q=c\{O_{med}\}^{1/2} \tag{4.15}$$

A similar form of q has been proposed recently by Ding & Venetsanopoulos (1987) for DW-MTM filtering of signal-dependent noise. Figure 4.7 shows the results of applying this filter with a 3 X 3 median window, a 7 X 7 averaging window and c=2 to the original images of Figure 4.1. Comparisons between the two figures shows that the DW-MTM has satisfactory performance. Speckle has been reduced substantially and the overall appearance of the scans is much cleaner. However, some drawbacks have been observed which are due to the following reasons. First, even the use of a small 3 X 3 window for calculating the median can cause loss of image detail. Then, although the DW-MTM filter can preserve high contrast edges, the averaging operation performed during the second phase of filtering can introduce a degree of blurring to weak edges such as the branch of the hepatic vein displayed at the top right corner of Figure 4.7.

Figure 4.7 : DW-MTM filtering applied to the original scans of Figure 4.1.

As far as computational efficiency is concerned, the DW-MTM filter is reasonably efficient with 100 s of CPU time needed to process a scan. The relatively long execution time is due to the large number of comparisons involved, which tend to be time consuming when they are performed in software but can be implemented relatively easily in hardware. The DW-MTM filter has the best performance among the filters considered so far in this chapter. The combination of median and linear characteristics, the use of the speckle local statistics and the efficiency of performing comparisons in hardware make this filter an attractive possibility for speckle suppression despite its drawbacks associated with signal preservation.

4.4. Adaptive filters

A successful noise reduction algorithm applied to ultrasonic images must satisfy several diverse and conflicting requirements. It must offer maximum noise reduction in uniform speckle areas, it must retain both high and low-contrast specular reflections and, perhaps most importantly, it must preserve and possibly enhance boundaries between areas of slightly different echogenicity. The linear and nonlinear filters mentioned above cannot satisfy all the requirements simultaneously because they are space-invariant, i.e. they perform the same type of operation to all parts of an image. Linear filters assume that the statistical properties of an image are location-invariant (e.g. the image is assumed to be stationary) which can be described by a global measure such as the frequency spectrum. However, the vast majority of images and certainly ultrasonic scans are inherently nonstationary. Nonlinear filters do not make any explicit assumptions about the stationarity of an image and have the additional advantage of edge preservation. Even so, they fail to satisfy the requirements mentioned above because signal preservation deteriorates rapidly as the window size increases to provide adequate noise reduction.

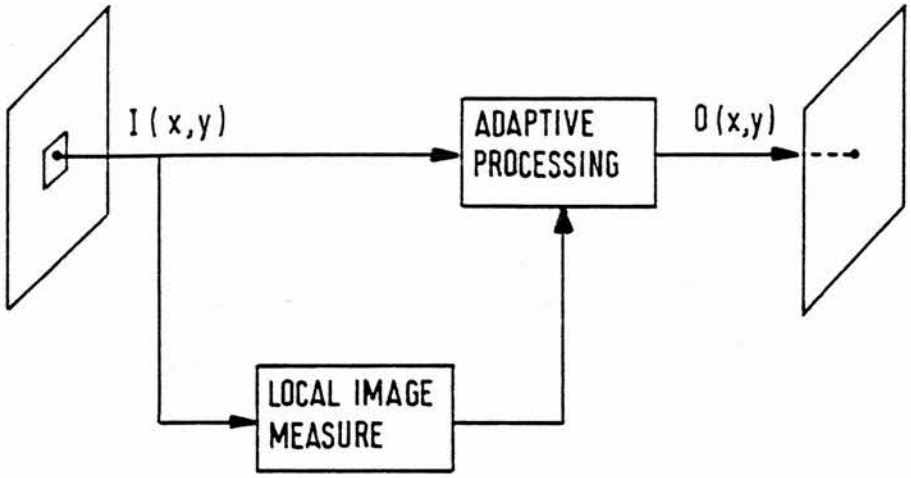

Figure 4.8 : General block diagram for adaptive processing. I(x,y), O(x,y) are the input and output grey levels at point (x,y).

An alternative approach which overcomes the limitations of space-invariant techniques is to use a space-varying or adaptive filter which adjusts the smoothing performed at each pixel according to the local image content (Figure 4.8). The local image content at each point can be described by a combination of image measures or features, calculated in a predefined neighbourhood of this point. These measures include first-order statistics (mean, variance), second-order statistics (autocorrelation, power spectrum), edge gradient information or other measures of local uniformity. Adaptive techniques acknowledge that an image is nonstationary on a global basis and assume instead that it consists of a large number of locally stationary areas. Provided that the local uniformity measures are appropriately chosen, the adaptive filter can determine if a point belongs to a locally stationary area and provide maximum noise reduction or if it is near a boundary between two or more locally stationary areas. In this case, the amount of smoothing can be minimized depending on how close the point is to the boundary or, alternatively, smoothing can be performed only along the direction of the boundary in order to improve its definition. Apart from the local image measures, the other important element of an adaptive filter is the type of

estimator used to produce a smoothed pixel from the noisy observations in its neighbourhood. The estimator can be determined in a heuristic manner or it can be designed so that it satisfies a criterion of optimality such as the minimum mean square error. Although the quality of the processed image depends heavily on the choice of a good estimator, measures which can provide an accurate description of the local image content are even more important because these are the ones that control the action of the estimator.

Adaptive techniques pay the price of computational complexity because the calculation of local image measures has to be repeated for each pixel of the image. However, this drawback is compensated by their ability to provide noise reduction while preserving the important features of an image. An evaluation of several noise smoothing algorithms (Mastin, 1985) has confirmed the importance a human observer gives to image sharpness and detail preservation and has demonstrated the superiority of adaptive techniques over their space invariant counterparts. A comprehensive review of adaptive techniques for image processing, including but not restricted to noise reduction, has been given by Tom (1985). In the rest of this section, some representative adaptive noise smoothing filters, both well-known and new, will be described.

4.4.1. Lee's modified algorithm

The first adaptive filter considered here is based on an algorithm suggested by Lee (1980) for suppression of additive, multiplicative or a combination of both types of noise. The same filter has been used for speckle suppression in synthetic aperture radar imaging (Lee, 1981; 1986). The filter operates by forming an output image where the grey scale level O(x,y) of a point (x,y) is the linear combination of the input grey scale level I(x,y) and the local mean $m_I(x,y)$ of the terms inside the filter window.

$$O(x,y)=m_I(x,y)+c[I(x,y)-m_I(x,y)]=cI(x,y)+(1-c)m_I(x,y) \quad (4.16)$$

The parameter c determines the amount of smoothing performed at each point (x,y). c=0 corresponds to maximum smoothing ($O(x,y)=m_I(x,y)$) whereas c=1 has no effect on the input ($O(x,y)=I(x,y)$). (4.16) is encountered in many signal processing applications which are not necessarily restricted to noise reduction. It is generally agreed that this equation was first introduced to image processing by Wallis (1976) who used it for space-varying contrast enhancement. Of particular relevance to this work is Dickinson's (1982) space-varying implementation of (4.16) for ultrasonic speckle suppression with c chosen to be proportional to the local mean of the input $m_I(x,y)$. The implications of this choice are that the amount of smoothing performed in regions of high grey scale level is reduced. Although, in this manner, blurring of bright edges is avoided, this is achieved at the expense of oversmoothing areas of low grey scale levels. Also, since the local mean cannot detect boundaries between areas of different echogenicity these are inevitably blurred by the filter.

Dickinson's filter is an example of how (4.16) can become adaptive if the value of c at each point is determined by the local image content. Lee's approach was to choose c so that the mean square error $E\{[O(x,y)-J(x,y)]^2\}$ between the output image O(x,y) and the noise-free image J(x,y) is minimum, where E{J} denotes the expected value (ensemble mean) of J. Obviously c is different for different image degradation models. For additive noise, i.e. $I(x,y)=J(x,y)+N(x,y)$ where N(x,y) is a zero mean, uncorrelated noise term which is statistically independent of J(x,y), the expression for c derived by Lee is exact. However, this is not true for multiplicative noise because he approximates the image degradation model by a Taylor series expansion of zero and first-order terms (Lee, 1980). A more accurate treatment of this

subject which can be applied to any type of signal-dependent noise has been given by Kuan et al (1985). The proof of the general form of c will be presented below in order to clarify some points which do not appear in the original derivation and, also, to state explicitly the assumptions made.

Consider the general image degradation model

$$\mathbf{i}=H\mathbf{j}+\mathbf{n} \tag{4.17}$$

j is the uncorrupted image, **n** is a zero mean, uncorrelated noise which in general can be signal-dependent, **i** is the noisy image which is available to us and H is a blurring matrix. The small-case variables in bold represent image arrays of M X M pixels which have been expressed as M^2 X 1 vectors. For example $\mathbf{i}^T$, which is the transpose of the vector **i**, is formed from the image I(x,y) in the following manner

$$\mathbf{i}^T=\{I(1,1),\ I(1,2),\ ...,\ I(1,M),\ I(2,1),\ ...,\ I(M,M)\} \tag{4.18}$$

We want to obtain an output vector **o** which is an estimate of **j** based on **i**. If we impose a linear constraint in the form **o** can take, the minimum mean square error solution is given by Sage & Melsa (pp 234-235, 1971) as

$$\mathbf{o}=E\{\mathbf{j}\}+C_{ji}C_i^{-1}(\mathbf{i}-E\{\mathbf{i}\}) \tag{4.19}$$

where C_{ji} is the cross-covariance matrix of **j**, **i** and C_i^{-1}, $E\{\mathbf{i}\}$ are the inverse of the autocovariance matrix and the expected value of **i** respectively.

The first assumption to be made is that the conditional expected value $E\{\mathbf{n}/\mathbf{j}\}$ is equal to zero. Then

$$E\{\mathbf{i}/\mathbf{j}\}=E\{H\mathbf{j}+\mathbf{n}/\mathbf{j}\}=HE\{\mathbf{j}/\mathbf{j}\}+E\{\mathbf{n}/\mathbf{j}\}=H\mathbf{j} \tag{4.20}$$

In other words, the noise **n** does not introduce bias to the signal.

Before we continue, the following theorem from probability theory is stated (Papoulis, pp. 208-209, 1981).

$$E\{g(x,y)\}=E_x\{E_y\{g(x,y)/x\}\} \tag{4.21}$$

where the subscripts x, y signify that the expected values E_x , E_y are calculated over x and y respectively. Then, if **j** corresponds to x and **i** to y

$$E\{[\mathbf{j}-E\{\mathbf{j}\}]\mathbf{n}^T\}=E_j\{E_n\{[\mathbf{j}-E\{\mathbf{j}\}]\mathbf{n}^T/\mathbf{j}\}\}=E_j\{[\mathbf{j}-E\{\mathbf{j}\}]E_n\{\mathbf{n}^T/\mathbf{j}\}\}=[0] \tag{4.22}$$

(4.22) will be used for the calculation of the covariance matrices C_{ji} and C_i in terms of C_j. By definition, C_{ji} is equal to

$$\begin{aligned} C_{ji}&=E\{[\mathbf{j}-E\{\mathbf{j}\}][\mathbf{i}-E\{\mathbf{i}\}]^T\}=E\{[\mathbf{j}-E\{\mathbf{j}\}][H(\mathbf{j}-E\{\mathbf{j}\})+\mathbf{n}]^T\} \\ &=C_jH^T+E\{[\mathbf{j}-E\{\mathbf{j}\}]\mathbf{n}^T\}=C_jH^T \end{aligned} \tag{4.23}$$

Similarly

$$\begin{aligned} C_i&=E\{[\mathbf{i}-E\{\mathbf{i}\}][\mathbf{i}-E\{\mathbf{i}\}]^T\}=E\{[H(\mathbf{j}-E\{\mathbf{j}\})+\mathbf{n}][H(\mathbf{j}-E\{\mathbf{j}\})+\mathbf{n}]^T\} \\ &=HC_jH^T+C_n+HE\{[\mathbf{j}-E\{\mathbf{j}\}]\mathbf{n}^T\}+E\{\mathbf{n}[\mathbf{j}-E\{\mathbf{j}\}]^T\}H^T \\ &=HC_jH^T+C_n \end{aligned} \tag{4.24}$$

(4.23) and (4.24) can be simplified if we assume that no blurring has occurred, that is, H=I where I is the unit diagonal matrix. Also, since the noise term **n** in (4.17) is assumed to be uncorrelated, its autocovariance will be a diagonal matrix $C_n=\sigma_n^2(x,y)I$ where $\sigma_n^2(x,y)$ is the nonstationary and signal-dependent noise variance. Now, a more controversial assumption is made about the noise-free vector **j**. **j** can be decomposed into a nonstationary mean component $E\{\mathbf{j}\}$ and a residual $\mathbf{j}_0=\mathbf{j}-E\{\mathbf{j}\}$ which is also nonstationary. We assume that the residual component $\mathbf{j}_0$ is uncorrelated. Then

the covariance $C_j=E\{[\mathbf{j}-E\{\mathbf{j}\}][\mathbf{j}-E\{\mathbf{j}\}]^T\}$ is equal to $\sigma_j^2(x,y)I$ where $\sigma_j^2(x,y)$ is the nonstationary variance of $\mathbf{j}$ at point (x,y). Since C_j is diagonal, from (4.23) it can be seen that C_{ji} is diagonal too and equal to C_j. Then, from (4.24) C_i is also diagonal and equal to $C_i=[\sigma_j^2(x,y)+\sigma^2{}_n(x,y)]I$. If we substitute these expressions into (4.19) and use scalar instead of vector notation we obtain

$$O(x,y)=m_J(x,y)+[\sigma_J^2(x,y)/(\sigma_J^2(x,y)+\sigma_N^2(x,y))][I(x,y)-m_I(x,y)] \tag{4.25}$$

where the ensemble statistics $E\{\mathbf{j}\}$, $E\{\mathbf{i}\}$, σ_j^2, σ_n^2 have been replaced by the local statistics $m_J(x,y)$, $m_I(x,y)$, σ_J^2, σ_N^2. The description of the filter is now complete provided that σ_J^2 and σ_N^2 can be expressed in terms of the local variance σ_I^2 of the observed noisy image I(x,y).

In order to apply this filter for ultrasonic speckle suppression, we rewrite the noise model of (2.13) using the notation of this section

$$I(x,y)=J(x,y)+N(x,y)=J(x,y)+[J(x,y)]^{1/2}U \tag{4.26}$$

where U is a zero mean, uncorrelated noise which is statistically independent of J(x,y), i.e. $E\{J(x,y)U\}=E\{J(x,y)\}E\{U\}=0$. U is assumed to be stationary, in other words its statistical properties are independent of the coordinates (x,y). The first-order statistics of N(x,y) are equal to

$$E\{N(x,y)\}=E\{[J(x,y)]^{1/2}U\}=E\{[J(x,y)]^{1/2}\}E\{U\}=0 \tag{4.27}$$

and

$$\begin{aligned}\sigma_N^2(x,y)&=E\{N^2(x,y)\}-E^2\{N(x,y)\}=E\{J(x,y)U^2\}\\&=E\{J(x,y)\}E\{U^2\}=m_J(x,y)\sigma_U^2\end{aligned} \tag{4.28}$$

where again we have assumed that ensemble and local statistics are equivalent. In a similar way we obtain

$$m_I(x,y)=m_J(x,y) \tag{4.29}$$

and

$$\sigma_I^2(x,y)=\sigma_J^2(x,y)+m_J(x,y)\sigma_U^2 \tag{4.30}$$

By using (4.27) - (4.30), equation (4.25) takes the form of (4.16) with c equal to

$$c=[\sigma_I^2(x,y)-m_I(x,y)\sigma_U^2]/\sigma_I^2(x,y)=1-m_I(x,y)\sigma_U^2/\sigma_I^2(x,y) \tag{4.31}$$

The practical implications of (4.31) can be appreciated by examining two extreme cases. For areas of uniform speckle with constant scattering strength, i.e. the variance of the noise-free image $\sigma_J^2(x,y)$ is equal to 0, from (4.30) $\sigma_I^2(x,y)=m_J(x,y)\sigma_U^2=m_I(x,y)\sigma_U^2$. Consequently, c=0 and maximum smoothing is performed. If on the other hand the point (x,y) is close to an edge, $\sigma_J^2(x,y)$ will have a large value and, as a result, $\sigma_I^2(x,y)$ will be considerably larger than $m_I(x,y)\sigma_U^2$. Then from (4.31) is easy to see that $c\simeq 1$ which results in minimum smoothing. In other words, near edges the best estimate O(x,y) of the noise-free value J(x,y) is the noisy signal I(x,y). The filter's operation can be described in terms of linear filtering as convolution of the input image I(x,y) with a impulse response h(x,y) which varies from point to point. For a 2K+1 X 2K+1 window, the central element h(K+1,K+1) of the convolution mask is equal to $c+(1-c)/(2K+1)^2$ whereas all the other elements are equal to $(1-c)/(2K+1)^2$.

In order to apply the filter described by (4.31), a value for σ_U^2 must be specified. From the graph of Figure 2.6 $\sigma_U^2=\sigma_I^2/m_I$ is approximately equal to 1.5. However, using a 9 X 9 window it was observed that this value caused loss of image detail. The best results were obtained with $\sigma_U^2=0.9$ and this is the value used for processing the images shown in Figure 4.9. This figure demonstrates

the ability of adaptive filters to suppress noise without affecting the true tissue information. The processed images represent a definite improvement over the original images of Figure 4.1. Speckle has been reduced considerably while the edges have been preserved and the visibility of small structures like the portal tracts in the left part of the top scan has been increased. The only criticism which can be made is about the filter's ability to preserve boundaries between areas of slightly different echogenicity. Points (x,y) along these boundaries have values of $\sigma_I^2(x,y)/m_I(x,y)$ which are not significantly higher than the ones expected from uniform areas of speckle. In this case, the linear averaging operation performed by the filter results in blurring of the boundaries, as it can be seen from the enlarged area of the bottom scan.

Despite the fact that the filter is adaptive , it is computationally very efficient with only 60 s of CPU time needed to process a scan on the MicroVax. This happens because the only time consuming task the filter faces is the calculation of the first-order local statistics. In our implementation (Appendix B), this task is performed in an efficient recursive way by taking advantage of the fact that when the filter window is moved one pixel to the right most of the terms are the same as before. In conclusion, Lee's algorithm combines efficiency in software due to its simplicity and good performance due to its adaptive nature. The only scope for improvement is the filter's ability to preserve subtle grey scale variations.

The basic idea of this filter has been used in many applications with minor or major modifications. Bamber & Daft (1986) used this filter, with c having a form similar to that of (4.31) apart from a scaling factor, for ultrasonic speckle suppression. Chan & Lim (1985) have attempted to overcome the problem of no smoothing near edges by using a cascade of one-dimensional filters operating along the 0°, 45°, 90° and 135° directions so that noise near an edge can be suppressed by the filter whose direction is

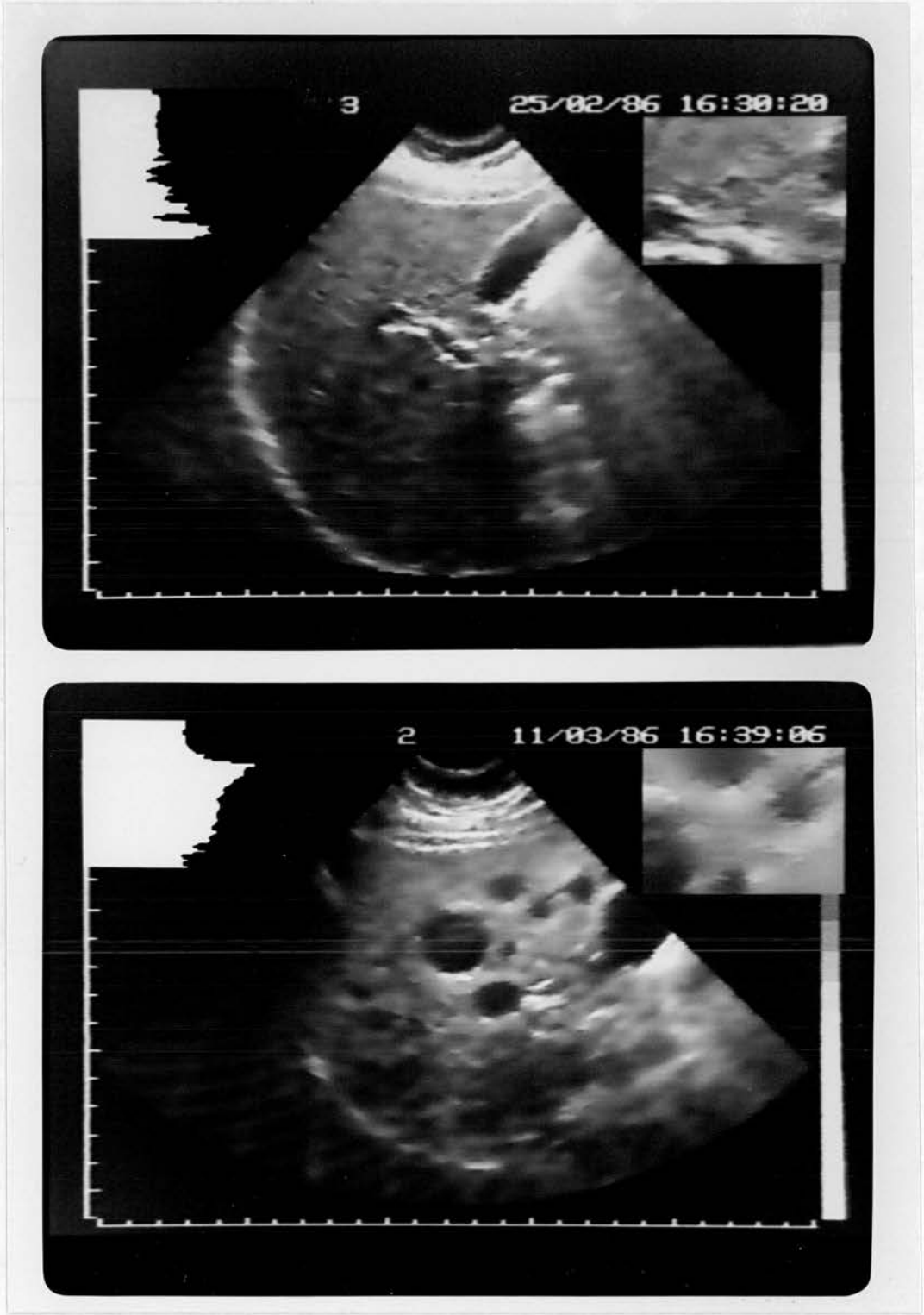

Figure 4.9 : Lee's modified filter applied to the original scans of Figure 4.1.

parallel to the edge axis. This approach seems interesting but its application to ultrasonic images did not prove particularly successful. The main reason is that, due to the strong correlation of grey scale levels between neighbours, a cascade of one-dimensional filters having a moderate window size cannot suppress speckle fully and results, instead, in an image with blotchy appearance. On the same subject of correlation, it has been already stated that the form of c given by (4.31) assumes that the autocovariance C_i of the noisy image I(x,y) is diagonal which means that the residual image, after the local mean has been subtracted, is nonstationary but uncorrelated. This is obviously not true for ultrasonic images and it is expected that if the speckle correlation could be taken into account better performance could be achieved. Kuan et al (1987) have done this for speckle suppression in simulated images using the general filtering equation (4.19). However a straightforward implementation of this equation involves the inversion of a $(512)^2 \times (512)^2$ matrix which represents a tremendous computational load. The same group have attempted to overcome this problem by dividing the image in smaller overlapping sections and processing each section separately but without very promising results. In this work, it has not been attempted to extend Lee's algorithm so that it includes information about the second-order statistics of the image because this represents a computationally demanding task which could not be carried out on the PDP11 in a reasonable time, of say, a few hours. However, it is recognized that the performance of the filter could be greatly enhanced by using combinations of first and second-order local statistics, something already done by Bamber & Cook-Martin (1987), in order to describe the local image content more accurately, even if the combinations of different local measures are not chosen according to a mathematical criterion of optimality but are determined in a heuristic manner instead.

4.4.2. Frost's modified algorithm

The filter presented here is a modified version of an adaptive algorithm suggested by Frost et al (1981) for speckle suppression in synthetic aperture radar imaging. A more complete description of the original algorithm can be found in a paper by the same authors which was published later (Frost et al, 1982) whereas the basis of its mathematical derivation has appeared in the proceedings of a conference on remote sensing (Frost et al, 1980). The starting point of this approach is that radar speckle can be regarded as multiplicative noise. This is a reasonable assumption. Lee (1981) has demonstrated the multiplicative nature of radar speckle by showing that its local mean is proportional to its local standard deviation, something which is also true for ultrasonic speckle after envelope detection (see Section 2.2). Under the multiplicative noise assumption, the minimum mean square error estimate of the true image in the frequency domain is derived. The estimate is similar to inverse/Wiener filter formulations. By assuming that the autocorrelation of the input image obeys an exponential decay model and noise is an uncorrelated random process, the filter's impulse response in the space domain is obtained. The filter is implemented by convolving the input image with the impulse response h(x,y), which for a 2K+1 X 2K+1 window is equal to

$$h(x,y)=(K_1\sigma_I^2/m_I^2)\exp(-K_2 d\sigma_I^2/m_I^2) \tag{4.32}$$

K_1 is a normalizing constant chosen so that the sum of the convolution coefficients is equal to 1, m_I and σ_I^2 are the local mean and variance of the terms inside the window, K_2 is a parameter which controls the amount of smoothing performed by the filter and d is the distance of the point (x,y) from the centre of the window (K+1,K+1)

$$d=[(K+1-x)^2+(K+1-y)^2]^{1/2} \tag{4.33}$$

In order to use this filter for ultrasonic speckle suppression, the term σ_I^2/m_I^2 has been replaced by σ_I^2/m_I in (4.32) because ultrasonic speckle on displays can be regarded as square root rather than multiplicative noise, having mean proportional to the variance instead of the standard deviation. The new impulse response is given by

$$h(x,y)=(K_1\sigma_I^2/m_I)\exp(-K_2\sigma_I^2/m_I) \qquad (4.34)$$

The filter described by (4.34) is adaptive because it includes the local statistics term σ_I^2/m_I which is calculated at each point of the image. For uniform areas of speckle, the local statistics term has a low value and the convolution coefficients of the filter decrease relatively slowly as we move away from the centre of the window (K+1,K+1), resulting in maximum noise reduction. However if part of an edge or other resolvable structure is included in the filter window, σ_I^2/m_I has a value higher than that expected for uniform speckle. Since this causes the convolution coefficients to fall sharply as we move away from the centre of the window, more emphasis is placed on the central terms and, therefore, signal preservation improves at the expense of noise suppression. The filter is similar to Lee's algorithm in the sense that they both convolve the input image with a space-varying mask and utilize the same local statistics quantity to describe the local image content. Their main difference is in their region of support, i.e. the neighbourhood around an input pixel which is used to calculate the output. In Lee' algorithm the region of support is always fixed and equal to the window size. On the contrary, from (4.34) it can be seen that as σ_I^2/m_I becomes larger an increasing number of convolution coefficients near the periphery of the window obtain very small values so that the actual window size is reduced near edges and only pixels close to the centre of the window contribute to the output.

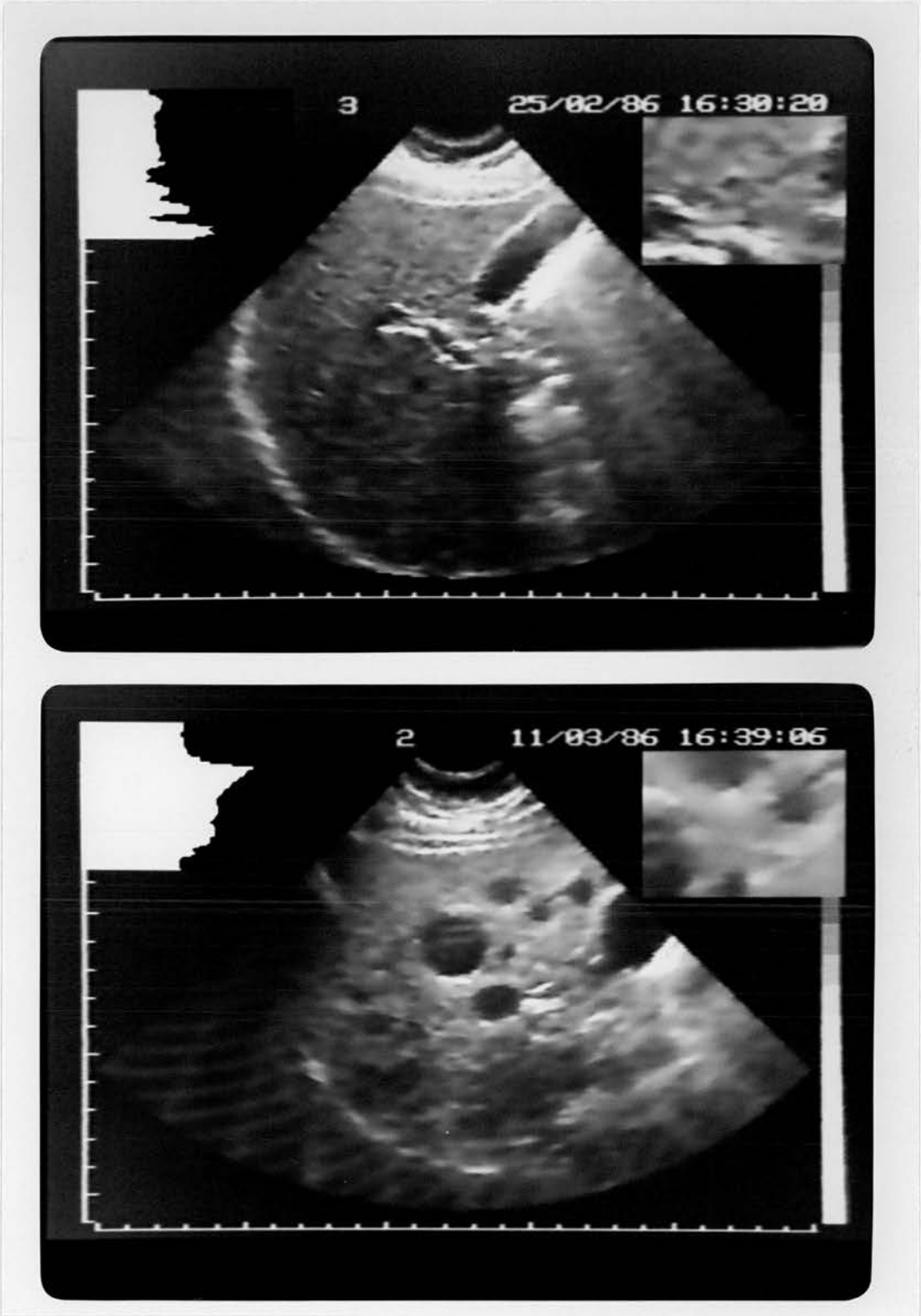

Figure 4.10 : Frost's modified filter applied to the original scans of Figure 4.1.

The best results using this filter were obtained with a window size of 9 X 9 and K_2=0.7. Figure 4.10 shows the original scans of Figure 4.1 after processing. The performance of the filter is satisfactory, although very similar to that of Lee's filter. Of course, there are slight differences between the two filters which, however, cannot appreciated very well by comparing the prints of Figures 4.9 and 4.10. The most important difference is that Frost's filter, due to its variable region of support, can preserve details and subtle grey scale variations somewhat better, as can be seen by comparing the magnified regions of Figures 4.9 and 4.10.

Computationally, Frost's algorithm is very inefficient. The Fortran subroutine listed in Appendix B takes 600 s of CPU time to process a scan, although it uses the fast recursive method mentioned in the previous subsection for calculating the local statistics. In fact, the local statistics represent only a very small fraction of the computations performed by the filter at each point of the image. The most time consuming operation is the calculation of the convolution coefficients for each point of the window, 81 of them for a 9 X 9 window, and the multiplication of these with the pixel intensities inside the window. A fast implementation of 300 s has been achieved by taking advantage of the fact that the convolution coefficients exhibit an 8-fold symmetry. Even so, the filter is still slow and the marginal improvement in performance over Lee's algorithm cannot justify the additional execution time and complexity.

4.4.3. Adaptive weighted median filtering

The filters based on Lee's and Frost's algorithms have demonstrated the superiority of adaptive techniques by offering considerable noise reduction and, at the same time, preserving edges and other resolvable structures. However, both filters produce an output value which is a linear combination of the input intensities. As a result, they tend to blur small structures and subtle

grey scale variations whose local statistics are not sufficiently different from those of uniform speckle so that they can be recognized by the filter. Therefore, it would be desirable to have a space-varying algorithm which combines adjustable smoothing with the signal preserving properties of nonlinear estimators like the median filter. These arguments have led to the development in this project of a new algorithm called the adaptive weighted median filter (AWMF).

The basis of the AWMF is the weighted median, a nonlinear class of median-type filters, which includes the pure median as a specific case. This class has been applied to astronomical images for object removal with the weight coefficients chosen so that specific desirable features of the original image are preserved (Brownrigg, 1984). More recently, a 3 X 3 weighted median capable of real-time operation has been developed for impulse suppression in frequency modulated satellite TV images (Perlman et al, 1987).

For the sake of simplicity, the filters examined in the next few paragraphs which describe the properties of the weighted median, are one-dimensional. The weighted median of a sequence $\{X_i\}$ is defined as the pure median of the extended sequence formed by repeating each term w_i times, where w_i is the weight coefficient which corresponds to X_i (Justusson, 1981). For example, if $w_1=2$, $w_2=3$ and $w_3=2$, the weighted median Y_{WM} of the sequence $\{X_1, X_2, X_3\}$ is equal to

$$Y_{WM}=\text{median}\{X_1, X_1, X_2, X_2, X_2, X_3, X_3\} \tag{4.35}$$

Intuitively, it is expected that as more emphasis is placed on the central weights of the window the ability of the weighted median to suppress noise decreases but also the signal preservation increases. This characteristic of the weighted median, which is confirmed below by using its statistical

properties, is very useful because it allows the design of an adaptive filter with median-type properties. One way of achieving this is by choosing a family of weights which decrease monotonically as we move away from the centre of the window and the rate of decrease is controlled by the local image content. Since the families we have experimented with offered comparable performance, the simplest and computationally most efficient of all was chosen. This is a family of linear weights with variable slope α. For a 2K+1-point window, the weight coefficient w_i at point i (i=1, ..., 2K+1) is given by

$$w_i=\left(w_{K+1}-\alpha|K+1-i|\right) \tag{4.36}$$

where (x) denotes the nearest integer to x if x is positive or zero if x is negative.

The weight family of (4.36) has been used to study the effects of the weight coefficients on the filter's smoothing characteristics. For the following applications, a window of 2K+1=9 points and a central weight $w_{K+1}=21$ have been chosen. Figure 4.11 plots the weights for three values of the slope α, with the pure median corresponding to $\alpha=0$. The analysis is based on some first and second-order probability density functions (pdf's) of the weighted median[1]. The derivation of the pdf's is presented in Appendix A but since the resulting expressions tend to be very long and cumbersome they will not be repeated here.

The variance of the output, when a constant signal corrupted by noise is filtered by the weighted median, gives an indication of the filter's ability to

[1]Very recently, further work on the properties of the weighted median, including some very interesting results on cascaded and recursive filters, has become available as a technical report (Yli-Harja et al, 1988).

suppress noise in uniform areas. By using the pdf $f_{WM}(x)$ of the weighted median when the input is a constant signal m plus uncorrelated additive noise having a symmetric pdf, the output variance σ^2_{WM} can be calculated from

$$\sigma^2_{WM} = \int (x-m)^2 f_{WM}(x)dx \tag{4.37}$$

The variance is plotted in Figure 4.12 as a function of the slope α for the case of Gaussian noise with mean 0 and variance 1.

As a quantitative index of the weighted median's performance in edge preservation when noise is present, the mean square error (MSE) has been used. Let us consider an ideal step edge of heights h_1, h_2 with the transition occurring at point M and corrupted by uncorrelated additive noise. Since for a filter size of 2K+1 points the window encounters the edge 2K times, the total MSE is defined by Pomalaza-Raez & McGillem (1984) as

$$\text{Total MSE} = \sum_{i=M-K}^{M+K-1} E\{(y_i-s_i)^2\} = \sum_{i=M-K}^{M+K-1} \int (x-s_i)^2 f_{WM}(x;i)dx \tag{4.38}$$

where

y_i is the filter output when the window is centred at point i
s_i is the signal value at that point before noise was added
$f_{WM}(x;i)$ is the pdf of the weighted median at point i when the input is an ideal edge corrupted by noise

The total MSE is plotted in Figure 4.13 for the case of uncorrelated Gaussian noise with mean 0 and variance 1 and edge heights $h_1=0$, $h_2=5$.

Figures 4.12 and 4.13 follow a similar pattern. For weights relatively close to the central value w_{K+1} (slope values $\alpha=0$ to 2) the filter behaves almost as a pure median offering maximum noise suppression but also introducing maximum distortion to edges corrupted by noise. However as the slope increases, i.e. as the weights fall more rapidly as we move away from the centre of the window, edge preservation improves at the expense of the ability to suppress noise. This happens because greater emphasis is placed on

the central weights while the effective window size is reduced since the weights at the periphery of the window become very small or even zero (see equation 4.36). For very large slope values, not shown in the graphs, the effective window size becomes 1 and the filter has no effect on the input. The behaviour of the filter can be predicted using the quantity ρ, defined as $\rho=[\sum w_i^2]/[\sum w_i]^2$. It has been found that signal preservation and noise reduction are proportional and inversely proportional to ρ, provided that the weights do not have significantly different values (Loupas et al, 1988).

By calculating the Fourier transform of the autocorrelation of the output when the input is a constant signal corrupted by uncorrelated additive noise, the power spectrum of the weighted median has been obtained for slope values α=0, 3 and 6 (Figure 4.14). This figure illustrates how the slope α modifies the low-pass characteristics of the weighted median. As the slope increases the bandwidth becomes wider while both ripple and attenuation in the stopband zone are reduced. It is interesting to note the similarity between this behaviour and that of weighted average (FIR) filters.

The analysis of the weighted median's properties for the one-dimensional case demonstrates that the selection of the weight coefficients represents a tradeoff between noise reduction and signal preservation. The AWMF takes advantage of this fact by adjusting the weights at each point of the image according to the local statistics of the terms inside the window. For a 2K+1 X 2K+1 window, the weight coefficient at (x,y) is equal to

$$w(x,y)=\left(w(K+1,K+1)-cd\sigma_I^2/m_I \right) \qquad (4.39)$$

where

c is a scaling constant
m_I, σ_I^2 are the local mean and variance of the of the input image
d is the distance of the point (x,y) from the centre of the window (K+1,K+1) defined by (4.33) and $\left(x\right)$ is defined by (4.36)

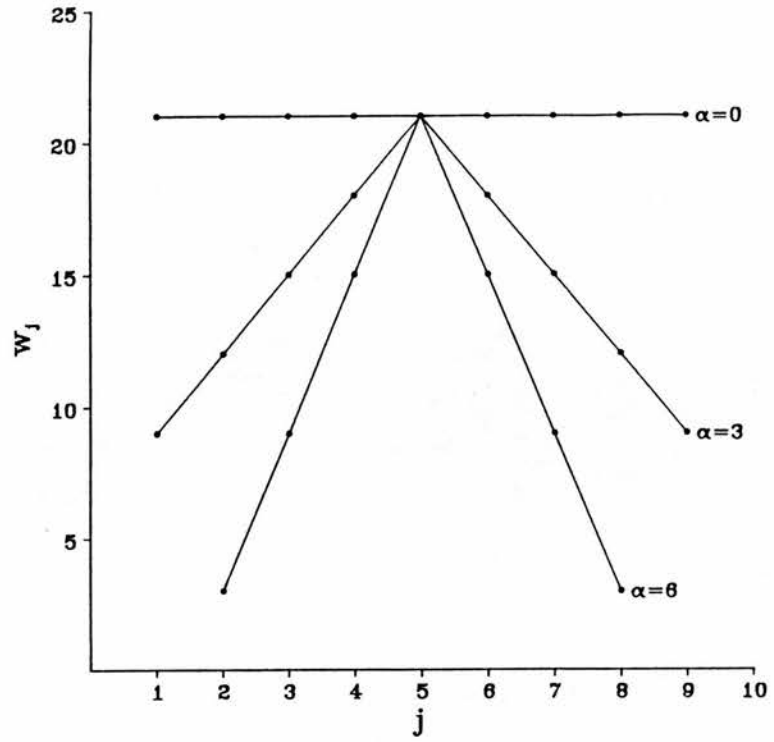

Figure 4.11 : A family of linear weight coefficients with variable slope α.

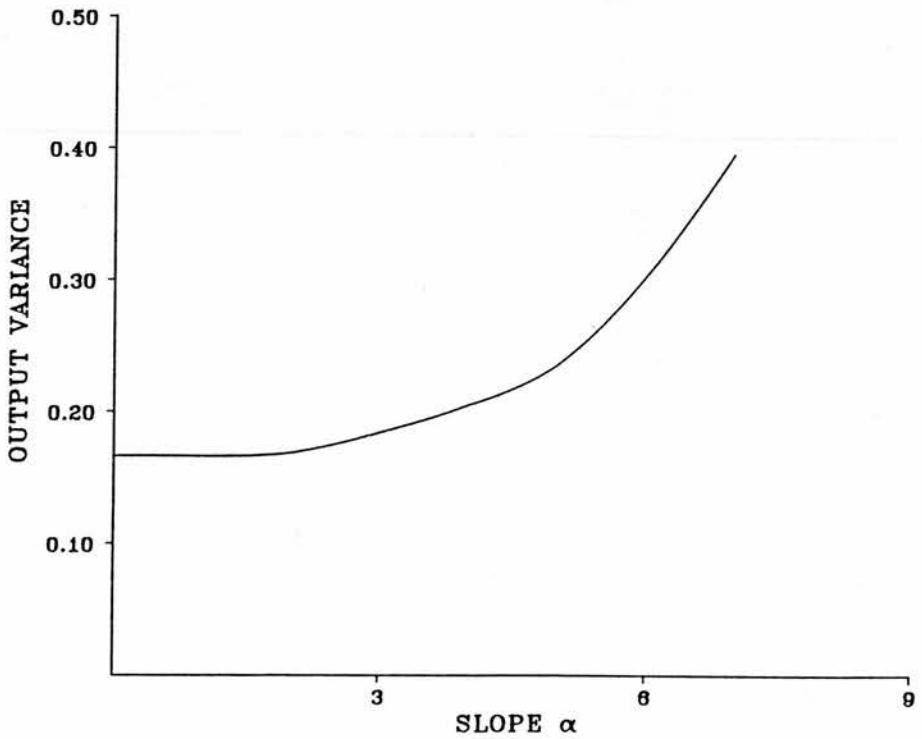

Figure 4.12 : Output variance of the weighted median as a function of the slope α of the weight coefficients. The input is a constant signal corrupted by uncorrelated, additive Gaussian noise.

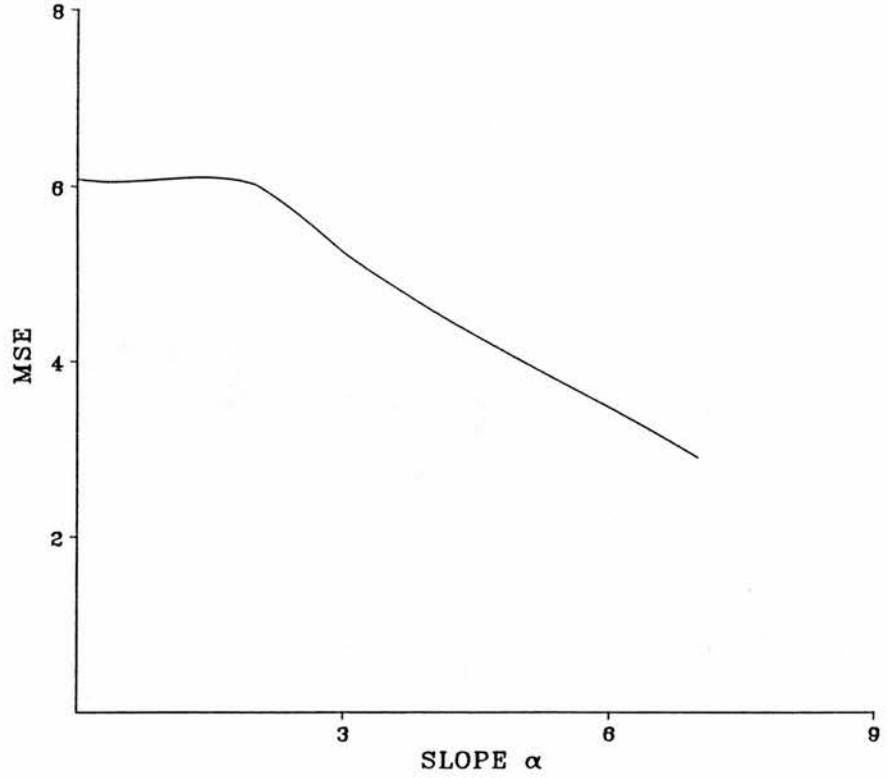

Figure 4.13 : Total Mean Square Error introduced by the weighted median as a function of the slope α of the weight coefficients. The input is an ideal step edge corrupted by uncorrelated, additive Gaussian noise.

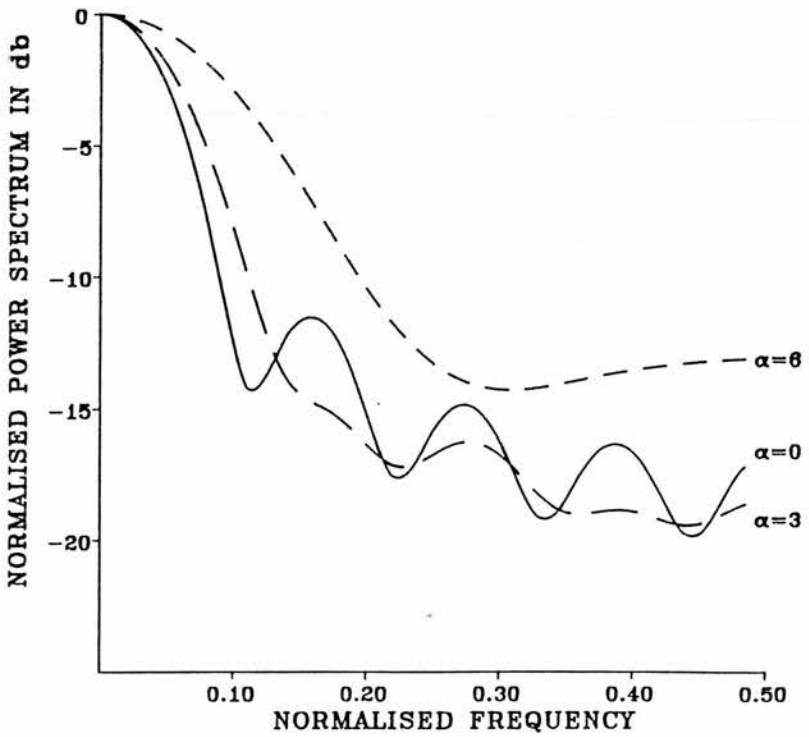

Figure 4.14 : Power spectrum of the weighted median for three sets of weights. The input is a constant signal corrupted by uncorrelated, additive Gaussian noise (quantized to 32 levels).

(4.39) is the two-dimensional equivalent of the weight equation (4.36) with the product $c\sigma_I^2/m_I$, which characterizes speckle, corresponding to the slope α. For uniform areas, where intensity fluctuations are due to noise, the quantity σ_I^2/m_I has a small value. From (4.39) it can be seen that the weights have values relatively close to the central value w(K+1,K+1) and, therefore, maximum noise reduction is performed. However, when the filter window includes a resolvable structure or a boundary between areas of different grey scale levels the local variance is larger than that expected form a uniform area having the same local mean. Consequently the slope $c\sigma_I^2/m_I$ increases and fine image detail can be preserved.

The output of the AWMF at a particular point is obtained following a three-step procedure. First, the local statistics and the weight coefficients are calculated. Then, the grey level histogram H(ℓ), ℓ=1, ..., max grey level (256 in our case), is formed by examining the grey level I(x,y) of each pixel (x,y) inside the window and incrementing H(I(x,y)) by the corresponding weight coefficient. Finally, the weighted median is determined as the minimum grey level O_{AWM} which satisfies

$$\sum_{\ell=1}^{O_{AWM}} H(\ell) \geq [\ \sum w(m,n)+1\ ]/2 \qquad (4.40)$$

where $\sum w(m,n)$ represents the sum of the weight coefficients.

Figure 4.15 shows the scans of Figure 4.1 after processing by the AWMF with window size 9 X 9, c=20 and w(K+1,K+1)=99. Comparisons between the two figures shows that speckle has been almost totally suppressed while high contrast edges are as sharp as in the original and even small details like the portal tracts at the left part of the top scan have been preserved and can be visualized better after speckle suppression. Also, due to its median-type

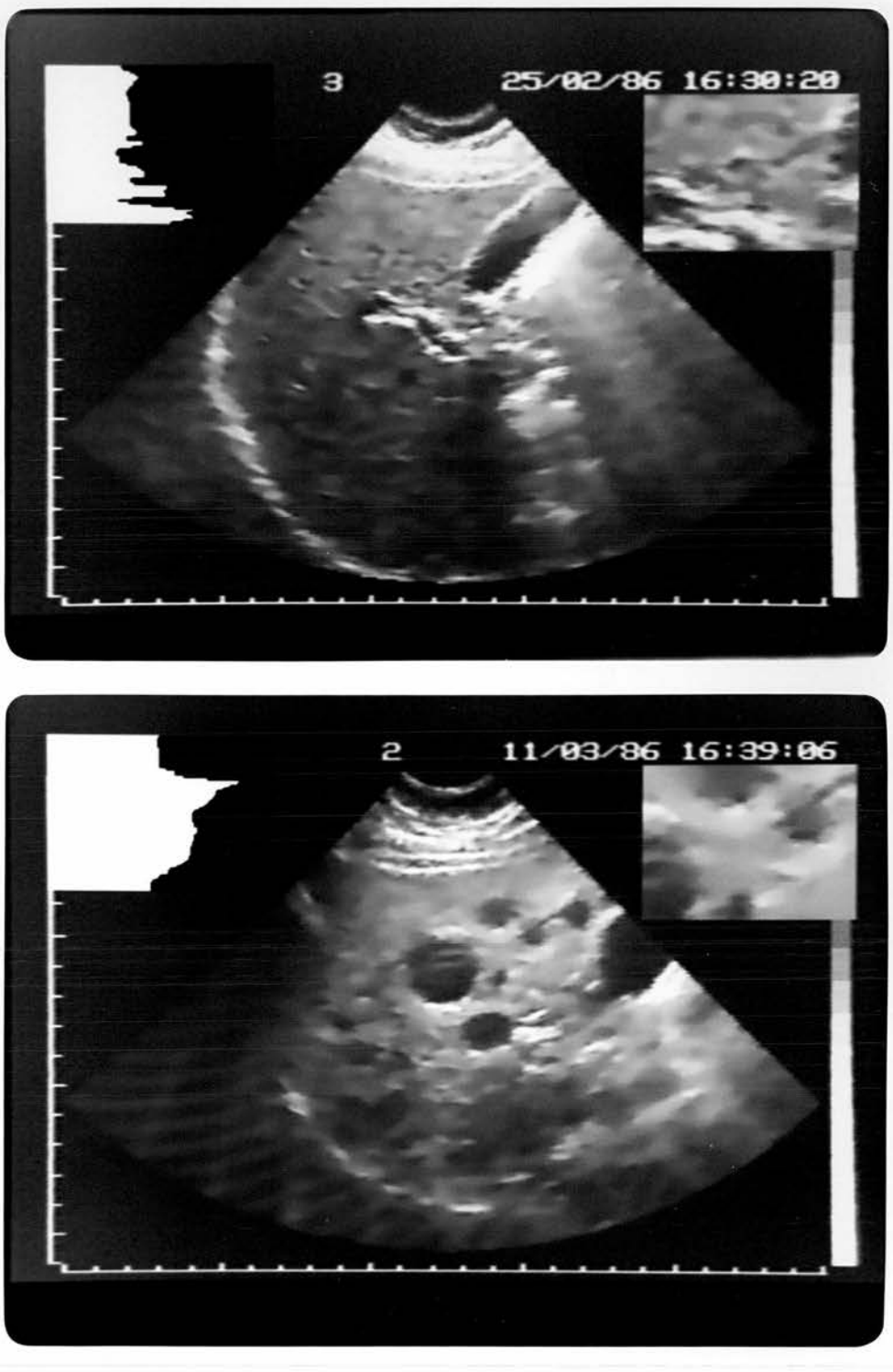

Figure 4.15 : Adaptive weighted median filtering applied to the original scans of Figure 4.1.

nature, the AWMF can preserve subtle grey scale variations better than Lee's or Frost's filters. This can be seen by comparing the appearance of the small branch of the hepatic vein (top scan) and the boundaries of the hypoechoic lesions in the magnified regions of Figures 4.9, 4.10, 4.15.

With 230 s of CPU time needed by the MicroVax to process a scan, the AWMF cannot be considered efficient or fast. The long execution time can be attributed to the need to calculate the weight coefficients at each pixel of the image and, more importantly, to the fact that Huang's fast median filtering algorithm (Huang et al, 1979) cannot be used because the weights vary from point to point. On the other hand, the AWMF can preserve boundaries between areas of slightly different echogenicity better than other adaptive filters. In our opinion, this approach succeeds in retaining the good points of median-type filters, the preservation of subtle grey scale variations being the most important, while it overcomes most of their drawbacks associated with loss of genuine image detail.

An alternative way of performing adaptive median-type filtering is to use a pure median filter with a variable-size window. A rather complex filter based on this idea which, nevertheless, can suppress different types of noise simultaneously has been proposed recently by Bernstein (1987). We have experimented with a simpler algorithm. This is a two-dimensional median filter with a window size 2L+1 X 2L+1 determined at each point of the image from the formula

$$L=\left(K(1-c\sigma_I^2/m_I)\right) \tag{4.41}$$

where 2K+1 X 2K+1 is the maximum window size and the rest of the symbols are defined as in (4.39).

This filter offers performance comparable to that of the AWMF,

something not surprising since both filters are based on the median and utilize the same local statistics criterion. An advantage of the variable-size median is that it is quite efficient with only 110 s of CPU time needed to process a scan on the MicroVax. The filter is only slightly less efficient than the DW-MTM filter (100 s) but it offers superior performance. One drawback of the variable-size median is that it is not able to perform fine adjustments of its smoothing characteristics, like the AWMF can, because its action can only be controlled by its window size. For example, if a maximum window of 9 X 9 points is used the filter can offer only 5 modes of action, from window sizes 9 X 9 to 1 X 1. On the other hand, Brownrigg (1986) has shown that for a given window length the weighted median acts in a very large, but finite, number of ways on the data depending on the selection of the weight coefficients. This inflexibility of the variable-size median compared to the adaptive weighted median results in slightly inferior image quality.

4.4.4. Directional filtering

The action of most adaptive filters varies from maximum noise smoothing in uniform areas where only noise is present to no smoothing at all near edges. While this prevents edge blurring and loss of image detail it does not do much to restore noisy edges and emphasize object boundaries. Another drawback, restricted only to techniques which use the first-order local statistics to determine the local image content like the adaptive filters of Sections 4.4.1 - 4.4.3, is that first-order statistics do not take into account how the pixel intensities are distributed inside the window. For example the 5 X 5 images of Figure 4.16 have identical means and variances but the square on the left is obviously noise whereas the square on the right consists of two separate regions. One approach which can overcome these drawbacks is to perform adaptive directional filtering.

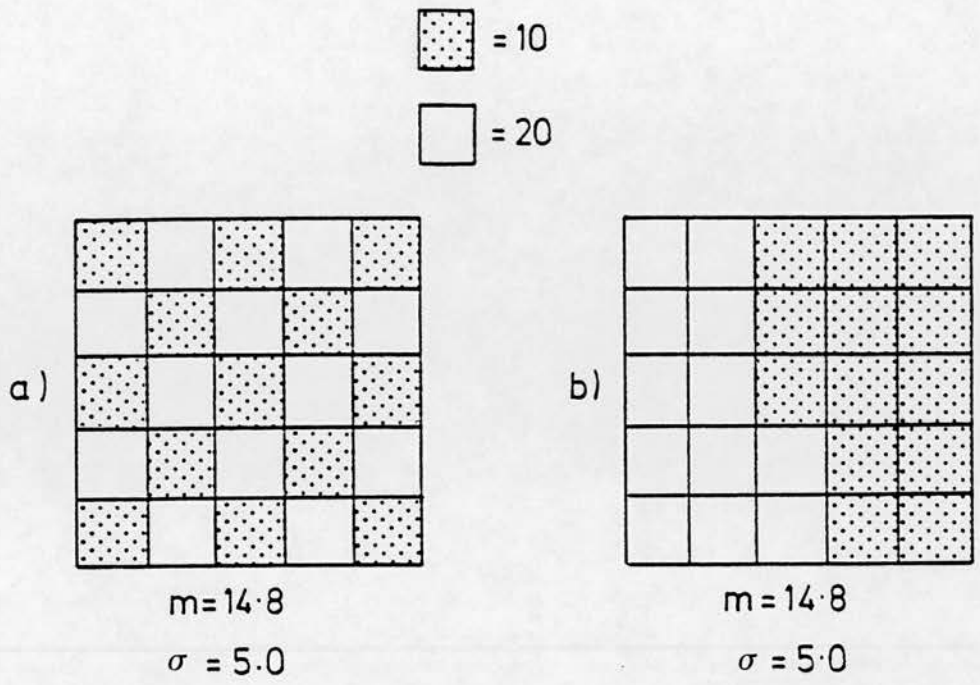

Figure 4.16 : 5 X 5 binary images having identical first-order statistics but displaying two obviously different patterns.

The human visual system possesses special mechanisms for edge detection which are "tuned" to specific orientations (Hubel & Wiesel, 1979). The directional information extracted by these edge detectors from a scene plays a very important role in the brain's attempt to determine the local image content (Peli, 1987). It makes sense therefore to develop image processing systems which simulate the operation of the human observer by utilizing the information about the orientation of structures contained in an image.

So far, directional processing has been used for feature extraction by means of a multilevel image transform (Granlund, 1978; 1981), texture discrimination (Ikonomopoulos & Munser, 1984), image coding (Ikonomopoulos & Kunt, 1985), image sharpening (Chanda et al, 1985) and enhancement of line structures in images of retinal fibre, fingerprints and seismic data (Peli, 1987). Also, two methods for noise suppression which utilize directional information have recently appeared in the scientific literature. Both of them are based on

Lee's adaptive algorithm. The first method, which has been mentioned already in Section 4.4.1, uses a cascade of one-dimensional filters operating along the four principal directions (Chan & Lim, 1985). The second method uses a two-dimensional filter, like the one described by (4.16), with directional information incorporated in the local mean (Kim & Jung, 1987).

A different approach to noise suppression by means of directional processing has been developed in this project. It is a two-stage technique which utilizes the directional information around a pixel, first to produce a smoothed image with noise suppressed both in uniform areas and near edges, and then to process the smoothed image with an adaptive band-pass filter in order to enhance edges and highlight boundaries between areas of different echogenicity. The second stage of the technique is not common at all in noise suppression algorithms but it was considered necessary because smoothing alone cannot sharpen edges and boundaries which draw the attention of a human observer to the presence of organs and lesions.

The directional filter is described in the following paragraphs. However, in order to illustrate the need for combined smoothing and sharpening around edges let us consider the computer generated image of Figure 4.17a. The 3D plot of the image is displayed on the left and its cross section on the right part of this figure. The image has uniform intensity equal to 60 apart from the two circular regions of intensity 30 and diameters 6 and 12 pixels and the three lines which are 3-pixel wide each and have intensities 100, 30 and 100, respectively. Figure 4.17b displays the same image after uncorrelated Gaussian noise with mean 0 and variance 100 was added. It can be seen that the low-contrast lesions have almost been buried by the noise and the line structures have been severely distorted. Figure 4.17c is obtained by processing the noisy image with a 9 X 9 adaptive weighted median which has been appropriately modified for the case of additive noise (the variance σ_I^2

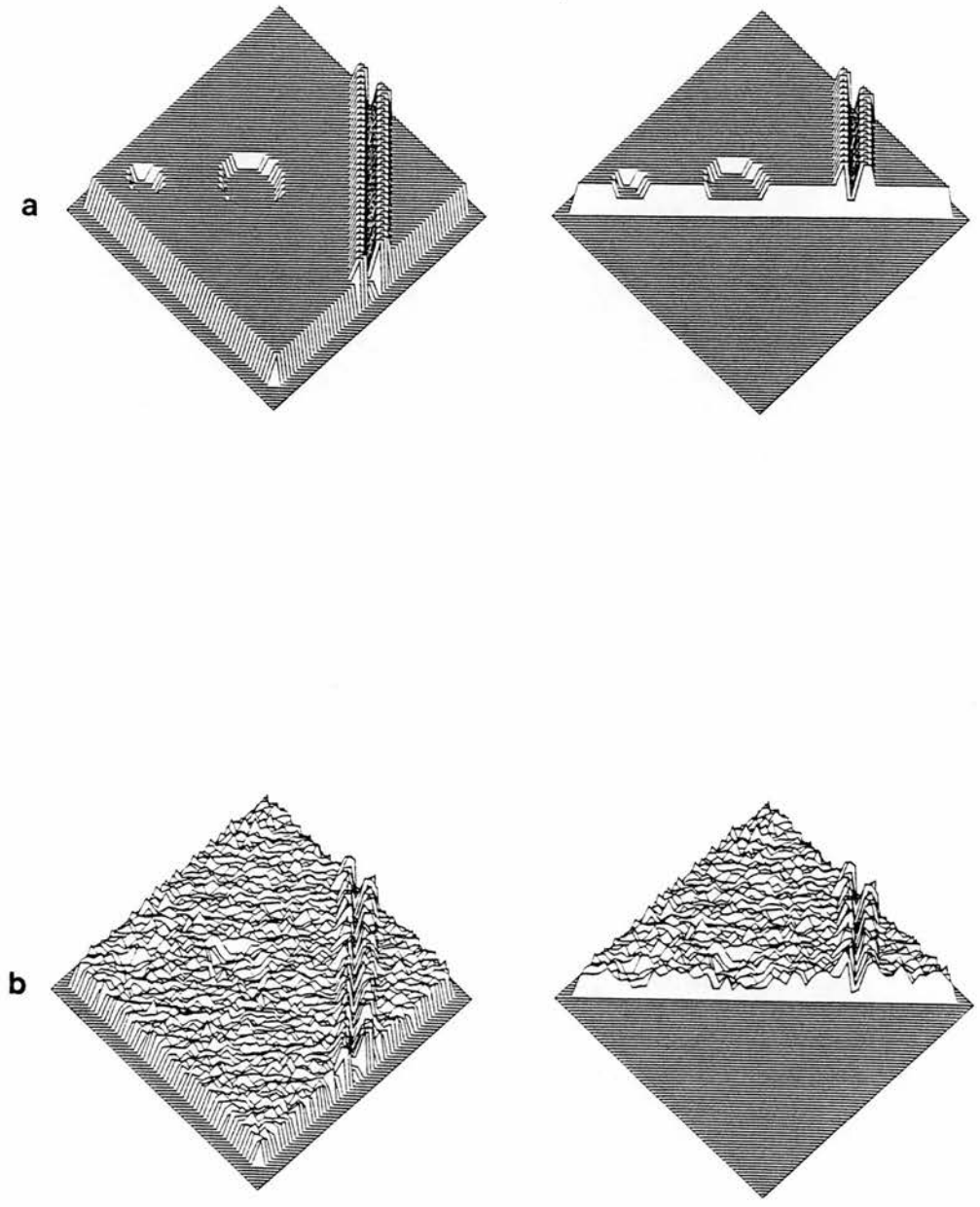

Figure 4.17 : Computer generated images. **(a)** – original. **(b)** – original plus uncorrelated, additive Gaussian noise.

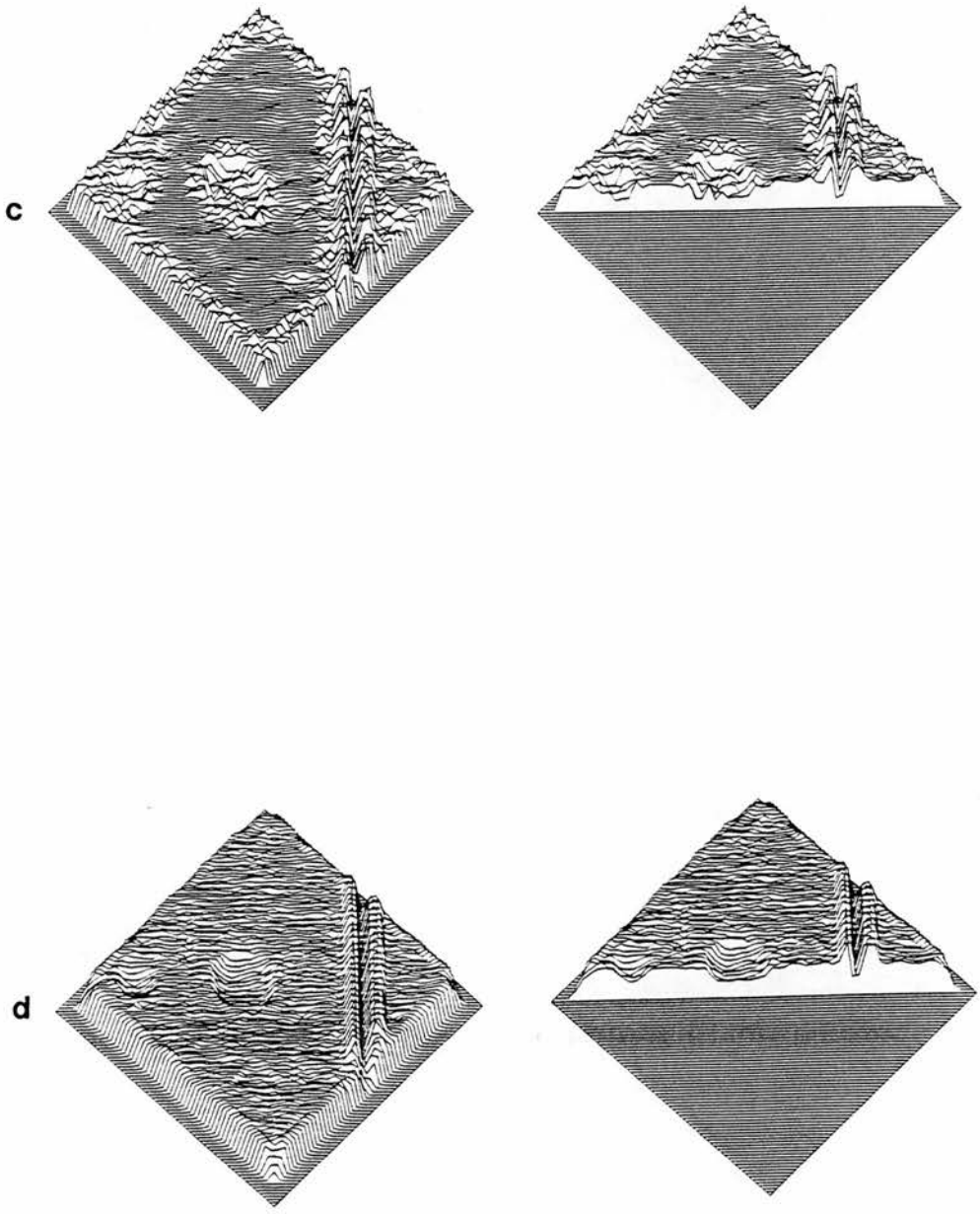

Figure 4.17 : Computer generated images. **(c), (d)** – adaptive weighted median and directional filtering applied to the noisy data of Figure 4.17b.

is used instead of σ_I^2/m_I to control its smoothing characteristics). Figure 4.17c demonstrates the inadequacy of this type of filtering for the restoration of edges corrupted by noise. Although the noise has been suppressed considerably in uniform areas, no smoothing has been performed near the circles and lines because they have been rightly classified by the local statistics criterion as edges. On the contrary, processing by the directional filter, with the same parameters as the ones mentioned below, suppresses noise in all parts of the image and enhances the visibility of the structures contained in the image (Figure 4.17d).

In order to perform directional filtering, the one-dimensional mean m_d and variance σ_d^2 around each point (x,y) are calculated along the directions 0°, 45°, 90° and 135° which correspond to d=1, 2, 3 and 4, respectively. From σ_d^2, the normalized variances σ_{dn}^2 are calculated as

$$\sigma_{dn}^2=\sigma_d^{2k}/(\sum_{d=1}^{4}\sigma_d^{2k}) \tag{4.42}$$

The output $O_1(x,y)$ of the smoothing stage is then given by

$$O_1(x,y)=\sum_{d=1}^{4}(m_d/\sigma_{dn}^2)\ /\ \sum_{d=1}^{4}(1/\sigma_{dn}^2) \tag{4.43}$$

The parameter k determines the relative contributions of the directional means m_d to the output $O_1(x,y)$. For k=0 all directions contribute equally whereas for k=+∞ the direction of minimum variance contributes exclusively.

The presence of an edge along a direction d results in minimum variance σ_d^2 along this direction. In this case, $1/\sigma_{dn}^2$ is considerably larger than the rest of the inverse normalized variances and smoothing parallel to the edge axis is performed, which improves its definition without introducing considerable blurring. On the other hand, if only noise is present all the

variances have similar values. As a result, $1/\sigma_{dn}^2 \simeq 1/4$ for d=1, ...,4 and by accepting equal contributions from all the directional means maximum smoothing is performed.

After the first stage is completed the normalized variances σ_{dn}^2 of the input image are used again to perform adaptive sharpening of the smoothed image, which enhances edges and lines without amplifying the noise. For each point (x,y), four one-dimensional band-pass filters are designed using the window method with a Kaiser window (Oppenheim & Schafer, Chapter 5, 1975; Rabiner et al, 1979). The normalized high-pass cutoff frequency f_H of the filters is fixed. However, the low-pass frequency f_{LM} is determined for each direction from $f_{LM}=f_L\sigma_{dn}^2$ so that f_{LM} obtains its maximum value f_L for directions vertical to an edge axis ($\sigma_{dn}^2 \simeq 1$) but approaches zero for directions parallel to an edge. Then, the pixels along each direction are convolved with the corresponding filter coefficients and the final output $O_2(x,y)$ is obtained from the partial results $O_{2d}(x,y)$ of the convolutions as

$$O_2(x,y)=\sum_{d=1}^{4} O_{2d}(x,y)\sigma_{dn}^2 \qquad (4.44)$$

This time it is the direction of maximum variance which contributes more to the final result.

The following parameters have been chosen for the directional filter. Smoothing window of 7 points, k=2, band-pass filter window of 7 points, Kaiser window attenuation 50 db, f_H=0.4 and f_L=0.1. The results of processing the scans of Figure 4.1 by the directional filter are shown in Figure 4.18. The first comment to be made is that edges , lines and boundaries have indeed been enhanced. Note, for example, the dark line on the bottom-right part of the gallbladder and the branch of the hepatic vein (top scan) or the boundaries of the hypoechoic lesions (bottom scan). Another comment is that noise has

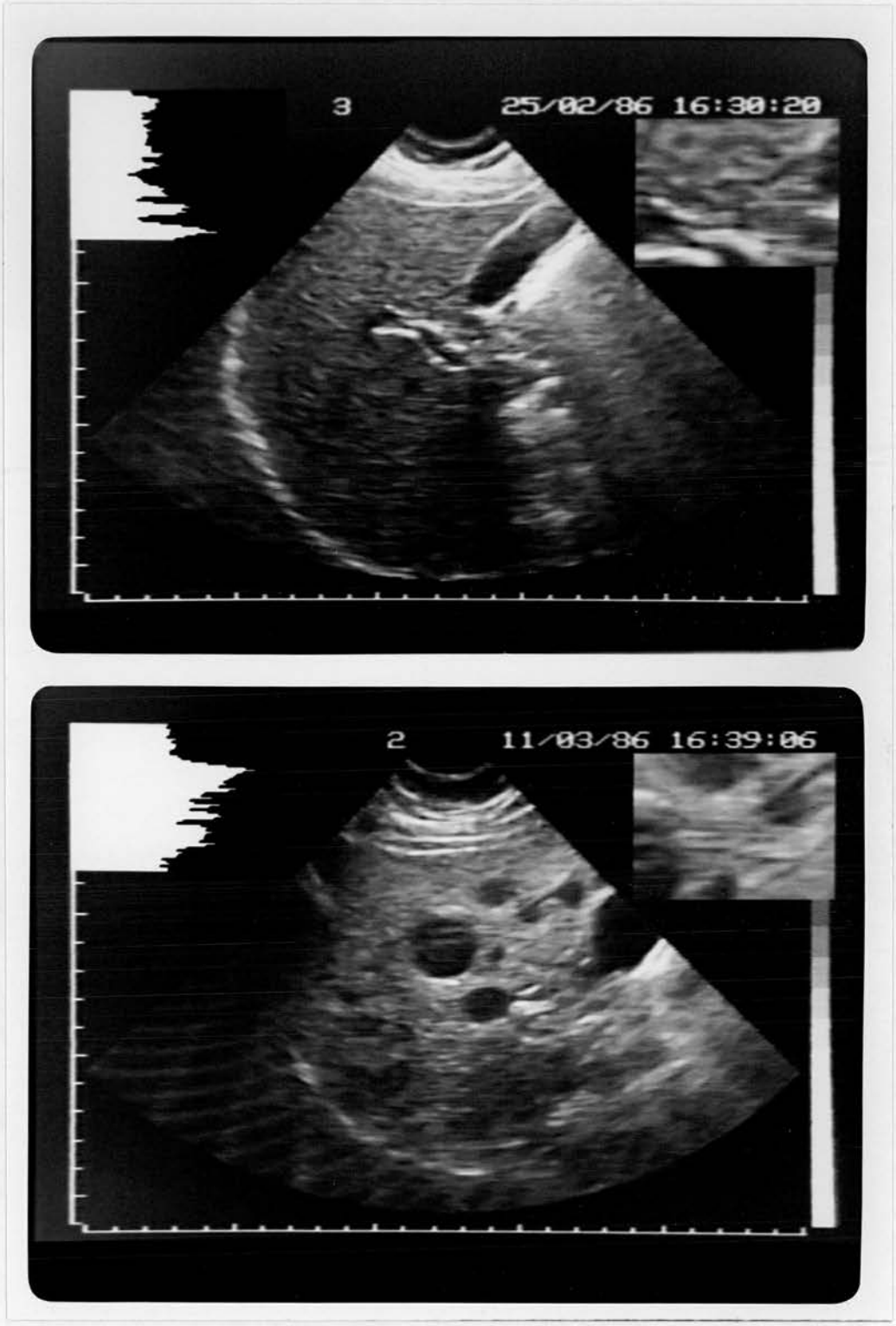

Figure 4.18 : Directional filtering applied to the original scans of Figure 4.1.

been reduced to some extent but not as much as in scans processed by the filters described before. The directional filter suppresses small speckle but preserves and even enhances coarser texture. This creates the subjective impression that more information can be seen in the tissue parenchyma of the processed scans, although the validity of this impression is questionable.

Directional filtering is extremely slow with 960 s of CPU time needed to process a scan on the MicroVax. The computational inefficiency is due to the two-stage filtering operation. An additional reason is that the basic operation at each point is performed four times along different directions, although this problem could be overcome in a parallel hardware implementation by using a number of processors operating simultaneously on data from different directions. It is recognized that this particular implementation of directional filtering is not necessarily optimum in the sense that many parts of the algorithm could be simplified considerably offering a substantial reduction in execution time. The reason for not having done this is that the idea could only be implemented after the purchase of the MicroVax when this project was approaching its completion. However, it is hoped that experimentation with different versions of the smoothing/sharpening algorithm could not only increase the computational efficiency of the filter but could also yield better performance.

4.4.5. Multiple filtering

A comparison based on the processed images of Section 4.4 suggests that techniques such as Lee's, Frost's and the adaptive weighted median filter are very efficient as far as speckle suppression in relatively uniform areas is concerned but not in edge enhancement while the directional filter is capable of enhancing edges and highlighting details but at the expense of inadequate noise reduction. Although computationally excessive, it is interesting to combine the strong points of several filters by adopting a multifiltering

approach, i.e. a number of algorithms are applied to the same image data and the output at each point is determined primarily by the filter which is most appropriate for processing the area which contains the point.

This approach is perfectly consistent with the concept of adaptive processing. In the introduction of Section 4.4 it was argued that the smoothing performed at each point must be adjusted according to the local image content. There is no reason why this idea could not be extended so that processing includes a number of filter types, since it is unlikely that one filter can be optimum for all parts of an image. In fact the human visual system, which most image processing algorithms attempt to simulate, could be modelled as a number of "filters" of various types, window geometries and sizes operating in parallel in order to extract the maximum amount of information from every part of an image.

As a first step in implementing a multiple filtering scheme, it was assumed that the pixels of an ultrasonic scan belong either to relatively uniform areas where speckle is the main source of grey level variations or to areas where low or high-contrast resolvable detail is present. The most suitable techniques to process these two area types were considered to be the adaptive weighted median and the directional filter respectively. From the methods tried, the one that produces the best results forms a composite image O(x,y) by combining information from the input image I(x,y) and the outputs of the adaptive weighted median $O_{AWM}(x,y)$ and directional filter $O_{DF}(x,y)$ in the following manner.

$$O(x,y)=cO_{AWM}(x,y)+(1-c)O_{DF}(x,y) \tag{4.45}$$

where

$$c=\exp[-\alpha(\beta m_I(x,y)/\sigma_I^2(x,y)-1)^2] \tag{4.46}$$

The by now familiar ratio σ_I^2/m_I of the local variance over the local mean is used to classify each point of the input image. If σ_I^2/m_I has a value close to the one expected from a uniform speckle area (equal to the parameter β in equation 4.46) $c \simeq 1$ and the adaptive weighted median contributes almost exclusively to the output. On the other hand, if σ_I^2/m_I is substantially larger (smaller) than β this implies the presence of high (low) contrast detail. In this case $c \simeq 0$ and the directional filter becomes the main contributor to the output. The parameter α controls the transition between the two filters. The values of of σ_I^2/m_I which result in equal contributions are given by

$$\sigma_I^2/m_I = \beta/\{1 \pm [(ln2)/\alpha]^{1/2}\} \tag{4.47}$$

Figure 4.19 displays the images of Figure 4.1 after multiple filtering with $\alpha=2$, $\beta=1$ and a 9 X 9 local statistics window. The parameters of the adaptive weighted median and directional filter were the same as the ones used for processing the images of Figure 4.15 and 4.18 respectively, with one exception. A smaller smoothing window of 5 points was chosen for the directional filter in order to obtain more edge/detail enhancement. Comparisons between the images of Figures 4.1 , 4.15 , 4.18 and 4.19 shows that multiple filtering offers both good speckle suppression and edge/detail enhancement; in other words it succeeds in combining the desirable features of the algorithms on which it is based.

Application of multiple filtering to a number of ultrasonic scans has shown that more impressive results can be expected when the original image contains poorly defined edges and small details obscured by speckle. An example is given in Figure 4.20. Multiple filtering (Figure 4.20d) offers as much speckle suppression in uniform areas as the adaptive weighted median (Figure 4.20c) does. At the same time, the composite image is definitely sharper than

both the original scan (Figure 4.20a) and the output of the directional filter (Figure 4.20b). The visibility of small vessels and other structures in the liver parenchyma has been improved significantly.

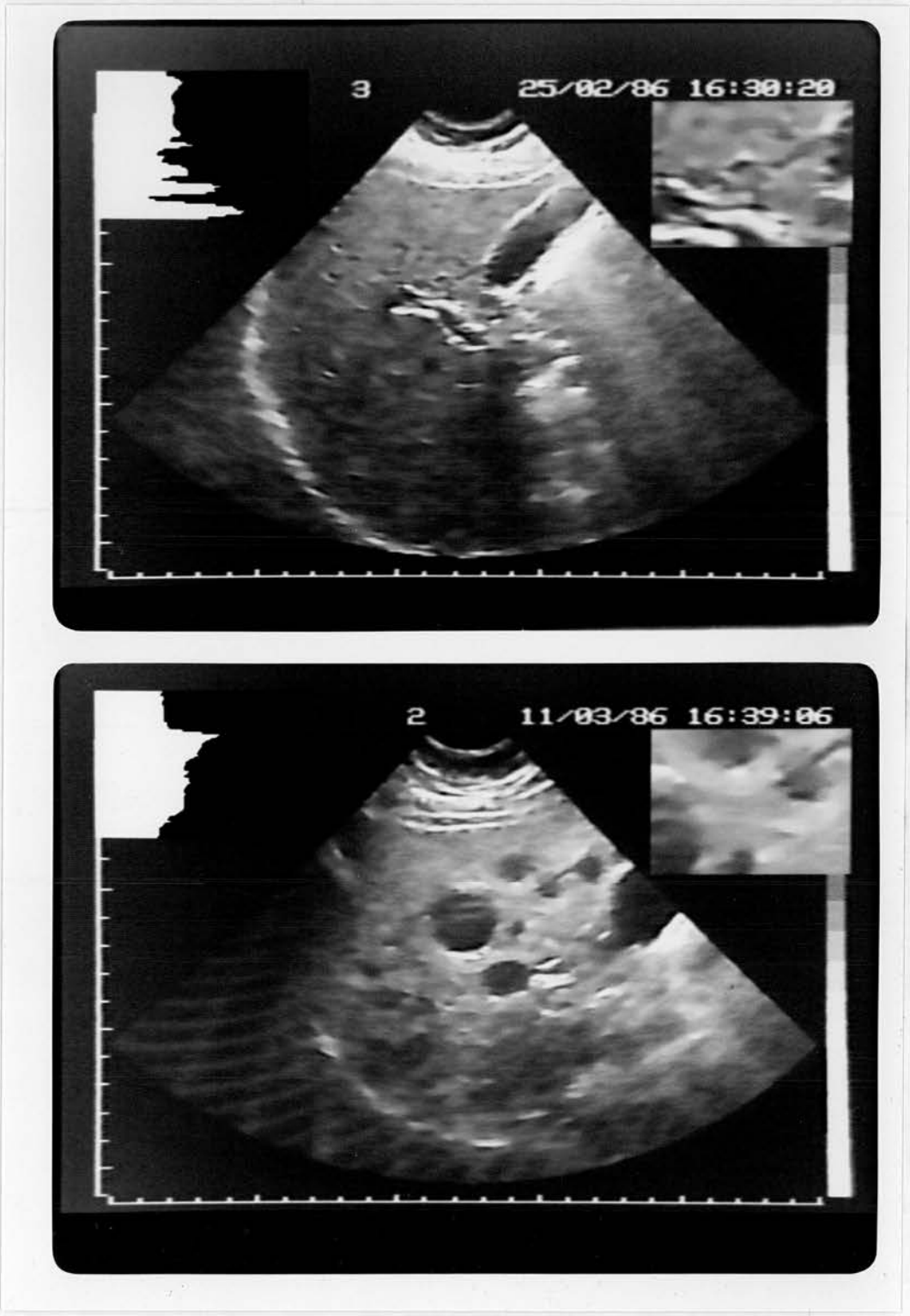

Figure 4.19 : Multiple filtering applied to the original scans of Figure 4.1.

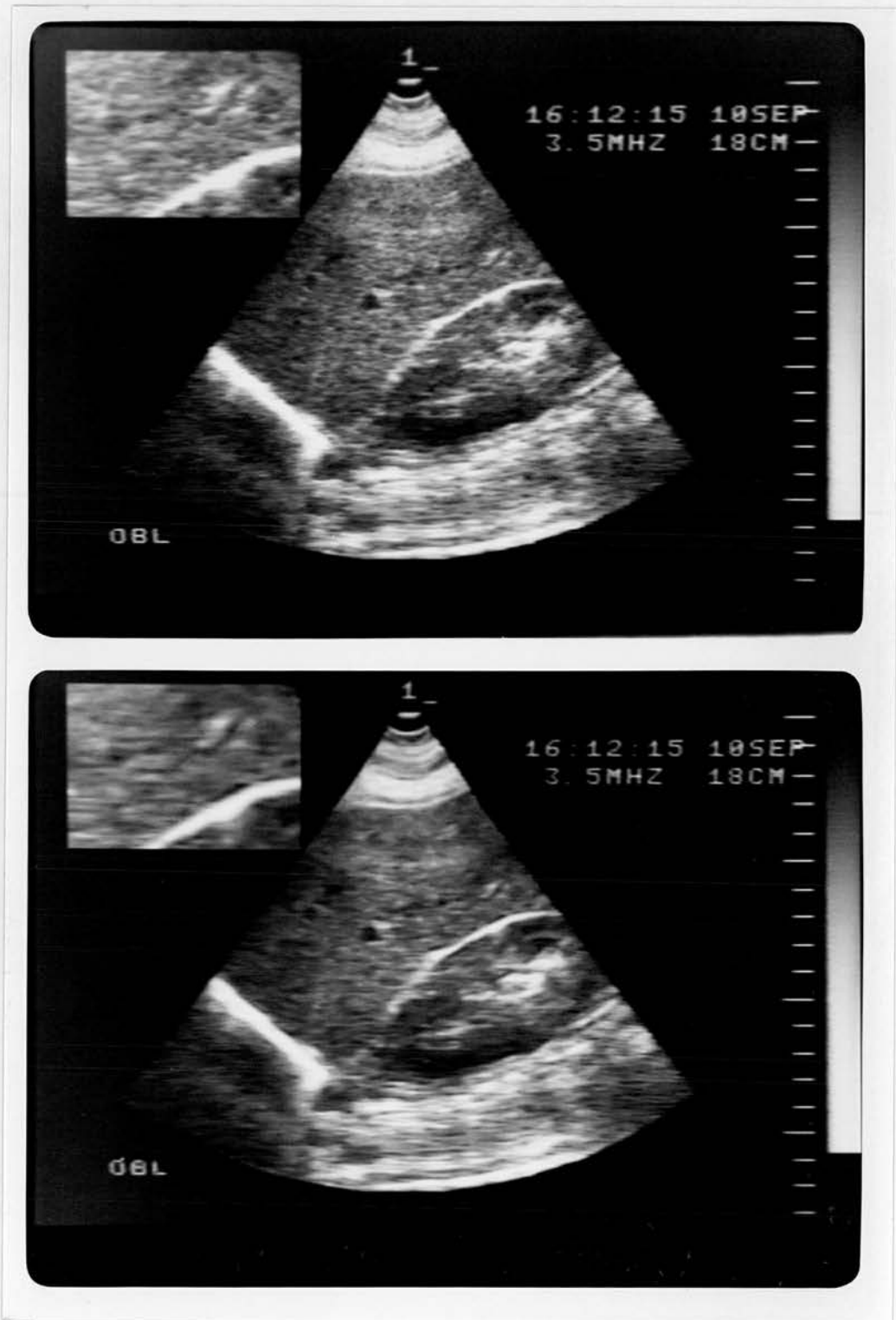

Figure 4.20 : **(a)** – Unprocessed scan of the liver and right kidney. **(b)** – Directional filtering. **(c)** – Adaptive weighted median filtering. **(d)** – Multiple filtering.

c

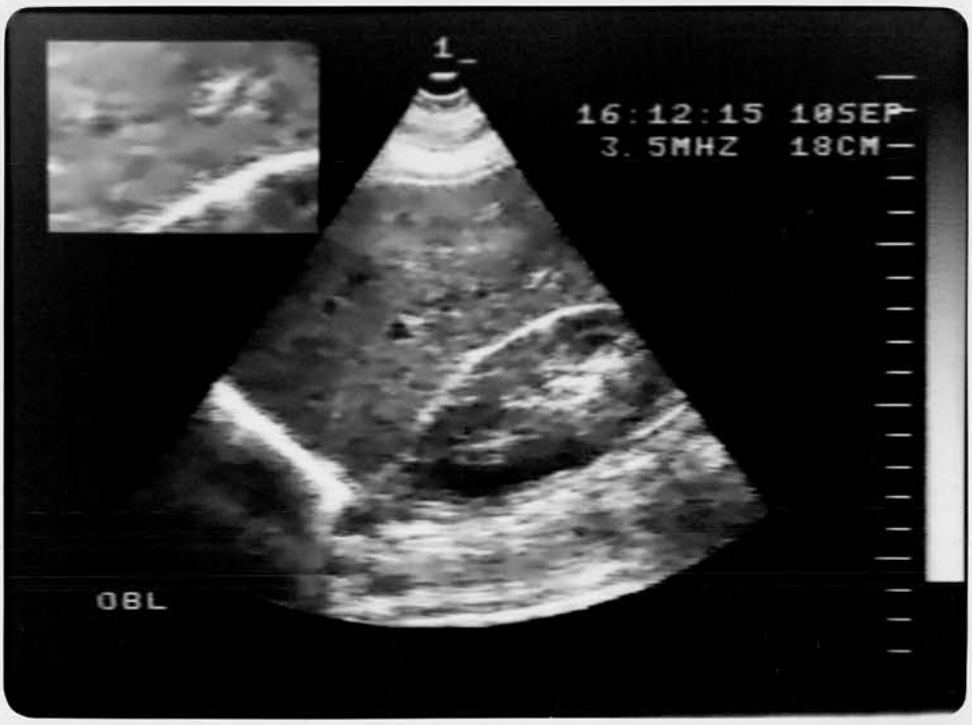

d

Figure 4.20 : **(a)** - Unprocessed scan of the liver and right kidney. **(b)** - Directional filtering. **(c)** - Adaptive weighted median filtering. **(d)** - Multiple filtering.

CHAPTER 5

REAL-TIME SPECKLE REDUCTION

5.1. Introduction

As mentioned in Section 2.4, a major requirement that a filtering technique must satisfy in order to gain acceptance in clinical practice is to be able to suppress speckle without introducing loss of genuine image detail. The adaptive filters of the previous chapter have demonstrated that it is possible to do this by using sophisticated computer image processing algorithms. Another equally important requirement, however, is that processing should be performed in real-time. "Real-time image processing" can be defined as processing at such a speed that the data rates of the input and output images are the same. In ultrasonic imaging, a real-time system must process a scan in 1/10 - 1/25 s, depending on the frame rate of the scanner. Due to their software implementation, the adaptive filters of Section 4.4 cannot offer this kind of speed. To give an example, they are anything between 600 times slower in the best case (Lee's algorithm and 10 frames/s) and 20000 times slower in the worst case (directional filtering and 25 frames/s). Clearly, what is needed is a hardware implementation.

Medical ultrasonics is not the only field where real-time image processing is highly desirable. Almost every interactive imaging technique could benefit from it. As a result, interest in this area has increased considerably during the last few years. The development of algorithms and hardware architectures which can satisfy the speed constraints imposed by real-time operation has become a major area of academic and commercial research. Hardware systems capable of real or near real-time operation include image processors such as the Crystal and the GOP (Granlund, 1981) or VLSI chips for linear filtering (Inmos Ltd, 1986a), median filtering (Oflazer, 1983; Bursky, 1987) and image moment generation (Hatamian, 1986). Designs based

on standard integrated circuits have also been developed for histogram equalization/contrast enhancement (Woods & Gonzalez, 1981; McCollum et al, 1988), two-dimensional recursive filtering (Ty & Venetsanopoulos, 1986), median filtering (Perlman et al; 1987) and edge detection (McCafferty et al, 1987).

5.1.1. Initial design considerations

The first step in designing a real-time image processing system is to decide if the system will be microprocessor-based or not. Microprocessors offer great flexibility because, after the input/output interface electronics have been built, it is fairly easy to modify or even change the algorithm used. Unfortunately, even the fastest "state of the art" devices like the transputer T414-20 (Inmos Ltd, 1986b) can only execute approximately 10 Million Instructions Per Second (MIPS) while our application requires the execution of a few hundred MIPS. Of course, it is possible to spread the processing tasks over a large number of processors operating in parallel on the input data. Parallel processors which are commercially available include the SIMD (single instruction multiple data) DAP and CLIP machines (Preston, 1986), and the MIMD (multiple instruction multiple data) Meiko Computing Surface (Bowler et al, 1987). However, the complexity and cost of those processors is not compatible with this project. Inevitably, the only other choice left is to design a system using dedicated integrated circuits which can perform only one function but in a very short time. For example, the addition of two 8-bit numbers can be performed in 15 ns using fast TTL chips (74S283) compared to 400 ns needed by a standard microprocessor like the Motorola 68000.

Another design consideration is the form of data to be processed. We chose to process the A-scan lines, after they have been digitized by the scanner but before scan conversion. Compared to the obvious choice of processing the TV image, which is available at the video output of the scanner,

this approach has the following advantages:

- There is no need for separate A/D and D/A converters which increase the complexity of the circuit.

- Filtering before scan conversion is more efficient. The smoothing and interpolation performed by the scan converter increase the spatial correlation of speckle and consequently larger window sizes are needed to suppress this artifact in the video image.

- The window geometry corresponds to the actual image formation both for linear (cartesian coordinates) and sector (polar coordinates) scans.

The main disadvantage of filtering the digitized A-scan lines instead of the video image is lack of flexibility and portability. Since the filter design is based on the specifications of a particular scanner, the circuit needs considerable modifications before it can be connected to a different machine.

It was decided to connect the filter to a Z/S mechanical sector scanner manufactured by GL Ultrasound Ltd, which had already been used in the evaluation of the frame averaging and software speckle suppression techniques. At that period the Z/S scanner was needed for another departmental project. However, this did not represent a serious problem because the development work could be carried out on a Fischer Ultrasound Marti scanner which shares the same electronics and scan converter (Hughes model 672) with the Z/S. The specifications of both scanners which are relevant to the design are : 6-bit A/D conversion, sampling period varying between 730 and 150 ns depending on the depth of penetration and line density equal to 1.1 vectors per 1°.

5.1.2. Simulations: Processing of A-scan lines in software

Because of the inflexibility and difficulties involved in implementing an image processing algorithm using dedicated hardware components, it is crucial

to form an idea about its performance before it is actually constructed. This can be achieved by simulating the algorithm's performance in software using real A-scan data. Ideally what is needed is an interface which can transfer the A-scan lines of a frame from a scanner to a computer and feed them back, after they have been processed, so that they can be displayed in the same format as the original scans. Since such an equipment was not available and building it is a major electronics project by itself, a system developed in the department for Adaptive Time Gain Compensation or ATGC (Pye et al, 1986), which could meet only the first of our requirements (transfer of data to a computer), was used instead.

The ATGC system can capture 32 consecutive A-scan lines, digitize them up to a depth of 197 mm at 8-bit, 4 MHz resolution and store them on a floppy disc. The fact that the system was linked to another Z/S scanner ensured that, apart from the different specifications of the A/D conversion, the input data used by the simulation programs would be identical to those processed by the hardware filter. Using the ATGC system, scans of liver and tissue mimicking phantoms were transferred to a PDP11/23 minicomputer. In order to display the A-scan lines as a conventional image, Fortran programs which implement different scan conversion algorithms (Ophir & Maklad, 1981; Robinson & Knight, 1982) were developed. An example of the phantom data used in the simulations is given by Figure 5.1. The reconstructed images formed from 100 A-scan lines is displayed in Figure 5.1a and 5.1b after scan conversion and interpolation respectively.

The A-scan data were used to examine the suitability of several window geometries, sizes and filter types. Application of the same filter to a scan, before and after scan conversion, demonstrated that processing is indeed more efficient when applied to the A-scan lines rather than to the final image, in the sense that a smaller window size is needed to achieve the same

a

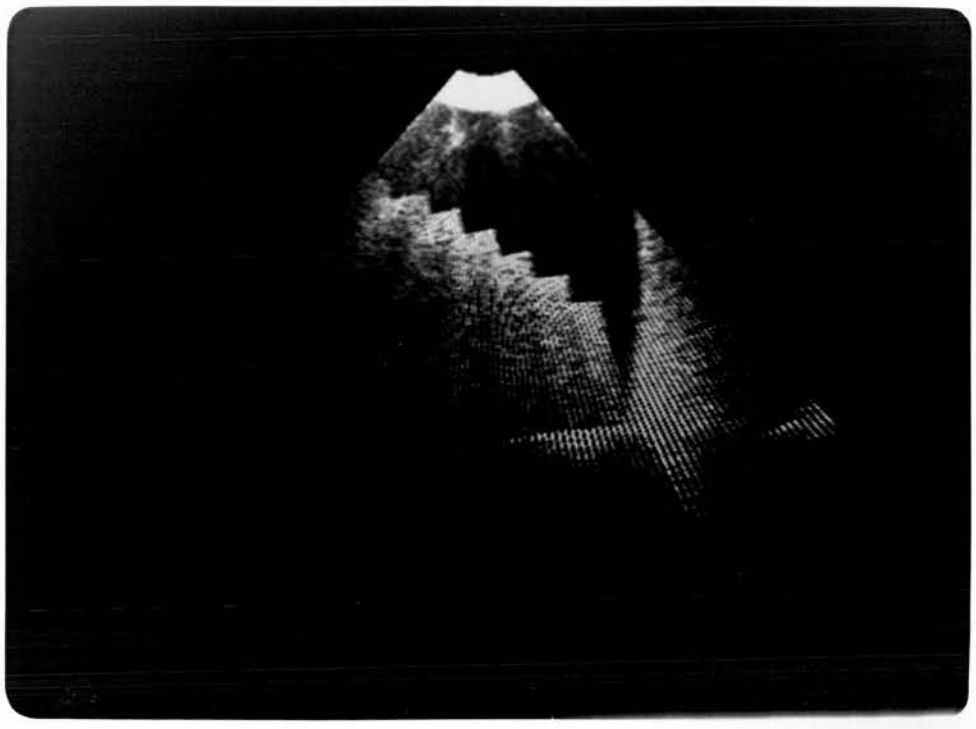

b

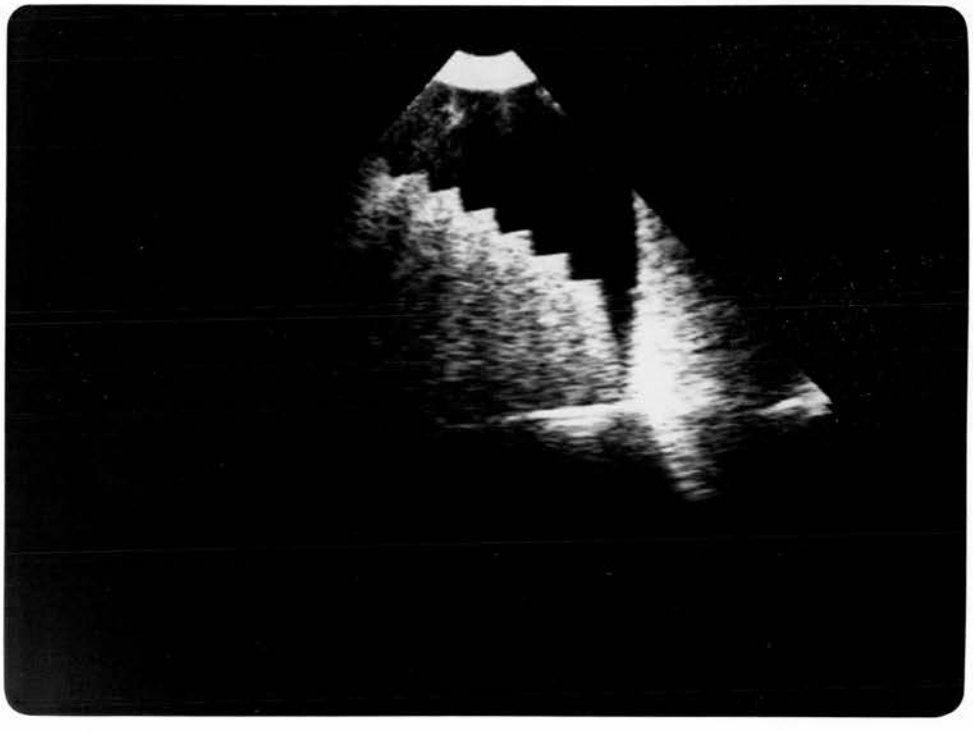

Figure 5.1 : A-scan data from ultrasonic phantom displayed as a grey scale image after scan conversion **(a)** and interpolation **(b)**.

degree of noise reduction. Another observation was that a cascade of two one-dimensional filters operating in the axial and lateral direction, i.e. along and across A-scan lines, gives results which are comparable to those obtained by a true two-dimensional filter. This has important implications for the complexity of the hardware because it offers considerable savings in the number of components needed. To give an example, a 7 X 3 average filter operating on 6-bit data needs forty two 4-bit adders compared to only fourteen needed by a 7 and a 3-point filter connected in cascade. The decomposition of a two-dimensional filter into a cascade of one-dimensional operations is one of the two most frequently used techniques to reduce the amount of computations needed for implementing a filter in software or hardware. The other technique, which is not suitable for our application, is repeated processing using a filter with a small window size.

After having specified the window geometry, experimentation continued in order to identify algorithms which offered satisfactory performance in terms of noise reduction/signal preservation but also were suitable for hardware implementation. Although Lee's algorithm (Section 4.4.1) combines these desirable characteristics, it was not chosen because of increased hardware complexity. In order to apply this filter, the local variance σ_I^2 of the terms I_i around each point must be calculated from the equation

$$\sigma_I^2=\sum_{i=1}^{2K+1} I_i^2/(2K+1)-[\sum_{i=1}^{2K+1} I_i/(2K+1)]^2 \qquad (5.1)$$

where 2K+1 is the window size. Calculating the terms I_i^2 is not a problem. It can be easily done using look-up tables stored in Programmable Read Only Memories (PROMs). However, all the subsequent stages of the filter must be designed to cope with 12-bit numbers, if the input data I_i are 6-bit wide, something which increases considerably the size of the circuit. Also, the

calculation of the filter's output from (4.25) needs floating-point multiplications and divisions which are very difficult to implement in hardware. Another candidate for hardware implementation was the DW-MTM filter (Section 4.3.2) which requires only simple fixed-point operations like magnitude comparisons. The algorithm which was finally chosen is very similar and equally efficient as the DW-MTM filter but it performed slightly better in the simulations.

5.2. The algorithm

The algorithm consists of two cascaded one-dimensional filters operating on vertical directions. First, axial processing is performed by means of sigma filtering. The sigma filter (Lee, 1983a), is a nonlinear edge preserving technique which compares favourably with other noise smoothing filters. More specifically, it introduces less distortion to noisy edges than the median (Pomalaza-Raez & McGillem, 1984) and offers equally satisfactory performance to that of Lee's local statistics algorithm in smoothing synthetic aperture radar images corrupted by speckle noise (Lee, 1983b). The sigma filter owes its signal preservation properties to the fact that at each point it attempts to identify those terms inside the window which are likely to belong to the same population as the central pixel and uses only these to calculate the output. The rest of the terms are assumed to come from a different population and are excluded from further calculations. For a 2K+1-point window which includes the terms I_1, ..., I_{2K+1}, the output O_{SG} is equal to

$$O_{SG}=\sum_{i=1}^{2K+1} w_i I_i / \sum_{i=1}^{2K+1} w_i \qquad (5.2)$$

where

$$w_i=1 \text{ for } |I_i-I_{K+1}|\leq q$$
$$w_i=0 \text{ for } |I_i-I_{K+1}|>q \qquad (5.3)$$

q is a threshold which depends on the standard deviation of noise. Through this quantity the filter utilizes information about the signal and noise statistics in an implicit manner, without having to calculate the local statistics around every point. By taking into account that the standard deviation of speckle is assumed to be proportional to the square root of the mean and by using the central pixel I_{K+1} as an approximation of the mean, the threshold q has the signal-dependent form

$$q=c\{I_{K+1}\}^{1/2} \tag{5.4}$$

Comparison between equations (5.2) - (5.4) and (4.13) - (4.15) shows that the sigma and DW-MTM filters are very similar. Their only difference is that the DW-MTM filter uses the median O_{med} of a smaller window as a first estimate of the true signal intensity whereas the sigma filter uses the central pixel I_{K+1} itself. The implication of this choice is that if a positive (negative) spike with very large (small) intensity compared to its neighbours occupies the centre of the window it will be preserved, because the other pixels fall outside the intensity range $[I_{K+1}-q, I_{K+1}+q]$ and the sum of (5.2) includes only the central pixel itself. In order to overcome the undesirable property of spike preservation, Lee (1983a) has suggested replacing the output O_{SG} by the average of the central pixel's immediate neighbours (4 in our case) if the number of pixels within the intensity range is smaller than or equal to a prespecified value M.

$$O'_{SG}=O_{SG} \qquad \text{if} \quad \sum_{i=1}^{2K+1} w_i - M > 0$$

$$O'_{SG}=[I_{K-1}+I_K+I_{K+2}+I_{K+3}]/4 \quad \text{otherwise} \tag{5.5}$$

Experimentation in software showed that the minimum window size of

the sigma filter to offer adequate noise reduction was equal to 17 points. In determining the window size of the hardware filter the quantity of interest is not the actual number of points but the spatial extent of the window, defined as

(spatial extent)=(window size)(speed of sound)/2(digitizing frequency)

For the simulation data, the digitizing frequency was 4 MHz at a depth of 197 mm. On the other hand, the Z/S scanner digitizes the echoes at 1.66 MHz for the same depth. Hence, a 7-point window has the same spatial extent as the 17-point window for the simulation. Ideally, a 9-point window would be preferable but it was not chosen because our aim was to keep the size of the circuit as small as possible.

The simulation showed that processing only in the axial direction produces images having a blotchy appearance, which could be removed by a 3-point lateral filter. The spatial extent of the window in the lateral direction is determined by the line density. Since the input data used for the simulation and for processing in hardware have equal line densities, a window size of 3 points was chosen for the hardware filter. For such a small window size it was observed that the sigma and median filters have similar performance, with the median offering considerable savings in the number of ICs required to implement it. For this reason, it was decided to perform lateral processing by means of median filtering. However, it must be noted that if a window of 5 or more points is needed, the sigma filter is preferable because it offers better signal preservation.

5.3. Design and implementation

After studying the circuit diagrams of the Hughes 672 scan converter, it was decided to insert the filter in the echo path directly after analog to digital conversion. It was considered essential for the filter to be as fast as

possible so that it could cope with a variety of digitizing frequencies. The design goal was to achieve a maximum speed of 150 ns per sample which corresponds to 330 Million Instructions Per Second, if we consider that in the software implementation of the algorithm approximately 50 Fortran statements are executed for every output value. This performance can be obtained by adopting a serial pipeline design. In a pipeline architecture, the processing task is decomposed into subtasks which are performed in cascaded stages, with the intermediate results transferred from one stage to the next using synchronous registers (Venetsanopoulos & Cappellini, 1986). Since the speed of the pipeline is determined by the slowest stage, parallel processing with several calculations performed simultaneously within a stage can be used to increase its performance.

The design was based on standard TTL integrated circuits and look-up tables implemented using fast PROMs. The circuit diagrams can be found in Appendix C. The filter requires the following signals from the scanner; ADCLK : clock of the A/D converter, LP : pulse which indicates the end of an A-scan line, $G_0 \ldots G_5$: 6-bit output of the A/D converter with G_0 denoting the Least Significant Bit. A brief description of the circuit follows.

5.3.1. Axial processing: Sigma filter

The 8-bit serial-in parallel-out registers (IC3 - IC8) of page 219 are used to implement a 6-bit, 7-word shift register with the data moving one position to the right at the low-to-high transition of the clock pulse ADCLK. The first and last term to enter the shift register, that is, the term which will be discarded after the next clock pulse and the most recent one, are denoted by I_1 and I_7, respectively.

The adders of page 220 calculate the 4-neighbour average of equation (5.5).

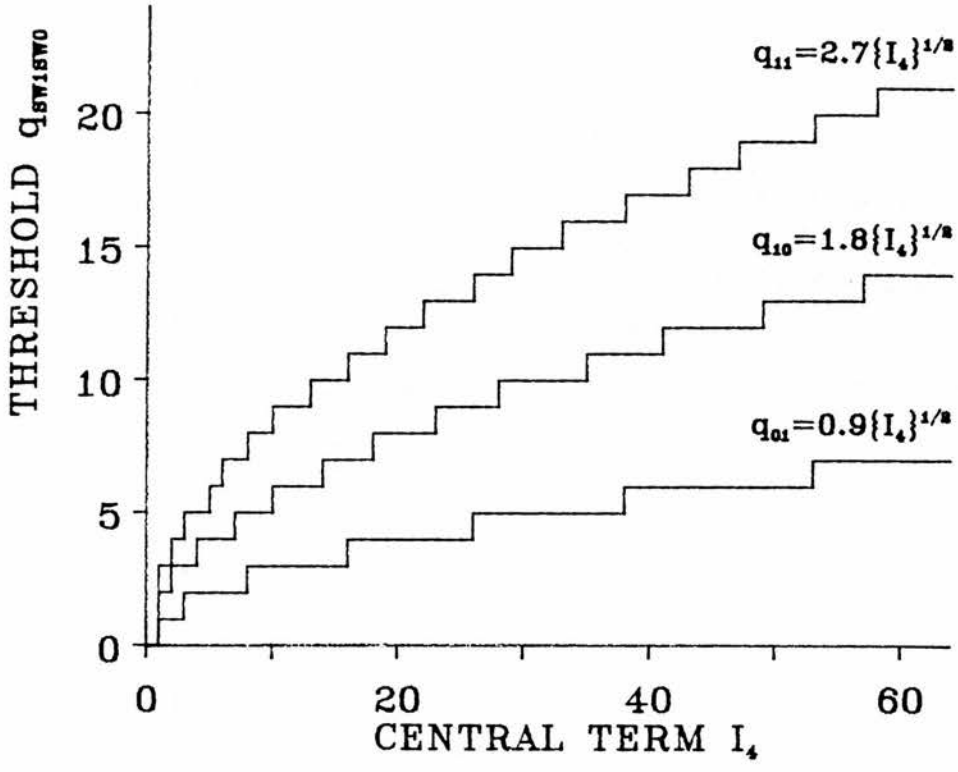

Figure 5.2 : Threshold curves used in the axial processing stage. The curve q_{00}, not shown here, is equal to zero for every value of I_4 and corresponds to no smoothing at all.

The weights w_i of equation (5.3) are calculated by the circuit of page 221. Two comparators and an AND gate set w_i to one if $I_4-q \leq I_i \leq I_4+q$ or zero otherwise. The values I_4-q, I_4+q are obtained from the look-up tables IC15, IC16. In order to be able to control the amount of smoothing performed by the filter, four sets of values have been stored in the look-up tables. These can be selected by the binary switches SW0 and SW1. When both switches are in the zero logical state the threshold q_{00} is equal to zero for every value of I_4 and consequently no smoothing is performed. The thresholds q_{SW1SW0} for the other three sets are displayed in Figure 5.2. A final comment on this part of the circuit is that in order to use as few ICs as possible, only the three most recent terms I_5, I_6, I_7 are compared with $I_4 \pm q$. The values of the weights w_5, w_6, w_7 are then stored and are used to calculate w_3, w_2, w_1 after one, two and three cycles respectively.

The registers of page 222 store the intermediate results of the first stage and transfer them to the second stage of the pipeline. The weights w_i are connected to the CLEAR inputs of the corresponding registers in order to implement the products $w_i I_i$.

The circuit of page 223 is a tree of 4-bit adders which perform the summation $\Sigma w_i I_i$, whereas the sum of the weights Σw_i is obtained from the look-up table stored in IC49.

Finally, another look-up table (IC51, IC52) performs the division $\Sigma w_i I_i / \Sigma w_i$ and the comparator IC50 and the multiplexers IC53, IC54 implement the spike suppression equation (5.5).

The design described above is a straightforward implementation of equations (5.2) - (5.5) which has proved perfectly adequate for our purpose. However, it is not efficient for large window sizes or input data having more than 6 bits. An alternative design which is suitable for a VLSI implementation because it possesses a systolic architecture (Kung, 1982), i.e. it is based on the regular repetition of a basic cell, is described below. Figure 5.3a shows the basic cell of this architecture. A1 is the input term, A2 is the central term of the window, A3 is the threshold q, A4 and A5 are the sums Σw_i, $\Sigma w_i I_i$ from the previous stage. The values stored in A2 - A5 are updated and transferred to B2 - B5 after a delay Z^{-1} equal to the sampling period. A 2K+1-point filter can be constructed by cascading 2K+1 cells, connected as in Figure 5.3b. The rightmost term of the window (the first to enter the shift register) is applied to all the A1 inputs and the sums Σw_i, $\Sigma w_i I_i$ are obtained from the B4, B5 outputs of the last cell. To clarify the operation of this circuit, Table 5.1 provides the output B5 of each cell of a 3-point filter at consecutive time instants t=1, 2, 3, 4. We assume that the rightmost position of the shift register is occupied for the first time at t=1. w_{ij} denotes the weight which corresponds to I_i and is

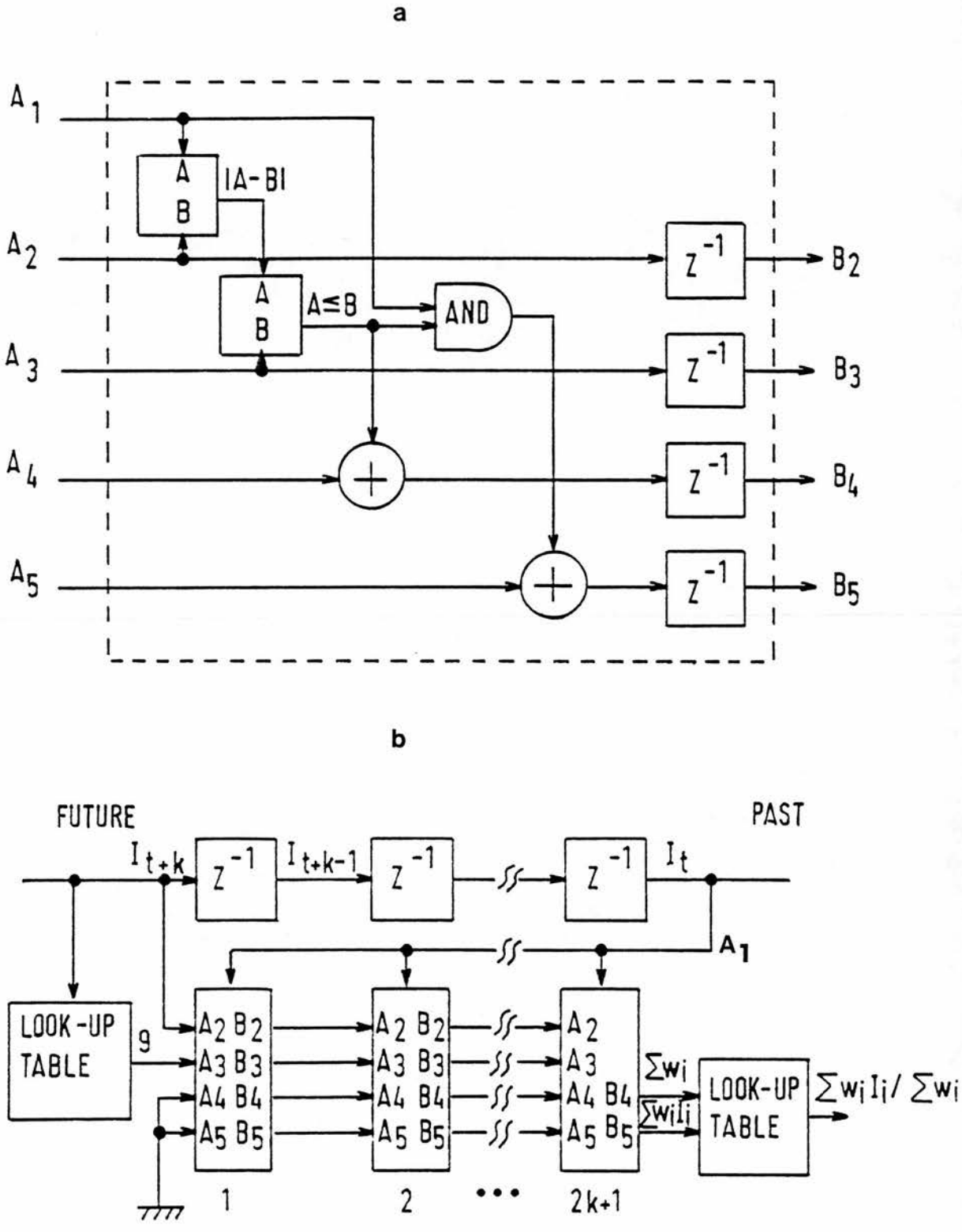

Figure 5.3 : VLSI implementation of sigma filter. **(a)** - Basic cell. **(b)** - Interconnection of 2K+1 cells to form a 2K+1-point filter.

calculated from the comparison between I_i and the central term of the window I_j.

Table 5.1

t	Cell 1	Cell 2	Cell 3
1	$w_{12}I_1$		
2	$w_{23}I_2$	$w_{12}I_1+w_{22}I_2$	
3	$w_{34}I_3$	$w_{23}I_2+w_{33}I_3$	$w_{12}I_1+w_{22}I_2+w_{32}I_3$
4	$w_{45}I_4$	$w_{34}I_3+w_{44}I_4$	$w_{23}I_2+w_{33}I_3+w_{43}I_4$

5.3.2. Lateral processing: median filter

In order to perform 3-point lateral filtering, the last two A-scan lines must be stored. This is achieved by the counters, RAMs and registers of page 225 which implement a variable-length (of up to 1024 points) shift register.The next step is to calculate the median of the input terms I_1, I_2, I_3 . The following design is very efficient for small window sizes. IC65 - IC67 compare each term with the rest. The results of the comparisons are then coded as a 2-bit word S1S0 which is used to select the appropriate term from the 3-to-1 multiplexer formed by IC68 - IC70 . Finally, the median is directed back to the scanner through the register IC73.

5.3.3. Construction and specifications

The circuit was constructed on a single board using wire wrapping (Figure 5.4). A separate board which simulates the scanner was built to test the numerical accuracy of the various parts of the hardware filter. The filter was found to produce accurate results up to a minimum clock period of 140 ns which corresponds to a maximum operating frequency of 7.14 MHz. During the construction, the combination of several factors such as a very high

operating frequency, a large number of ICs changing logic state simultaneously and the inferiority of wire wrapping compared to printed circuit construction created problems that are not generally encountered in a less complex design. The most important of all was the sensitivity to glitches in the power and ground lines. In fact, the first prototype to be constructed could only produce accurate results up to a frequency of a few hundred kHz. At higher frequencies, some ICs would occasionally be locked in an oscillating state. Several attempts were made to solve this problem, but it was finally overcome only after designing and building a new circuit with better power distribution lines.

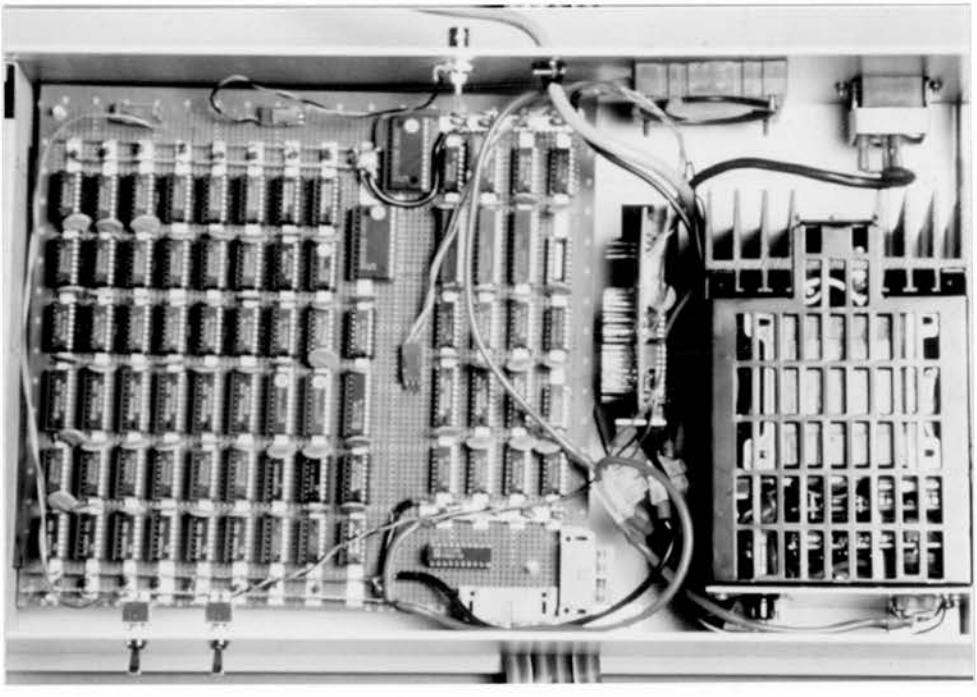

Figure 5.4 : Prototype hardware filter.

The final circuit contains 73 ICs and has an approximate cost of £300. Both these figures are rather modest compared to other designs such as a 3 X 3 median filter which needs more than 200 hundred ICs (Perlman et al,

1987) or a two-dimensional recursive filter which has an estimated cost of $5000 (Ty & Venetsanopoulos, 1986). The circuit is relatively compact but its complexity and size could be further reduced if custom or semicustom devices such as Programmable Logic Arrays had been used.

To summarize, the specifications and main features of the real-time speckle suppression filter are:

- Power consumption 12 Watts
- 6-bit input data
- 7-point Sigma filter along the axial direction
- 3-point median filter along the lateral direction
- Processing at video rates (max operating frequency 7.14 MHz)
- Adjustable smoothing (3 settings)
- Simple and cost effective construction.

5.4. Applications

The hardware filter was connected to the Z/S scanner through two 16-way ribbon cables. Its smoothing action was controlled by a hand-held switch box which selected one of the threshold curves q_{SW1SW0}. A few examples of processing, taken from the clinical evaluation of the hardware filter, are presented below.

Figure 5.5a shows an unprocessed scan of normal liver and the right kidney (threshold q_{00}) whereas Figure 5.5b displays the result of light smoothing (threshold q_{01}). This figure demonstrates the filter's ability to preserve both strong edges and small detail. The noise reduction offered can

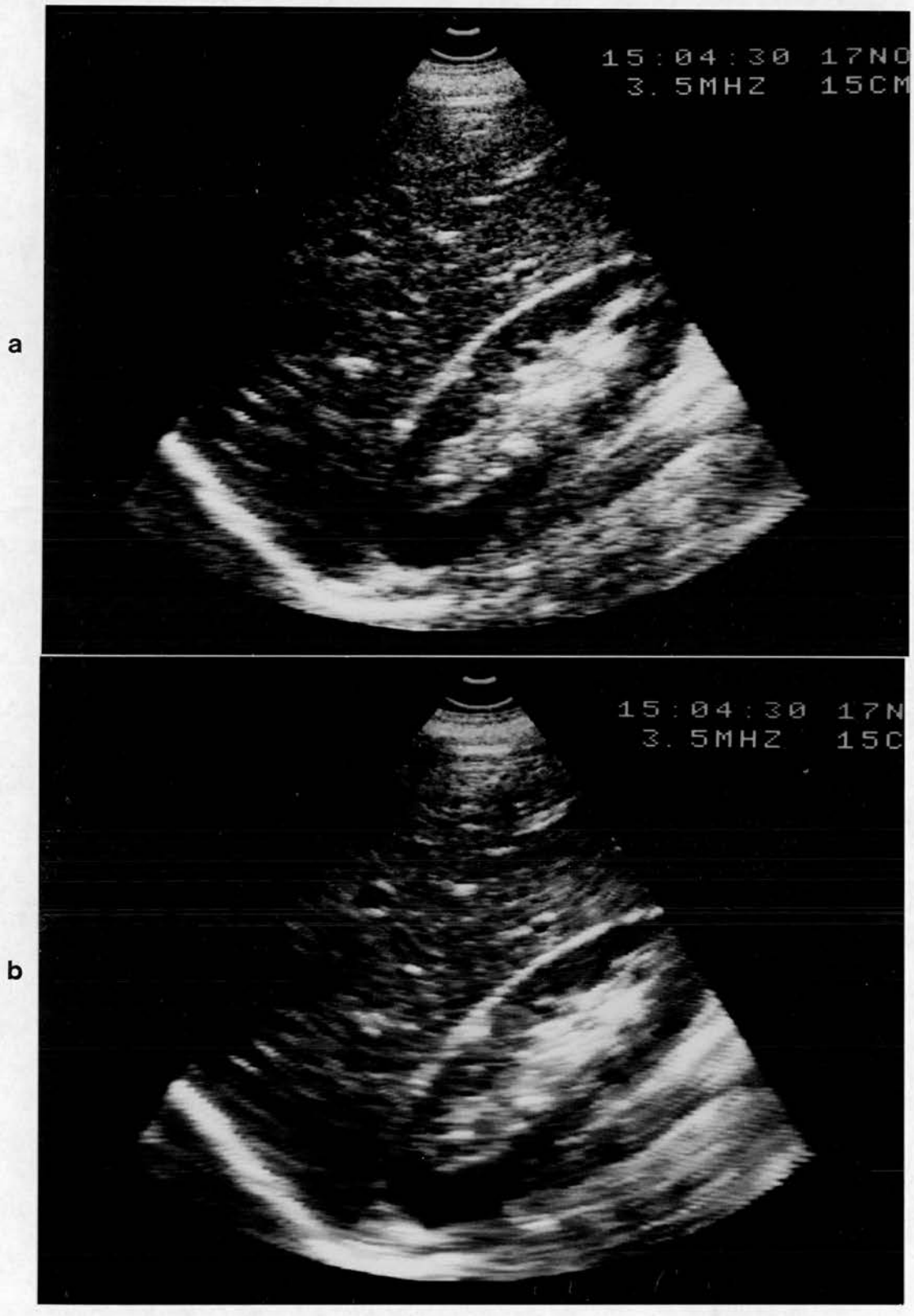

Figure 5.5 : Scan of normal liver and kidney. **(a)** – Original. **(b)** – Processed using the light smoothing curve q_{01}.

be appreciated better by comparing the magnified regions of Figure 5.6.

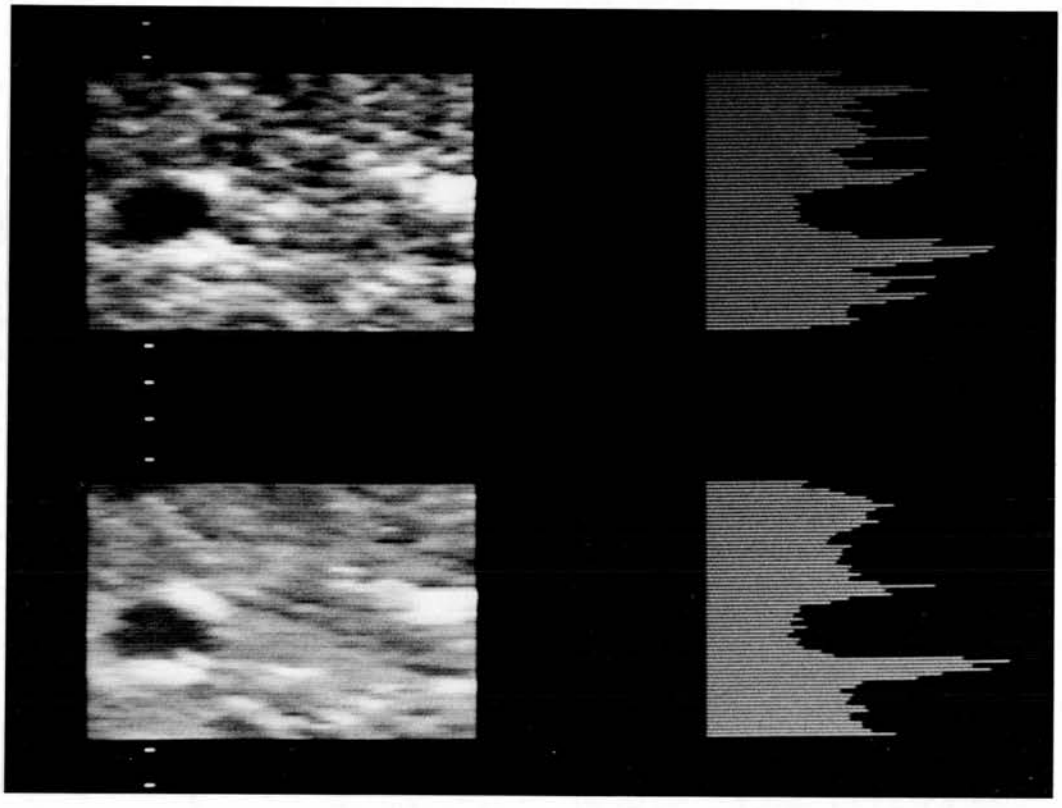

Figure 5.6 : Magnified regions of Figure 5.5a and 5.5b plus vertical intensity profiles along the dotted line.

The effect speckle has on contrast resolution is demonstrated by the scans of diffuse liver disease shown in Figure 5.7. Slight differences in echogenicity within the liver parenchyma, which were previously masked by the presence of speckle, become more apparent in the processed image of Figure 5.7b, which was obtained using the light smoothing threshold q_{01}.

Finally, an example of heavier smoothing (threshold q_{10}) is presented in Figure 5.8. The original scan (Figure 5.8a) is an oblique view through the upper abdomen showing the gallbladder, an aortic aneurysm and part of the liver. The processed scan (Figure 5.8b) is of course smoother than the original but also exhibits better contrast and boundary definition. However, a slight degradation of bright structures can be observed in the processed image. This

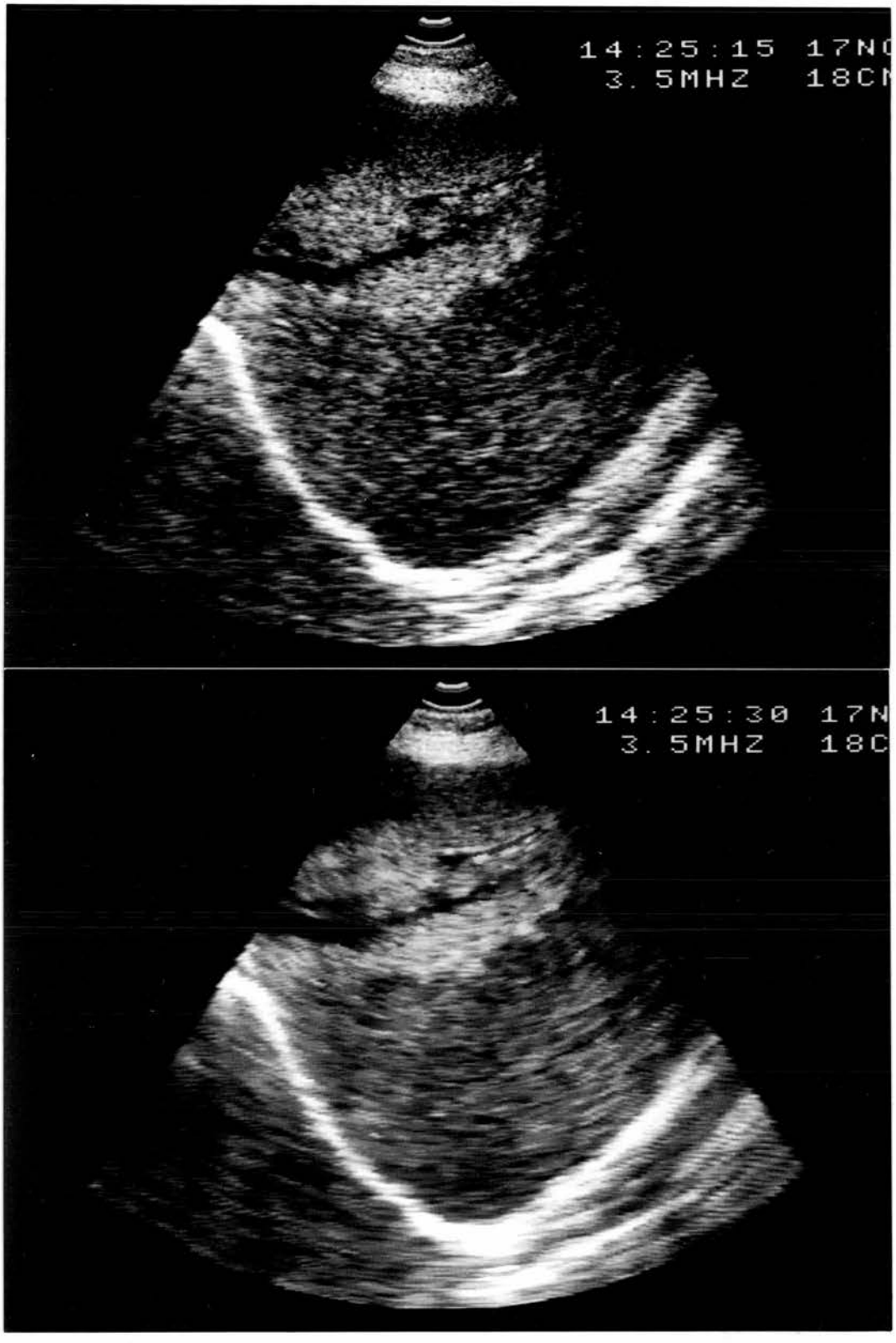

a

b

Figure 5.7 : Diffuse liver disease. **(a)** – Original. **(b)** – Processed using the light smoothing curve q_{01}.

Figure 5.8 : Liver, gallbladder and aortic aneurysm. **(a)** - Original. **(b)** - Processed using the heavy smoothing curve q_{10}.

is due to the shape of the threshold curves used (see Figure 5.2). Better signal preservation can be achieved if the threshold q obtains small values for high signal intensities. An interesting idea which we plan to implement in the near future is to set the threshold curve interactively using a number of sliding potentiometers. In this way, it will be possible to try a large number of curves very easily and determine the most suitable.

Although the filter design was based on the specifications of the Z/S scanner, it was considered important to assess its performance with more than one machine. For this reason, the hardware was modified by redesigning its timing circuits and the filter was connected to a Siemens Sonoline SX and a Dynamic Imaging Concept 1 scanner. Unfortunately, both scanners perform 4-bit A/D conversion. The inadequacy of using only 16 grey scale levels to display an image was clearly demonstrated after noise reduction, with the scans exhibiting "false contouring" (Gonzalez & Wintz, Chapter 2, 1987) which is the main artifact associated with poor quantization. In our opinion, digital smoothing is not suitable for direct application on 4-bit data from ultrasonic scans.

In conclusion, the prototype filter described here has demonstrated that speckle suppression can be performed in real-time without loss of genuine image detail. Furthermore, this can be achieved by using an algorithm of moderate complexity and readily available integrated circuits without the need for "exotic" and highly complex devices.

CHAPTER 6

CLINICAL EVALUATION OF SPECKLE SUPPRESSION TECHNIQUES

6.1. Introduction

The application of image processing in medicine aims at improving the quality of an image and increasing its perceivable information content. The degree of success (or failure) of a technique in achieving these aims varies considerably from image to image because of different anatomical views, pathological findings and quality of the original data. It is therefore very important to assess the usefulness of an image processing technique as objectively as possible before applying it in a clinical environment. However, a discrepancy seems to exist between the large number of techniques proposed in the literature and the very few reports (positive or negative) on their clinical benefits. This is certainly the case for noise suppression in ultrasonic imaging. Although a respectable amount of work in this area has been accumulated over the years, as far as we know, evaluation data can be found only in one paper which has examined the effect of digital averaging in cardiac border definition (Petrovic et al, 1986). In our opinion, the lack of evaluation results does not imply that researchers have ignored the need for an objective assessment of their work. It rather demonstrates the difficulties involved in organizing and carrying out this task in a satisfactory way. A list of image processing evaluation studies in other diagnostic modalities, mainly nuclear medicine, can be found in two review articles by Todd-Pokropek (1980) and Sharp (1987).

A large number of evaluation methods attempts to determine the effect of a processing, or more generally a diagnostic, technique on the detectability of abnormalities contained in an image. The most comprehensive and realistic method is based on the analysis of Receiver Operating Characteristic (ROC) curves derived from clinical data (Swets et al, 1979). ROC

curves have been used for evaluating a wide range of techniques, including noise smoothing filters applied to radioisotope images (Rai et al, 1979). The main drawback of this approach is that a large number of images with unequivocally established pathology, what is usually referred to as "ground" or "absolute truth", must be available. This necessitates either biopsy or autopsy to be performed on patients or alternatively a follow-up period of several years. Obviously, it is very difficult to complete the collection of this kind of data within the time limits imposed by a Ph.D. project.

The problem of the "absolute truth" can be overcome by using clinical images, which are known to be normal, with artificial (computer generated) abnormalities superimposed on them (Houston et al, 1979). However, the clinical relevance of results obtained from such studies is determined primarily by how realistically the computer generated artifacts can simulate true pathology. We have explored this approach but without much success.

Phantoms which contain targets of varying sizes and intensities can also overcome the problem of establishing the "absolute truth". A phantom of this type, which has been designed for studying the detectability of lesions in ultrasonic scans (Smith et al, 1983), has recently become commercially available (Contrast/detail phantom, Nuclear Associates). The use of this phantom would have allowed us to determine the effect of speckle suppression on the contrast resolution of a scan, but unfortunately we did not have access to it.

Instead of trying to determine the presence of an abnormality, an alternative evaluation approach is to investigate the effect a processing technique has on image quality (Cohen et al, 1978; Sharp et al, 1982; Jaffe et al, 1982). This approach was followed here by using clinical data and asking experienced observers to judge the quality of the images before and after

speckle suppression. In order to form a more complete picture of the effectiveness of speckle suppression, image quality was defined in terms of several criteria. The methodology followed in the clinical evaluation is described in the next section.

6.2. Methodology

Three groups of speckle suppression techniques were evaluated; namely frame averaging, software spatial filtering and hardware spatial filtering. The frame averaging techniques of Chapter 3 were evaluated first because although recursive averaging has been incorporated into scanners for a number of years and is being used by clinicians in routine scanning, to our knowledge no assessment of its clinical value has appeared in the literature so far. From the software techniques presented in Chapter 4, the adaptive weighted median and directional filters were chosen to be evaluated partly because they are original and partly because they possess desirable features, i.e. preservation of low-contrast areas and enhancement of edges/boundaries respectively, which are not found in other filters. Finally, the hardware filter of Chapter 5 was included in the evaluation because the ability to operate in real-time makes it suitable for use in a clinical environment.

The evaluation was based on abdominal images obtained during routine scanning. Frame averaging and hardware spatial filtering were applied to between one and three anatomical views for each patient. The views had been previously identified by the radiologist during the clinical examination of the patient. The data used for the software spatial filters were recorded on video tape and later transferred to a computer for processing. No attempt was made to select a special group of patients. Apart from the frame averaging trial, where a large proportion of the patients had breast cancer and were scanned because of suspected liver metastasis, the rest represented a typical sample of the cases referred to the X-ray department for abdominal scanning.

A number of scanners was used to acquire the images in order to draw more general conclusions about the value of speckle suppression.

The original and processed scans were photographed on standard X-ray film using an EMI Multi-Imager 6 (2 by 2 scans per film) and an Agfa Gevaert Scopix 100 imager (3 by 3 scans per film). No attempt was made to randomize the relative positions of the scans on the film because each processing technique produced distinctive and easily recognizable results. At the end of the evaluation 293 sets, each one including three or four scans of the same view, had been obtained (1024 images in total).

The number of observers who took part in the evaluation was determined by the availability of experts willing to participate. The images of the first two groups were evaluated by a consultant radiologist (PLA) and a physicist (WNMcD), both with long experience in medical ultrasonics, who judged the medical and technical aspects respectively of processing. For the evaluation of the hardware spatial filter, it was possible to include two more observers; a consultant radiologist (SRW) and a physicist (SDP). The observers judged the images, which were displayed on a light box, in sessions lasting between one and two hours, spending an average time of 2 - 4 minutes per set.

Five quality indices were evaluated. The observers were asked to give marks to the images of each set according to their noise level, contrast, boundary definition[1] and, in the case of the radiologists, diagnostic information. The images were rated on a four-point numerical scale with 1

[1] A certain overlap exists between contrast and boundary definition in the sense that they can be determined by the presentation of either bright echoes (e.g. vessel walls) or midgrey level areas of slightly different echogenicity (e.g. hypoechoic lesion in normal tissue background). It was left to the observers to decide which of the two features, i.e. bright echoes and tissue regions, was more important for each particular scan.

indicating very poor quality and 4 excellent quality . The observers were allowed to give equal marks if they believed that some or all the images of a set were comparable. The observers were also asked to rank the images of a set in order of preference with mark 1 given to the best image. This last category can be considered as an index of overall quality.

6.3. Statistical analysis

After seeking advice from the Department of Medical Statistics, it was decided to analyse and present the results of the evaluation separately for each scanner, because the success or failure of a processing technique is determined to a great extent by the technical characteristics of the original image. A similar decision was taken for the observers, since each individual bases his judgements about the quality of an image on a different set of criteria.

When comparing experimental results, statistical methods can help in answering the question: are the observed differences between the means of the various samples real or can they be attributed to chance ? In order to give an answer, the null hypothesis H_0 (the samples come from the same population - no real differences exist) must be tested against the alternative hypothesis H_A (the samples belong to more than one population - the observed differences are real). Testing the null hypothesis at an n% level of significance means that there is a probability P=n/100 of rejecting H_0 while it is true. The smaller n is the higher the differences between the means must be before we accept them as real and, therefore, the more confident we are that our data are indeed distinguishable. For this evaluation, the commonly used, and rather strict, 1% level of significance was chosen.

Since each group of processing techniques included more than two image types, the statistical analysis was performed in two steps. For the noise,

contrast, boundary definition and diagnostic information categories two-way classification analysis of variance (Snedecor & Cochran, Chapter 14, 1980) was used first to determine if at least one image type was different from the rest. Then, and only if the answer to the previous test was positive (i.e. not all types belonged to the same population), multiple comparisons in pairs were performed using the Studentized Range criterion (Snedecor & Cochran, Chapter 12, 1980) in order to decide which differences between the means were statistically significant. The marks for the overall quality category, which are ranks, were analysed by applying the two-way classification Friedman test followed by multiple comparisons between the means using a criterion based on the standard normal percentage points (Daniel, Chapter 7, 1978).

The results of the comparisons can be deduced from the Q values[2] included in Tables 6.1 - 6.7, which give the minimum absolute difference two means must have in order to be distinguishable at a 1% level of significance. The ↑ and ↓ signs preceding the means of the processed images indicate that a speckle suppression technique is better or worse respectively, compared to the original. For the case of frame averaging, the arrows refer to comparisons between images obtained at the same time, i.e. unprocessed I and recursive averaging - unprocessed II and integration.

6.4. Frame averaging

Two speckle suppression techniques were tested in this evaluation: recursive averaging and integration. The images were obtained over a period of six months using the GL Ultrasound Ltd Z/S and Siemens Sonoline SX scanners, both of which had 3.5 MHz mechanical sector probes. For each

[2]For the overall quality category, Q is determined by the number of samples and level of significance. However, for the first four categories Q depends also on the actual marks and consequently may have different values from one category to the other.

anatomical view a set of two unprocessed and two processed scans was recorded on X-ray film following the protocol described in Section 3.5 . A number of sets had to be excluded because the scans were not anatomically comparable. The evaluation results of the remaining sets, one hundred and one sets from fifty one patients for the Z/S and forty four sets from twenty two patients for the SX scanner, are presented in Tables 6.1 and 6.2.

6.4.1. Results

The first observation from Tables 6.1 and 6.2, is that no significant differences exist between unprocessed image I and II for all categories, scanners and observers, something expected since both image types are scans of the same anatomical views.

The analysis of the radiologist's marks for the Z/S scanner shows that both processing techniques produced images with lower noise level. The averaging process enhanced the appearance of poorly defined boundaries but at the same time blurring due to patient movement reduced the brightness of edges and small details and resulted in loss of contrast. The improvement in noise and boundary definition was reflected on the overall quality category where there was a marked difference in favour of the processed scans. Diagnostic information was the only category without significant differences. Although the marks of the physicist follow a similar pattern, it seems that he was more sensitive to the noise level of an image and this influenced his judgement about the performance of noise reduction techniques in a positive way. He believed that there was an improvement in contrast, probably because he thought that loss of contrast in the presentation of bright echoes was offset by gain in contrast between areas of slightly different echogenicity after noise smoothing, and he expressed a stronger overall preference for the processed images than the radiologist.

TABLE 6.1 : EVALUATION OF FRAME AVERAGING

Means ± Standard Deviations for the GL Ultrasound Ltd Z/S scanner
101 sets of images from 51 patients

Radiologist (PLA)

Image Type	[1] Noise	[1] Contrast	[1] Boundary Definition	[1] Diagnostic Information	[2] Overall Quality
Unprocessed Image I	2.12±0.68	2.77±0.44	2.28±0.63	2.45±0.71	2.77±1.02
Recursive Averaging	↑2.78±0.56	↓2.57±0.53	↑2.70±0.50	2.62±0.66	↑1.81±0.86
Unprocessed Image II	2.09±0.63	2.73±0.49	2.22±0.62	2.39±0.69	3.12±0.93
Integration	↑2.90±0.54	↓2.34±0.60	↑2.61±0.60	2.45±0.68	↑2.30±1.17
[3] Q	0.16	0.16	0.21	0.19	0.57

Physicist (WNMcD)

Image Type	[1] Noise	[1] Contrast	[1] Boundary Definition	[2] Overall Quality
Unprocessed Image I	1.77±0.59	2.28±0.75	2.47±0.75	3.22±0.84
Recursive Averaging	↑2.75±0.64	↑2.77±0.63	↑2.80±0.68	↑1.71±0.80
Unprocessed Image II	1.98±0.66	2.34±0.73	2.46±0.83	3.13±0.86
Integration	↑3.32±0.58	↑2.72±0.73	2.58±0.81	↑1.93±1.03
[3] Q	0.22	0.31	0.31	0.57

[1] 1 = poor ; 4 = excellent quality
[2] 1 = first ; 4 = last in order of preference
[3] Minimum statistically significant difference between two means at 1% level

TABLE 6.2 : EVALUATION OF FRAME AVERAGING

Means ± standard deviations for the Siemens Sonoline SX scanner
44 sets of images from 22 patients

Radiologist (PLA)

Image Type	[1] Noise	[1] Contrast	[1] Boundary Definition	[1] Diagnostic Information	[2] Overall Quality
Unprocessed Image I	2.27±0.54	2.66±0.47	2.43±0.50	2.39±0.61	2.11±0.83
Recursive Averaging	↑2.70±0.50	2.41±0.49	2.66±0.47	2.34±0.67	1.98±1.10
Unprocessed Image II	2.25±0.53	2.66±0.47	2.39±0.53	2.30±0.69	2.43±0.91
Integration	↑2.70±0.50	↓2.09±0.70	2.27±0.65	↓2.02±0.72	↓3.48±0.94
[3] Q	0.22	0.28	0.29	0.27	0.87

Physicist (WNMcD)

Image Type	[1] Noise	[1] Contrast	[1] Boundary Definition	[2] Overall Quality
Unprocessed Image I	1.84±0.52	2.16±0.47	2.48±0.75	3.20±0.94
Recursive Averaging	↑2.89±0.49	2.32±0.63	2.68±0.59	↑1.89±0.86
Unprocessed Image II	2.02±0.69	2.02±0.34	2.50±0.72	2.61±1.11
Integration	↑3.64±0.53	2.00±0.64	2.48±0.89	2.30±1.10
[3] Q	0.36	+∞	+∞	0.87

[1] 1 = poor ; 4 = excellent quality
[2] 1 = first ; 4 = last in order of preference
[3] Minimum statistically significant difference between two means at 1% level

It is interesting to note that the performance of frame averaging techniques, and especially integration, was generally poorer for the images obtained with the SX scanner. Comparison with the marks given by the radiologist for the Z/S scanner shows that the margin in favour of the processed images was reduced or, in the case of integration, was reversed. For the radiologist, recursive averaging and integration were no longer significantly better than the original images as far as boundary definition is concerned. Also, the contrast of the processed images deteriorated and integration reduced the diagnostic information of a scan. Overall, the radiologist judged integration to be inferior whereas no significant differences exist between the other image types. The physicist still ranked the processed images at the top of his preference but the margin from the unprocessed images was reduced. The poorer performance of frame averaging can be explained by the fact that the SX scanner produces images which are generally less noisy and more balanced compared to those obtained by the Z/S scanner. As a result, the blurring introduced by the frame averaging techniques weighs more in the observers' judgement than the noise reduction offered.

6.4.2. Discussion

The results of the evaluation suggest that frame averaging can improve the quality of a scan. The amount of improvement is related to the quality of the original image with better results expected for noisier scans. Recursive averaging is generally preferable to integration because it offers superior and more consistent performance. One could argue that the blurring introduced by integration and, as a result of that, its relatively poor performance is due to the large number of frames chosen to be integrated (32 in this case), and consequently the two techniques would have had comparable performance if a smaller number of frames had been chosen. Although this is probably true, recursive averaging is still preferred because it

produces a live instead of a frozen picture.

The main drawback of recursive averaging is that its effect on an image is determined in a random and uncontrollable manner by patient movement. With the "right" amount of movement (the term "right" meaning that the movement is adequate to produce a relatively smooth image but not excessive so that heavy blurring is introduced) an image of better quality than the original can be obtained. This has been demonstrated already in Figure 3.4 , one of the best sets of the series, and another successful example is given in Figure 6.1. In this figure, the appearance of the irregular and poorly defined boundaries between liver and kidney in the original has clearly been enhanced in the processed image and the differences in the echogenicity of the two organs can be appreciated better. If, however, the position of the tissue being imaged relative to the ultrasound beam does not change, the amount of smoothing performed is negligible and the processed image looks very similar to the original apart from a slight loss of contrast, as demonstrated by Figure 3.5 . At the other extreme, large amounts of movement, caused either when the operator moves the probe rapidly over the body surface of a patient or when a moving structure is imaged, result in a severely blurred image. No such images were acquired for the evaluation since they are useless from a clinical point of view.

In conclusion and without overlooking the image quality improvement that recursive averaging can offer, it is not considered as the solution to the problem of ultrasonic speckle because its effectiveness in suppressing this artifact is determined primarily by random factors and cannot be controlled by the users.

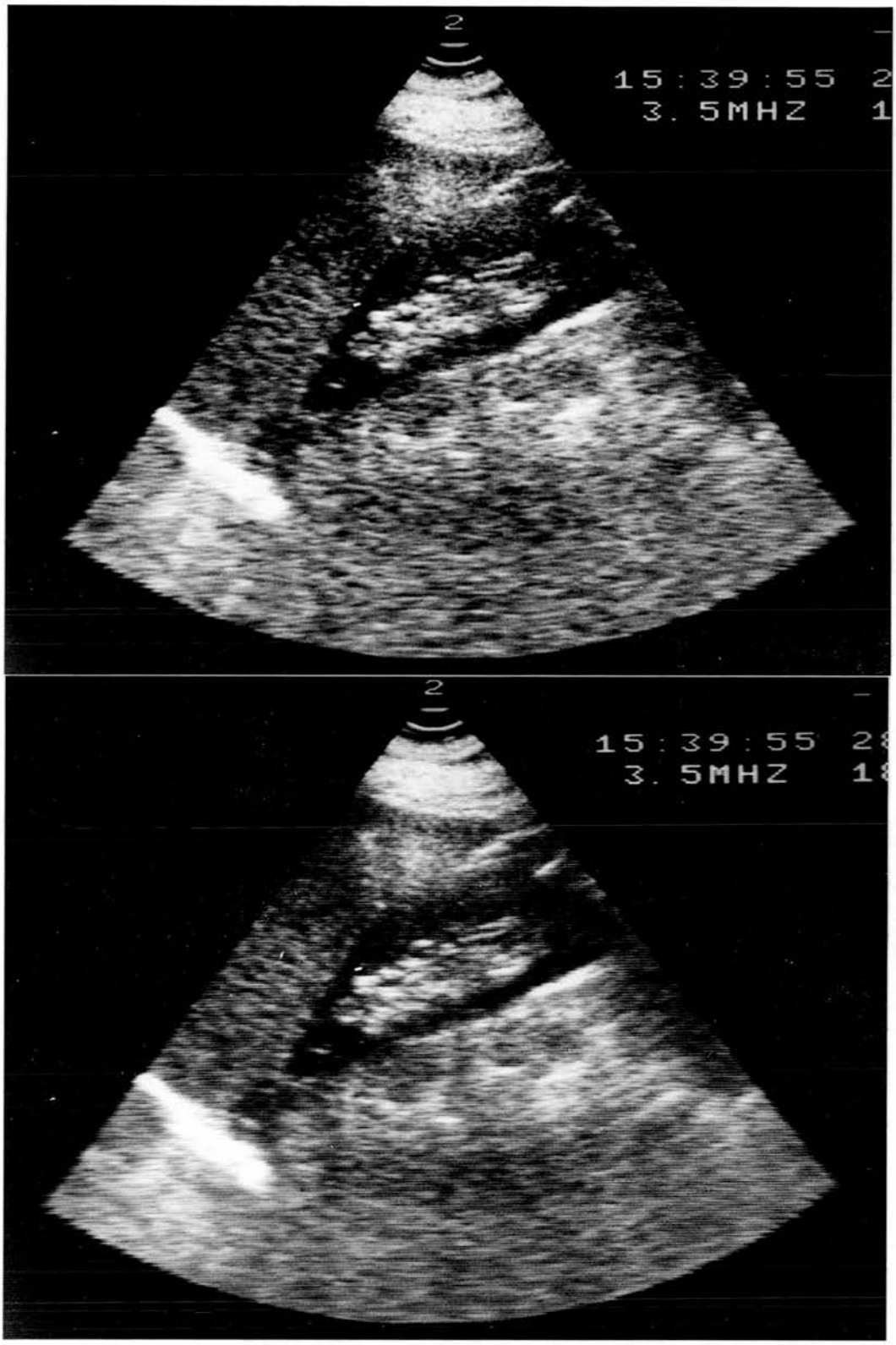

Figure 6.1 : A successful application of recursive averaging to a scan of normal liver and kidney. **(a)** – Original. **(b)** – Processed.

6.5. Software spatial filtering

The adaptive weighted median and directional filters were included in this evaluation. The filters were applied to abdominal scans acquired using the GL Ultrasound Z/S (twenty two patients), Siemens Sonoline SX (nineteen patients) and Acuson 128 (sixteen patients) real-time scanners, all of which had 3.5 MHz transducers. In total, seventy five scans (twenty five from each scanner) were recorded on video tape during clinical examination and transferred to the MicroVax for processing and storage. For the Z/S and SX scanners, the filter parameters mentioned in Sections 4.4.3 - 4.4.4 were used, that is, 9 X 9 window, c=20 for the adaptive weighted median, 7-point smoothing window, k=2, 7-point band-pass window, Kaiser window attenuation 50db, f_L=0.1, f_H=0.4 for the directional filter. The Acuson images, which exhibit a more pronounced speckle pattern, were processed using a 11 X 11 window, c=0.16 for the adaptive weighted median and a 9-point smoothing window for the directional filter, with the other parameters same as before. It would have been preferable if the observers had viewed the original and processed images directly on the computer display. However, due to practical problems, the images were recorded on X-ray film and were viewed using a light box. The results of the evaluation are presented in Tables 6.3 - 6.5.

6.5.1. Results

By comparing the results for the three scanners, a pattern similar to the one found in the frame averaging evaluation emerges. More specifically, the results indicate that the greatest improvement is obtained by processing images of poor quality acquired using the Z/S scanner. On the other hand, processing applied to the SX images, which are quite smooth and of good quality, offers the least improvement. The Acuson is one of the most advanced scanners available at the moment with excellent spatial resolution and image quality which is definitely superior to that of the Z/S and SX scanners.

TABLE 6.3 : EVALUATION OF SOFTWARE SPATIAL FILTERING

Means ± Standard Deviations for the GL Ultrasound Ltd Z/S scanner
25 sets of images from 22 patients

Radiologist (PLA)

Image Type	[1] Noise	[1] Contrast	[1] Boundary Definition	[1] Diagnostic Information	[2] Overall Quality
Unprocessed Image	2.28±0.53	2.84±0.67	2.40±0.49	2.52±0.64	1.80±0.57
Ad W Median Filtering	↑3.32±0.55	2.72±0.53	2.64±0.56	2.36±0.62	↓2.84±0.46
Directional Filtering	↑2.92±0.48	2.84±0.54	↑3.04±0.45	2.68±0.61	1.36±0.56
[3] Q	0.31	+∞	0.37	+∞	0.83

Physicist (WNMcD)

Image Type	[1] Noise	[1] Contrast	[1] Boundary Definition	[2] Overall Quality
Unprocessed Image	1.16±0.37	2.16±0.37	2.04±0.53	3.00±0.00
Ad W Median Filtering	↑2.92±0.48	2.36±0.62	2.32±0.95	↑1.48±0.50
Directional Filtering	↑2.32±0.55	2.12±0.32	↑2.84±0.46	↑1.52±0.50
[3] Q	0.34	+∞	0.33	0.83

[1] 1 = poor ; 4 = excellent quality
[2] 1 = first ; 3 = last in order of preference
[3] Minimum statistically significant difference between two means at 1% level

TABLE 6.4 : EVALUATION OF SOFTWARE SPATIAL FILTERING

Means ± standard deviations for the Siemens Sonoline SX scanner
25 sets of images from 19 patients

Radiologist (PLA)

Image Type	[1] Noise	[1] Contrast	[1] Boundary Definition	[1] Diagnostic Information	[2] Overall Quality
Unprocessed Image	2.52±0.57	2.40±0.57	2.56±0.50	2.64±0.62	1.56±0.57
Ad W Median Filtering	↑2.80±0.49	2.40±0.56	2.40±0.69	↓2.16±0.61	↓2.96±0.20
Directional Filtering	2.72±0.45	2.40±0.57	2.76±0.51	2.76±0.59	1.48±0.50
[3] Q	0.24	+∞	+∞	0.31	0.83

Physicist (WNMcD)

Image Type	[1] Noise	[1] Contrast	[1] Boundary Definition	[2] Overall Quality
Unprocessed Image	1.68±0.55	2.20±0.63	2.32±0.61	3.00±0.00
Ad W Median Filtering	↑3.44±0.50	2.40±0.49	2.48±0.64	↑1.24±0.43
Directional Filtering	↑2.56±0.50	2.32±0.55	↑2.92±0.63	↑1.76±0.43
[3] Q	0.23	+∞	0.36	0.83

[1] 1 = poor ; 4 = excellent quality
[2] 1 = first ; 3 = last in order of preference
[3] Minimum statistically significant difference between two means at 1% level

TABLE 6.5 : EVALUATION OF SOFTWARE SPATIAL FILTERING

Means ± Standard Deviations for the Acuson 128 scanner
25 sets of images from 16 patients

Radiologist (PLA)

Image Type	[1] Noise	[1] Contrast	[1] Boundary Definition	[1] Diagnostic Information	[2] Overall Quality
Unprocessed Image	2.32±0.47	2.72±0.45	2.36±0.48	2.64±0.48	1.64±0.62
Ad W Median Filtering	↑2.72±0.45	2.68±0.47	2.60±0.49	2.56±0.50	↓2.92±0.27
Directional Filtering	↑2.68±0.47	2.72±0.45	↑2.84±0.37	2.76±0.43	1.44±0.50
[3] Q	0.28	+∞	0.28	+∞	0.83

Physicist (WNMcD)

Image Type	[1] Noise	[1] Contrast	[1] Boundary Definition	[2] Overall Quality
Unprocessed Image	1.64±0.56	2.20±0.49	2.08±0.48	3.00±0.00
Ad W Median Filtering	↑3.24±0.59	2.44±0.57	2.24±0.59	↑1.68±0.47
Directional Filtering	↑2.52±0.64	2.52±0.50	↑3.00±0.49	↑1.32±0.50
[3] Q	0.35	+∞	0.32	0.83

[1] 1 = poor ; 4 = excellent quality
[2] 1 = first ; 3 = last in order of preference
[3] Minimum statistically significant difference between two means at 1% level

However, because the appearance of speckle is quite pronounced, the results for the Acuson fall somewhere between those of the other two scanners.

Looking at the results in more detail, it is clear that both observers believed that processing resulted in images with reduced noise level. However, it is interesting to note that the margin between the adaptive weighted median and the directional filter is much wider for the physicist than for the radiologist. This is probably due to the fact that the two observers have different sensitivities to noise or even different understanding of what the term "noise" means.

Contrast was the only category where processed and unprocessed images were equivalent for both observers and all three scanners.

The filters offered improvement in boundary definition but the differences were statistically significant only for the directional filter.

As far as diagnostic information is concerned, the radiologist believed that the directional filter offered a slight improvement which, however, was too small to be significant. The only significant difference in this category was found for images from the SX scanner processed by the adaptive weighted median filter where the radiologist believed that processing reduced the diagnostic information.

Finally, in the overall quality category the radiologist judged the adaptive weighted median filtered images to be significantly worse than the other two image types. At the same, time he ranked the directional filter first but the margin from the unprocessed images was too small to be significant. The highest difference in favour of the directional filter was found for the Z/S images. This difference would have been significant if more than eighty eight images had been included in the evaluation. On the other hand, the physicist

believed that both filters produced better results. In fact, as can be seen from the zero standard deviation of the unprocessed images, he ranked them always third. The filter ranked first varies from scanner to scanner but overall the physicist expressed a stronger preference for the adaptive weighted median filter.

6.5.2. Discussion

The results of the evaluation suggest that the radiologist and the physicist form their judgements using different criteria. To begin with, it seems that their understanding of the term "noise" is quite different and so are their expectations from processing. The physicist is fully aware of the origin and implications of speckle. Consequently, he treats speckle purely as an undesirable signal and judges the various filters according to how efficiently they can suppress speckle without introducing loss of genuine image detail. On the other hand, the radiologist tends to place less emphasis on speckle suppression and more emphasis on the suppression of signals such as random intensity fluctuations within vessels, cysts, etc, which he is fully convinced are artifactual. Another problem, especially as far as diagnostic information is concerned, is the radiologist's lack of familiarity with the processed images. Since speckle suppression is still an area of research and not an established technique in clinical practice, radiologists have not been exposed to it. As a consequence, they probably feel more confident and are more efficient in interpreting a conventional scan, something for which they have been trained and have accumulated considerable experience, rather than one with suppressed speckle. A comment to this effect was made by the radiologist who took part in the evaluation. He remarked that looking at the processed images made him feel uncomfortable as if there was something missing. This problem, i.e. the lack of texture, was not encountered in the evaluation of frame averaging techniques because although they reduce speckle they still

produce images with a familiar textured appearance. After the above discussion, it is not surprising that the radiologist expressed a preference for the directional filter which offers modest noise reduction but retains the coarser texture, whereas the physicist preferred the adaptive weighted median filter which offers almost complete speckle suppression.

In our opinion, based on the seventy five sets of images from this evaluation but also on the whole involvement in this project, the main advantage of the adaptive weighted median filter is the ability to preserve subtle grey scale variations within the tissue parenchyma. Its major drawback is that under certain circumstances it produces amorphous regions of constant or nearly constant grey level, which evoke the visual impression of structures that have no physical correlate. This behaviour is characteristic of all median-type filters. Bovik (1987) who studied it in detail used the term "blotching effect" to describe it and found that it is related to the window size of the filter used. In this evaluation, blotching was most noticeable in Acuson images which tend to have a large speckle size, especially in the far field. This was probably the reason why the physicist, who was generally more in favour of the adaptive weighted median filter, preferred the directional filter in the evaluation of the Acuson images (Table 6.5).

As far as the directional filter is concerned, its strength lies in the fact that it can combine noise reduction with improved boundary definition. The main problem associated with it, or at least with the present implementation, is that it can only suppress speckle of small size.

The advantages and drawbacks discussed above are demonstrated by the following two figures which display scans of metastatic liver disease. Figure 6.2 is an example of successful processing. The radiologist judged both the processed images to be superior to the original. He also believed that the

adaptive weighted median filter (Figure 6.2b) offered more diagnostic information, probably because it enhanced the visibility of the metastatic deposits (compare the enlarged regions of Figures 6.2a, 6.2b). On the other hand, the processed images of Figure 6.3 were judged to be inferior to the original. Figure 6.3b demonstrates the distracting blotching effect while Figure 6.3c demonstrates the inadequate noise reduction offered by the directional filter.

a

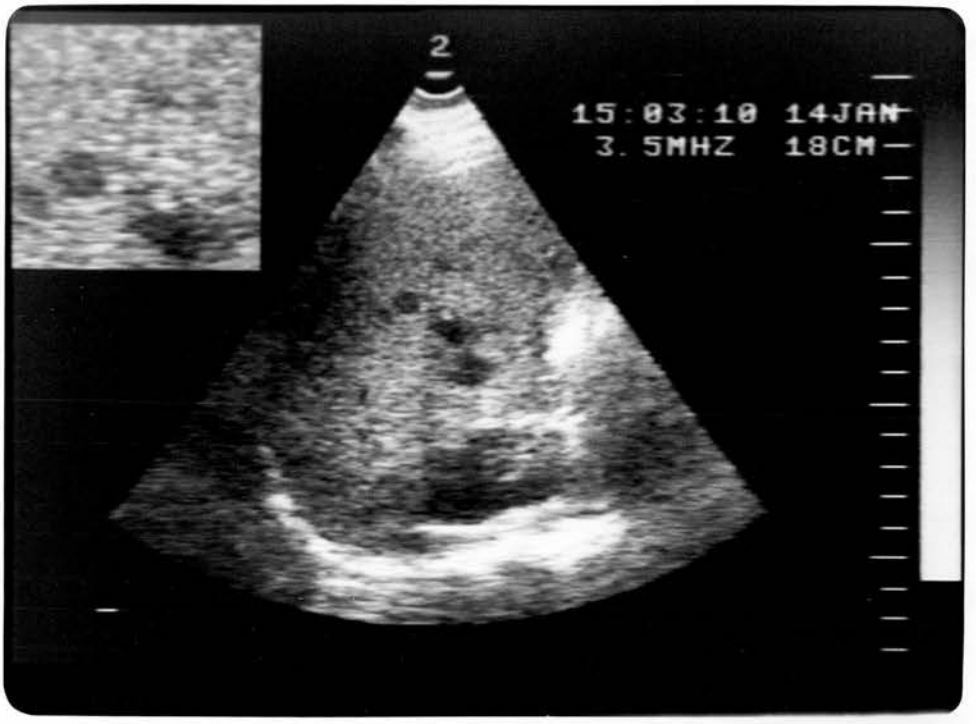

b

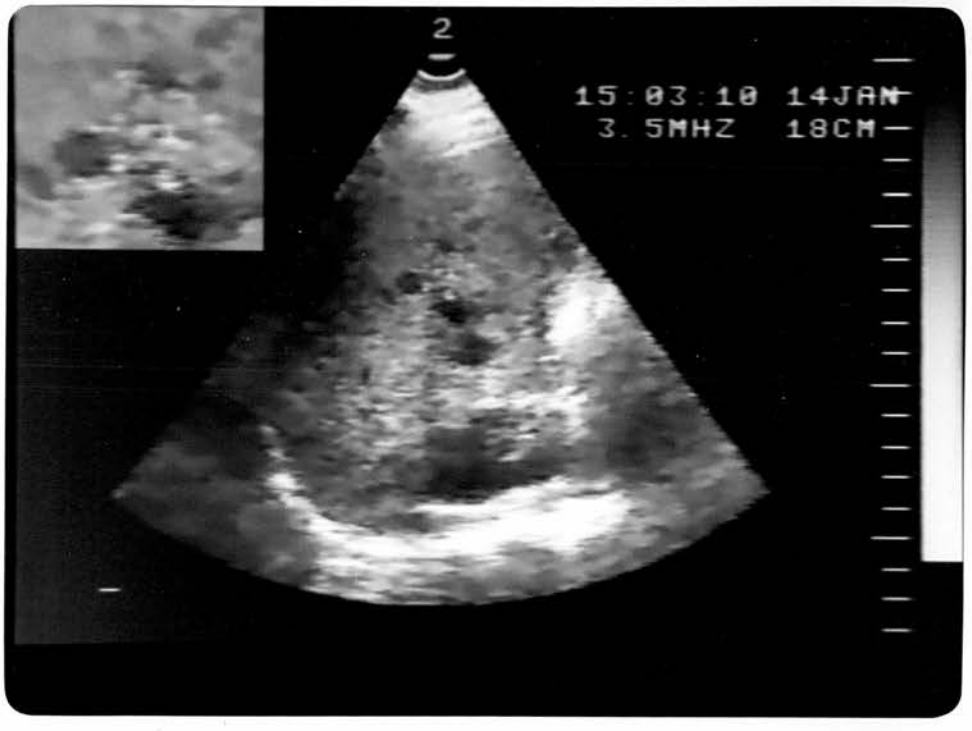

Figure 6.2 : A successful application of software spatial filtering to a scan of liver metastasis. **(a)** - Original. **(b)** Processed by the adaptive weighted median filter.

c

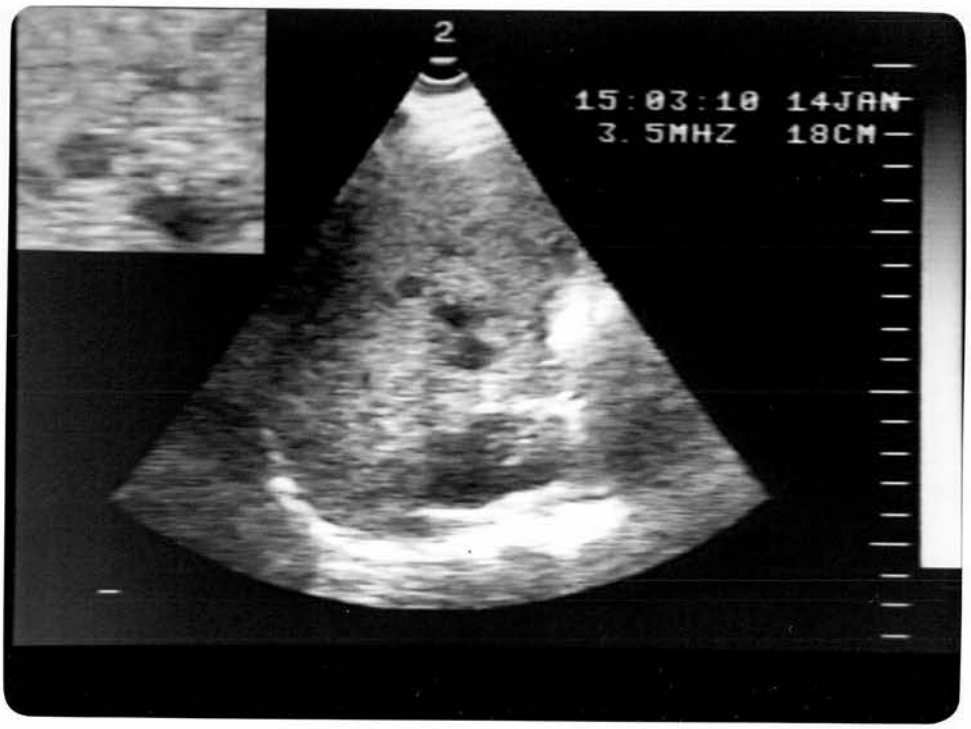

Figure 6.2 : (c) – Directional filtering applied to the original scan of Figure 6.2a.

a

b

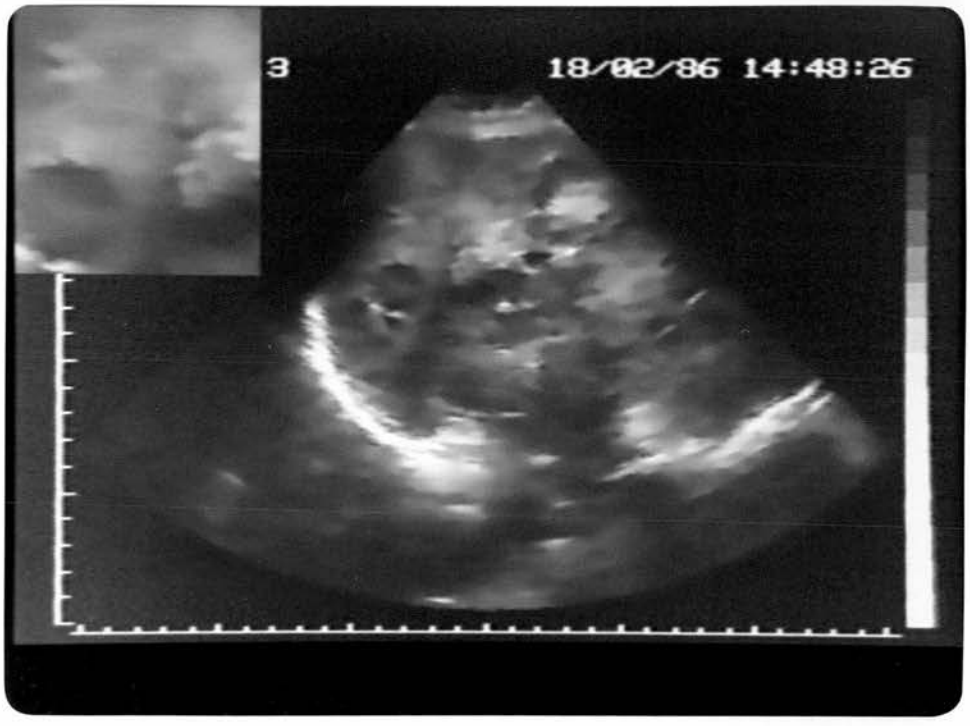

Figure 6.3 : An unsuccessful application of software spatial filtering to a scan of liver metastasis. **(a)** – Original. **(b)** – Processed by the adaptive weighted median filter.

c

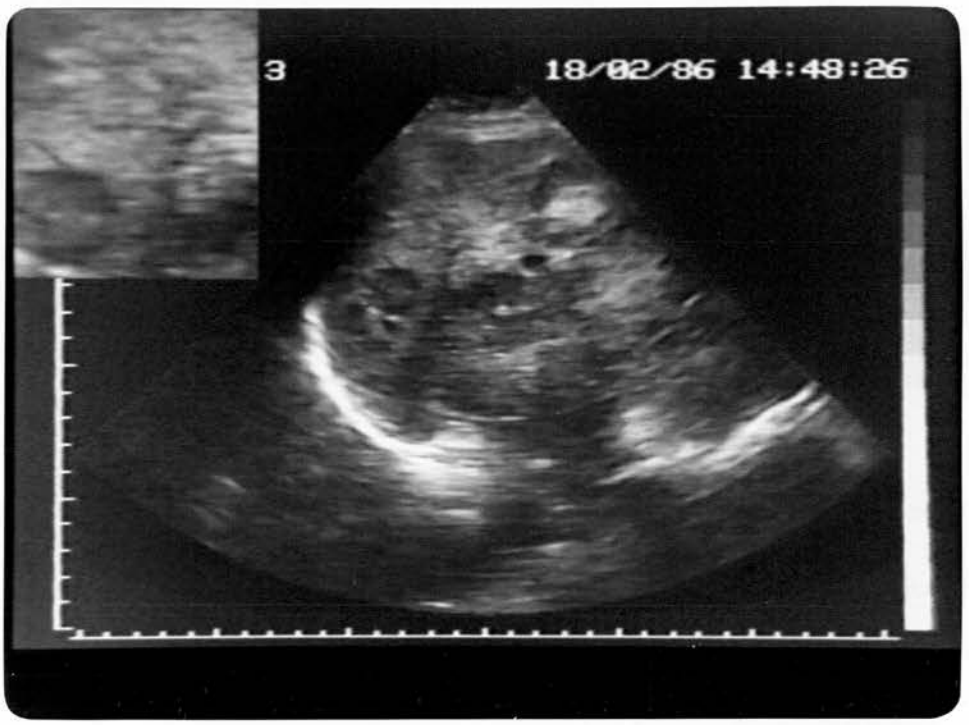

Figure 6.3 : **(c)** – Directional filtering applied to the original scan of Figure 6.3a.

6.6. Hardware spatial filtering

The evaluation of the real-time filter was based on scans obtained interactively during clinical examination of patients. The acquisition of data was carried out over a period of three months using the GL Ultrasound Ltd Z/S scanner interfaced to the hardware filter. Two or three suitable views from each patient were included in the evaluation. For each view, a set of three scans corresponding to no smoothing (threshold curve q_{00}), light smoothing (threshold curve q_{01}) and heavy smoothing (threshold curve q_{10}) were recorded on X-ray film. In total, eighty sets from thirty two patients were obtained but a number of them was excluded because the scans were not anatomically comparable. The remaining sets, seventy three of them from thirty patients, were evaluated by two consultant radiologists and two physicists. The results are presented in Tables 6.6, 6.7.

6.6.1. Results

The difference in attitude that radiologists and physicists have towards smoothed images, something already observed in the previous noise reduction evaluations of this chapter, was confirmed by the results of the two new observers (SRW and SDP) in the current evaluation. In general, the physicists are strongly in favour of the processed images whereas the radiologists tend to be cautious or even against processing.

Noise was the only category where the statistical analysis of the evaluation marks produced identical results for the four observers. All of them believed that the processed images had significantly less noise. However, comparison between Tables 6.6 and 6.7 shows that, in quantitative terms, the radiologists found less improvement than the physicists.

Contrast was a category where no statistically significant differences were found, with the exception of one of the physicists (SDP) who gave

TABLE 6.6 : EVALUATION OF HARDWARE SPATIAL FILTERING

Means ± Standard Deviations for the GL Ultrasound Ltd Z/S scanner
73 sets of images from 30 patients

Radiologist (PLA)

Image Type	[1] Noise	[1] Contrast	[1] Boundary Definition	[1] Diagnostic Information	[2] Overall Quality
Unprocessed Image	2.14±0.61	2.67±0.55	2.26±0.65	2.29±0.65	1.91±0.82
Light Smoothing	↑2.39±0.72	2.67±0.53	2.43±0.70	2.33±0.69	1.97±0.69
Heavy Smoothing	↑2.56±0.68	2.69±0.52	2.44±0.70	2.43±0.70	2.12±0.91
[3] Q	0.18	+∞	+∞	+∞	0.50

Radiologist (SRW)

Image Type	[1] Noise	[1] Contrast	[1] Boundary Definition	[1] Diagnostic Information	[2] Overall Quality
Unprocessed Image	2.75±0.58	3.01±0.40	2.79±0.59	2.99±0.59	1.37±0.54
Light Smoothing	↑2.90±0.49	2.99±0.47	2.88±0.56	2.88±0.66	↓1.96±0.68
Heavy Smoothing	↑2.94±0.45	3.00±0.42	2.82±0.57	2.90±0.60	↓2.66±0.64
[3] Q	0.14	+∞	+∞	+∞	0.52

[1] 1 = poor ; 4 = excellent quality
[2] 1 = first ; 3 = last in order of preference
[3] Minimum statistically significant difference between two means at 1% level

TABLE 6.7 : EVALUATION OF HARDWARE SPATIAL FILTERING

Means ± Standard Deviations for the GL Ultrasound Ltd Z/S scanner
73 sets of images from 30 patients

Physicist (WNMcD)

Image Type	[1] Noise	[1] Contrast	[1] Boundary Definition	[2] Overall Quality
Unprocessed Image	1.10±0.29	2.29±0.63	1.64±0.58	2.92±0.32
Light Smoothing	†2.12±0.33	2.16±0.60	†2.22±0.60	†1.79±0.52
Heavy Smoothing	†2.79±0.40	2.23±0.54	†2.27±0.65	†1.29±0.48
[3] Q	0.14	+∞	0.22	0.50

Physicist (SDP)

Image Type	[1] Noise	[1] Contrast	[1] Boundary Definition	[2] Overall Quality
Unprocessed Image	1.17±0.37	1.79±0.50	2.00±0.53	2.83±0.50
Light Smoothing	†2.60±0.49	†2.58±0.57	†2.50±0.62	†1.53±0.53
Heavy Smoothing	†2.92±0.36	†2.74±0.55	†2.36±0.71	†1.64±0.65
[3] Q	0.18	0.21	0.28	0.50

[1] 1 = poor ; 4 = excellent quality
[2] 1 = first ; 3 = last in order of preference
[3] Minimum statistically significant difference between two means at 1% level

significantly higher marks to the processed images.

As far as boundary definition is concerned, all the observers gave higher marks to the processed images but only the results of the physicists are statistically significant.

In the diagnostic information category the radiologists judged all the image types to be equivalent, in other words no significant differences were observed. However, it is interesting to note that one radiologist (PLA) was slightly in favour and the other (SRW) slightly against the processed images.

Finally, in the overall quality category the radiologists believe that processing did not improve the quality of the original images. One radiologist (PLA) judged processed and unprocessed images to be equivalent whereas the other (SRW) believed that processing produced significantly worse images. On the other hand, both physicists expressed a strong preference in favour of the processed images. One of them (WNMcD) ranked the heavily smoothed images first while the other (SDP) judged both processed images to be equivalent.

6.6.2. Discussion

The different criteria that physicists and radiologists use to form their opinion about processing have already been discussed in several occasions throughout this chapter. The main reasons were considered to be the fact that radiologists may not be fully aware of the origin and implications of acoustic speckle and also the lack of familiarity with speckle reduced images. The results of the second radiologist (SRW), who had not been exposed to speckle suppression before, seem to support the argument that the less accustomed one is in interpreting smoothed scans, the less likely he is to prefer them. This is demonstrated from the data of Table 6.6 (bottom) where the evaluation marks of all image types are almost identical for the first four categories but a

very clear difference in favour of the unprocessed images exists in the overall quality category. Admittedly, the lack of familiarity is not the only reason for this pattern. The radiologist commented that he found it difficult to judge the scans in an isolated manner without knowledge of the clinical history of each patient (in fact he evaluated only sixty six out of the seventy three sets). Also, he felt that in many cases the images of a set had comparable quality and he ranked them only in order to conform to the evaluation protocol.

An interesting observation from the evaluation marks of the radiologists, which is not apparent from Table 6.6, is that in the majority of the cases where the processed images were ranked first they also had a higher diagnostic content and contained pathological findings. This observation is consistent with our opinion that real-time speckle suppression techniques should be incorporated into ultrasound scanners not in order to replace the conventional way of presenting an image but to be used as an alternative form of displaying the echo information in cases of suspected pathology in parenchymal tissues.

The prototype hardware filter demonstrated that speckle suppression can be performed in real-time without loss of genuine image detail. However, the processed scans revealed some problems of the current filter design and hinted at possible improvements. The problems are mainly related to the shape of the threshold curve q_{SW1SW0} (see Figure 5.2) and the filter size.

As far as light smoothing (threshold curve q_{01}) is concerned, inspection of the processed scans showed that consistently good quality and satisfactory signal preservation can be expected from this type of filtering. An example is presented in Figure 6.4 which displays a kidney with carcinoma. From this figure it can be seen that processing offers better presentation of low-contrast detail inside the kidney and improved boundary definition. Both

radiologists agreed that the processed scan had better image quality and offered more diagnostic information. The main drawback of this threshold curve is that it does not provide adequate noise reduction. One way to produce a smoother image is to use a curve which corresponds to higher thresholds. However, the application of the curve q_{10} to the seventy three scans of this evaluation demonstrated that this is not the best approach. The problem of blurring bright edges, which is associated with high thresholds, has already been discussed in Section 5.4 and a way of overcoming it has been proposed there. A more serious problem is that due to the small axial window size, on some occasions filtering tends to join together small speckles instead of smoothing them. This results in the distracting blotchy appearance demonstrated by the processed scan of Figure 6.5. This scan was judged to be of inferior quality by the majority of the observers and I personally consider it to be the worst processed scan of the series. Therefore, it seems that in order to obtain adequate noise reduction a filter having a bigger window in the axial direction, of say 9 or 11 points instead of the 7 currently used, must be designed.

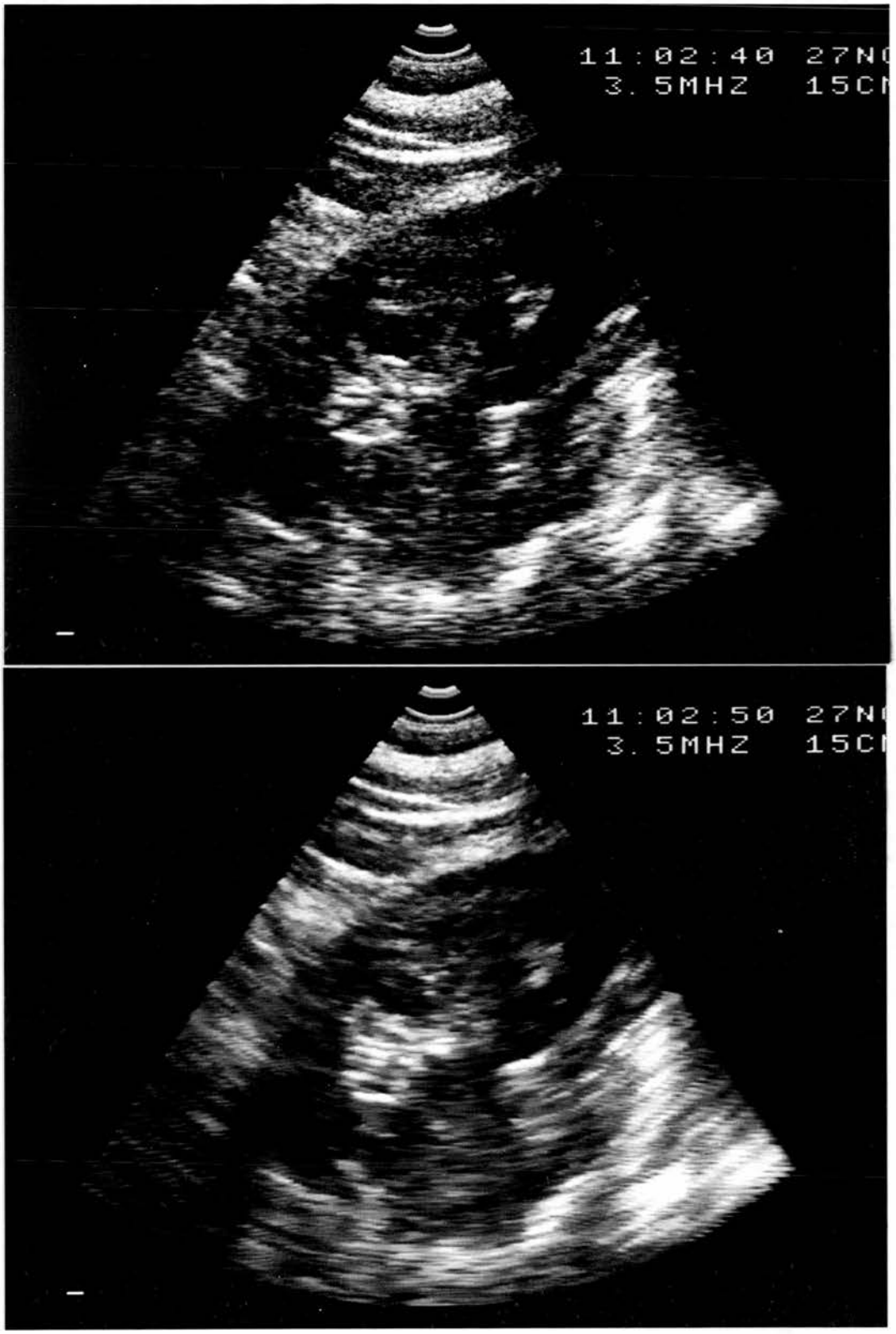

Figure 6.4 : A successful application of hardware spatial filtering to a scan showing a tumour distal to the right kidney. **(a)** - Original. **(b)** - Processed using the light smoothing curve q_{01}.

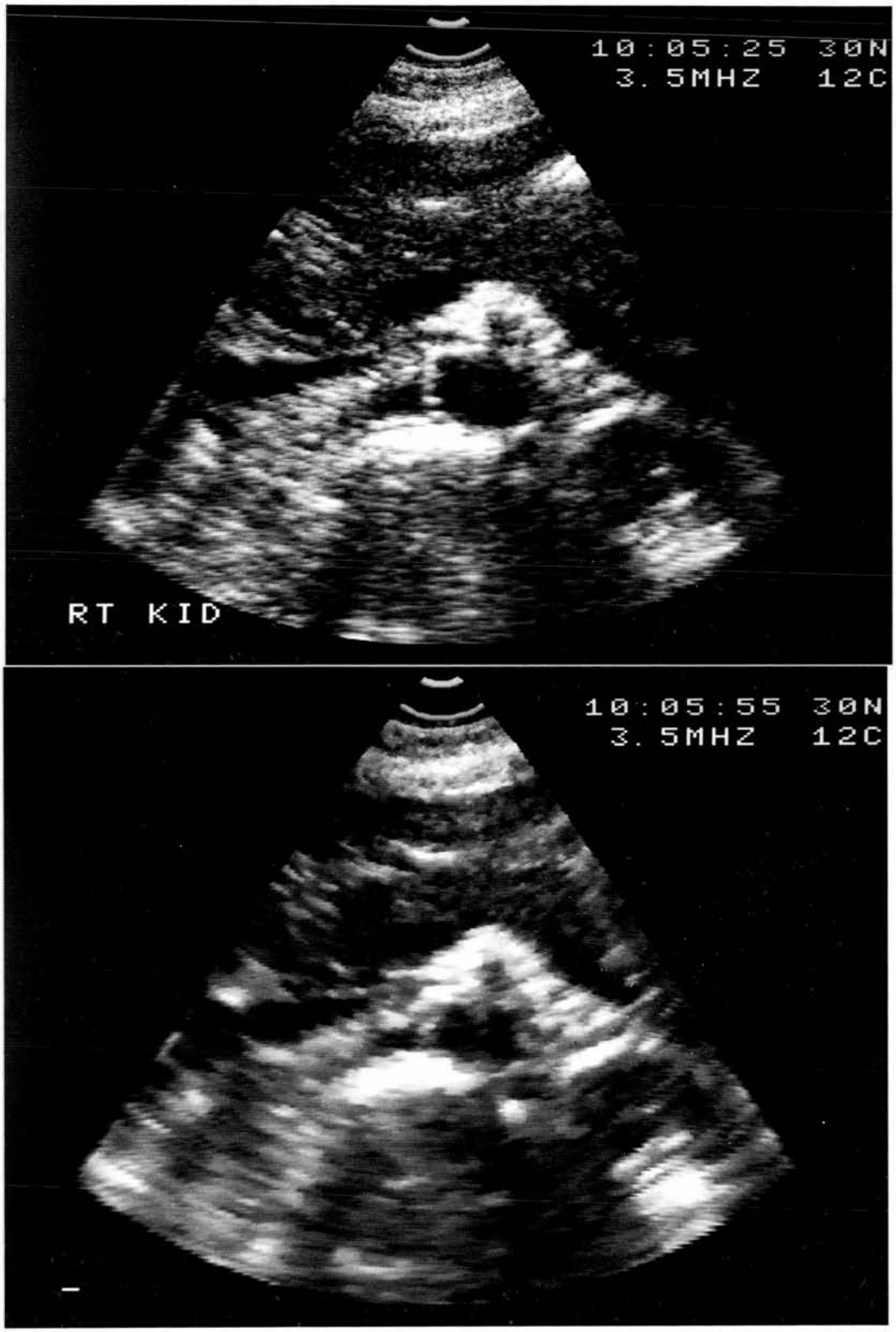

a

b

Figure 6.5 : An unsuccessful application of hardware spatial filtering to a scan of pancreas. **(a)** – Original. **(b)** – Processed using the heavy smoothing curve q_{10}.

6.7. Conclusions

The evaluations described in this chapter covered a wide range of digital noise reduction techniques applied to medical ultrasonic images primarily to suppress speckle: frame averaging techniques which are effective only when the transducer's position relative to the imaged structure is changed between frames; adaptive spatial filtering implemented in software and with emphasis either on complete speckle suppression or on combined noise reduction and edge enhancement; hardware spatial filtering which offers real-time operation. The techniques were applied to a number of images acquired using different scanners and the processed images were evaluated by panels of radiologists and physicists. The evaluation results provided some conclusions but also left some questions unresolved.

The first conclusion from this study is that speckle suppression can be performed in most cases without loss of diagnostic information (with the exception of integration and adaptive weighted median filtering applied to images from the Siemens Sonoline SX scanner). Processing can, obviously, reduce the noise level of an image but it can also improve the boundary definition and on certain occasions the overall quality of an image. Processing seems to be more successful when applied to images containing pathology.

Another conclusion is that the amount of improvement offered by processing is directly related to the quality of the original image. Better results can be expected for noisy, poor quality input scans. It is therefore reasonable to assume that in order to obtain the best possible results, a processing technique should be optimized for a particular scanner.

Finally, an observation from the evaluation results, which I believe it to be true in general, is that radiologists and physicists have different attitudes, different expectations and use different criteria to judge the success

or failure of processing. In our opinion, this can be attributed mainly to the fact that although interest in acoustic speckle is constantly increasing, it is still confined to the scientific community. As a consequence, physicians are not fully aware of the artifactual nature of speckle and are not accustomed to interpret speckle reduced images.

What the evaluations did not provide was a conclusive answer to the question of how useful speckle suppression is from the diagnostic point of view. There are several reasons for that: the relatively small number of images from each scanner included in the evaluations (especially in the software spatial filtering study), the lack of many scans with suspected or definite pathology and, more importantly, the difficulty a radiologist faces when he is asked to form an opinion about the diagnostic content of a single scan. This last reason is easily explainable when we consider that during clinical examination the diagnosis is based on several views obtained by scanning a patient interactively. Some of these problems had been identified in advance but it was not possible to overcome them due to practical difficulties.

In order to obtain a definite answer about the diagnostic usefulness of speckle suppression, more rigorous and comprehensive studies must be performed. The effect of speckle suppression on the detectability of low-contrast lesions should be investigated by using suitable contrast phantoms (Smith et al, 1983) but also by organizing a large scale clinical trial, perhaps on a selected group of patients, so that an adequate number of scans with suspected abnormalities can be acquired. However, at the same time it is equally important to develop and introduce real-time speckle suppression techniques in clinical practice because these techniques will reach their full potential only when physicians have become exposed to speckle reduced images and have accumulated sufficient experience to interpret them.

CHAPTER 7

FURTHER DEVELOPMENTS AND OTHER USES

7.1. Other applications of noise suppression

So far, noise suppression has been applied to abdominal scans, where speckle is most prevalent, in order to make their diagnostic information content more suitable for human interpretation. In this section some other possible uses of noise suppression are considered.

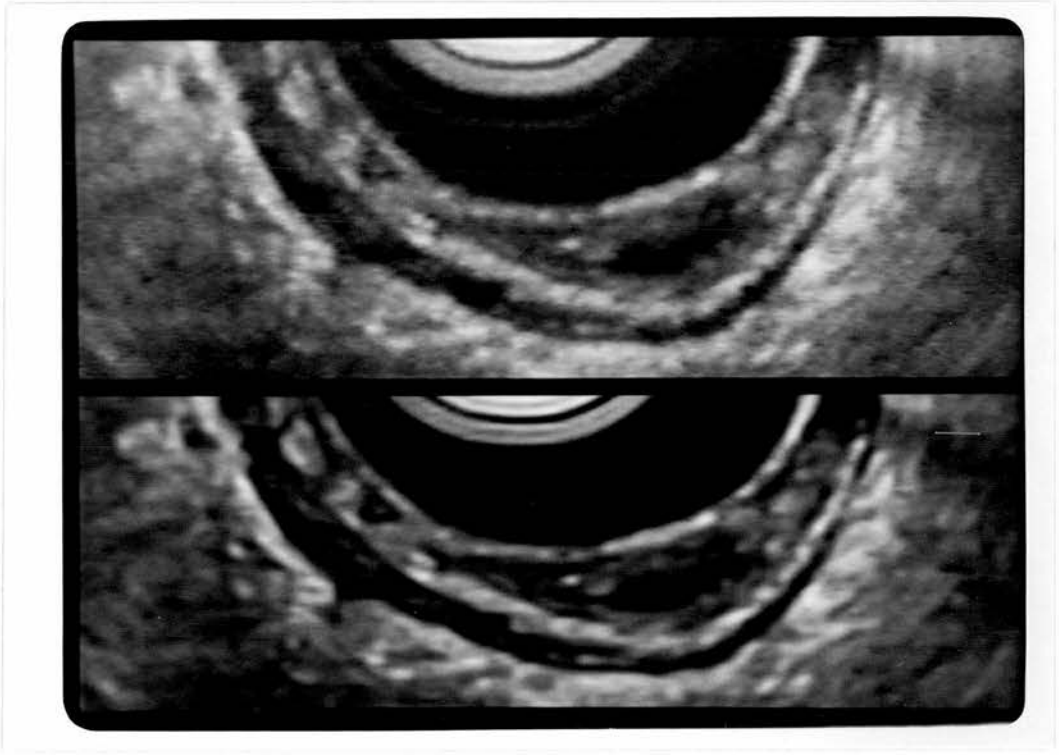

Figure 7.1 : Scan of a rectal tumour (top) processed by the directional filter (bottom).

In the ultrasonic visualization of many parts of the human body, the presentation of interfaces, edges and line structures is of major clinical importance. Such parts include the infant hip, the foetal head and also the rectum because the management of patients with rectal cancer may be determined by a staging method based on how many layers of the rectal wall have been attacked by the tumour (Beynon et al, 1987). We have experimented with hip, head and rectal scans and found that the directional filter can

improve their quality because it combines noise suppression with edge enhancement. An example is given in Figure 7.1. The top image is part of a transverse scan of an annular rectal tumour. As can be seen from the bottom image, processing improves the definition and sharpens the boundaries of the tumour and rectal wall and enhances the low contrast detail of the scan. Our experience so far suggests that this type of filtering could be of diagnostic benefit to the areas mentioned above.

Alternatively, image sharpening and possibly increased spatial resolution could be achieved using deconvolution techniques (Schomberg et al, 1983; Vaknine & Lorenz, 1984) instead of the directional filter. However, since deconvolution techniques are extremely sensitive to random intensity fluctuations, noise suppression using a detail-preserving filter must precede deconvolution. The use of noise suppression as a preprocessing tool before further machine processing is very important because it is the quality of the input data that determines the success or failure of many techniques such as colour coding, adaptive histogram equalization and contrast enhancement, image segmentation and pattern recognition. The usefulness of noise suppression in machine processing techniques which are relevant to ultrasonic imaging is demonstrated by the examples given below.

Edge detection is the first step of almost every computer vision task. An important application of edge detection in echocardiography is the identification of the cardiac borders (Wolfe et al, 1987). These can then be used to measure automatically the dimensions of several structures, an operation which provides valuable diagnostic information. Automatic quantitative measurements are also of interest in other fields, primarily obstetrics. Figure 7.2 shows the results of applying a simple edge detector, known as the Sobel operator (Gonzalez & Wintz, Chapter 7, 1987), to the original scan of Figure 4.1a and the adaptive weighted median filtered scan of

a

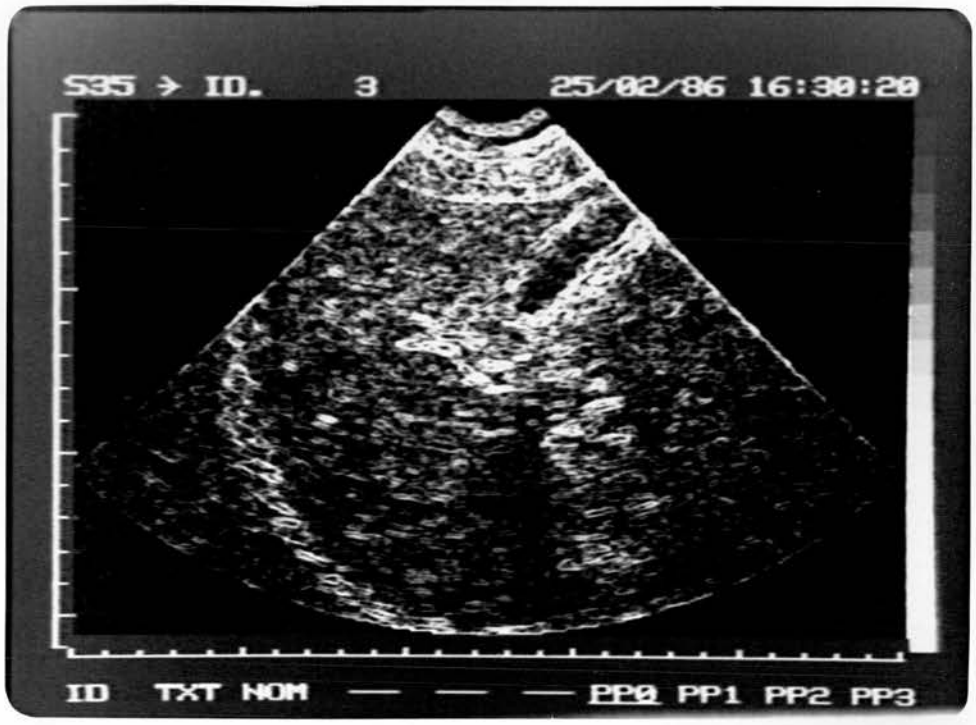

b

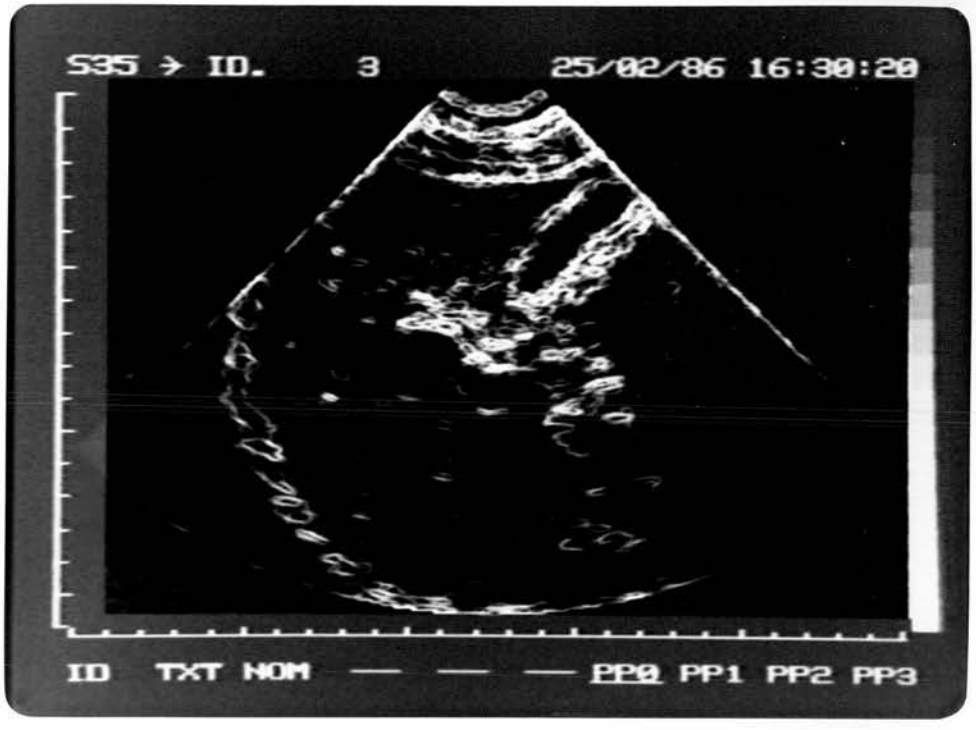

Figure 7.2 : **(a)** – Sobel edge detection operator applied to the unprocessed scan of Figure 4.1a. **(b)** – The same operator applied to the speckle reduced image of Figure 4.15a.

Figure 4.15a . By comparing the two images of Figure 7.2 it is clear that edge detection is far more successful when applied to a scan with reduced noise. Due to the sensitivity of the edge detector to speckle noise, the top image of Figure 7.2 contains so many erroneous edge points that it is almost impossible for an edge linking algorithm to trace the boundaries of the true structure. In contrast, the number of erroneous points due to noise has been reduced significantly in the bottom image and the real edges stand out clearly.

Recently, interest has been expressed in using multiple scans of a three-dimensional volume to reconstruct any plane within that volume (Halliwell et al, 1988). In this way, it is possible to visualize anatomical planes of clinical interest which cannot be scanned directly. The reconstruction is performed by interpolating between the multiple scans. In general, interpolation based on noisy data produces poor results. We have used the real-time hardware filter of Chapter 5 to investigate the effect that noise suppression before interpolation has on the reconstructed image. An ultrasonic phantom, which contains tissue mimicking material with wires embedded in it, was used in the experiments. A three-dimensional volume was scanned by moving the probe at 2 mm intervals in a direction perpendicular to the scan plane. At each position of the probe three images, unprocessed - light smoothing (threshold q_{01}) - heavy smoothing (threshold q_{10}), were recorded on video tape. Twenty one scans for each smoothing setting were obtained. These were transferred to a computer and programs were written to reconstruct a slice perpendicular to the scan plane. Figure 7.3a shows one of the multiple (unprocessed) scans with the bright markers on the left and right of the sector defining the intersection between the scan and reconstruction planes. The results of the reconstruction are presented in Figure 7.3b. From top to bottom, the images were formed using unprocessed, lightly smoothed and heavily smoothed data. Comparison of the images shows that noise

suppression before reconstruction can produce images of better quality with "cleaner" appearance and better defined boundaries, as it can be seen by the longitudinal cross-section of the wire. Another possibility is that by performing noise suppression on the original data, fewer slices would be needed in order to obtain a reconstructed image of acceptable quality. In this way considerable reduction in storage and processing requirements could be achieved.

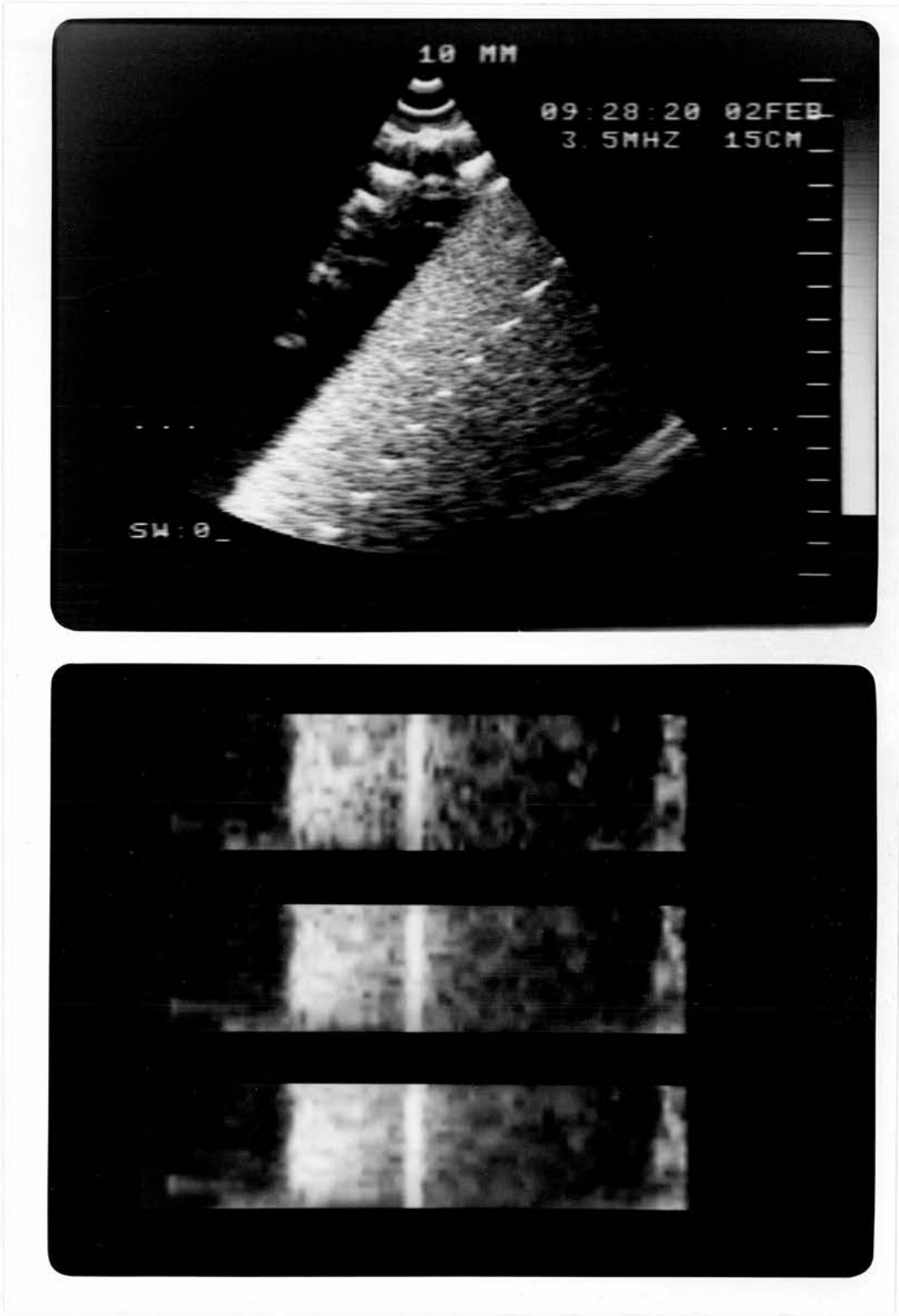

Figure 7.3 : Reconstruction of a plane from multiple scans. **(a)** - One of the multiple unprocessed scans. The bright markers define the reconstructed plane. **(b)** - From top to bottom, reconstructed plane using unprocessed, lightly smoothed and heavily smoothed data.

7.2. Future research directions

Based on the experience gained from this project, two directions for further research, related to different aspects of adaptive/signal-preserving filtering, have been identified as being worth pursuing.

As far as adjusting the filter's smoothing action according to the local image content is concerned, it is believed that first-order statistics have been fully explored. It is regarded as unlikely that new filters based on first-order statistics can be found which offer substantially better results. However, there is still considerable scope for improvement by exploring higher-order statistics and other textural properties of speckle, i.e. by taking into account the spatial arrangement of grey levels within an area. By using features based on these properties it should be possible to determine the boundaries between differently textured regions as opposed to only the location of intensity discontinuities, which is what first-order statistics can offer. Provided that segmentation with an acceptable degree of accuracy can be achieved, adaptive processing can be performed with variable shape windows, so that only pixels belonging to the same region are included in the calculations, and possibly using different filters according to the type of region to be processed.

A comprehensive survey of features and techniques used in texture modelling, classification and segmentation has been given by Haralick (1986). These include the autocorrelation function, which has already been used for ultrasonic speckle suppression (Bamber & Cook-Martin, 1987), the co-occurence matrix and the edge content and orientation per unit image area. The theory of Markov random fields has also found applications in texture analysis. Of particular interest here is a statistical approach to the texture analysis problem which models the image data as a Markov random field characterized by a class of probability distributions known as Gibbs distributions. This class, first introduced for modelling molecular interactions in

ferromagnetic materials, has increasingly been used in image processing over the last few years for tasks such as restoration (Geman & Geman, 1984) and modelling/segmentation (Derin & Elliot, 1987) with very promising results. Unfortunately most of the textural analysis methods, and the Gibbs distributions in particular, are computationally extremely demanding. Consequently, their application is restricted to small image segments with very few grey levels and containing a small number of region types. For this reason, future research should not only be concerned with identifying textural features capable of characterizing ultrasonic scans with reasonable accuracy but also with investigating how a suitable feature could be modified so that the amount of computations is reduced to an acceptable level.

The other direction which is considered to be worth pursuing is hardware for real-time operation. In contrast to the last few paragraphs, the challenge here is to reproduce the results already obtained with software methods but at a fraction of the time originally needed, rather than to achieve superior performance using more complex and sophisticated algorithms. It has already been mentioned in Chapter 5 that conventional microprocessors are incompatible with real-time operation. Also, image processing systems based on medium or large scale integration digital circuits, like the hardware filter of Chapter 5, can only implement algorithms of moderate complexity and size. Therefore, the emphasis should be in developing algorithms and architectures suitable for parallel and/or VLSI implementation. A point to be taken into account is that it would be preferable to process the data as early as possible in the image formation process. Ideally this should be done just before or after the radiofrequency detection stage in order to minimize the effect of the various signal processing stages performed inside the scanner. Finally, it would be highly desirable to include the time dimension in the processing by using information obtained at consecutive frames. A group of techniques which is

suitable for temporal processing includes algorithms such as the DW-MTM and Sigma filters. These filters have moderate complexity and can be implemented in hardware relatively easily. Also, because of their edge-preserving properties they do not affect abrupt signal changes in the time dimension and ,consequently, they can prevent blurring due to motion. Recursive implementations of these filters could be investigated as a means of increasing the efficiency of the hardware.

References

ABBOT J G & Thurstone F L (1979). Acoustic speckle: theory and experimental analysis. *Ultrasonic Imaging, 1,* 303-324.

AHMAD M O & Sundararajan D (1987). A fast algorithm for two-dimensional median filtering. *IEEE Transactions on Circuits and Systems, 34,* 1364-1374.

ARSENAULT H H & Denis M (1983). Image processing in signal-dependent noise. *Canadian Journal of Physics, 61,* 309-317.

ATAMAN E , Aatre V K & Wong K M (1980). A fast method for real-time median filtering . *IEEE Transactions on Acoustics, Speech and Signal Processing, 28,* 415-421.

BAMBER J C & Dickinson R J (1980). Ultrasonic B-scanning: a computer simulation. *Physics in Medicine and Biology, 25,* 463-479.

BAMBER J C & Daft C (1986). Adaptive filtering for reduction of speckle in ultrasonic pulse-echo images. *Ultrasonics, 24,* 41-44.

BAMBER J C & Cook-Martin G (1987). Texture analysis and speckle reduction in medical echography. In *SPIE Proceedings Vol 768,* 120-127.

BARTRUM R J Jr & Crow H C (1980). Ultrasound echo averaging: a simple method for improving image perception. *Journal of Clinical Ultrasound, 8,* 63-64.

BAUM G & Greenwood I (1958). The application of ultrasonic locating techniques to ophthalmology. *Archives of Ophthalmology, 60,* 263-279.

BEDNAR J B & Watt T L (1984). Alpha-trimmed means and their relationship to median filters. *IEEE Transactions on Acoustics, Speech and Signal Processing, 32,* 145-153.

BERNSTEIN R (1987). Adaptive nonlinear filters for simultaneous removal of different kinds of noise in images. *IEEE Transactions on Circuits and Systems, 34,* 1275-1291.

BEYNON J , Roe A M , Foy D M A , Channer J L , Virjee J & McMortensen N J (1987). Preoperative staging of local invasion in rectal cancer using endoluminal ultrasound. *Journal of the Royal Society of Medicine, 80,* 23-24.

BILLON A C (1988). Use of grey tone morphology for speckle smoothing in echography (abstract). *Ultrasonic Imaging, 10,* 66.

BOVIK A C , Huang T S & Munson D C Jr (1983). A generalization of median filtering with linear combinations of order statistics. *IEEE Transactions on Acoustics, Speech and Signal Processing, 31,* 1342-1350.

BOVIK A C (1987). Streaking in median filtered images. *IEEE Transactions on Acoustics, Speech and Signal Processing, 35,* 493-503.

BOWLER K C , Kenway R D , Pawley G S & Roweth D (1987). *An Introduction to OCCAM 2 and the Computing Surface.* Department of Physics, University of Edinburgh.

BRACEWELL R N (1986). *The Fourier Transform and its Applications.* McGraw-Hill:

New York.

BROWNRIGG D R K (1984). The weighted median filter. *Communications of the American Association for Computer Machinery, 27,* 807-818.

BROWNRIGG D R K (1986). Generation of representative members of an RrSst weighted median filter class. *IEE Proceedings Part F, 133,* 445-448.

BURCKHARDT C B (1978). Speckle in ultrasound B-mode scans. *IEEE Transactions on Sonics and Ultrasonics, 25,* 1-6.

BURSKY D (1987). CMOS four-chip set processes images at 20-MHz data rates. *Electronic Design, May 28 issue,* 39-46.

CAPPELLINI V & Emiliani P R (1986). Two-dimensional digital systems and applications: the state of the art. In *Multidimensional Systems,* edited by S G Tzafestas (Marcel Dekker: New York), 1-35.

CHAN P & Lim J S (1985). One-dimensional processing for adaptive image restoration. *IEEE Transactions on Acoustics, Speech and Signal Processing, 33,* 117-126.

CHANDA B , Chaudhuri B B & Majumder D D (1985). Image sharpening incorporating human visual response. *Signal Processing, 9,* 57-65.

CHIN R T & Yeh C L (1983). Quantitative evaluation of some edge-preserving noise-smoothing techniques. *Computer Vision, Graphics and Image Processing, 23,* 67-91.

CHIVERS R C (1977). The scattering of ultrasound by human tissues - some theoretical models. *Ultrasound in Medicine and Biology, 3,* 1-13.

CHIVERS R C , Davies I J & Duarte F M (1986). Perceptual studies on ultrasonic B-scan textures. *Physics in Medicine and Biology, 31,* 627-634.

COHEN G , Barnes J O & Pœa P M (1978). The effects of the film/screen combination on tomographic image quality. *Radiology, 129,* 515-520.

CORNSWEET T N (1970). *Visual Perception.* Academic Press: New York.

CRIMMINS T R (1985). Geometric filter for speckle reduction. *Applied Optics, 24,* 1438-1443.

CUNNINGHAM J J & Bacani M (1985). Reduced-speckle imaging. A simple technique for improving real-time sonograms. *Applied Radiology, Jan/Feb issue,* 91-94.

DANIEL W W (1978). *Applied Nonparametric Statistics.* Houghton Mifflin Company: Boston.

DAVENPORT W B Jr & Root W L (1958). *An Introduction to the Theory of Random Signals and Noise.* Prentice-Hall: Englewood Cliffs, New Jersey.

DAVID H A (1981). *Order Statistics.* Wiley: New York.

DAVIS L S & Rosenfeld A (1978). Noise cleaning by iterated local averaging. *IEEE Transactions on Systems Man and Cybernetics, 8,* 705-710.

DEEKSHATULU B L , Kulkarni A D & Rao G K (1985). Quantitative evaluation of enhancement techniques. *Signal Processing, 8,* 369-375.

DERIN H & Elliot H (1987). Modelling and segmentation of noisy textured images using Gibbs random fields. *IEEE Transactions on Pattern Analysis and Machine Intelligence, 9,* 39-55.

DEUTSCH R (1962). *Nonlinear Transformations of Random Processes.* Prentice-Hall: Englewood Cliffs, New Jersey.

DICKINSON R J (1982). Reduction of speckle in ultrasound B-scans by digital signal processing. In *Acoustical Imaging Vol 12,* edited by E A Ash & C R Hill (Plenum Press: New York), 213-224.

DICKINSON R J (1986). Reflection and scattering. In *Physical Principles of Medical Ultrasonics,* edited by C R Hill (Ellis Horwood: Chichester, Sussex), 225-260.

DING R & Venetsanopoulos A N (1987). Generalized homomorphic and adaptive order statistics filters for the removal of impulsive and signal-dependent noise. *IEEE Transactions on Circuits and Systems, 34,* 948-955.

DONALD I , MacVicar J & Brown T G (1958). Investigation of abdominal masses by pulsed ultrasound. *Lancet, 1,* 1188-1194.

FATEMI M & Kak A C (1980). Ultrasonic B-scan imaging: theory of image formation and a technique for restoration. *Ultrasonic Imaging, 2,* 1-47.

FELLINGHAM L L & Sommer F G (1984). Ultrasonic characterization of tissue structure in the *in vivo* human liver and spleen. *IEEE Transactions on Sonics and Ultrasonics, 31,* 418-428.

FERRARI L , Jones J , Gonzalez V & Behrens M (1982). Acoustical imaging using the phase of echo waveforms. In *Acoustical Imaging Vol 12,* edited by E A Ash & C R Hill (Plenum Press: New York), 635-641.

FIASCONARO J G (1979). Two-dimensional nonrecursive filters. In *Picture Processing and Digital Filtering,* edited by T S Huang (Springer-Verlag: Berlin), 69-129.

FLAX S W , Glover G H & Pelc N J (1981). Textural variations in B-mode echography: a stochastic model. *Ultrasonic Imaging, 3,* 235-257.

FOSTER D R , Arditi M , Foster F S , Patterson M S & Hunt J W (1983). Computer simulations of speckle in B-scan images. *Ultrasonic Imaging, 5,* 308-330.

FRIEDEN B R (1979). Image enhancement and restoration. In *Picture Processing and Digital Filtering,* edited by T S Huang (Springer-Verlag: Berlin), 177-248.

FROST V S , Stiles J A & Holtzman J C (1980). Radar image preprocessing. In Proceedings of *1980 Machine Processing of Remotely Sensed Data Symposium,* Purdue University, Lafayette, Indiana, 140-146.

FROST V S , Stiles J A , Shanmugan K S , Holtzman J C & Smith S A (1981). An adaptive filter for smoothing noisy radar images. *Proceedings of the IEEE, 69,* 133-135.

FROST V S , Stiles J A , Shanmugan K S & Holtzman J C (1982). A model for radar images and its application to adaptive digital filtering of multiplicative noise.

IEEE Transactions on Pattern Analysis and Machine Intelligence, 4, 157-166.

GALLAGHER N C Jr & Wise G L (1981). A theoretical analysis of the properties of median filters. *IEEE Transactions on Acoustics, Speech and Signal Processing, 29,* 1136-1141.

GALLOWAY R L , McDermott B A & Thurstone F L (1988). A frequency diversity process for speckle reduction in real-time ultrasonic images. *IEEE Transactions on Ultrasonics, Ferroelectrics and Frequency Control, 35,* 45-49.

GARRET W J , Kossoff G & Carpenter D (1975). Grey scale compound scan echography of the normal upper abdomen. *Journal of Clinical Ultrasound, 3,* 199-204.

GEHLBACH S M & Sommer F G (1987a). Speckle reduction processing. In *SPIE Proceedings Vol 768,* 178-184.

GEHLBACH S M & Sommer F G (1987b). Frequency diversity speckle processing. *Ultrasonic Imaging, 9,* 92-105.

GEMAN S & Geman D (1984). Stochastic relaxation, Gibbs distributions and the Bayesian restoration of images. *IEEE Transactions on Pattern Analysis and Machine Intelligence, 6,* 721-741.

GONZALEZ R C & Wintz P (1987). *Digital Image Processing.* Addison-Wesley: Reading, Massachusetts.

GOODMAN J W (1975). Statistical properties of laser speckle patterns. In *Laser Speckle and Related Phenomena,* edited by J C Dainty (Springer-Verlag: Berlin), 9-75.

GOODMAN J W (1976). Some fundamental properties of speckle. *Journal of the Optical Society of America, 66,* 1145-1150.

GRANLUND G H (1978). In search of a general picture processing operator. *Computer Graphics and Image Processing, 8,* 155-173.

GRANLUND G H (1981). The GOP parallel image processor. In *Digital Image Processing,* edited by L Bolc & Z Kulpa (Springer-Verlag: Berlin), 200-227.

GRANRATH D J (1981). The role of human visual models in image processing. *Proceedings of the IEEE, 69,* 552-561.

HALLIWELL M (1987). Ultrasonic imaging in medical diagnosis. *IEE Proceedings Part A, 134,* 179-187.

HALLIWELL M , Key H , Jenkins D & Wells P N T (1988). Multiplanar prostatic scanning (abstract). *British Journal of Radiology, 61,* 545.

HARALICK R M (1986). Statistical image texture analysis. In *Handbook of Pattern Recognition and Image Processing,* edited by T Y Young & K S Fu (Academic Press: New York), 242-279.

HATAMIAN M (1986). A real-time two-dimensional moment generating algorithm and its single chip implementation. *IEEE Transactions on Acoustics, Speech and Signal Processing, 34,* 546-553.

HECKER R & Pöppl S J (1982). Structured noise removal by using a high flexible 2D FIR digital filter. In *SPIE Proceedings, vol 375,* 87-91.

HEYGSTER G (1982). Rank filters in digital image processing. *Computer Graphics and Image Processing, 19,* 148-164.

HIGSON G R (1987). Seeing things more clearly. *British Journal of Radiology, 60,* 1049-1057.

HILL C R (1986). Introduction. In *Physical Principles of Medical Ultrasonics,* edited by C R Hill (Ellis Horwood: Chichester, Sussex), 15-17.

HOUSTON A S & Macleod M A (1979). An intercomparison of computer assisted image processing and display methods in liver scintigraphy. *Physics in Medicine and Biology, 24,* 559-570.

HUANG T S , Yang G J & Tang G Y (1979). A fast two-dimensional median filtering algorithm. *IEEE Transactions on Acoustics, Speech and Signal Processing, 27,* 13-18.

HUBEL D H & Wiesel T (1979). Brain mechanisms of vision. *Scientific American , 241, No. 3,* 150-162.

HUBER P (1981). *Robust Statistics.* Wiley: New York.

HUSSEY M (1985). *Basic Physics and Technology of Medical Diagnostic Ultrasound.* MacMillan: London.

IKONOMOPOULOS A & Unser M (1984). A directional filtering approach to texture discrimination . In Proceedings of *Seventh International Conference on Pattern Recognition,* Montreal, Canada, 87-89.

IKONOMOPOULOS A & Kunt M (1985). High compression image coding via directional filtering. *Signal Processing, 8,* 179-203.

INMOS LTD (1986a). *Product Overview: IMS A100 Cacsadable Image Processor.* Inmos Ltd: Bristol.

INMOS LTD (1986b). *Product Overview: The Transputer Family.* Inmos Ltd: Bristol.

INSANA M F , Wagner R F , Garra B S , Brown D G & Shawker T H (1986). Analysis of ultrasound image texture via generalized Rician statistics. *Optical Engineering, 25,* 743-748.

IOANNIDIS A , Kazakos D & Watson D D (1984). Application of median filtering on nuclear medicine scintigram images. In Proceedings of *Seventh International Conference on Pattern Recognition,* Montreal, Canada, 33-36.

ITOH K , Yasuda Y , Aihara T , Koyano A & Konishi T (1985). Acoustic intensity histogram pattern diagnosis of liver diseases. *Journal of Clinical Ultrasound, 13,* 449-456.

JAFFE C C & Harris D J (1980a). Physical factors influencing numerical echo-amplitude data extracted from B-scan ultrasound images. *Journal of Clinical Ultrasound, 8,* 327-333.

JAFFE C C & Harris D J (1980b). Sonographic tissue texture: influence of transducer

focusing pattern. *American Journal of Roentgenology, 135,* 343-347.

JAFFE C C , Orphanoudakis S C & Ablow R C (1982). The effect of a television digital noise reduction device on fluoroscopic image quality and dose rate. *Radiology, 144,* 789-792.

JENNET B (1984). *High Technology Medicine.* Nuffield Provincial Hospitals Trust: London.

JOURNAL OF THE OPTICAL SOCIETY OF AMERICA (1976). *Special Issue on Speckle,* Vol 66, No. 11.

JULESZ B , Gilbert E N , Shepp L A & Frisch H L (1973). Inability of humans to discriminate between visual textures that agree in second-order statistics - Revisited. *Perception, 2,* 391-405.

JULESZ B (1975). Experiments in the visual perception of texture. *Scientific American, 232, No. 4,* 34-43.

JUSTUSSON B I (1981). Median filtering: statistical properties. In *Two-Dimensional Digital Signal Processing II,* edited by T S Huang (Springer-Verlag: Berlin), 161-196.

KARPUR P , Shankar P M , Rose J L & Newhouse V L (1987). Split spectrum processing : optimizing the parameters using minimization. *Ultrasonics, 25,* 204-208.

KATO H & Matsumoto G (1982). Design of circularly symmetric 2-D FIR digital filters using a Fourier reconstruction technique. *IEEE Transactions on Acoustics, Speech and Signal Processing, 30,* 505-508.

KERR A T , Patterson M S , Foster F S & Hunt J W (1986). Speckle reduction in pulse echo imaging using phase insensitive and phase sensitive signal processing techniques. *Ultrasonic Imaging, 8,* 11-28.

KIM N C & Jung S H (1987). Adaptive image restoration using local statistics and directional gradient information. *Electronics Letters, 23,* 610-611.

KIMME-SMITH C & Jones J P (1984). The relative effects of system parameters on texture in grey-scale ultrasonograms. *Ultrasound in Medicine and Biology, 10,* 299-307.

KOSSOFF G , Garret W J , Carpenter D A , Jellins J & Dadd M J (1976). Principles and classification of soft tissues by grey scale echography. *Ultrasound in Medicine and Biology, 2,* 89-105.

KOSSOFF G , Robinson D E , Dadd M , Carpenter D A , Knight P & Gill R (1985). UI XTC (Ecstasy) scanner. A two transducer imaging tissue characterization scanner (abstract). In Proceedings of *Fourth Meeting of the World Federation for Ultrasound in Medicine and Biology and First World Congress of Sonographers,* Sydney, Australia, 493-494.

KOZMA A & Christensen C R (1976). Effects of speckle on resolution. *Journal of the Optical Society of America, 66,* 1257-1260.

KREMKAU F W & Taylor K J W (1986). Artifacts in ultrasound imaging. *Journal of Ultrasound in Medicine, 5,* 227-237.

KUAN D T , Sawchuk A A , Strand T C & Chavel P (1985). Adaptive noise smoothing filter for images with signal-dependent noise. *IEEE Transactions on Pattern Analysis and Machine Intelligence, 7,* 165-177.

KUAN D T , Sawchuk A A , Strand T C & Chavel P (1987). Adaptive restoration of images with speckle. *IEEE Transactions on Acoustics, Speech and Signal Processing, 35,* 373-383.

KUHLMANN F & Wise G L (1981). On second moment properties of median filtered sequences of independent data. *IEEE Transactions on Communications, 29,* 1374-1379.

KUNDU A , Mitra S K & Vaidyanathan P P (1984). Application of two-dimensional generalized mean filtering for removal of impulse noises from images. *IEEE Transactions on Acoustics, Speech and Signal Processing, 32,* 600-609.

KUNG H T (1982). Why systolic architectures ? *IEEE Computer, 15,* Jan issue, 37-46.

LEE J S (1980). Digital image enhancement and noise filtering by use of local statistics. *IEEE Transactions on Pattern Analysis and Machine Intelligence, 2,* 165-168.

LEE J S (1981). Speckle analysis and smoothing of synthetic aperture radar images. *Computer Graphics and Image Processing, 17,* 24-32.

LEE J S (1983a). Digital image smoothing and the sigma filter. *Computer Vision, Graphics and Image Processing, 24,* 255-269.

LEE J S (1983b). A simple speckle smoothing algorithm for synthetic aperture radar images. *IEEE Transactions on Systems, Man and Cybernetics, 13,* 85-89.

LEE J S (1986). Speckle suppression and analysis for synthetic aperture radar images. *Optical Engineering, 25,* 636-643.

LEE Y H & Kassam S A (1985). Generalized median filtering and related nonlinear filtering techniques. *IEEE Transactions on Acoustics, Speech and Signal Processing, 33,* 672-683.

LEEMAN S & Seggie D A (1987). Speckle reduction via phase. In *SPIE Proceedings vol 768,* 173-177.

LIAO G Y , Nodes T A & Gallagher N C Jr (1985). Output distributions of two-dimensional median filters. *IEEE Transactions on Acoustics, Speech and Signal Processing, 33,* 1280-1295.

LOUPAS T , McDicken W N & Allan P L (1987). Noise reduction in ultrasonic images by digital filtering. *British Journal of Radiology, 60,* 389-392.

LOUPAS T , McDicken W N & Allan P L (1988). An adaptive weighted median filter for speckle suppression in medical ultrasonic images. Accepted for publication by *IEEE Transactions on Circuits and Systems.*

MAGNIN P A , von Ramm O T & Thurstone F L (1982). Frequency compounding for speckle contrast reduction in phased array images. *Ultrasonic Imaging, 4,* 267-281.

MAHER K P , Mallone J F , Hurley G D & McInerney D P (1988). Evaluation of the

processing functions of a digital subtraction angiography image processor. *British Journal of Radiology, 61,* 62-68.

MAILLOUX G E , Bertrand M , Stampfler R & Ethier S (1984). Texture analysis of ultrasound B-mode images by segmentation. *Ultrasonic Imaging, 6,* 262-277.

MAILLOUX G E , Bertrand M , Stampfler R & Ethier S (1985). Local histogram information content of ultrasound B-mode echographic texture. *Ultrasound in Medicine and Biology, 11,* 743-750.

MARAGOS P & Schafer R W (1987a). Morphological filters - part I: their set-theoretic analysis and relations to linear shift-invariant filters. *IEEE Transactions on Acoustics, Speech and Signal Processing, 35,* 1153-1169.

MARAGOS P & Schafer R W (1987b). Morphological filters - part II: their relations to median, order-statistics and stack filters. *IEEE Transactions on Acoustics, Speech and Signal Processing, 35,* 1170-1184.

MARGULIS A R & Shea W J Jr (1986). Advances in imaging technology and their impact on medicine. *British Journal of Radiology, 59,* 309-315.

MASTIN G A (1985). Adaptive filters for digital noise smoothing: an evaluation. *Computer Vision, Graphics and Image Processing, 31,* 103-121.

MAX J (1960). Quantizing for minimum distortion. *IRE Transactions on Information Theory, 6,* 7-12.

McCARTY K & Stewart W (1984). *The Cardiff Test System Instruction Manual.* Diagnostic Sonar: Livingston, Edinburgh.

McCLELLAN J H & Chan D S K (1977). A 2-D FIR filter structure derived from the Chebyshev recursion. *IEEE Transactions on Circuits and Systems, 24,* 372-378.

McCOLLUM A J , Bowman C C & Daniels P A (1988). A histogram modification unit for real-time image enhancement. *Computer Vision, Graphics and Image Processing, 42,* 387-398.

McDICKEN W N (1981). *Diagnostic Ultrasonics - Principles and Use of Instruments.* Wiley: New York.

McPHERSON D D , Aylward P E , Knosp B M , Bean J A , Kerber R E , Collins S M & Skorton D J (1986). Ultrasound characterization of acute myocardial ischemia by quantitative texture analysis. *Ultrasonic Imaging, 8,* 227-240.

MELTON H E Jr & Magnin P A (1984). A-mode speckle reduction with compound frequencies and compound bandwidths. *Ultrasonic Imaging, 6,* 159-173.

MIDDLETON D (1960). *An Introduction to Statistical Communication Theory.* McGraw-Hill: New York.

MORIKUBO H , Takada E , Tsuchidate M & Shida S (1985). Image processing by microcomputer to the ultrasonogram of the thyroid, the breast and the abdominal organs (abstract). In Proceedings of *Fourth Meeting of the World Federation for Ultrasound in Medicine and Biology and First World Congress of Sonographers,* Sydney, Australia, 561.

MORRISON D C (1979). *Medical Ultrasonics: A Computer Analysis of Echoes from*

Soft Tissues. Ph.D. Thesis, University of Edinburgh.

MORRISON D, McDicken W & Wild R (1980). Statistical variations in echo amplitudes and their effect on interpretation of grey-scale images. *Applied Radiology, 9,* 109-112.

NEWHOUSE V L , Bilgutay N M , Saniie J & Furgason E S (1982). Flaw-to-grain echo enhancement by split-spectrum processing. *Ultrasonics, 20,* 59-68.

NICHOLAS D , Nassiri D K , Garbutt P & Hill C R (1986). Tissue characterization from ultrasound B-scan data. *Ultrasound in Medicine and Biology, 12,* 135-143.

NIEMINEN A , Heinonen P & Neuvo Y (1987). A new class of detail-preserving filters for image processing. *IEEE Transactions on Pattern Analysis and Machine Intelligence, 9,* 74-90.

NODES T A & Gallagher N C Jr (1984). The output distribution of median type filters. *IEEE Transactions on Communications, 32,* 532-541.

OFLAZER K (1983). Design and implementations of a single-chip 1-D median filter. *IEEE Transactions on Acoustics, Speech and Signal Processing, 31,* 1164-1168.

OOSTERVELD B J , Thijssen J M & Verhoef W A (1985). Texture of B-mode echograms: 3-D simulations and experiments of the effects of diffraction and scatterer density. *Ultrasonic Imaging, 7,* 142-160.

OPHIR J & Maklad N F (1979). Digital scan converters in diagnostic ultrasound imaging. *Proceedings of the IEEE, 67,* 654-664.

OPPENHEIM A V , Schafer R W & Stockham T G (1968). Nonlinear filtering of multiplied and convolved signals. *Proceedings of the IEEE, 56,* 1264-1294.

OPPENHEIM A V & Schafer R W (1975). *Digital Signal Processing*. Prentice-Hall: Englewood Cliffs, New Jersey.

PAPOULIS A (1981). *Probability, Random Variables and Stochastic Processes*. McGraw-Hill: New York.

PARKER D L & Pryor T A (1982). Analysis of B-scan speckle reduction by resolution limited filtering. *Ultrasonic Imaging, 4,* 108-125.

PELI E (1987). Adaptive enhancement based on a visual model. *Optical Engineering, 26,* 655-660.

PERLMAN S S , Eisenhandler S , Lyons P W & Shumila M J (1987). Adaptive median filtering for impulse noise elimination in real-time TV signals. *IEEE Transactions on Communications, 35,* 646-652.

PETROVIC O , Feigenbaum H , Armstrong W F , Ryan T , West S R , Green-Hess D , Stewart J , Mattson-Friedmeyer J L & Fineberg N (1986). Digital averaging to facilitate two-dimensional echocardiographic measurements. *Journal of Clinical Ultrasound, 14,* 367-372.

PITAS I & Venetsanopoulos A N (1986a). Nonlinear mean filters in image processing. *IEEE Transactions on Acoustics, Speech and Signal Processing, 34,* 573-584.

PITAS I & Venetsanopoulos A N (1986b). Nonlinear order statistics filters for image

filtering and edge detection. *Signal Processing, 10,* 395-413.

POMALAZA-RAEZ C A & McGillem C D (1984). An adaptive nonlinear edge-preserving filter. *IEEE Transactions on Acoustics, Speech and Signal Processing, 32,* 571-576.

PORCELLO L J , Massey N G , Innes R B & Marks J M (1976). Speckle reduction in synthetic aperture radars. *Journal of the Optical Society of America, 66,* 1305-1311.

PRATT W K (1978). *Digital Image Processing.* Wiley: New York.

PRESTON K Jr (1986). Cellular logic arrays for image processing. In *Handbook of Pattern Recognition and Image Processing,* edited by T Y Young & K S Fu (Academic Press: New York), 394-436.

PROCEEDINGS OF THE IEEE (1987). *Special Issue on Hardware and Software for Digital Signal Processing,* Vol 75, No. 9.

PYE S D , Wild S R , McDicken W N & Anderson T (1986). Automatic swept gain in ultrasonic imaging. In *Institute of Physical Sciences in Medicine, Report No. 47,* edited by J A Evans (Institute of Physical Sciences in Medicine: London), 173-175.

PYE S D , Wild S R & McDicken W N (1988). Clinical trial of a new adaptive TGC system for ultrasound imaging. *British Journal of Radiology, 61,* 523-526.

RABINER L R , McGonegal C A & Paul D (1979). FIR windowed filter design program - WINDOW. In *Programs for Digital Signal Processing,* (IEEE Press: New York), 5.2.1-5.2.19.

RAETH U , Schlaps D , Limberg B , Zuna I , Lorenz A , van Kaick G , Lorenz W J & Kommerell B (1985). Diagnostic accuracy of computerized B-scan texture analysis and conventional ultrasonography in diffuse parenchymal and malignant liver disease. *Journal of Clinical Ultrasound, 13,* 87-99.

RAI G S , Haggith J W , Fenwick J D & James O (1979). Clinical evaluation of computer processing of liver gamma camera scans. *British Journal of Radiology, 52,* 116-123.

RAO V V B & Rao K S (1986). A new algorithm for real-time median filtering. *IEEE Transactions on Acoustics, Speech and Signal Processing, 34,* 1674-1675.

RAWSON E G , Nafarrate A B , Norton R E & Goodman J W (1976). Speckle-free rear-projection screen using two close screens in slow relative motion. *Journal of the Optical Society of America, 66,* 1290-1294.

RITENOUR E R , Nelson T R & Raff U (1984). Applications of the median filter to digital radiographic images. In Proceedings of *1984 International Conference on Acoustics, Speech and Signal Processing,* San Diego, California, 23.1.1-23.1.4.

ROBINSON D E & Knight P C (1981). Computer reconstruction techniques in compound pulse-echo imaging. *Ultrasonic Imaging, 3,* 217-234.

ROBINSON D E & Knight P C (1982). Interpolation scan conversion in pulse-echo ultrasound. *Ultrasonic Imaging, 4,* 297-310.

SAGE A P & Melsa J L (1971). *Estimation Theory with Applications to Communications and Control.* McGraw-Hill: New York.

SCHOMBERG H , Vollmann W & Mahnke G (1983). Lateral inverse filtering of ultrasonic B-scan images. *Ultrasonic Imaging, 5,* 38-54.

SCHUSTER E , Knoflach P , Huber K & Grabner G (1986). An interactive processing system for ultrasonic compound imaging, real-time image processing and texture analysis. *Ultrasonic Imaging, 8,* 131-150.

SEGGIE D A & Leeman S (1987). Deterministic approach towards ultrasound speckle reduction. *IEE Proceedings Part A, 134,* 188-192.

SEGGIE D A , Doherty G M & Leeman S (1987). Pulse-echo imaging via zero manipulation. *Journal of the Acoustical Society of America, 81,* 1465-1470.

SERRA J (1982). *Image Analysis and Mathematical Morphology.* Academic Press: New York.

SHARP P F , Chesser R B & Mallard J R (1982). The influence of picture element size on the quality of clinical radionuclide images. *Physics in Medicine and Biology, 27,* 913-926.

SHARP P F (1987). Image perception. *IEE Proceedings Part A, 134,* 211-224.

SHATTUCK D P & von Ramm O T (1982). Compound scanning with a phased array. *Ultrasonic Imaging, 4,* 93-107.

SHATTUCK D P , Weinshenker M D , Smith S W & von Ramm O T (1984). Explososcan: a parallel processing technique for high speed ultrasound imaging with linear phased arrays. *Journal of the Acoustical Society of America, 75,* 1273-1282.

SHAWKER T H , Moran B , Linzer M , Parks S I , James S P , Stromeyer F W & Barranger J A (1981). B-scan echo amplitude measurement in patients with diffuse infiltrative liver disease. *Journal of Clinical Ultrasound, 9,* 293-301.

SKLANSKY J , Sankar P V & Walter R J Jr (1986). Biomedical image analysis. In *Handbook of Pattern Recognition and Image Processing,* edited by T Y Young & K S Fu (Academic Press: New York), 629-647.

SMITH S W & Lopez H (1982). A contrast-detail analysis of diagnostic ultrasonic imaging. *Medical Physics, 9,* 4-12.

SMITH S W , Wagner R F , Sandrik J M & Lopez H (1983). Low contrast detectability and contrast/detail analysis in medical ultrasound. *IEEE Transactions on Sonics and Ultrasonics, 30,* 164-173.

SMITH S W & Wagner R F (1984). Ultrasound speckle size and lesion signal to noise ratio: verification of theory. *Ultrasonic Imaging, 6,* 174-180.

SNEDECOR G W & Cochran W G (1980). *Statistical Methods.* The Iowa State University Press: Iowa.

SOMMER F G & Sue J Y (1983). Image processing to reduce ultrasonic speckle. *Journal of Ultrasound in Medicine, 2,* 413-415.

SOMMER F G , Fellingham-Joynt L L , Carroll B A & Macovski A (1981). Ultrasonic characterization of abdominal tissues via digital analysis of backscattered waveforms. *Radiology, 141,* 811-817.

STEVENSON R L & Arce G R (1987). Morphological filters: statistics and further syntactic properties. *IEEE Transactions on Circuits and Systems, 34,* 1293-1305.

SWETS J A , Pickett R M , Whitehead S F , Getty D J , Schnur J A , Swets J B & Freeman B A (1979). Assessment of diagnostic technologies. *Science, 205,* No. 4407, 753-759.

THIJSSEN J M , Oosterveld B J & Romijn R L (1987). Texture in amplitude modulated (AM) and phase derivative (PD) echograms. In *SPIE Proceedings Vol 768,* 162-167.

TODD-POKROPEK A (1980). Image processing in nuclear medicine. *IEEE Transactions on Nuclear Science, 27,* 1080-1094.

TOM V T (1985). Adaptive filter techniques for digital image enhancement. In *SPIE Proceedings Vol 528,* 29-42.

TRAHEY G E , Smith S W & von Ramm O T (1986a). Speckle pattern correlation with lateral aperture translation: experimental results and implications for spatial compounding. *IEEE Transactions on Ultrasonics, Ferroelectrics and Frequency Control, 33,* 257-264.

TRAHEY G E , Allison J W , Smith S W & von Ramm O T (1986b). A quantitative approach to speckle reduction via frequency compounding. *Ultrasonic Imaging, 8,* 151-164.

TRAHEY G E , Allison J W , Smith S W & von Ramm O T (1987). Speckle reduction achievable by spatial compounding and frequency compounding: experimental results and implications for target detectability. In *SPIE Proceedings Vol 768,* 185-192.

TUKEY J W (1971). *Exploratory Data Analysis.* Addison-Wesley: Reading, Massachusetts (preliminary edition, final edition 1977).

TY K M & Venetsanopoulos A N (1986). A fast filter for real-time image processing. *IEEE Transactions on Circuits and Systems, 33,* 948-957.

TYAN S G (1981). Median filtering: deterministic properties. In *Two-Dimensional Digital Signal Processing II,* edited by T S Huang (Springer-Verlag: Berlin), 197-217.

UHR L (1986). Parallel architectures for image processing, computer vision and pattern recognition. In *Handbook of Pattern Recognition and Image Processing,* edited by T Y Young & K S Fu (Academic Press: New York), 437-469.

VAKNINE R & Lorenz W J (1984). Lateral filtering of medical ultrasonic B-scans before image generation. *Ultrasonic Imaging, 6,* 152-158.

VELLEMAN P F (1977). Robust nonlinear data smoothers. Definitions and recommendations. *Proceedings of the National Academy of Science USA, 74,* 434-436.

VENETSANOPOULOS A N & Cappellini V (1986). Real-time image processing. In

Multidimensional Systems, edited by S G Tzafestas (Marcel Dekker: New York), 345-399.

WAGNER R F ,Smith S W , Sandrik J M & Lopez H (1983). Statistics of speckle in ultrasound B-scans. *IEEE Transactions on Sonics and Ultrasonics, 30,* 156-163.

WAGNER R F , Insana M F & Brown D G (1985). Progress in signal and texture discrimination in medical imaging. In *SPIE Proceedings Vol 535,* 57-63.

WAGNER R F , Insana M F & Brown D G (1986). Unified approach to the detection and classification of speckle texture in diagnostic ultrasound. *Optical Engineering, 25,* 738-742.

WAGNER R F , Insana M F & Brown D G (1987a). Statistical properties of radio-frequency and envelope-detected signals with applications to medical ultrasound. *Journal of the Optical Society of America Part A, 4,* 910-922.

WAGNER R F , Insana M F , Brown D G & Smith S W (1987b). Statistical physics of medical ultrasonic images. In *SPIE Proceedings Vol 768,* 22-27.

WALLIS R H (1976). An approach to the space-variant restoration and enhancement of images. In Proceedings of *Symposium on Current Mathematical Problems in Image Science,* Naval Postgraduate School, Monterey, California, 10-12.

WELLS P N T & Halliwell M (1981). Speckle in ultrasonic imaging. *Ultrasonics, 19,* 225-229.

WELLS P N T (1986). The prudent use of diagnostic ultrasound. *British Journal of Radiology, 59,* 1143-1151.

WELLS P N T (editor) (1987). *The Safety of Diagnostic Ultrasound.* British Institute of Radiology: London (British Journal of Radiology, supplement 20).

WENDT P D , Coyle E J & Gallagher N C Jr (1986). Some convergence properties of median filters. *IEEE Transactions on Circuits and Systems, 33,* 276-286.

WOLFE E R , Delp E J , Meyer C R , Bookstein F L & Buda A J (1987). Accuracy of automatically determined borders in two-dimensional echocardiography using a cardiac phantom. *IEEE Transactions on Medical Imaging, 6,* 292-296.

WOODS R E & Gonzalez R C (1981). Real-time digital image enhancement. *Proceedings of the IEEE, 69,* 643-654.

YLI-HARJA O , Astola J & Neuvo Y (1988). *Analysis of the Properties of Median and Weighted Median Filters Using Threshold Logic and Stack Filter Representation.* Research Report 10/1988, Department of Information Technology, Lappeenranta University of Technology, Finland.

YOSHIDA C , Nakajima M & Yuta S (1985). Real time speckle reduction in ultrasound echo imaging (abstract). In Proceedings of *Fourth Meeting of the World Federation for Ultrasound in Medicine and Biology and First World Congress of Sonographers,* Sydney, Australia, 544.

YOSHIDA C ,Nakajima M & Yuta S (1986). Real time speckle reduction in ultrasound imaging. *Japanese Journal of Medical Ultrasound, 13,* 305-314.

YOUNG T Y & Liu P S (1986). VLSI array architectures for pattern analysis and image

processing. In *Handbook of Pattern Recognition and Image Processing,* edited by T Y Young & K S Fu (Academic Press: New York), 471–496.

ZAGZEBSKI J A , Madsen E L & Goodsitt M M (1985). Quantitative tests of a three-dimensional grey scale texture model. *Ultrasonic Imaging, 7,* 252–263.

Appendix A : Statistical properties of the weighted median

This appendix presents the derivation of some first and second-order statistical properties of the weighted median which have been used in Section 4.4.3 of the main text. Due to the nonlinear nature of the weighted median, the resulting equations tend to be long and cumbersome. However, they are in a closed form and can be implemented on a computer in a straightforward manner. In the following, an N-point weighted median filter is assumed, having weight coefficients $\{w_1, w_2, ..., w_N\}$. Capital and small case letters are used to distinguish random variables from the actual values they take, e.g. $X=x$. Finally, $F_i(x)$ and $f_i(x)$ denote the cumulative distribution function (cdf) and the probability density function (pdf) of the random variable X_i .

First-order statistics

The pdf of the weighted median when the input sequence includes samples from one, two and three distributions is presented below. These three inputs correspond to the cases of a constant signal, an ideal (step) edge and an impulse corrupted by uncorrelated , additive noise.

Case I : Let $\{X_1, X_2, ..., X_m\}$ be independent, identically distributed (i.i.d.) random variables with distribution function $F_m(x)$ and density function $f_m(x)$. The output of an N-point weighted median filter (N=m) has a pdf $f_{WM}(x)$ given by

$$f_{WM}(x) = f_m(x) \sum_{j=1}^{m} \sum_{q=-w_j+1}^{w_j-1} f_G^j(q; m, 0) \qquad (A.1)$$

Case II : Let $\{X_1, X_2, ..., X_{m+n}\}$ be independent random variables and let $\{X_1, ..., X_m\}$, $\{X_{m+1}, ..., X_{m+n}\}$ have distribution functions $F_m(x)$, $F_n(x)$ and density functions $f_m(x)$, $f_n(x)$ respectively. The output of an N-point weighted median filter (N=m+n) has a pdf $f_{WM}(x)$ given by

$$f_{WM}(x)=f_m(x)\sum_{j=1}^{m}\sum_{q=-w_j+1}^{w_j-1}\sum_{r=-S^j(m,0)}^{S^j(m,0)} f_G^j(r;m,0)f_G(q-r;n,m) +$$

$$+ f_n(x)\sum_{j=m+1}^{m+n}\sum_{q=-w_j+1}^{w_j-1}\sum_{r=-S(m,0)}^{S(m,0)} f_G(r;m,0)f_G^j(q-r;n,m) \qquad (A.2)$$

Case III : Let $\{X_1, X_2, \ldots, X_{m+n+p}\}$ be independent random variables and let $\{X_1, \ldots, X_m\}$, $\{X_{m+1}, \ldots, X_{m+n}\}$, $\{X_{m+n+1}, \ldots, X_{m+n+p}\}$ have distribution functions $F_m(x)$, $F_n(x)$, $F_p(x)$ and density functions $f_m(x)$, f_n, $f_p(x)$ respectively. The output of an N-point weighted median filter (N=m+n+p) has a pdf $f_{WM}(x)$ given by

$$f_{WM}(x)=f_m(x)\sum_{j=1}^{m}\sum_{q=-w_j+1}^{w_j-1}\sum_{r=-S^j(m,0)}^{S^j(m,0)}\Bigg[f_G^j(r;m,0)$$

$$\sum_{s=-S(n,m)}^{S(n,m)} f_G(s;n,m)f_G(q-s-r;p,m+n)\Bigg] +$$

$$+ f_n(x)\sum_{j=m+1}^{m+n}\sum_{q=-w_j+1}^{w_j-1}\sum_{r=-S(m,0)}^{S(m,0)}\Bigg[f_G(r;m,0) \qquad (A.3)$$

$$\sum_{s=-S^j(n,m)}^{S^j(n,m)} f_G^j(s;n,m)f_G(q-s-r;p,m+n)\Bigg] +$$

$$+ f_p(x)\sum_{j=m+n+1}^{m+n+p}\sum_{q=-w_j+1}^{w_j-1}\sum_{r=-S(m,0)}^{S(m,0)}\Bigg[f_G(r;m,0)$$

$$\sum_{s=-S(n,m)}^{S(n,m)} f_G(s;n,m)f_G^j(q-s-r;p,m+n)\Bigg]$$

The quantities S, S^j, f^G and f_G^j used in equations (A.1) - (A.3) are defined as

$$S(\ell,t)=\sum_{i=1}^{\ell} w_{t+i} \quad , \quad S^j(\ell,t)=\sum_{\substack{i=1\\ i\neq j}}^{\ell} w_{t+i} \qquad (A.4)$$

and

$$f_G(r;\ell,t)=\sum_{k=0}^{\ell}[F_\ell(x)]^{\ell-k}[1-F_\ell(x)]^k\sum_{j_1=1}^{\ell-k+1}\sum_{j_2=j_1+1}^{\ell-k+2}\cdots$$

$$\cdots\sum_{j_k=j_{k-1}+1}^{\ell}\delta\left(r+S(\ell,t)-2\sum_{i=1}^{k}w_{t+j_i}\right)$$

$$f_G^j(r;\ell,t)=\sum_{k=0}^{\ell-1}[F_\ell(x)]^{\ell-k-1}[1-F_\ell(x)]^k\sum_{\substack{j_1=1\\ j_1\neq j}}^{\ell-k+1}\sum_{\substack{j_2=j_1+1\\ j_2\neq j}}^{\ell-k+2}\cdots \tag{A.5}$$

$$\cdots\sum_{\substack{j_k=j_{k-1}+1\\ j_k\neq j}}^{\ell}\delta\left(r+S^j(\ell,t)-2\sum_{i=1}^{k}w_{t+j_i}\right)$$

where $\delta(r)$ is the delta function (Bracewell, Chapter 5, 1986).

Proof

Before proceeding in the actual proof it is necessary to obtain some results which will be used extensively later. We define $g_i(x)=q$ as

$$q=g_i(x)=w_i\,\mathrm{sgn}(X_i-x) \tag{A.6}$$

where

$$\mathrm{sgn}(x)=\begin{cases}1 & \text{if } x>0\\ -1 & \text{if } x<0\end{cases} \tag{A.7}$$

The pdf $f_i(q)$ of the function $g_i(x)=q$ can be written as

$$f_i(q)=F_i(x)\,\delta(q+w_i)+(1-F_i(x))\,\delta(q-w_i) \tag{A.8}$$

where $F_i(x)$ is the distribution function of the random variable X_i.

Again, we define

$$q=G(x;\ell,t)=\sum_{i=1}^{\ell}w_{t+i}\,\mathrm{sgn}(X_{t+i}-x) \tag{A.9}$$

The function $G(x;\ell,t)=q$ is the sum of $g_i(x)$, $i=t+1, \ldots, t+\ell$. Hence, its pdf $f_G(q;\ell,t)$ is given as the convolution of the individual pdf's $f_i(q)$ (Papoulis, Chapter 7, 1981).

$$f_G(q;\ell,t)=f_{t+1}(q)*f_{t+2}(q)*\ldots*f_{t+\ell}(q) \tag{A.10}$$

Assume that the random variables X_i are identically distributed with cumulative distribution function $F_\ell(x)$. By taking into account the convolution property of the delta function, $f(x)*\delta(x)=f(x)$, and by substituting (A.8) into (A.10) the following expression is obtained.

$$f_G(r;\ell,t)=\sum_{k=0}^{\ell}[F_\ell(x)]^{\ell-k}[1-F_\ell(x)]^{k}\sum_{j_1=1}^{\ell-k+1}\sum_{j_2=j_1+1}^{\ell-k+2}\cdots$$
$$\cdots\sum_{j_k=j_{k-1}+1}^{\ell}\mathfrak{s}\left(r+S(\ell,t)-2\sum_{i=1}^{k}w_{t+j_i}\right) \tag{A.11}$$

where

$$S(\ell,t)=\sum_{i=1}^{\ell}w_{t+i} \tag{A.12}$$

The function $G^j(x;\ell,t)$ results from $G(x;\ell,t)$ if the term X_j is excluded.

$$G^j(x;\ell,t)=\sum_{\substack{i=1\\ i\neq j}}^{\ell}w_{t+i}\,\mathrm{sgn}(X_{t+i}-x) \tag{A.13}$$

Again, by substituting (A.8) into (A.10) and noting that there are only $\ell-1$ terms in the convolution, since X_j is not included, the pdf $f^j_G(q;\ell,t)$ is obtained.

$$f_G^j(r;\ell,t)=\sum_{k=0}^{\ell-1}[F_\ell(x)]^{\ell-k-1}[1-F_\ell(x)]^k \sum_{\substack{j_1=1\\ j_1\neq j}}^{\ell-k+1}\ \sum_{\substack{j_2=j_1+1\\ j_2\neq j}}^{\ell-k+2}\cdots$$

$$\cdots\ \sum_{\substack{j_k=j_{k-1}+1\\ j_k\neq j}}^{\ell} s\left(r+S^j(\ell,t)-2\sum_{i=1}^{k}w_{t+j_i}\right) \tag{A.14}$$

where

$$S^j(\ell,t)=\sum_{\substack{i=1\\ i\neq j}}^{\ell} w_{t+i} \tag{A.15}$$

Case I : Now we can proceed to the derivation of the pdf $f_{WM}(x)$ of the weighted median X_{WM}, which can be defined as

$$f_{WM}(x)=\sum_{j=1}^{m} P(X_j=x)P(X_j=X_{WM}/X_j=x)$$

Since $\{X_1, \ldots, X_m\}$ are identically distributed, $P(X_j=x)=f_m(x)$ and

$$f_{WM}(x)=f_m(x)\sum_{j=1}^{m} P(X_j=X_{WM}/X_j=x) \tag{A.16}$$

The probability of $X_j=x$ being the weighted median of the input sequence is equal by definition to the probability of $X_j=x$ being the pure median of the extended sequence which has S(m,0) terms in total (S(m,0) has been defined in equation A.12) and is formed by repeating each term X_i, w_i times. The latter probability can be expressed as the probability that from the remaining $S^j(m,0)$ terms (this quantity has been defined in equation A.15) k are smaller and $S^j(m,0)-k$ are larger than X_j . The minimum and maximum values of k are equal to

$$k_{min}+w_j=(S(m,0)+1)/2 \quad , \quad k_{max}+1=(S(m,0)+1)/2$$

If we subtract the number of terms which are larger from the number of terms which are smaller than X_j, the difference q must fall in the interval $[-w_j+1, w_j-1]$. Therefore

$$P(X_j = X_{WM} / X_j = x) = P(q \in [-w_j + 1, w_j - 1]) \tag{A.17}$$

The difference q is actually given by the function $G^j(x;m,0)$, defined in (A.13) . By using its pdf $f^j_G(q;m,0)$ (see equation A.14) we have

$$P(X_j = X_{WM} / X_j = x) = \sum_{q=-w_j+1}^{w_j-1} f^j_G(q;m,0) \tag{A.18}$$

Substitution of (A.18) into (A.16) yields (A.1) .

Case II : The pdf $f_{WM}(x)$ of the weighted median X_{WM} can be expressed as

$$f_{WM}(x) = \lim_{dx \to 0} [P(x \leq X_{WM} \leq x+dx)] / dx \tag{A.19}$$

(A.19) can be split into two mutually exclusive events A and B.

Event A : One of the random variables X_1, ..., X_m (say X_j) falls into [x, x+dx] and the rest m−1 and n variables are distributed in such a way that $X_j = X_{WM}$.

Event B : One of the random variables X_{m+1}, ..., X_{m+n} (say X_j) falls into [x, x+dx] and the rest m and n−1 variables are distributed in such a way that $X_j = X_{WM}$.

Then

$$f_{WM}(x) = \lim_{dx \to 0} [P(A) + P(B)] / dx \tag{A.20}$$

The corresponding probabilities of the events A and B are

$$P(A) = f_m(x)\,dx \sum_{j=1}^{m} P(X_j = X_{WM} / X_j \in [x, x+dx]) \tag{A.21}$$

and

$$P(B)=f_n(x)\,dx \sum_{j=m+1}^{m+n} P(X_j=X_{WM}/X_j\epsilon[x,x+dx]) \qquad (A.22)$$

If X_j belongs to the m-distribution (event A), the number of terms of the same distribution which are larger than X_j minus the number of terms which are smaller than X_j is given by $G_j(x,m,0)$. According to (A.17) the probability of X_j being the weighted median is equal to the probability that the *total* difference q falls into $[w_j+1,\ w_j+1]$. Using the pdf's $F^j_G(q;m,0)$, $f_G(q;n,m)$ of the partial differences $G^j(x;m,0)$ and $G(x;n,m)$, this can be written as

$$P(A)=f_m(x)\,dx \sum_{j=1}^{m} \sum_{q=-w_j+1}^{w_j-1} \sum_{r=-S^j(m,0)}^{S^j(m,0)} f^j_G(r;m,0)\,f_G(q-r;n,m) \qquad (A.23)$$

In a similar way

$$P(B)=f_n(x)\,dx \sum_{j=m+1}^{m+n} \sum_{q=-w_j+1}^{w_j-1} \sum_{r=-S(m,0)}^{S(m,0)} f_G(r;m,0)\,f^j_G(q-r;n,m) \qquad (A.24)$$

Finally substitution of (A.23) and (A.24) into (A.20) results in (A.2).

Case III : (A.3) can be proved by following the same methodology of Case II .

Second-order statistics

This section presents the derivation of the weighted median's autocorrelation function R(k) when the input is a constant signal corrupted by uncorrelated additive noise. Assume that the sequence of random variables $\{X_i\}$ is filtered by an N-point weighted median filter with weight coefficients $\{w_i\}$. From the definition (Section 4.4.3), the majority of the terms in the extended sequence formed by taking w_j copies of each term X_j are less than or equal to the weighted median Y_{WM} . Hence, the probability that the weighted median is less than or equal to x is given by

$$P(Y_{WM}<x)=P\left(\sum_{i=1}^{N} w_i \operatorname{sgn}(X_i-x)<0\right) \tag{A.25}$$

We define the function G(x) as

$$G(x)=\sum_{i=1}^{N} w_i \operatorname{sgn}(X_i-x)$$

which is very similar to G(x;ℓ,t), defined by (A.9) . Following a methodology similar to the one used to derive (A.10), it can be proved that the pdf of G(x) is equal to

$$f_G(q;N;F(x);S;w)=\sum_{\nu=0}^{N}[F(x)]^{N-\nu}[1-F(x)]^{\nu}\sum_{j_1=1}^{N-\nu+1}\sum_{j_2=j_1+1}^{N-\nu+2}\cdots \tag{A.26}$$

$$\cdots\sum_{j_k=j_{k-1}+1}^{N}\delta\left(q+S-2\sum_{i=1}^{\nu} w_{j_i}\right)$$

where S is the sum of the weight coefficients

$$S=\sum_{i=1}^{N} w_i \tag{A.27}$$

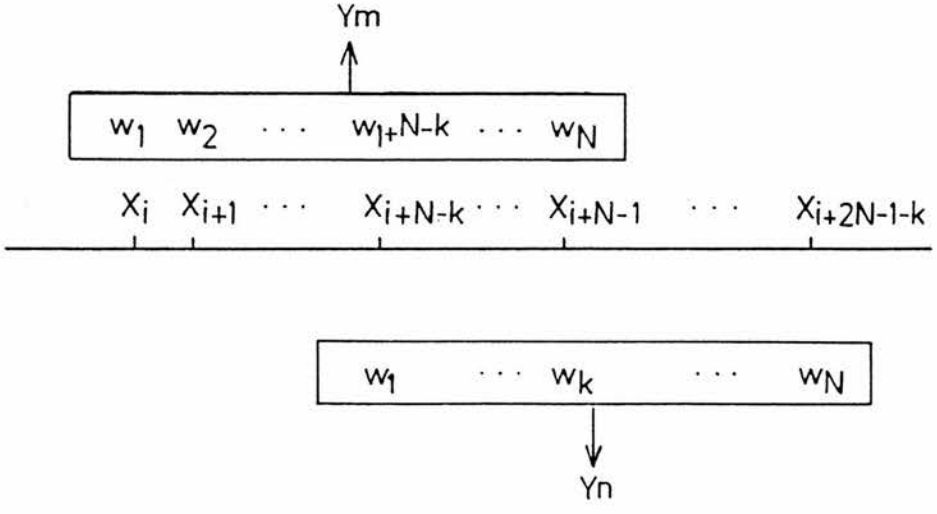

Figure A.1 : Correspondence between the terms of an input sequence and the weight coefficients of two overlapping windows.

Equation A.26 is the basis for the calculation of the joint cumulative distribution function $F(y_m, y_n)$ of the weighted median. Figure A.1 shows two N-point windows having k common terms and the corresponding weight coefficients. The joint cdf will be derived by calculating the conditional probability given an event Ω_i and then summing over all possible events (Theorem of total probability, Papoulis, Chapter 2, 1981) . This approach was suggested by Kuhlmann & Wise (1981) for the calculation of the joint cdf of the pure median.

$$F(y_m, y_n) = P(Y_m \leq y_m, Y_n \leq y_n) = \sum_i P(Y_m \leq y_m, Y_n \leq y_n / \Omega_i) P(\Omega_i) \qquad (A.28)$$

Ω_i is the event that a set of terms belonging to the overlap are less than or equal to y_m . The summation in (A.28) includes all the possible events Ω_i which, for an overlap size of k terms, are 2^k .

Let

A_i = {terms belonging to the overlap : $X_i \leq y_m$}

A_i^c = {terms belonging to the overlap : $X_i > y_m$}

B_m = {terms belonging to the m-window but not to the overlap}

B_n = {terms belonging to the n-window but not to the overlap}

In the following, $N(R)$, $w_i(\ell,R)$, $S(\ell,R)$ denote the number of terms of the ℓ-window which belong to a set R, the weight coefficients which correspond to these terms and the sum of the weights respectively. The probability $P(\Omega_i)$ is given by David (1970)

$$P(\Omega_i) = [F(y_m)]^{N(A_i)} [1-F(y_m)]^{N(A_i^c)} \qquad (A.29)$$

Also

$$P(Y_m \lessgtr y_m, Y_n \lessgtr y_n / \Omega_i) = P(Y_m \lessgtr y_m / \Omega_i) P(Y_n \lessgtr y_n / \Omega_i) \qquad (A.30)$$

Using (A.25) and noting that, due to the event Ω_i, the terms in the overlap have a fixed magnitude in respect to y_m

$$P(Y_m \lessgtr y_m / \Omega_i) = P\left(\sum_{j=1}^{N(B_m)} w_j(m, B_m) \operatorname{sgn}(X_j - y_m) \lessgtr S(m, A_i) - S(m, A_i^c) \right)$$

By using (A.26) this can be written as

$$P(Y_m \lessgtr y_m / \Omega_i) = \sum_{p=-S(m,B_m)}^{S(m,A_i)-S(m,A_i^c)-1} f_G(p; N(B_m); F(y_m); w(m, B_m); S(m, B_m)) \qquad (A.31)$$

For the derivation of $P(Y_n \lessgtr \Omega_i)$ two cases must be distinguished.

Case I : $y_n \leq y_m$

$$P(Y_n \lessgtr y_n / \Omega_i) = P\left(\sum_{j=1}^{N(B_n)} w_j(n, B_n) \operatorname{sgn}(X_i - y_n) + \right.$$

$$\left. + \sum_{j=1}^{N(A_i)} w_j(n, A_i) \operatorname{sgn}(X_j - y_n) \lessgtr -S(n, A_i^c) \right)$$

which can be written as

$$P(Y_n \lessgtr y_n / \Omega_i) = \sum_{q=-S(n,B_n)}^{N(B_n)} \sum_{r=-S(n,B_n)-S(n,A_i)}^{-S(n,A_i^c)-1} f_G(q; N(B_n); F(y_n); w(n, B_n); S(n, B_n)) *$$

$$* f_G(r-q; N(A_i); F(y_n / X_i \lessgtr y_m); w(n, A_i); S(n, A_i)) \qquad (A.32)$$

where f_G is given by (A.26) and $F(y_n / X_i \leq y_m)$ by

$$F(y_n / X_i \lessgtr y_m) = P(X_i \lessgtr y_n / X_i \lessgtr y_m) = \begin{cases} F(y_n)/F(y_m) & \text{if } y_n \lessgtr y_m \\ 1 & \text{if } y_n > y_m \end{cases}$$

Case II : $y_n > y_m$

In a similar way it can be proved that

$$P(Y_n<y_n/\Omega_i)=\sum_{q=-S(n,B_n)}^{S(n,B_n)}\sum_{r=-S(n,B_n)-S(n,A_i^c)}^{S(n,A_i)-1} f_G(q;N(B_n);F(y_n);w(n,B_n);S(n,B_n))* \\ * f_G(r-q;N(A_i^c);F(y_n/X_i>y_m);w(n,A_i^c);S(n,A_i^c)) \quad (A.33)$$

where f_G is given by (A.26) and $F(y_n/X_i>y_m)$ by

$$F(y_n/X_i>y_m)=P(X_i<y_n/X_i>y_m)=\begin{cases} 0 & \text{if } y_n<y_m \\ F(y_n)/(1-F(y_m)) & \text{if } y_n>y_m \end{cases}$$

The joint cumulative distribution function $F(y_m,y_n)$ can now be obtained by substituting (A.29) - (A.33) into (A.28) and summing over all possible events Ω_i . The resulting expression is valid for any type of input distribution as long as the random variables are identically distributed. However, in order to obtain the joint density $f(y_m,y_n)$ it will be assumed that the input random variables are discrete. If the random variable X take the values $\{y_i, i=1, ..., L\}$ the joint density is equal to the (discrete) derivative of the joint cdf

$$f(y_m,y_n)=F(y_m,y_n)+F(y_{m-1},y_{n-1})-F(y_{m-1},y_n)-F(y_m,y_{n-1})$$

where it must be noted that

$$F(y_i,y_j)=0 \qquad \text{if} \quad i \text{ or } j=0 \quad (A.34)$$

The autocorrelation R(k) is then calculated by

$$R(k)=\sum_{i=1}^{L}\sum_{j=1}^{L} y_i y_j f(y_i,y_j) \quad (A.35)$$

where k is equal to the number of terms in the overlap and L is the input alphabet size.

Equation (A.35) has been used to calculate the results presented in

Figure 4.14 . The noise distribution considered was Gaussian quantized to 32 levels in the minimum square error sense (Max, 1960).

APPENDIX B : PROGRAM LISTINGS

PROGRAM SPECKLEFILTER

The following program performs processing of ultrasonic images using one of the speckle suppression filters described in Chapter 4. The code is written in Vax Fortran (an extension of Fortran 77) and runs on a DEC MicroVax II minicomputer under the MicroVMS V4.4 operating system.

Images have 576 rows by 512 columns by 256 grey scale levels and are stored on disc as random access files of 577 records. Each row of the image corresponds to a 512-byte record, with the first record of the file containing the image header.

The name of the input image, coordinates of region to be processed, filter type to be used and its corresponding parameters are specified by the user. The main program reads the image data, stores them in an input array, calls the appropriate filter subroutine and, when processing is completed, writes the results back to the disc.

In order to achieve maximum efficiency only the pixels inside a sector scan are processed, if desirable.

VARIABLES

FILNAM	Byte array containing filename of image to be processed
LINE	Byte array containing grey scale levels of a row
IN,OUT	Integer arrays containing input and output image data
TR,BR	User-specified first/last row numbers of region to be processed
TC,BC	The corresponding column numbers
LIML,LIMR	Integer arrays containing column numbers of first/last points to be processed along a row. type has been specified.
ISCANT	User-specified scanner type
IFILTN	User-specified filter type

The filter parameters are defined at the beginning of the appropriate filter subroutines

```
      BYTE FILNAM(32),CONVC(32),LINE(512),BYTEMP
      CHARACTER*1 TEMP
      DIMENSION LIML(576),LIMR(576)
      INTEGER IN(512,576),OUT(512,576),TR,TC,BR,BC
      EQUIVALENCE (BYTEMP,TEMP)

      COMMON/A/ TR,TC,BR,BC,LIML,LIMR,IFILTN,ISCANT
      COMMON/B/ IN,OUT
      COMMON/F1/ CONVC
      COMMON/F234567/ NW,FILPAR,MW
      COMMON/F7/ NWH,IWID,VWF,EDF,FL,FH,BETA

***   SPECIFY IMAGE TO BE PROCESSED
20    WRITE(6,40)
40    FORMAT(' ENTER FILE NAME :')
      READ(5,60)FILNAM
60    FORMAT(32A1)

***   OPEN RANDOM ACCESS FILE CONTAINING IMAGE DATA
      OPEN(UNIT=8,NAME=FILNAM,ACCESS='DIRECT',
     * RECORDSIZE=128,ASSOCIATEVARIABLE=IREC8,ERR=20)

***   SELECT REGION TO BE PROCESSED,FILTER TO BE USED
***   AND SCANNER TYPE
      WRITE(6,80)
80    FORMAT(' ENTER TOP-LEFT/BOTTOM-RIGHT ROW,COLUMN'/
     * ' ,FILTER NUMBER AND SCANNER TYPE (6I4)')
      READ(5,100)TR,TC,BR,BC,IFILTN,ISCANT
100   FORMAT(6I4)

***   SPECIFY FILTER PARAMETERS
      GOTO(120,160,220,320,320,320,380)IFILTN
120   WRITE(6,140)
140   FORMAT(' ENTER FILE NAME FOR FIR COEFFICIENTS :')
      READ(5,60)CONVC
      GOTO 500
160   WRITE(6,180)
180   FORMAT(' ENTER WINDOW SIZE (I3)')
      READ(5,200)NW
200   FORMAT(I3)
      GOTO 500
220   WRITE(6,240)
240   FORMAT(' ENTER AVERAGING,MEDIAN WINDOW SIZES',
     * ' AND FILTER PARAMETER (2I3,F8.4)')
      READ(5,260)NW,MW,FILPAR
260   FORMAT(2I3,F8.4)
      GOTO 500
320   WRITE(6,340)
340   FORMAT(' ENTER WINDOW SIZE AND FILTER PARAMETER'
     * ' (I3,F8.4)')
      READ(5,360)NW,FILPAR
360   FORMAT(I3,F8.4)
      GOTO 500
380   WRITE(6,400)
400   FORMAT(' ENTER SMOOTHING,SHARPENING ',
     * ' WINDOW LENGTHS, VARIANCE WEIGHTING FACTOR,'/
     * ' WINDOW WIDTH AND EXP DECAY FACTOR,'/
     * ' LOW/HIGH CUTOFF FREQUENCIES '/
     * '  AND BETA FOR KAISER WINDOW (3I3,5F8.4)'
      READ(5,420)NW,NWH,VWF,IWID,EDF,FL,FH,BETA
420   FORMAT(3I3,5F8.4)
500   CONTINUE

***   TRANSFER IMAGE DATA FROM DISC TO MEMORY
      DO 520  IR=1,576
      IREC8=IR+1
      READ(8'IREC8)(LINE(IC),IC=1,512)
***   TRANSFORM BYTE VALUES TO INTEGERS
***   STORE THEM INTO INPUT AND OUTPUT ARRAYS
      DO 520  IC=1,512
      IPIX=LINE(IC)
      IF(IPIX.LT.0)IPIX=IPIX+256
      IN(IC,IR)=IPIX
      OUT(IC,IR)=IPIX

520   CONTINUE

***   →FOR EVERY ROW IR
      DO 540 IR=TR,BR
***   CALCULATE COLUMNS OF FIRST/LAST POINT
***   TO BE PROCESSED ALONG IR
      CALL LIMCOL(IR)
540   CONTINUE

***   CALL SELECTED FILTER SUBROUTINE
      GOTO(560,580,600,620,640,660,680)IFILTN
560   CALL FILT1
      GOTO 740
580   CALL FILT2
      GOTO 740
600   CALL FILT3
      GOTO 740
620   CALL FILT4
      GOTO 740
640   CALL FILT5
      GOTO 740
660   CALL FILT6
      GOTO 740
680   CALL FILT7
740   CONTINUE

***   TRANSFER OUTPUT IMAGE DATA FROM MEMORY TO DISC
      DO 780 IR=TR,BR
***   TRANSFORM INTEGER VALUES TO BYTES
      DO 760 IC=1,512
      ITEMP=OUT(IC,IR)
      TEMP=CHAR(ITEMP)
      LINE(IC)=BYTEMP
760   CONTINUE
      IREC8=IR+1
      WRITE(8'IREC8)(LINE(IC),IC=1,512)
780   CONTINUE

      STOP
      END
```

SUBROUTINE LIMCOL(IR)

This subroutine calculates the column numbers of the first/last points to be processed along row IR and stores them in arrays LIML, LIMR. For linear scanners, the column numbers are row-independent and equal to the user-specified values. For sector scanners, they are determined by the sector geometry.

VARIABLES

IR	Current image row
IR0,IC0,RAD,THETA	Centre coordinates,radius and half-angle of the sector
LIMLT,LIMRT	Column numbers of leftmost/rightmost points of the sector
TC,BC	User-specified first/last column of region to be processed
IC1,IC3	Column numbers defined by the intersection of row IR with the linear segments of the sector
IC2,IC4	Corresponding quantities for the circular segment of the sector
ILC,IRC	Columns of firts/last points to be processed along row IR
LIML,LIMR	Arrays containing ILC,IRC values

```
      DIMENSION LIML(576),LIMR(576)
      INTEGER TR,TC,BR,BC
      COMMON/A/ TR,TC,BR,BC,LIML,LIMR,IFILTN,ISCANT

***   GEOMETRICAL DATA FOR SCANNERS
      GOTO(10,20,40,60,80)ISCANT

***   LINEAR SCANNER
10    ILC=TC
      IRC=BC
      GOTO 120


***   GL Z/S SCANNER - OSCILLATING PROBE
20    IR0=25
      IC0=228
      THETA=0.4742
      RAD=460.
      LIMLT=48
      LIMRT=410
      GOTO 100
***   GL Z/S SCANNER - ROTATING PROBE
40    IR0=32
      IC0=228
      THETA=0.6023
      RAD=454.
      LIMLT=22
      LIMRT=442
      GOTO 100
***   SIEMENS SX SCANNER
60    IR0=34
      IC0=253
      THETA=0.6142
      RAD=460.
      LIMLT=32
      LIMRT=480
      GOTO 100
***   ACUSON SCANNER
80    IR0=60
      IC0=258
      THETA=0.6012
      RAD=440.
      LIMLT=46
      LIMRT=472
100   CONTINUE

***   CALCULATE COLUMN NUMBERS
***   OF FIRST/LAST POINTS TO BE PROCESSED
      ANGF=(IR-IR0)*SIN(THETA)/COS(THETA)
      RADF=SQRT(RAD**2-FLOAT(IR-IR0)**2)
      IC1=IC0-ANGF
      IC2=IC0-RADF
      IC3=IC0+ANGF
      IC4=IC0+RADF
      TC=MAX0(TC,IC1,IC2,LIMLT)
      BC=MIN0(BC,IC3,IC4,LIMRT)

***   STORE RESULTS
120   LIML(IR)=ILC
      LIMR(IR)=IRC

      RETURN
      END
```

SUBROUTINE FILT1

Two-dimensional linear (FIR) filter

VARIABLES

IN,OUT,TR,BR,LIML,LIMR	See main program
CONVC	Name of file containing filter data
NW	Window length/width. Actual window size is NW X NW
FIR	Real array containing filter coefficients
SF,SUM	Sums of filter coefficients and convolution partial results

```
      BYTE CONVC(32)
      DIMENSION LIML(576),LIMR(576),FIR(31,31)
      INTEGER IN(512,576),OUT(512,576),TR,TC,BR,BC
      COMMON/A/ TR,TC,BR,BC,LIML,LIMR,IFILTN,ISCANT
      COMMON/B/ IN,OUT
      COMMON/F1/ CONVC

***   OPEN SEQUENTIAL ACCESS FILTER DATA FILE
      OPEN(UNIT=9,NAME=CONVC,TYPE='OLD')

***   READ WINDOW LENGTH/WIDTH
      READ(9,20)NW
20    FORMAT(I2)


***   READ FILTER COEFFICIENTS
      DO 60 I=1,NW
      READ(9,40)(FIR(J,I),J=1,NW)
40    FORMAT(31F12.8)
60    CONTINUE

***   CALCULATE WINDOW PARAMETERS
      NW2=(NW-1)/2
      N=NW2+1
      NSQ=NW*NW

***   →FOR EVERY ROW IR
      DO 100 IR=TR,BR
***   →AND FOR EVERY POINT TO BE PROCESSED ALONG IR
      DO 100 IC=LIML(IR),LIMR(IR)

***   CONVOLVE IMAGE DATA WITH FILTER COEFFICIENTS
      SUM=0.
      SF=0.
      DO 80 I=1,NW
      IRM=IR+I-N
      DO 80 J=1,NW
      ICM=IC+J-N
      WC=FIR(J,I)
      SF=SF+WC
      SUM=SUM+WC*IN(ICM,IRM)
80    CONTINUE

***   STORE NEAREST INTEGER OF RESULT
      OUT(IC,IR)=INT(SUM/SF+0.5)

100   CONTINUE

      RETURN
      END
```

SUBROUTINE FILT2

Two-dimensional median filter implemented using Huang's fast algorithm. This algorithms takes advantage of the fact that only

a small fraction of the pixels inside the window is deleted and an equal number is added every time the window moves one position to the right.

VARIABLES

IN,OUT,TR,BR,LIML,LIMR	See main program
NW	Window length/width. Actual window size is NW X NW
HIST	Integer array containing the grey level histogram of the pixels inside the window
MDN	Median value at a particular point
LTMDN	Number of pixels inside the window with grey level less than the median

```
      DIMENSION LIML(576),LIMR(576),IN(512,576)
      INTEGER OUT(512,576),HIST(256),TR,TC,BR,BC
      COMMON/A/ TR,TC,BR,BC,LIML,LIMR,IFILTN,ISCANT
      COMMON/B/ IN,OUT
      COMMON/F234567/ NW,FILPAR,MW

***   CALCULATE WINDOW PARAMETERS
      NW2=(NW-1)/2
      N=NW2+1
      NSQ=NW*NW
      NSQ2=(NSQ-1)/2

***   →FOR EVERY ROW IR
      DO 180 IR=TR,BR

***   INITIALIZE HISTOGRAM
      DO 20  I=1,256
      HIST(I)=0
20    CONTINUE

***   CALCULATE MEDIAN FOR THE FIRST POINT OF IR
      IC=LIML(IR)


***   FORM GREY LEVEL HISTOGRAM
      DO 40 I=1,NW
      IRM=IR+I-N
      DO 40 J=1,NW
      ICM=IC+J-N
      IPIX=IN(ICM,IRM)+1
      HIST(IPIX)=HIST(IPIX)+1
40    CONTINUE

***   FIND [(NW*NW-1)/2]th LARGEST VALUE
      LTMDN=0
      DO 60 I=1,256
      LTMDN=LTMDN+HIST(I)
      IF(LTMDN.GT.NSQ2)GOTO 80
60    CONTINUE

***   MEDIAN HAS BEEN FOUND
80    MDN=I
      OUT(IC,IR)=MDN-1

***   →FIND MEDIAN VALUE FOR THE REST OF THE POINTS
***    TO BE PROCESSED ALONG IR
      DO 180 IC=LIML(IR)+1,LIMR(IR)

***   UPDATE HISTOGRAM AND LTMDN
      ICM=IC-N
      DO 100 I=1,NW
      IRM=IR+I-N
      IPXOLD=IN(ICM,IRM)+1
      HIST(IPXOLD)=HIST(IPXOLD)-1
      IF(IPXOLD.LE.MDN)LTMDN=LTMDN-1
      IPXNEW=IN(ICM+NW,IRM)+1
      HIST(IPXNEW)=HIST(IPXNEW)+1
      IF(IPXNEW.LE.MDN)LTMDN=LTMDN+1
100   CONTINUE

***   FIND CURRENT MEDIAN USING PREVIOUS MEDIAN VALUE
      IF(LTMDN.GT.NSQ2)GOTO 120
      GOTO 140
120   TEMP=LTMDN-HIST(MDN)
      IF(TEMP.LE.NSQ2)GOTO 160
      LTMDN=TEMP
      MDN=MDN-1
      GOTO 120
140   IF(LTMDN.GT.NSQ2)GOTO 160
      MDN=MDN+1
      LTMDN=LTMDN+HIST(MDN)
      GOTO 140

***   STORE MEDIAN VALUE
160   OUT(IC,IR)=MDN-1

180   CONTINUE

      RETURN
      END
```

SUBROUTINE FILT3

Double window modified trimmed mean (DW-MTM) filter. The variance of noise is assumed to be proportional to its mean. The median is calculated as in **SUBROUTINE FILT2** .

VARIABLES

IN,OUT,TR,BR,LIML,LIMR	See main program
NW	Averaging window length/width. Actual window size is NW X NW
MW	Median window length/width. Actual window size is MW X MW
HIST,MDN,LTMDN	See **SUBROUTINE FILT2**
MED	Integer array containing median values O_{med} of row IR
Q	Threshold q defined as $q=c[O_{med}]^{1/2}$
FILPAR	Constant c in the above expression. Controls the amount of smoothing performed
IDIF	Absolute difference between a pixel and median O_{med}
ICOUNT,SUM	Number and sum of terms inside the window whose difference from the median O_{med} is not greater than the threshold q

```
      DIMENSION LIML(576),LIMR(576),MED(512),IN(512,576)
      INTEGER OUT(512,576),HIST(256),TR,TC,BR,BC
      COMMON/A/ TR,TC,BR,BC,LIML,LIMR,IFILTN,ISCANT
      COMMON/B/ IN,OUT
      COMMON/F234567/ NW,FILPAR,MW

***   CALCULATE AVERAGING,MEDIAN WINDOW PARAMETERS
      NW2=(NW-1)/2
      N=NW2+1
      NSQ=NW*NW
      MW2=(MW-1)/2
      M=MW2+1
      MSQ=MW*MW
      MSQ2=(MSQ-1)/2

***   →FOR EVERY ROW IR
      DO 220  IR=TR,BR

***   →PERFORM MW X MW MEDIAN FILTERING
      DO 20  I=1,256
      HIST(I)=0
20    CONTINUE

      IC=LIML(IR)
      DO 40 I=1,MW
      IRM=IR+I-M
      DO 40 J=1,MW
      ICM=IC+J-M
      IPIX=IN(ICM,IRM)+1
      HIST(IPIX)=HIST(IPIX)+1
40    CONTINUE

      LTMDN=0
      DO 60 I=1,256
```

```
      LTMDN=LTMDN+HIST(I)
      IF(LTMDN.GT.MSQ2)GOTO 80
60    CONTINUE
80    MDN=I
      MED(IC)=MDN-1

      DO 180 IC=LIML(IR)+1,LIMR(IR)

      ICM=IC-M
      DO 100 I=1,MW
      IRM=IR+I-M
      IPXOLD=IN(ICM,IRM)+1
      HIST(IPXOLD)=HIST(IPXOLD)-1
      IF(IPXOLD.LE.MDN)LTMDN=LTMDN-1
      IPXNEW=IN(ICM+MW,IRM)+1
      HIST(IPXNEW)=HIST(IPXNEW)+1
      IF(IPXNEW.LE.MDN)LTMDN=LTMDN+1
100   CONTINUE

      IF(LTMDN.GT.MSQ2)GOTO 120
      GOTO 140
120   TEMP=LTMDN-HIST(MDN)
      IF(TEMP.LE.MSQ2)GOTO 160
      LTMDN=TEMP
      MDN=MDN-1
      GOTO 120
140   IF(LTMDN.GT.MSQ2)GOTO 160
      MDN=MDN+1
      LTMDN=LTMDN+HIST(MDN)
      GOTO 140

160   MED(IC)=MDN-1

180   CONTINUE

***   →FOR EVERY POINT TO BE PROCESSED ALONG IR
      DO 220  IC=LIML(IR),LIMR(IR)

***   CALCULATE THRESHOLD q
      MDN=MED(IC)


      Q=FILPAR*SQRT(FLOAT(MDN))

***   CALCULATE ICOUNT AND SUM
      ICOUNT=0
      SUM=0.
      DO 200 I=1,NW
      IRM=IR+I-N
      DO 200 J=1,NW
      ICM=IC+J-N
      IPIX=IN(ICM,IRM)
      IDIF=IABS(IPIX-MDN)
      IF(IDIF.GT.Q)GOTO 200
      ICOUNT=ICOUNT+1
      SUM=SUM+IPIX
200   CONTINUE

***   STORE NEAREST INTEGER OF RESULT
      OUT(IC,IR)=INT(SUM/ICOUNT+0.5)

220   CONTINUE

      RETURN
      END
```

SUBROUTINE FILT4

Lee's modified algorithm. Fast calculation of local statistics by **SUBROUTINE IMSTAT(IR)** . The variance of noise is assumed to be proportional to its mean.

VARIABLES

IN,OUT,TR,BR,LIML,LIMR	See main program
NW	Window length/width. Actual window size is NW X NW
AV,VAR	Arrays containing the local mean and variance of points to be processed along IR
C	Weighting factor. Controls contributions of the input and the local mean to the output value
FILPAR	Used for the calculation of C. Controls the amount of smoothing performed.

```
      DIMENSION LIML(576),LIMR(576),AV(512),VAR(512)
      INTEGER IN(512,576),OUT(512,576),TR,TC,BR,BC
      COMMON/A/ TR,TC,BR,BC,LIML,LIMR,IFILTN,ISCANT
      COMMON/B/ IN,OUT
      COMMON/F234567/ NW,FILPAR,MW
      COMMON/STAT/ AV,VAR

***   →FOR EVERY ROW IR
      DO 20  IR=TR,BR

***   CALCULATE LOCAL STATISTICS
      CALL IMSTAT(IR)

***   →FOR EVERY POINT TO BE PROCESSED ALONG IR
      DO 20  IC=LIML(IR),LIMR(IR)

***   CALCULATE WEIGHTING FACTOR C
      ICPIX=IN(IC,IR)
      A=1.-AV(IC)*FILPAR**2/VAR(IC)
      IF(A.LT.0.)A=0.

***   STORE NEAREST INTEGER OF RESULT
      OUT(IC,IR)=INT(AV(IC)+A*(ICPIX-AV(IC))+0.5)

20    CONTINUE

      RETURN
      END
```

SUBROUTINE FILT5

Frost's modified algorithm. Fast calculation of local statistics by **SUBROUTINE IMSTAT(IR)** . The variance of noise is assumed to be proportional to its mean.

VARIABLES

IN,OUT,TR,BR,LIML,LIMR	See main program
NW	Window length/width. Actual window size is NW X NW
AV,VAR	Arrays containing the local mean and variance of points to be processed along IR
DIST	Array containing distance of each point inside the window from the centre
A	Local statistics factor, $A=c\sigma^2/m$
FILPAR	Constant c in the above expression. Controls the amount of smoothing performed
WC	Filter coefficient at a particular point
SF,SUM	Sums of filter coefficients and convolution partial results

```
      DIMENSION LIML(576),LIMR(576),AV(512),VAR(512)
      DIMENSION DIST(31,31)
      INTEGER IN(512,576),OUT(512,576),TR,TC,BR,BC
      COMMON/A/ TR,TC,BR,BC,LIML,LIMR,IFILTN,ISCANT
      COMMON/B/ IN,OUT
      COMMON/F234567/ NW,FILPAR,MW
      COMMON/STAT/ AV,VAR

***   CALCULATE WINDOW PARAMETERS
      NW2=(NW-1)/2
      N=NW2+1
      NSQ=NW*NW

***   CALCULATE DISTANCES FROM CENTRE OF WINDOW
      DO 20  I=1,NW
      DO 20  J=1,NW
      DIST(I,J)=(I-N)**2+(J-N)**2
      DIST(I,J)=SQRT(DIST(I,J))
```

```
20    CONTINUE

***   →FOR EVERY ROW IR
      DO 60 IR=TR,BR

***   CALCULATE LOCAL STATISTICS
      CALL IMSTAT(IR)

***   →FOR EVERY POINT TO BE PROCESSED ALONG IR
      DO 60 IC=LIML(IR),LIMR(IR)

***   CALCULATE LOCAL STATISTICS FACTOR
      A=FILPAR*VAR(IC)/AV(IC)

***   CALCULATE FILTER COEFFICIENTS
***   CONVOLVE IMAGE DATA WITH THEM
      SUM=0.
      SF=0.
      DO 40 I=1,NW
      IRM=IR+I-N
      DO 40 J=1,NW
      ICM=IC+J-N
      WC=EXP(-A*DIST(I,J))
      SF=SF+WC
      SUM=SUM+WC*IN(ICM,IRM)
40    CONTINUE

***   STORE NEAREST INTEGER OF RESULT
      OUT(IC,IR)=INT(SUM/SF+0.5)

60    CONTINUE

      RETURN
      END
```

SUBROUTINE FILT6

Adaptive weighted median filter. Fast calculation of local statistics by **SUBROUTINE IMSTAT(IR)** . The variance of noise is assumed to be proportional to its mean.

VARIABLES

IN,OUT,TR,BR,LIML,LIMR	See main program
NW	Window length/width. Actual window size is NW X NW
AV,VAR	Arrays containing the local mean and variance of points to be processed along IR
DIST	Array containing the distance of each point inside the window from the centre
A	Local statistics factor, $A=c\sigma^2/m$
FILPAR	Constant c in the above expression. Controls the amount of smoothing performed
WF	Weight coefficient at a particular point
HIST	Gray level histogram of terms inside the window
MDN	Weighted median of the terms inside the window, i.e. median of the extended sequence formed by repeating each term as many times as the corresponding weight coefficients
LTMDN	Number of terms with grey level less than the weighted median

```
      DIMENSION LIML(576),LIMR(576)
      DIMENSION AV(512),VAR(512),DIST(31,31)
      INTEGER IN(512,576),OUT(512,576),TR,TC,BR,BC
      INTEGER WF(31,31),HIST(256)
      COMMON/A/ TR,TC,BR,BC,LIML,LIMR,IFILTN,ISCANT
      COMMON/B/ IN,OUT
      COMMON/F234567/ NW,FILPAR,MW
      COMMON/STAT/ AV,VAR

***   CALCULATE WINDOW PARAMETERS
      NW2=(NW-1)/2
      N=NW2+1

***   CALCULATE DISTANCES FROM CENTRE OF THE WINDOW
      DO 20  I=1,N
      DO 20  J=1,N
      DIST(I,J)=(I-N)**2+(J-N)**2
      DIST(I,J)=SQRT(DIST(I,J))
20    CONTINUE

***   →FOR EVERY ROW TO BE PROCESSED
      DO 220  IR=TR,BR

***   CALCULATE LOCAL STATISTICS
      CALL IMSTAT(IR)

***   →FOR EVERY POINT TO BE PROCESSED ALONG IR
      DO 220  IC=LIML(IR),LIMR(IR)

***   CALCULATE LOCAL STATISTICS FACTOR
      A=FILPAR*VAR(IC)/AV(IC)

***   CALCULATE WEIGHT COEFFICIENTS
      DO 80 J=1,MW
      DO 80 I=1,MW
      WF(I,J)=99.-A*DIST(I,J)
      IF(WF(I,J).LT.0)WF(I,J)=0
80    CONTINUE

***   INITIALIZE GREY LEVEL HISTOGRAM
      DO 140 I=1,256
      HIST(I)=0
140   CONTINUE

***   CALCULATE HISTOGRAM OF EXTENDED SEQUENCE
      IWFS=0
      DO 160 I=1,NW
      IRM=IR+I-N
      DO 160 J=1,NW

      ICM=IC+J-N
      IWFS=IWFS+WF(I,J)
      IPIX=IN(ICM,IRM)+1
      HIST(IPIX)=HIST(IPIX)+WF(I,J)
160   CONTINUE

***   FIND MEDIAN OF EXTENDED SEQUENCE
      LTMDN=0
      IWFS2=(IWFS-1)/2
      DO 180 I=1,256
      LTMDN=LTMDN+HIST(I)
      IF(LTMDN.GT.IWFS2)GOTO 200
180   CONTINUE

***   STORE RESULT
200   MDN=I
      OUT(IC,IR)=MDN-1

220   CONTINUE

      RETURN
      END
```

SUBROUTINE IMSTAT(IR)

Local statistics subroutine. Called by **SUBROUTINE FILT4, FILT5 & FILT6** to calculate the local mean and variance of points along a specific row. Fast implementation based on the observation that when an NW X NW window is shifted one position to the right, a column of NW terms leaves and a new one enters the window but the rest NW^2-2NW terms remain the same.

VARIABLES

IN,OUT,TR,BR,LIML,LIMR	See main program
NW	Window length/width. Actual window size is NW X NW
SUM,SQSUM	Arrays containing the sum and sum of squares of terms belonging to a particular column of the window

SUMT,SQSUMT	Total sum and sum of squares of terms inside the window
SUMN,SQSUMN	Sum and sum of squares of terms belonging to the rightmost (most recently included) column of the window
AV,VAR	Arrays containing the local mean and variance of points to be processed along row IR

```
      DIMENSION LIML(576),LIMR(576)
      DIMENSION SUM(31),SQSUM(31),AV(512),VAR(512)
      INTEGER IN(512,576),OUT(512,576),TR,TC,BR,BC
      COMMON/A/ TR,TC,BR,BC,LIML,LIMR,IFILTN,ISCANT
      COMMON/B/ IN,OUT
      COMMON/F234567/ NW,FILPAR,NW
      COMMON/STAT/ AV,VAR

***   CALCULATE WINDOW PARAMETERS
      NW2=(NW-1)/2
      N=NW2+1
      NSQ=NW*NW

***   INITIALIZE ARRAYS
      DO 20  I=1,NW
      SUM(I)=0.
      SQSUM(I)=0.
20    CONTINUE

***   CALCULATE LOCAL STATISTICS
***   OF FIRST POINT TO BE PROCESSED
      IC=LIML(IR)
      SUMT=0.
      SQSUMT=0.
      DO 60 J=1,NW
      ICM=IC+J-N
      DO 40 I=1,NW
      IRM=IR+I-N
      PIX=IN(ICM,IRM)

      SUM(J)=SUM(J)+PIX
      SQSUM(J)=SQSUM(J)+PIX**2
40    CONTINUE
      SUMT=SUMT+SUM(J)
      SQSUMT=SQSUMT+SQSUM(J)
60    CONTINUE
      AV(IC)=SUMT/NSQ+0.001
      VAR(IC)=SQSUMT/NSQ-AV(IC)**2+0.001

***   →CALCULATE LOCAL STATISTICS FOR THE REST
***   OF THE POINTS TO BE PROCESSED ALONG IR
      DO 120  IC=LIML(IR)+1,LIMR(IR)

***   CALCULATE SUM AND SUM OF SQUARES FOR NEW COLUMN
      SUMN=0.
      SQSUMN=0.
      ICM=IC+NW2
      DO 80 I=1,NW
      IRM=IR+I-N
      PIX=IN(ICM,IRM)
      SUMN=SUMN+PIX
      SQSUMN=SQSUMN+PIX**2
80    CONTINUE

***   CALCULATE TOTAL SUM AND SUM OF SQUARES
      SUMT=SUMT+SUMN-SUM(1)
      SQSUMT=SQSUMT+SQSUMN-SQSUM(1)

***   CALCULATE LOCAL STATISTICS
      AV(IC)=SUMT/NSQ+0.001
      VAR(IC)=SQSUMT/NSQ-AV(IC)**2+0.001

***   UPDATE SUM ARRAYS BY SHIFTING THEM
***   ONE POSITION TO THE LEFT
      DO 100 I=1,NW-1
      SUM(I)=SUM(I+1)
      SQSUM(I)=SQSUM(I+1)
100   CONTINUE
      SUM(NW)=SUMN
      SQSUM(NW)=SQSUMN

120   CONTINUE

      RETURN
      END
```

SUBROUTINE FILT7

Directional smoothing/sharpening

VARIABLES

IN,OUT,TR,BR,LIML,LIMR	See main program
NW,NWH	Window lengths for smoothing/sharpening
IWID	Width of directional windows (usually IWID=1)
EDF	Exponential decay factor. Determines relative contributions of terms along the window width
WIDC	Weight coefficients for the terms along the window width
ICONTR	Indicates processing stage; 1 : smoothing - 2 : sharpening
IND	Indicates direction of processing; 1 : horizontal - 3 : vertical - 3,4 : diagonal
DAV,DVAR	Arrays containing the local directional mean and variance of the terms inside the window
VWF	Variance weighting factor
VARN	Array containing normalized directional variances of every image point
BETA	Attenuation of Kaiser window for bandpass filter design
WKAISER	Array containing Kaiser window coefficients
FL,FH	User specified low and high cutoff frequency of bandpass filter
FLM	Actual low cutoff frequency at each point
BPCOEF	Array containing bandpass filter coefficients

```
      DIMENSION LIML(576),LIMR(576)
      DIMENSION VARN(4,512,576),DAV(4),DVAR(4)
      DIMENSION WIDC(31),WKAISER(31),BPCOEF(31)
      INTEGER IN(512,576),OUT(512,576),TR,TC,BR,BC
      COMMON/A/ TR,TC,BR,BC,LIML,LIMR,IFILTN,ISCANT
      COMMON/B/ IN,OUT
      COMMON/F234567/ NW,FILPAR,NW
      COMMON/F7/ NWH,IWID,VWF,EDF,FL,FH,BETA

***   CALCULATE WINDOW PARAMETERS AND CONSTANTS
      NW2=(NW-1)/2
      N=NW2+1
      NWH2=(NWH-1)/2
      NH=NWH2+1
      IWID2=(IWID-1)/2
      IW=IWID2+1
      PI=4.*ATAN(1.)

***   CALCULATE WEIGHTS ALONG THE WINDOW WIDTH
      SUM=0.
      DO 20  I=1,IWID
      WIDC(I)=EXP(-EDF*(I-IW)**2)
      SUM=SUM+WIDC(I)
20    CONTINUE
      DO 40 I=1,IWID
      WIDC(I)=WIDC(I)/SUM
40    CONTINUE

***   CALCULATE KAISER WINDOW COEFFICIENTS
      CALL KAISER(NWH,WKAISER,BETA)
```

```
      ICONTR=0
***   UPDATE PROCESSING STAGE INDICATOR
60    ICONTR=ICONTR+1

***   →FOR EVERY ROW IR
      DO 680 IR=TR,BR

***   →AND FOR EVERY POINT TO BE PROCESSED ALONG IR
      DO 680 IC=LIML(IR),LIMR(IR)

      IF(ICONTR.EQ.2)GOTO 340

***   PERFORM SMOOTHING
      SUMNV=0.
      SUMNVI=0.

***   →FOR EVERY DIRECTION
      DO 300 IND=1,4

***   CALCULATE MEAN AND VARIANCE
      SUM=0.
      SQSUM=0.
      DO 280 K=1,NW

***   ALONG THE WINDOW LENGTH
      GOTO(80,100,120,140)IND
80    I=IR
      J=IC+K-N
      GOTO 160
100   I=IR+K-N
      J=IC-K+N
      GOTO 160
120   I=IR+K-N
      J=IC
      GOTO 160
140   I=IR+K-N
      J=IC+K-N
160   CONTINUE

***   AND ALONG THE WINDOW WIDTH

      PIX=0.
      DO 270 L=1,IWID
      GOTO(180,200,220,240)IND
180   IM=I+L-IW
      JM=J
      GOTO 260
200   IM=I+L-IW
      JM=J+L-IW
      GOTO 260
220   IM=I
      JM=J+L-IW
      GOTO 260
240   IM=I+L-IW
      JM=J-L+IW
260   PIX=PIX+IN(JM,IM)*WIDC(L)
270   CONTINUE
      SUM=SUM+PIX
      SQSUM=SQSUM+PIX**2

280   CONTINUE

      DAV(IND)=SUM/NW+0.001
      DVAR(IND)=SQSUM/NW-DAV(IND)**2+0.001
      TEMP=DVAR(IC)**VWF
      SUMNV=SUMNV+TEMP
      SUMNVI=SUMNVI+1/TEMP

300   CONTINUE

***   CALCULATE NORMALIZED VARIANCES AND OUTPUT
      OUTP=0.
      DO 320  IND=1,4
      VARN(IND,IC,IR)=DVAR(IND)**VWF/SUMNV
      OUTP=OUTP+DAV(IND)/VARN(IND,IC,IR)
320   CONTINUE

***   STORE NEAREST INTEGER OF RESULT
      OUT(IC,IR)=INT(OUTP/SUMNVI+0.5)
      GOTO 680

***   PERFORM SHARPENING
340   CONTINUE

      OUTP=0.
      VSUM=0.

***   →FOR EVERY DIRECTION
      DO 660 IND=1,4

***   CALCULATE BANDPASS FILTER COEFFICIENTS
      TEMP=0.
      FLM=FL*VARN(IND,IC,IR)
      FD=FH-FLM
      FS=FH+FLM
      BPCOEF(NH)=2*FD*WKAISER(1)
      BPSUM=BPCOEF(NH)
      DO 400 M=2,NH
      C=PI*(M-1)
      BPCOEF(M+NWH2)=2*SIN(C*FD)*COS(C*FS)*WKAISER(M)/C
      BPSUM=BPSUM+2*BPCOEF(M+NWH2)
400   CONTINUE
      DO 420  M=NH,NWH
      BPCOEF(M)=BPCOEF(M)/BPSUM
      BPCOEF(NWH+1-M)=BPCOEF(M)
420   CONTINUE

***   CONVOLVE IMAGE DATA WITH FILTER COEFFICIENTS
      DO 640 K=1,NWH

      GOTO(440,460,480,500)IND

440   I=IR
      J=IC+K-NH
      GOTO 520
460   I=IR+K-NH
      J=IC-K+NH
      GOTO 520
480   I=IR+K-NH
      J=IC
      GOTO 520

500   I=IR+K-NH
      J=IC+K-NH
520   CONTINUE

      PIX=0.
      DO 630 L=1,IWID
      GOTO(540,560,580,600)IND
540   IM=I+L-IW
      JM=J
      GOTO 620
560   IM=I+L-IW
      JM=J+L-IW
      GOTO 620
580   IM=I
      JM=J+L-IW
      GOTO 620
600   IM=I+L-IW
      JM=J-L+IW
620   PIX=PIX+IN(JM,IM)*WIDC(L)
630   CONTINUE
      BPC=BPCOEF(K)
      TEMP=TEMP+PIX*BPC
640   CONTINUE
      TEMP=TEMP*VARN(IND,IC,IR)
      OUTP=OUTP+TEMP
660   CONTINUE

***   STORE NEAREST INTEGER OF RESULT
      OUT(IC,IR)=INT(OUTP+0.5)

680   CONTINUE

***   IF SHARPENING IS COMPLETED STOP
      IF(ICONTR.EQ.2)GOTO 720

***   IF SMOOTHING IS COMPLETED
***   TRANSFER SMOOTHED DATA TO INPUT ARRAY
      DO 700 I=TR,BR
      DO 700 J=LIML(I)-NWH,LIMR(I)+NWH
      IN(J,I)=OUT(J,I)
```

```
700   CONTINUE

***   GO BACK TO PERFORM SHARPENING
      GOTO 60

720   CONTINUE

      RETURN
      END
```

SUBROUTINE KAISER(NF,W,BETA)

This subroutine calculates the Kaiser window coefficients for one-dimensional bandpass filter design. Called from **SUBROUTINE FILT7**

VARIABLES

NF	Window size
W	Kaiser window coefficients
BETA	Attenuation of Kaiser window in db
BES	Modified Bessel function of the first kind (zero order)

```
      DIMENSION W(31)
      REAL INO
      N=(NF+1)/2
      BES=INO(BETA)
      XIND=(NF-1)**2
      DO 20  I=1,N
      XI=4.*(I-1)**2
      W(I)=INO(BETA*SQRT(1.-XI/XIND))/BES
20    CONTINUE
      RETURN
      END
```

REAL FUNCTION INO(X)

This function evaluates the zero-order modified Bessel function of the first kind as a polynomial series of up to 25 terms.

```
      Y=X/2.
      T=1.E-08
      E=1.
      DE=1.
      DO 20  I=1,25
      XI=I
      DE=DE*Y/XI
      SDE=DE**2
      E=E+SDE
      IF(E*T-SDE)20,20,40
20    CONTINUE
40    INO=E
      RETURN
      END
```

Appendix C : Circuit diagrams

This Appendix presents the circuit diagrams of the real-time hardware filter of Chapter 5. The following signals from the scanner are required.

- ADCLK : A/D converter clock.

- LP : End of A-scan line pulse.

- $G_0 ... G_5$: 6-bit A/D converter output (G_0 is the LSB).

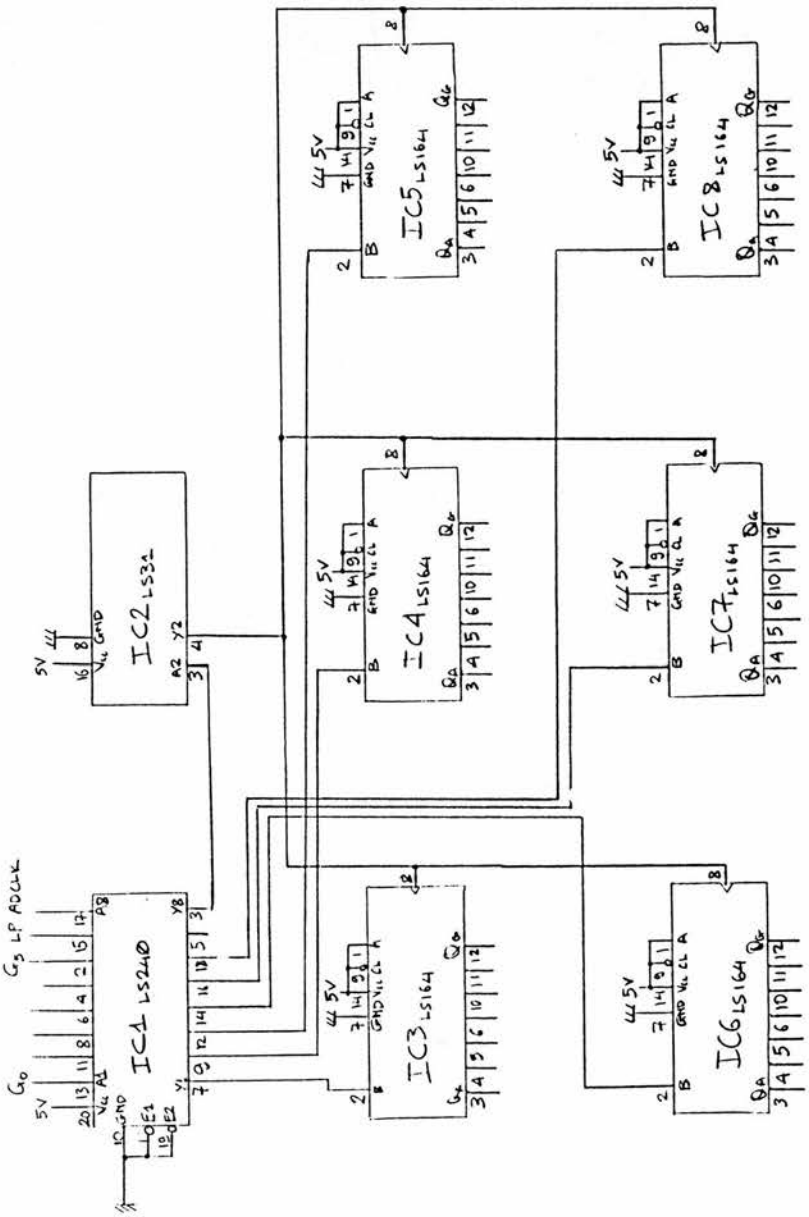
IC1 LS240
IC2 LS32
IC3 LS164
IC4 LS164
IC5 LS164
IC6 LS164
IC7 LS164
IC8 LS164
5V
GND
G0
G5 LP ADCLK

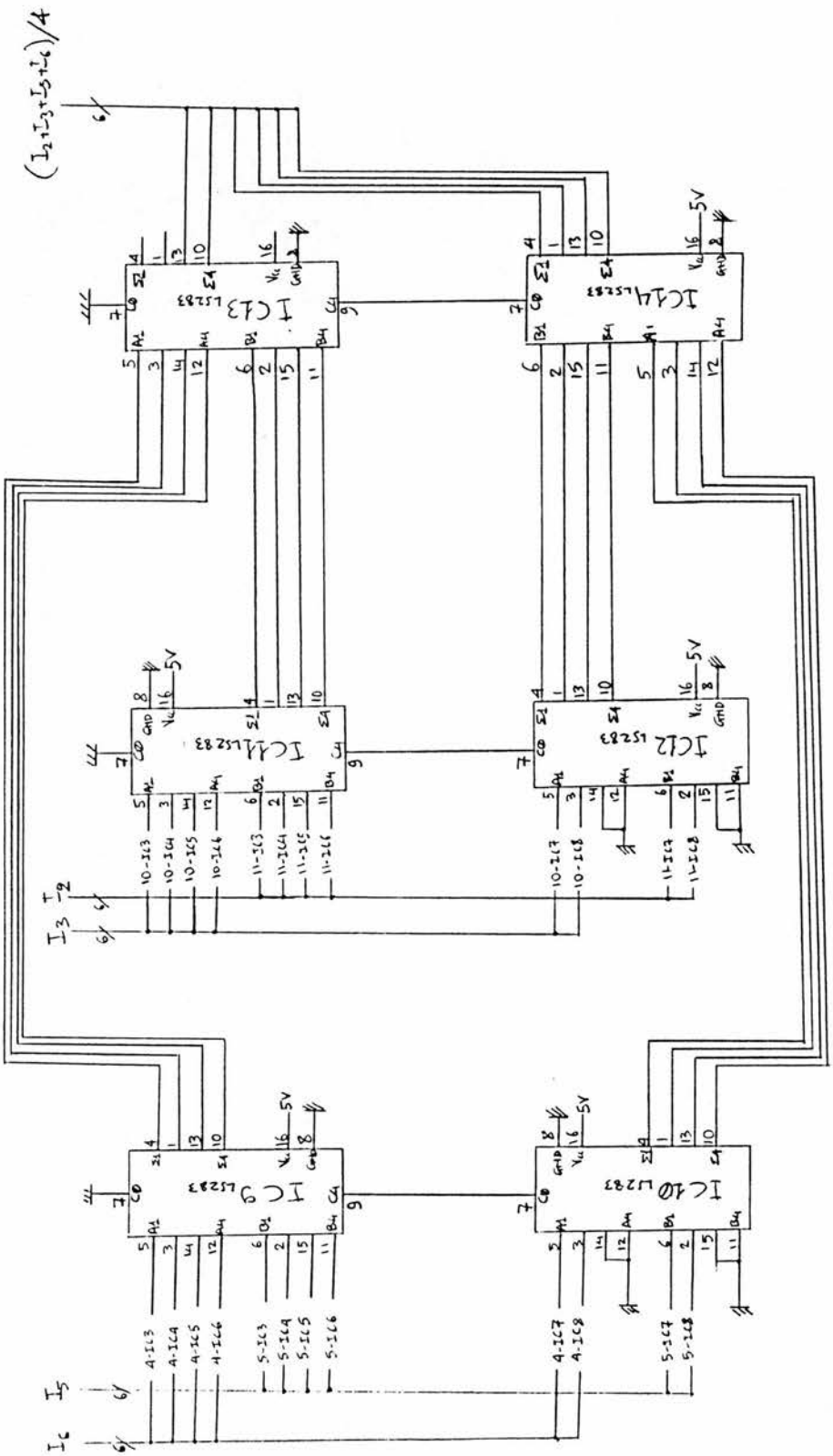
(I2+I3+I5+I6)/4
IC3 LS283
IC4 LS283
IC1 LS283
IC2 LS283
IC9 LS283
IC10 LS283
5V
I3
I5
I6

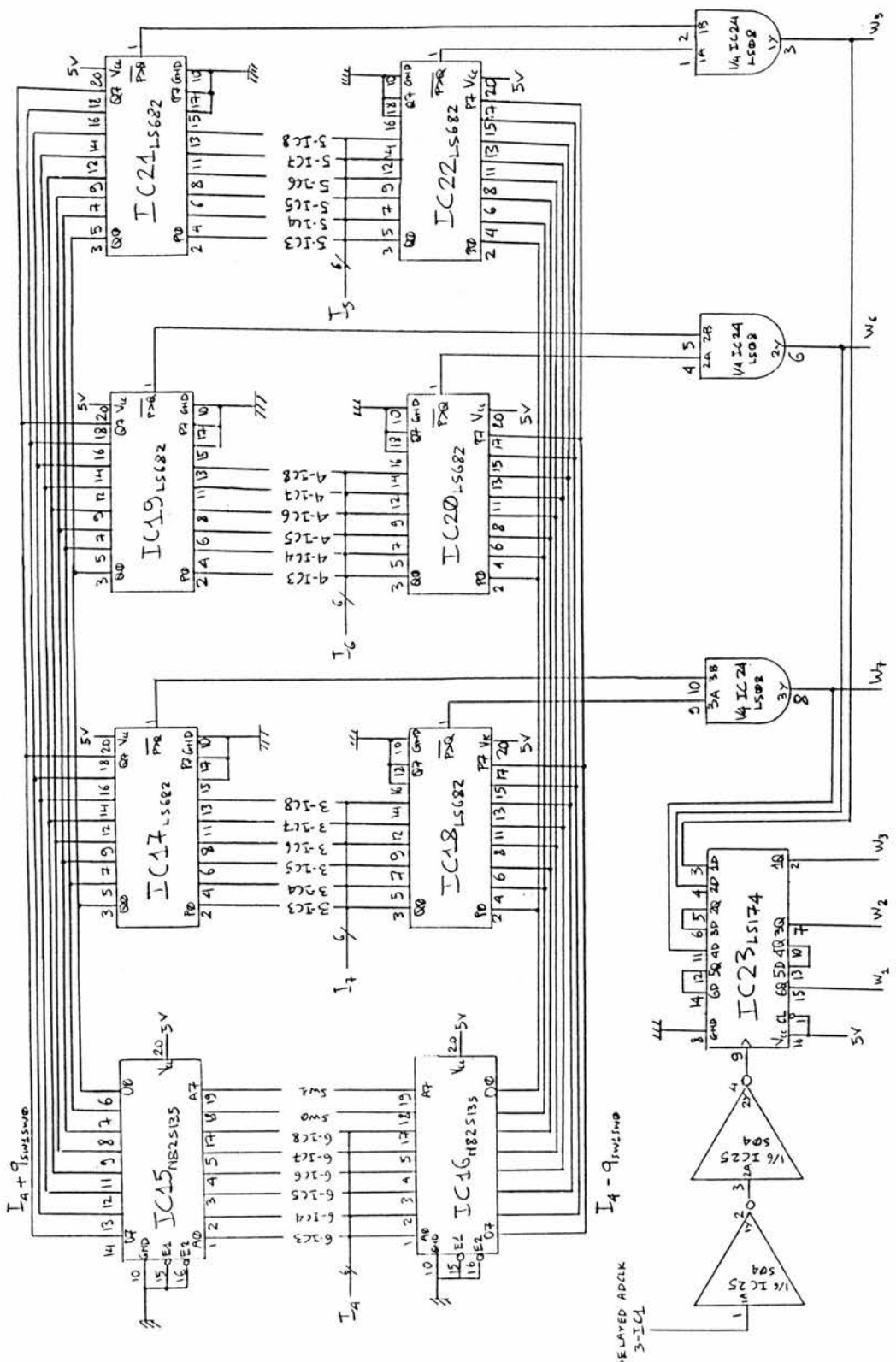
IC21 LS682
IC22 LS682
IC19 LS682
IC20 LS682
IC17 LS682
IC18 LS682
IC15 N82S135
IC16 N82S135
IC23 LS174
1/4 IC24 LS08
1/6 IC25 S04
DELAYED ADCLK
3-IC1
5V
GND

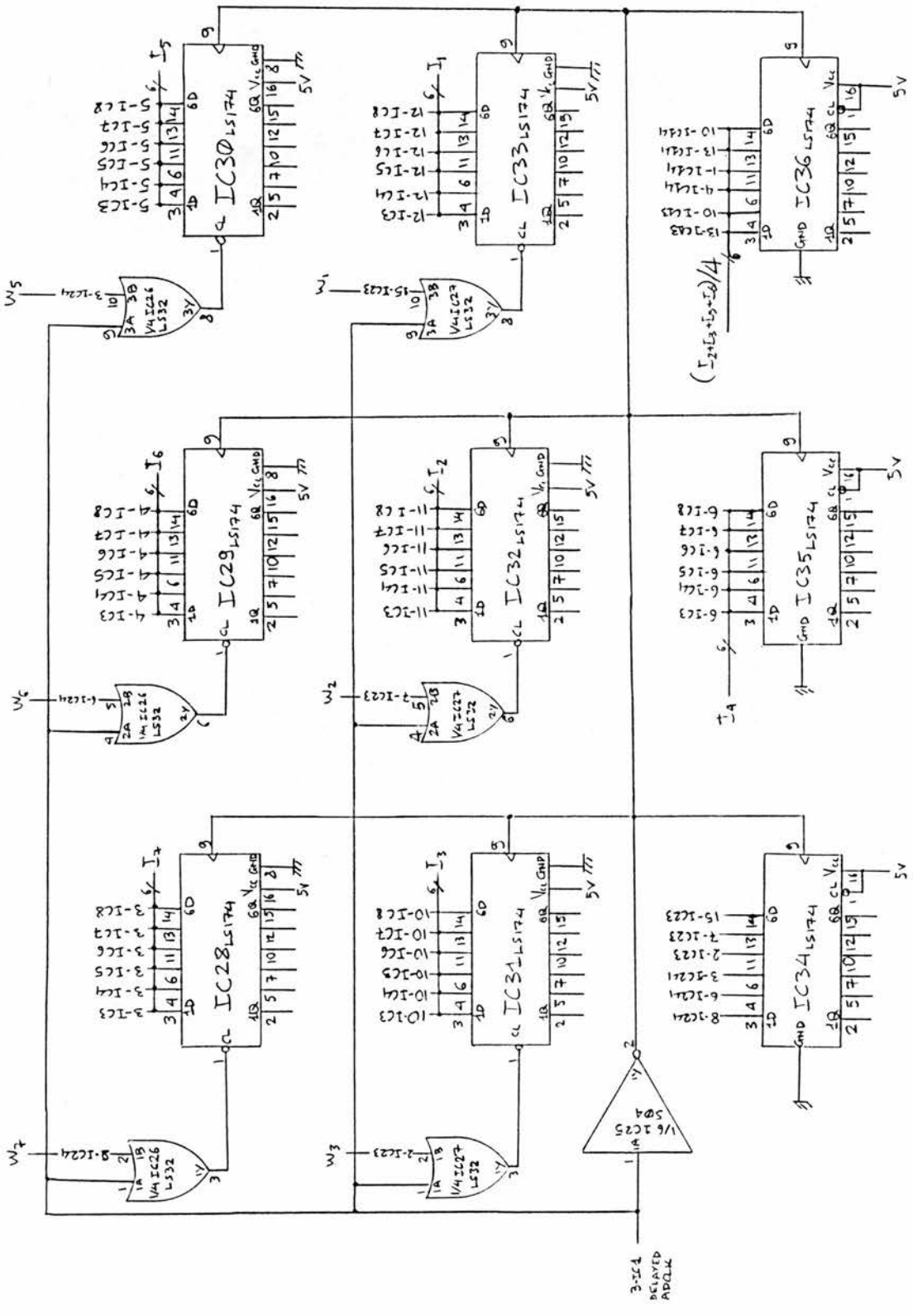

Appendix C : Circuit diagrams

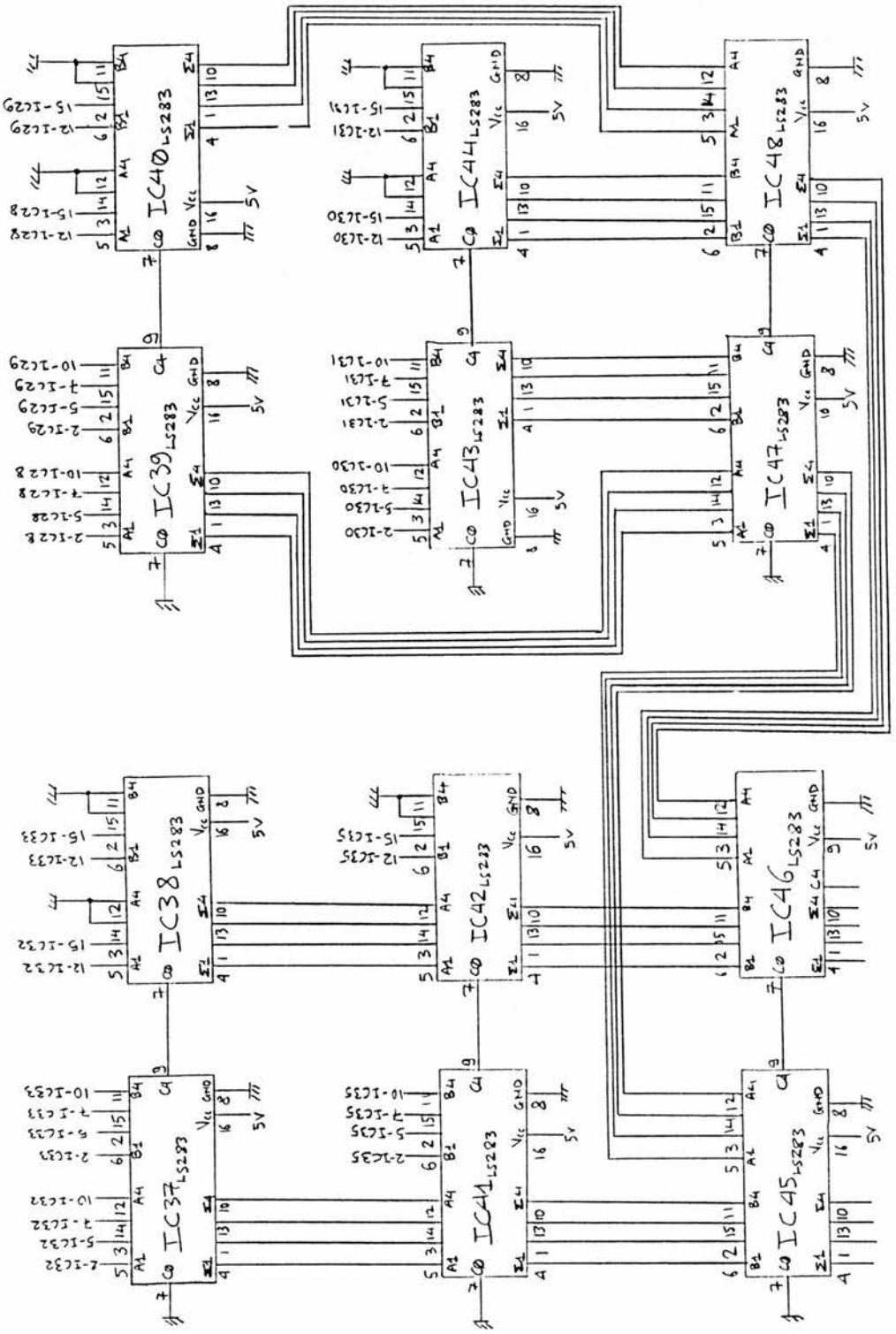
IC40 LS283
IC41 LS283
IC48 LS283
IC39 LS283
IC43 LS283
IC47 LS283
IC38 LS283
IC42 LS283
IC46 LS283
IC37 LS283
IC44 LS283
IC45 LS283
5V
GND

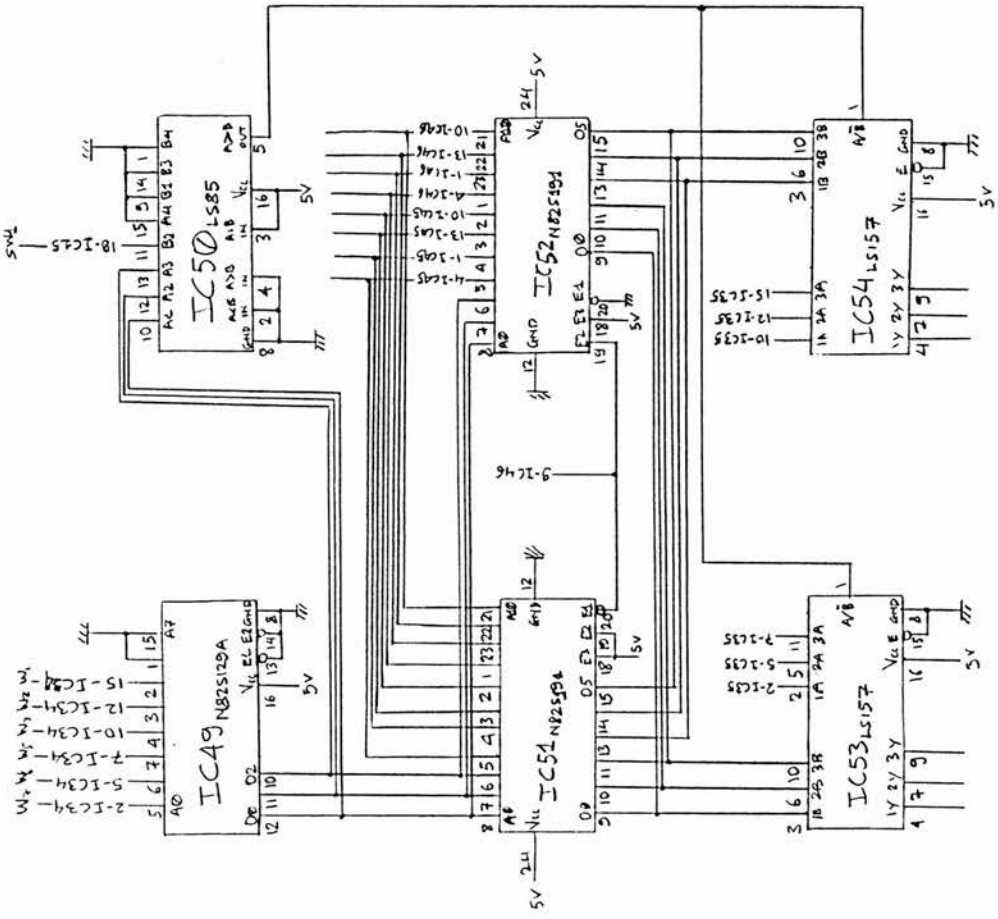
IC49 N82S128A
IC50 LS85
IC51 N82S96
IC52 N82S96
IC53 LS157
IC54 LS157
5V

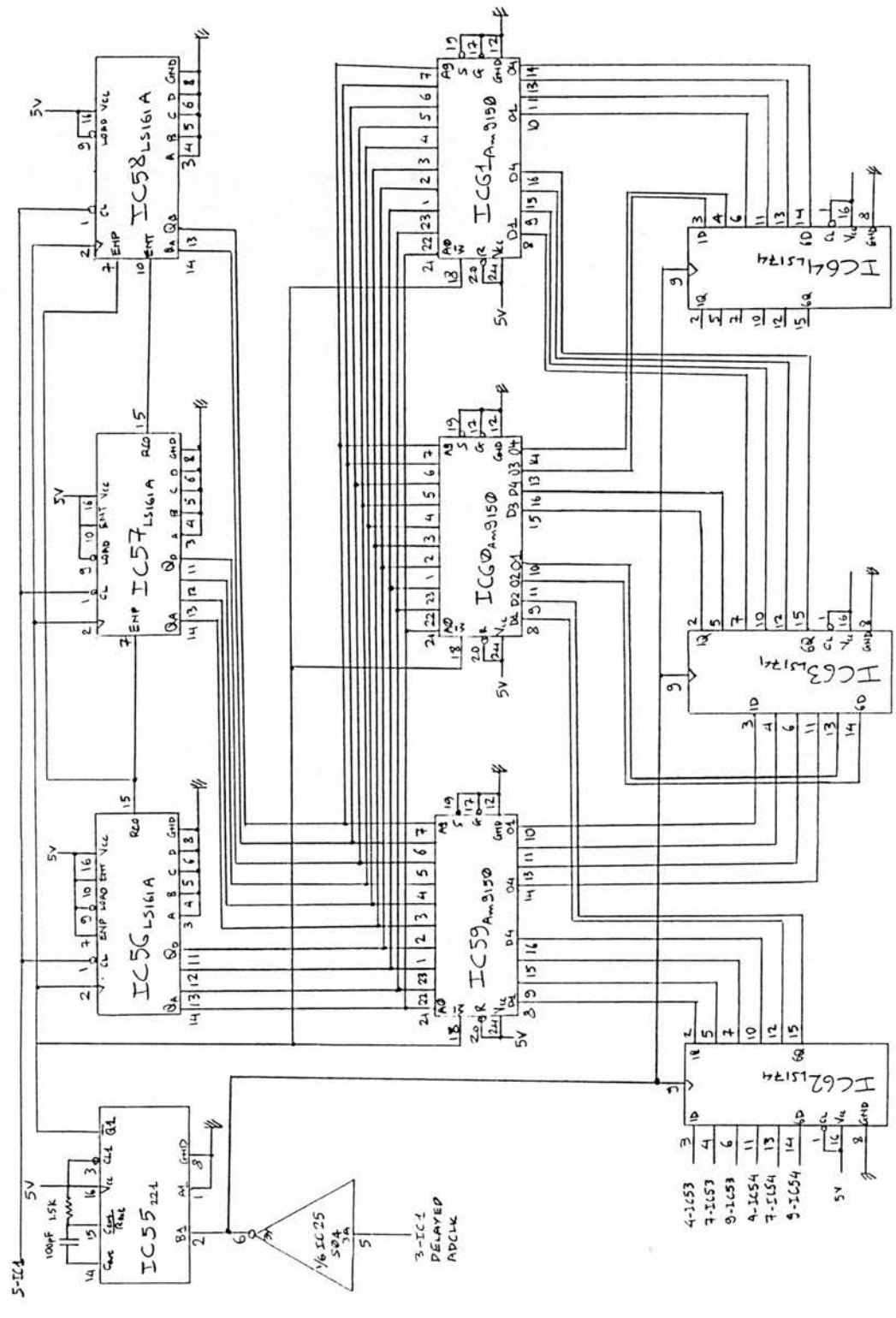
IC58 LS161A
IC57 LS161A
IC56 LS161A
IC55 LS221
IC61 Am9150
IC60 Am9150
IC59 Am9150
IC64 LS174
IC63 LS174
IC62 LS174
1/6 IC25 SN7404
100pF 1.5K
5V
LP
5-IC1
3-IC1 DELAYED ADCLK
4-IC53
7-IC53
9-IC53
4-IC54
7-IC54
9-IC54

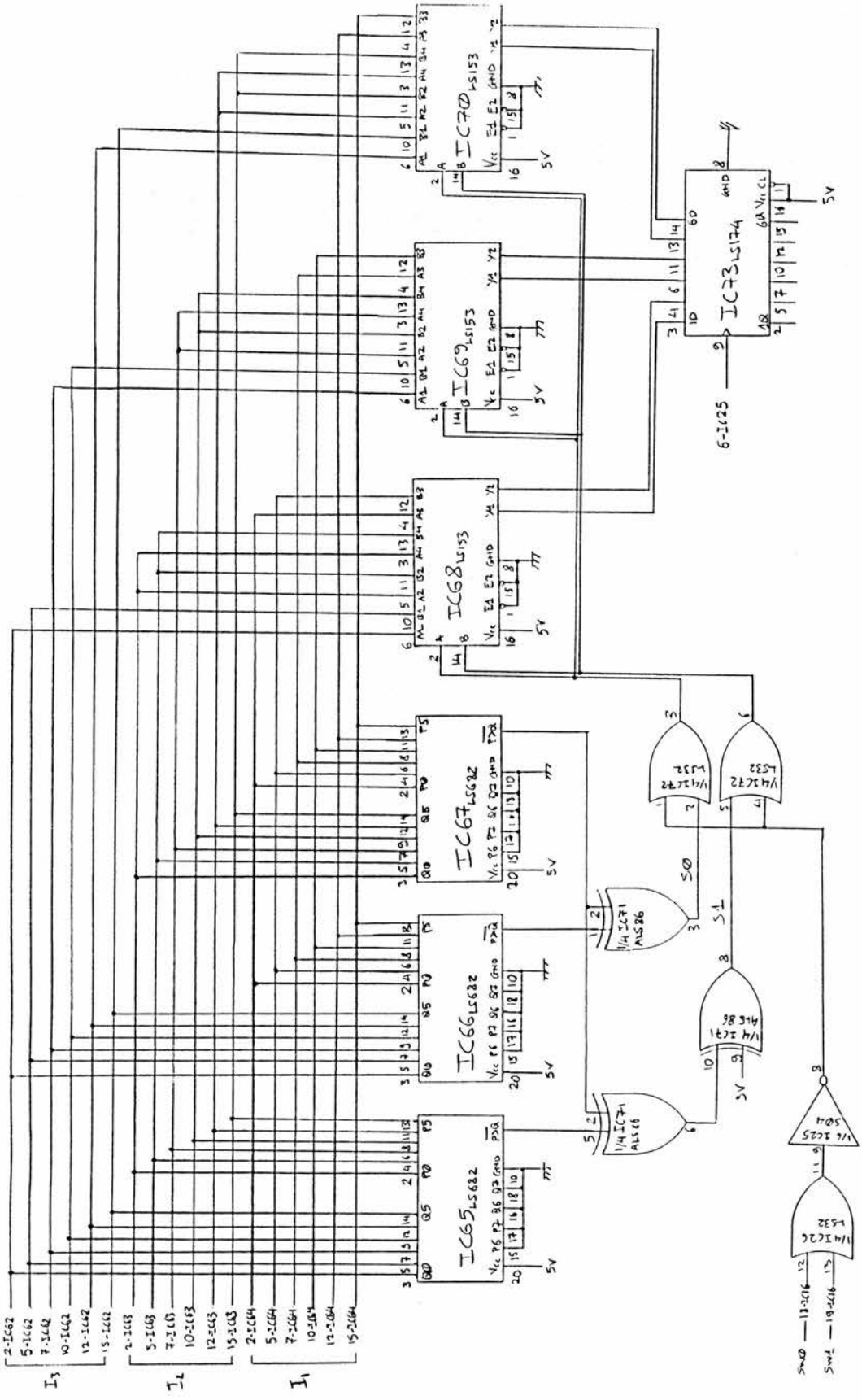
IC65 LS682
IC66 LS682
IC67 LS682
IC68 LS153
IC69 LS153
IC70 LS153
IC73 LS174
1/4 IC71 ALS86
1/4 IC72 LS32
1/4 IC74 ALS86
1/4 IC75 S04
1/4 IC76 LS32
5V
6-I125
I3
I2
I1

Acknowledgements

I am very grateful to my supervisor Norman McDicken for his advice, guidance and encouragement throughout this project. I also wish to thank Professor J R Greening, Dr P Tothill and Professor W N McDicken who, as Heads of the Department of Medical Physics during the last four years, made the departmental facilities available to me.

I wish to express my thanks to Dr P L Allan for his interest, advice on medical aspects of processing and the considerable amount of time he and his registrars devoted in the clinical trials. For their participation as observers in the clinical evaluations I am indebted to Dr P L Allan, Dr S R Wild, Professor W N McDicken and especially Dr S D Pye who also provided many valuable comments and whose careful and thorough reading of the draft helped reduce the number of mestakes and inconsistencies found in this thesis.

I wish to thank Martin Connell for introducing me to the field of image processing, for assistance with various aspects of computing and for many helpful discussions. I also wish to thank Tom Anderson for his help during the design and construction of the electronics.

I thank my fellow students for their help and encouragement and especially Nicholas Nicholson for his very constructive comments.

My thanks are due to the Scottish Home and Health Department for equipment grants. The receipt of a Scholarship from the State Scholarship Foundation of Greece (Oct 1984 - June 1987) and a British Council Fellowship (Oct 1987 - Sep 1988) are gratefully acknowledged. I also thank my family for their financial and moral support. The weekly deliveries of nonfiltered Camel cigarettes, 30000 of them during the last four years, may not have been the healthiest present but they have definitely contributed to my well-being.

Finally, I would like to express my thanks to the typist of this thesis for his excellent work and to a few friends who made life more interesting, and sometimes more difficult, over the last few years.

I declare that the work contained in this thesis was done by myself and the thesis was composed by myself.

Thanasis Loupas

July 1988